Optical code multiplex schemes as economical upgrade on existing DWDM systems to simplify costly channel monitoring

(Verwenden optischen Codemultiplexes zum kostengünstigen Aufrüsten bestehender DWDM Systeme zur Vereinfachung aufwändiger Kanalüberwachung)

Vom Fachbereich Elektrotechnik und Informationstechnik
der Universität Kaiserslautern
zur Verleihung des akademischen Grades
Doktor der Ingenieurwissenschaften (Dr.-Ing.)
genehmigte Dissertation

von

Dipl.-Ing. Jochen Eckert

aus Saarlouis

D 386

Tag der mündlichen Prüfung: 09.11.2001

Dekan des Fachbereiches: Prof. Dr.-Ing. R. Urbansky

Promotionskomission:
Vorsitzender: Prof. Dr.-Ing. R. Urbansky
1. Berichterstatter: Prof. Dr.-Ing. R. Zengerle
2. Berichterstatter: Prof. Dr.-Ing. (em.) W. E. Heinlein

Table of Contents

Table of Contents iii

Preface v

Chapter 1 Introduction 7
1.1 Fibreoptic Communication - State of the Art . . . 7
1.2 Motivation and task . . . 9
1.3 Overview and essential results . . . 10

Chapter 2 Optical CDMA 13
2.1 Characteristics and potential fields of application . . . 13
2.1.1 Local area and broadcast networks . . . 20
2.1.2 High bit rate point-to-point links . . . 21
2.1.3 Robust and secure transmission . . . 22
2.2 Code generation and detection . . . 24
2.2.1 Code generation by electrical signal processing . . . 24
2.2.2 Code generation by optical signal processing . . . 25
2.2.3 Code detection . . . 27
2.3 Current codes . . . 29
2.3.1 Optical orthogonal codes . . . 30
2.3.2 Prime sequence codes . . . 33
2.3.3 Quadratic congruence codes . . . 34
2.3.4 Two-dimensional codes . . . 36

Chapter 3 New codes for OCDMA and hybrid OCDMA/WDMA-techniques 39
3.1 Code generation . . . 40
3.2 Code properties . . . 49
3.2.1 Correlation constraints . . . 49
3.2.2 Size . . . 54
3.2.3 Bit error ratio . . . 60
3.2.3.1 Bit error ratio of modified optical orthogonal codes . . . 60
3.2.3.2 Bit error ratio of the errorfree subset of modified optical orthogonal codes . . . 62
3.3 Simulation results . . . 65
3.3.1 Size . . . 65
3.3.2 Bit error ratio . . . 70
3.4 Potential fields of application . . . 76
3.4.1 Synchronized CDMA system . . . 76
3.4.2 Hybrid WDMA/CDMA system . . . 78

Chapter 4 The propagation characteristics of single-mode fibres 81
4.1 Propagation of single wavelength light in optical transmission fibres . . . 82
4.1.1 The Nonlinear Schrödinger Equation . . . 83

4.1.2 Attenuation . . . 89
4.1.3 Dispersion . . . 91
4.1.4 Nonlinear refraction - Self-phase modulation . . . 95
4.1.5 Stimulated Raman Scattering . . . 97
4.1.6 Stimulated Brillouin Scattering . . . 98
4.2 Propagation of multiple-carrier wavelength light signals in optical transmission fibres . 100
4.2.1 Cross-phase modulation . . . 101
4.2.2 Four-wave mixing . . . 104
4.2.3 Stimulated Raman scattering . . . 107
4.2.4 Stimulated Brillouin scattering . . . 110
4.3 Consideration of nonlinear effects in WDM system simulations . . . 111

Chapter 5 The simulation of the optical transmission system 115
5.1 The optical transmitter . . . 115
5.2 The optical encoder and decoder . . . 116
5.3 The optical link . . . 117
5.4 The optical receiver . . . 118
5.4.1 The optical filters . . . 119
5.4.2 The receiving diodes . . . 120
5.4.3 The equalizer and synchronizer . . . 121
5.5 Performance evaluation measures . . . 122
5.5.1 The Q factor . . . 122
5.5.2 The eye diagram and the eye penalty factor . . . 126

Chapter 6 Crossphase modulation as dominant nonlinear effect in a SSMF/DCF based WDM transmission system 129
6.1 Input powers . . . 131
6.2 Channel numbers . . . 135
6.3 Channel spacing . . . 139
6.4 Bandpass filter characteristics . . . 143
6.5 Link length . . . 144

Chapter 7 Characteristics of the hybrid OCDMA/ WDMA transmission system 147
7.1 The structure of the system model . . . 147
7.2 Appropriate codes for a hybrid system . . . 151
7.3 Simulation results . . . 152
7.3.1 Input powers . . . 152
7.3.2 Channel spacing . . . 155
7.3.3 Link length . . . 159

Chapter 8 Summary 163

Zusammenfassung 165

List of Symbols 171

List of Acronyms 175

References 177

Lebenslauf 185

Preface

Thanks to Prof. Dr.-Ing. Heinlein for being supervisor of this work.

Many thanks to Prof. Dr.-Ing. Zengerle for being my supervisor, for giving me the chance to work in his department, to realize my research work and for giving me valuable suggestions during the development of this thesis.

Thanks to Mrs. Edel and to Mrs. Distler for their great cooperation and their perfect organizing ability.

Also, many thanks to my colleagues Steffen Reichel, Stefan Leonhard and Wolfgang Lenz for the inspiring discussions, for their helpful hints and answers on my questions and the hours that we spent together.

Very special thanks to Ralf Stemler, who always had an ear for my concerns, were they private or professional. I will miss the interesting and entertaining discussions.

And, of course, very, very special thanks to my parents who have always supported me on my course of life.

Chapter 1

Introduction

1.1 Fibreoptic Communication - State of the Art

The traffic load on telecommunication links has seen a tremendous increase during the last years. Especially due to the internet with its exponentially growing number of participants all over the world and more and more multimedia applications, a further increase in line capacity is one of the major tasks for telecommunication engineers and scientists at the beginning of the new millennium. This high transmission capacity can only be offered by optical fibres. But not only trunk traffic lines have seen higher data payloads, local and metropolitan networks (LAN, MAN) are widely being enhanced regarding capacity and maximum bandwidth. Companies, scientific institutes, hospitals and federal and communal authorities use the advantages that connected computer systems manifoldly offer. First projects examine the economic aspects, the acceptance, daily usage and social changes of fibre-to-the-home (FTTH) and the applications (e.g. pay-per-view TV, fast internet connections) the vast bandwidth offers. Networking has become the catchword of the communication industry.

Neglecting the uneconomic possibility of adding further fibres, developments to increase bandwidths in the last few years have mainly gone in two directions. One approach has been the increase in bit rates on a single transmission channel, the so-called time division multiple access (TDMA) or as optical alternative, the optical TDMA (OTDMA) [2] [66]. The other approach has been the more effective usage of the frequency spectrum that can be exploited on a fibre optic transmission channel, namely by adding multiple wavelength carriers on the same fibre, the so-called wavelength division multiple access (WDMA) [2] [66].

Starting with less than 10 GBit/s with a single carrier wavelength at the beginning of the last decade, transmission bit rates of laboratory systems exceed the TBit/s range [54] [78], e.g. with 132 wavelength channels, each carrying a 20 GBit/s TDMA signal. The increase in data bandwidth has lead - due to the great number of WDM channels - to a very high accumulated optical input power that is inserted into the fibre. The then occurring nonlinear effects like cross-phase modulation (XPM), four-wave mixing (FWM), polarization mode dispersion (PMD), stimulated Raman scattering (SRS) and stimulated Brillouin scattering (SBS) partially show strong impacts on the performance of the transmission quality (see section 4.2 and 4.3). Namely, the bit error ratio (BER) can increase to unacceptable levels if not certain conditions concerning e.g. power levels, carrier wavelengths and separations are met.

The tremendous increase in usable bandwidth has further become possible through the development or enhancement of various system components that enable a transparent link between transmitter and receiver. Optical add-drop multiplexer (OADM), optical amplifiers such as the erbium doped fibre amplifier (EDFA), tunable optical filters, star couplers (SC), wavelength routers (WR), wavelength converters (WC) and optical cross-connects (OXC) are viable components for operation of an optically transparent network. Although the „transparency“ of these components makes transmissions with arbitrary bitrate possible, their behavior is far from being ideal. They may introduce interchannel crosstalk which adds up to the crosstalk introduced by the nonlinear nature of the optical fibre. Furthermore, all these components show a significant dependence on temperature and aging effects, making an exact, strict and continuous channel monitoring absolutely essential.

A multiple access scheme widely neglected in optical systems in the last years has been the optical code division multiple access (OCDMA) technique. However, since necessary bandwidths both in access and backbone networks rise further and further, an additional access scheme can offer better bandwidth utilization ([41] et al.). Though CDMA has become very well known in mobile communication applications, especially in 3rd generation mobile systems as UMTS (Universal mobile telecommunication system), its application to fibre optics suffers from the almost exclusive deployment of intensity modulated direct detection (IM-DD) systems. Furthermore, bit rates are several orders of magnitude higher than in mobile networks, where the possibility to modulate the carrier’s phase enables the system designer to transmit bipolar signals and introduce codes with short lengths but still sufficient correlation constraints [58].

In contrast to that, an IM-DD system only allows the detection of „power-on“ or „power-off“ and the developed bipolar codes loose their nice characteristics in a unipolar environment. All the alternative ways (e.g. [12][23][35][46][61][62]) have the disadvantage of very long codelengths, thus making a use for high bit rate applications impossible, where the need for short codelengths is absolutely necessary.

1.2 Motivation and task

The fibre optic transmission systems that are currently developed for future use are very prone for imponderabilities of the system components. Be it by temperature changes or mechanical stress or even aging effects, especially laser diodes and optical filters, but also add/drop multiplexers show a significant dependence on outer influences. Laser diodes shift their carrier wavelengths, filters and multiplexers alter their transmission and their reflection profile, resp. [13][22]. Furthermore, some components like e.g. distributed feedback (DFB) lasers cannot be produced exactly with a specific and designated carrier wavelength. Quality checks after the production show a wide range of wavelengths between the different pieces, and the needed carrier wavelength is then selected during deployment by tuning the temperature of the component to the necessary value. This kind of production and deployment bears economical inefficiency, since carrier wavelengths in use on optical links are standardized to certain values according to the ITU grid.

Furthermore, wavelengths as well as the perfect tuning of all components to the specific channel must closely be monitored and observed during operation of the transmission link. With increasing number of transmitters and receivers, this ties even further resources.

But even if the lumped system components would show an - unrealistically - ideal behavior, there would still be interchannel crosstalk resulting from the nonlinear effects that the signals adept by travelling over the fibre. This crosstalk which mainly stems from the XPM can only be overcome by a sufficient spectral separation of the different wavelength channels. This demand is opposite to the demand for a number of channels as large as possible, or a channel spacing as small as possible. The ITU grid has fixed the separation to 0.4 nm (or 50 GHz, 3rd optical window) or integer multiples of that. An even smaller separation would be desirable to maximize the number of channels.

Thus, a smaller separation is only possible with a skillful coding of adjacent channels.

With suitable codes, the separation could be lowered to zero, enabling new channels to be added in the spectral transmission window. Furthermore, coding of the adjacent channels also lowers the effects of the crosstalk, improving system performance and BER of all involved channels.

Convenient codes must be capable of coding high bit rate signals. It is thus inevitable that the lengths of the codesequences are to be kept as short as possible. The codes must further be applicable in unipolar systems, so that the coding and decoding process can be used as upgrade of existing links. Furthermore, to be independent from electronic restrictions, signal processing i.e. coding and decoding has to be performed optically.

This work deals with the development of codes that meet these requirements and the comparison of a system upgraded with coding/decoding units and a standard system.

1.3 Overview and essential results

An overview on OCDMA is given in Chapter 2. Being an asynchronous multiple access scheme, OCDMA is especially well suited for local area applications with its bursty kind of traffic. OCDMA enables every user to access the transmission medium at any given time without waiting time. Further applications include broadcast networks with only one (or a only few) transmitters but many receivers. This system structure enables the operator to install costly equipment at the few transmitters and cheap of-the-shelf mass products at the receivers. Even in high bit rate point-to-point links, OCDMA as sole or as part of a hybrid access scheme can offer interesting advantages over the common access schemes. Other applications appreciate the increased security aspect of a coded transmission. Chapter 2 also points out the different possibilities of code generation and detection and presents the current codes that were developed throughout the last years.

Chapter 3 presents the new codes that were developed by the author. They are especially suited for OCDMA and hybrid OCDMA/WDMA applications. The theoretical code properties such as correlation constraints, code size and probability of error are depicted, followed by corresponding simulation results. It will be shown, that the new codes show superior behavior regarding code size and bit error probability. Chapter 3 ends with the potential fields of applications for the newly derived codes.

In order to perform reliable transmission link system simulations, it is first necessary to develop a system model for the simulated transmission medium, see Chapter 4. It is based on

the nonlinear Schrödinger equation which is solved by the split-step Fourier algorithm. The characteristic properties of single mode fibres as attenuation, dispersion, self-phase modulation and stimulated scattering processes are investigated for single- and multichannel systems. Finally, the consideration of these effects in the system simulations is stated.

Besides the transmission medium, the simulated optical system consists of components like the transmitter, the optical encoder and decoder units, optical amplifiers, filters and receiver diodes. Their functionalities and models are described in Chapter 5. Furthermore, the possibilities for the evaluation of the received signal quality is explained. Whereas in a pure TDM or WDM system, the bit error ratio is commonly calculated from the so-called Q factor, signal quality in the hybrid OCDM/WDM system is estimated from the eye penalty factor. This has become necessary since the sampled amplitude values of the received output signal are no longer Gaussian distributed due to the coded transmission.

Therefore, Chapter 6 presents simulation results of an 8 channel WDM system (10 GBit/s per channel) which show both signal quality factors. A 400 km link built up of 8 sections of 50 km standard single-mode fibre with pre- and postcompensation, followed by optical filter and EDFA, is simulated with varying input powers, numbers of active channels, channel spacings, bandpass filter widths and finally various link lengths. The results show a strong impact of signal powers and channel spacings on the received signal quality, mainly due to XPM. The system's bit error ratio increases dramatically as soon as input powers exceed 12 mW and as soon as the channel spacing goes below 0.3 nm due to spectral overlap of adjacent channels. Generally, the system performance fluctuates strongly with varying system parameters.

This strong dependence is drastically reduced in case of a coded transmission, for which the necessary system structure and the appropriate codes as well as simulation results are presented in Chapter 7. An eight channel hybrid OCDM/WDM transmission system (with 10 GBit/s input data signal) is simulated, varying the same parameters as in the uncoded case of Chapter 6. The results prove that even in the case of zero carrier spacing of all channels, all 8 channels can be decoded with bit error rates well below 10^{-12}. Furthermore, the bit error rate is well below acceptable levels for all kinds of input parameter sets, which make the hybrid system very robust against outer influences or aging effects of its components.

Chapter 8 finally gives a short summary of the obtained results.

Chapter 2

Optical CDMA

Whereas time division multiplexing (TDM) has been used as multiple access scheme since the beginning of technical feasibility of transmission systems and wavelength division multiplexing (WDM) has been focussed on at the end of the last millennium in optical communications, optical code division multiplexing (OCDM) is still widely unknown and unrecognized. But since bit rates are further pushed ahead and dense wavelength division multiplexing (DWDM) systems slowly reach their minimum channel spacing, OCDM turns into an interesting alternative to more and more complex TDM or WDM systems with increasingly high component requirements.

In section 2.1, a closer look is taken at the basic fundamentals of optical code division multiple access (OCDMA), potential implementation schemes are named and advantages and disadvantages of OCDMA are assessed. Section 2.2 presents different possibilities of code generation with a closer look at optical code generation. Finally, in section 2.3 an overview on current codes and their characteristics is given.

2.1 Characteristics and potential fields of application

The CDMA technique has its origin in the spread spectrum (SS) technique. SS has been developed in the 1940's as military radio application which offers high security transmission. In an SS transmission, the input signal is coded in such a way, that its spectrum spreads over a much wider range than the original signal. At the receiver, the spreaded signal is decoded and its original form is restored. While despreading the input signal, unwanted noise or intentional jamming signals are spreaded, i.e. though input signal and distortion might carry the same power, the power spectral density of the distortion covers a wider area, thus enabling

the receiver to detect the input signal and noticing some additional, but only weak noise (see Figure 2.1). Furthermore, a despreading of the input signal is impossible without exact knowledge of the code sequence, thus increasing the security of the transmission.

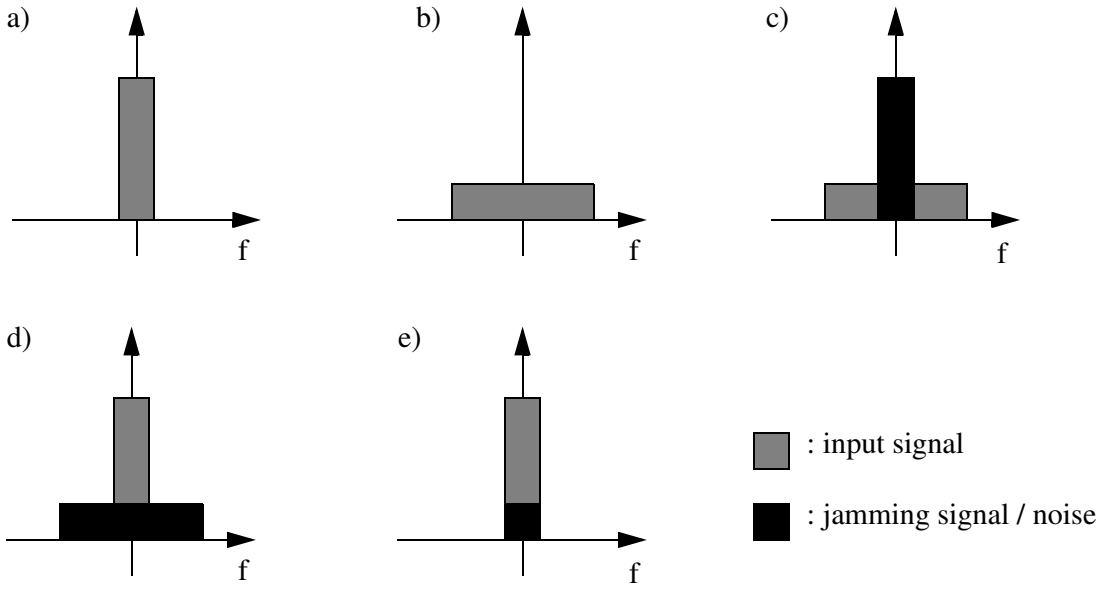

Figure 2.1: Principle of spread spectrum communication.
a) Spectrum of input signal. b) Spectrum of coded input signal (to be transmitted). c) Jamming signal/noise overlapping input signal during transmission. d) Decoded signal, input signal is compressed, jamming signal/noise is spreaded. e) Filtered signal at receiver, input signal can be detected.

If each of the users is assigned to its own code sequence which is orthogonal to all others, they can all access the transmission medium at the same time at the same carrier frequency, resulting in the so-called CDMA. CDMA has been of high attractiveness as multiple access scheme in radio applications because of

- non-sensitivity against narrow-band jamming signals
- efficient use of transmission medium in bursty traffic scenarios
- high security due to coded transmission.

In fibre optic applications, these first-sight advantages are less interesting. Narrow-band jamming signals are not to be expected on a fibre link, traffic is, if not in local area networks, rather of continuous nature than of bursty. Still, OCDMA can be of interest. Again, in LAN applications with bursty traffic environment, CDMA is a first choice multiple access scheme due to low coordination necessary between different users. Whereas in TDMA schemes, all users are assigned to fixed time frames or, in WDMA schemes, to a fixed wavelength, this is

not the case in CDMA transmission. In case of temporal or spectral overlapping, system performance decreases immediately in pure TDMA/WDMA applications. Especially in DWDM systems, wavelength drift has serious influence on an acceptable bit error ratio (see 2.1.3). This fact can be overcome by an „upgrade“ of the DWDM system with OCDM. OCDM in a WDM transmission system can also help to weaken the effects of nonlinearities (see 2.1.2).

Several methods have been developed for coding, two of them have come into closer focus during the last years [2] [26]:

- Direct sequence (DS) CDMA, a temporal coding technique. Each mark of the input bit sequence is encoded into a whole sequence of marks and spaces (the code sequence, also called chip sequence), each space is encoded into another orthogonal code sequence. In case of unipolar environment as is in fibre optic transmission, a space is not encoded, since a space carries no energy. Thus, there is no signal in that time slot that can be encoded.
- Frequency hop (FH) CDMA, a spectral coding technique. The carrier frequency is shifted periodically according to a certain, preassigned code. All channels share the entire bandwidth by using different carrier wavelengths at different times according to a certain code. Since FH CDMA requires tuneable laser sources for optic applications or the creation of a supercontinuum with subsequent filtering [70][80][81], this CDMA scheme has not been further taken into consideration in this work, because one of the aims of this work has been the improvement of system performance without extending the system’s complexity.

For the rest of this work, CDMA will denote direct sequence CDMA.

CDMA can thus be divided into two categories:

- Incoherent CDMA.
- Coherent CDMA. Coherent CDMA requires the exact knowledge of the carrier’s phase. Though coherent detection increases the receiver sensitivity by approx. 10 dB [77], the system’s complexity is extremely increased [36][37][49]. In case of a fibre optic transmission system, tracking the phase of the light wave means an additional effort which is out of all proportion to the expected improvement of performance. For these reasons, coherent CDMA has also not been considered in this work.

By restriction to incoherent CDMA, another advantage is the possible use of the widely

used IM-DD (intensity modulated direct detection) systems. Signal detection in these systems is equivalent to power measurement, i.e. on-off keying („full“ power for transmitting a mark, zero power for space) is used with only very few exceptions. These systems are modeled as *positive systems*, i.e. a system that can not manipulate its signals to add to zero, since optical power can not be negative.

This circumstance is of tremendous importance and a huge difference to code division multiple access radio systems, where tracking of the carrier's phase can easily be accomplished and enables coherent CDMA. By being able to modulate and detect the carrier phase, bipolar codes (marks are represented by „+1“, spaces by „-1“ or „$+\pi$“ and „$-\pi$“, resp.) can be chosen. Bipolar codes have been under examination for several years [57].

In positive systems, unipolar codes must be used. Whenever an information „1“-bit is to be transmitted, a whole code sequence consisting of „0“s and „1“s is transmitted. An information „0“-bit is not encoded.

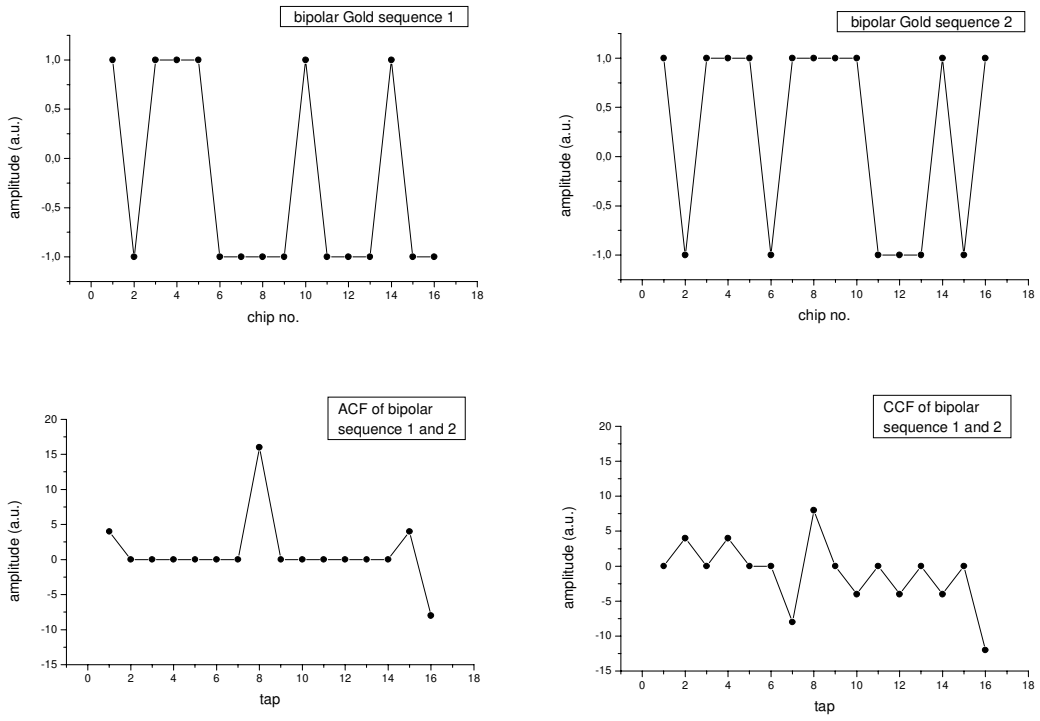

Figure 2.2: 16-chip bipolar Gold sequences and their autocorrelation (ACF) and crosscorrelation functions (CCF)

However, a transfer of bipolar codes into unipolar codes includes a complete change of the code's characteristic. A small example using Gold codes [69] shall intensify this fact.

As Figure 2.2 indicates, in the case of a bipolar environment, both sequences have equal maximum values of their autocorrelation at sampling instant and a crosscorrelation maximum which is much lower than the autocorrelation maximum, thus enabling a clear distinction between desired (autocorrelation) and undesired signal (crosscorrelation) at the receiver. If the same code is used in a unipolar environment, the autocorrelations show different peak values and, even worse, the crosscorrelation shows the same peak value as the autocorrelation of sequence #1, making a distinction between them by pure sampling absolutely impossible, see Figure 2.3.

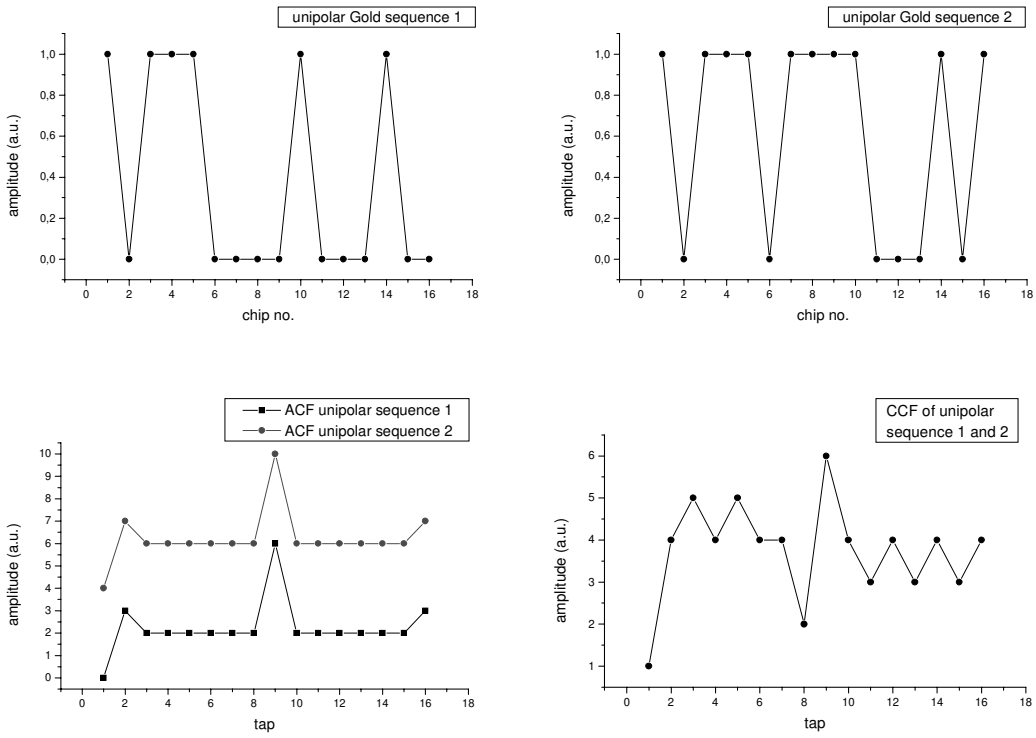

Figure 2.3: 16-chip unipolar Gold sequences and their ACFs and their CCF

New codes were developed, see 2.3, which consider the positive nature of fibre optic transmission systems and the incoherent detection process. Due to this unavoidable fact, the mode of action of these codes is different to that in a bipolar environment where the magnitude of the crosscorrelation can be kept low by a summation of „+1“ and „-1“, or the destructive interference of phase „+π“ and „-π“. In a purely positive environment, crosscorrelation must be kept low by the prevention of a superposition of too many „1“s (so-called hit incidents).

A CDMA system thus has the principal structure as shown in Figure 2.4.

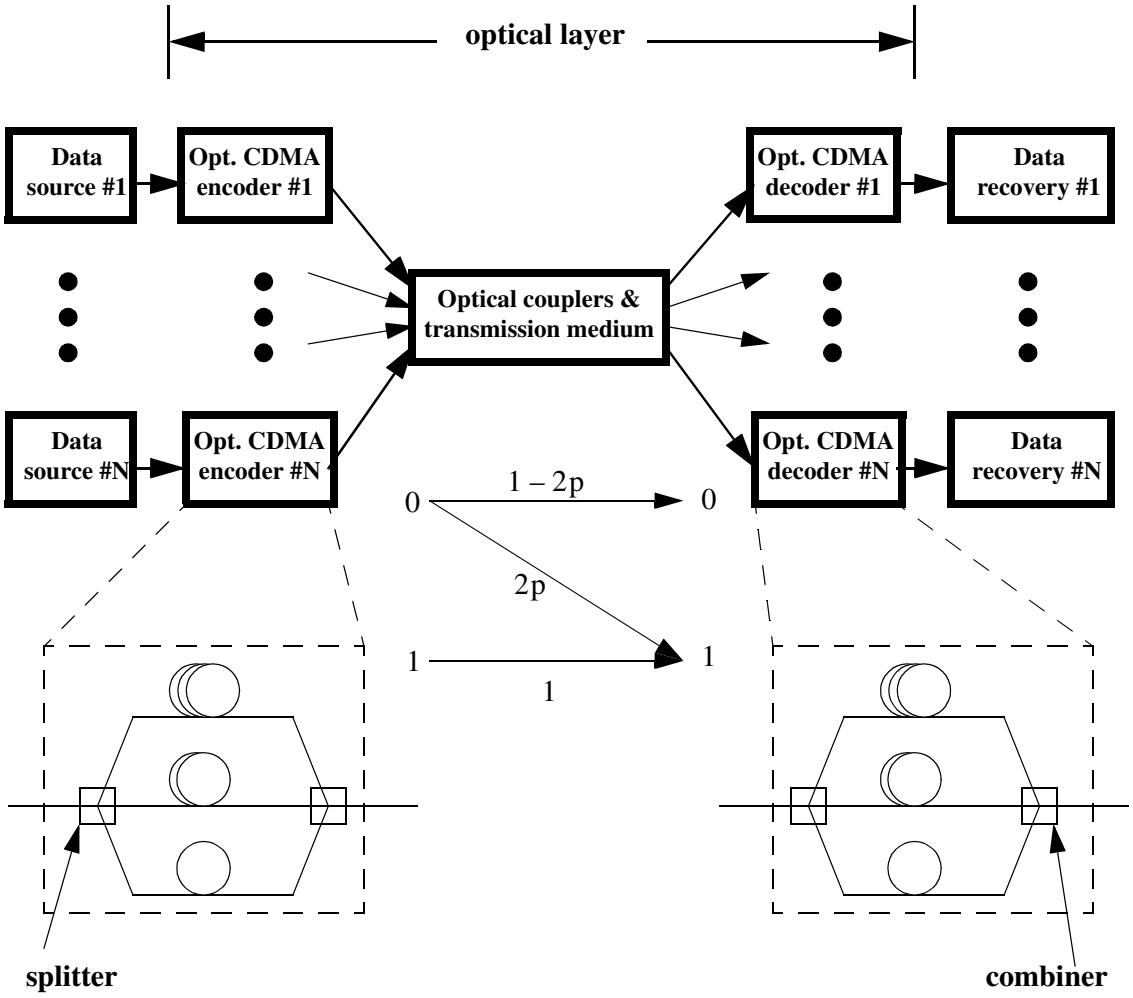

Figure 2.4: Principal structure of OCDMA transmission system

The binary, but unipolar data signal of source #n is

$$b_n(\mu) = \sum_{t=-\infty}^{\infty} b_t^{(n)} p_M(\mu - t \cdot M) \quad , \tag{2.1}$$

where $b_t^{(n)}$ is the data sequence of user #n, taking on values of „0“ and „1“ for each t with equal probability and $p_M(\mu)$ a rectangular pulse of duration T as described in Chapter 5.

The unique signature sequence of user #n $p_n(\mu)$ is described by

$$p_n(\mu) = \sum_{j=-\infty}^{\infty} a_j^{(n)} p_{M_c}(\mu - j \cdot M_c) \quad , \tag{2.2}$$

where $a_j^{(n)}$ is the code sequence or chip sequence, resp., of user #n, taking on values of „0“ and „1“. $p_{M_c}(\mu)$ is the rectangular pulse of duration T_c. The output signal of the encoder thus follows as

$$s_n(\mu) = s_n b_n(\mu) p_n(\mu), \tag{2.3}$$

s_n being the nth user's intensity. The overall baseband signal of all transmitters is the summation of all single signals:

$$s(\mu) = \sum_{n=1}^{N} s_n(\mu) \quad . \tag{2.4}$$

Since this chapter is dedicated to the influence of multiuser interference, thermal and quantum noise is neglected for now, as is the signal distortion due to dispersion and nonlinear effects on the fibre. In that case, the received signal resembles the transmitted one

$$r(\mu) = g \cdot s(\mu) = g \cdot \left(s_1 b_1(\mu) p_1(\mu) + \sum_{n=2}^{N} s_n b_n(\mu) p_n(\mu) \right) \tag{2.5}$$

where g is an amplitude factor ($0 < g \leq 1$) due to signal attenuation on the fibre. User #1 shall be the wanted user which is to be detected.

If $r(\mu)$ is decoded, the corresponding signal is then obtained by

$$\begin{aligned} \varphi_{r,\,p_1}(i) &= \sum_{\mu=0}^{K-1} r(\mu) p_1(\mu + i) \\ &= g \sum_{\mu=0}^{K-1} s_1 b_1(\mu) p_1(\mu) p_1(\mu + i) + g \sum_{\mu=0}^{K-1} \sum_{n=2}^{N} s_n b_n(\mu) p_n(\mu) p_1(\mu + i) \\ &= g \sum_{\mu=0}^{K-1} p_1(\mu) p_1(\mu + i) \quad + \quad I_1 \end{aligned} \tag{2.6}$$

I_1 being the interference term. The sampling of $\varphi_{r,\,p_1}(i)$ leads to

$$\begin{aligned} \underline{\varphi}_{r,\,p_1}(i) &= \varphi_{r,\,p_1}(i) \delta\left(i - k\frac{K-1}{2} \right) = \varphi_{r,\,p_1}\left(k\frac{K-1}{2} \right) \\ &= w + \text{interference} \end{aligned} \tag{2.7}$$

where w is the weight of the code, i.e. the number of „1“s in a codeword.

Common to all codes, see also 2.3, is the demand for certain threshold levels, that both the autocorrelation and the crosscorrelation peak do not exceed.

$$\left|\varphi_{p_n,\,p_n}(i)\right| = \left|\sum_{\mu=0}^{K-1} a_\mu^{(n)} a_{\mu+i}^{(n)}\right| = \begin{cases} w & \text{for } i = 0 \\ \le \rho_a & \text{for } 1 \le i \le K-1 \end{cases} \tag{2.8}$$

$$\left|\varphi_{p_n,\,p_m}(i)\right| = \left|\sum_{\mu=0}^{K-1} a_\mu^{(n)} a_{\mu+i}^{(m)}\right| \le \rho_c \qquad \text{for } 0 \le i \le K-1,\ n \ne m \tag{2.9}$$

w, ρ_a and ρ_c are constants. In unipolar systems, it is impossible to keep $\rho_a = \rho_c = 0$ as required by strict orthogonality. Whereas (2.8) is necessary for correct synchronization ((2.8) demands a narrow peak in the ACF), (2.9) is necessary to ensure a low probability of error in a multiuser environment. If w is lower than the interference term, i.e. the sum of the sampled CCF peaks, a bit error occurs.

In order to keep ρ_c low and thus prevent too many hit incidents, one possibility is the use of long codewords with only a few marks. Optical orthogonal codes (see 2.3) use codewords where the ratio of codelength to number of marks is less than 1/5. I.e. that for accommodating a greater number of users, codelengths of over 1000 have to be employed. Clearly, there are fields of application where such codelengths can not be accepted, since they imply a chiprate which is at least 1000 times higher than the bitrate. This is the case in high bit rate applications. To distinguish between the different potential applications for a CDMA system, in 2.1.1 to 2.1.3 different scenarios and requirements for the necessary codes are pointed out.

2.1.1 Local area and broadcast networks

Fibre optic transmission systems that need to connect a large number of users within a local area, so that any user can connect to any other desired user, are called *local area networks* (LAN). A LAN offers the advantage of a random access of the user to the network. This does not hold for *broadcast networks*[1] (BCN), where information is transmitted from one transmitter to a group of subscribers. Broadcasting several dozens of video channels over cable television and pay-per-view applications are examples for this kind of network architecture. Despite the difference in the access scheme, both network types have a lot in common. They are thus discussed in the same chapter where the differences between them and the point-to-

[1] Some publications prefer the term *distribution* network to broadcast network. However, there is no difference in the structure of both systems.

point links are pointed out. LAN and BCN can be characterized by these facts:

- short distances (< 10 km) between transmitters and receivers,
- chromatic dispersion is no constraint,
- normally in-line amplification is not required due to short distances, thus making it to a *passive optical network* (PON),
- power budget is dominated by passive splitter losses,
- many transmitter/receiver pairs with relatively low bitrate in the MBit/s regime add up to a large overall bandwidth in the GBit/s or even TBit/s regime.

The main profit of employing a CDMA based access scheme in a LAN/BCN is the lack of synchronization of all users. If the code sequences are carefully chosen, each user can transmit at any desired time without the need for synchronization with the other users. In that case, the underlying codes should offer the following characteristics:

- small number of marks in the code sequence, since the system is dominated by splitter losses and a partition of the energy of one bit into many chips is not desirable
- since the bitrate of each user is in the order of several MBit/s, length of codewords can exceed 1000,
- the code family must accommodate both many (in the order of hundreds) users in the network as well as many simultaneous users,
- bit error ratios of 10^{-6} or less can be accepted.

Optical CDMA based research work mainly focused on these kind of codes in the past. The most important codes in this field are depicted in section 2.3. Codes which go beyond this field of application and can, at the same time, improve the system performance in LAN/BCN applications are described in Chapter 3.

2.1.2 High bit rate point-to-point links

Point-to-point links represent the simplest way of transmitting information from one point to another via a fibre optic. In order to efficiently utilize the bandwidth of the transmission fibre, point-to-point links are mostly driven with high bit rates or multiple wavelengths. Here the main characteristics are:

- predominantly long (> 50 km) distances between transmitter and receiver,
- synchronous network
- electrical or optical amplification necessary due to long fibre links,
- dispersion compensation necessary,
- power budget is dominated by fibre losses,
- only few transmitter/receiver pairs per wavelength but with high bitrates in the GBit/s regime, adding up to an overall bitrate in the TBit/s regime,
- stringent reliability requirements on system performance.

Designing a CDMA based access scenario would require different characteristics of the suitable codes than in the case of LAN/BCN. However, including codes to the transmitting signals will show additional advantages in terms of system performance, system robustness, system reliability and system structure, see Chapter 6 and Chapter 7. These codes must meet the following requirements:

- since bit rates are in the GBit/s regime, lengths of codewords must be kept below 100 to ensure feasibility
- code family must accommodate only several tens of users, but all of them must be able to communicate simultaneously
- bit error rates must be less than 10^{-9} or even 10^{-12}

Codes which fulfill these needs are developed in Chapter 3. Their impact on actual transmission systems is described in Chapter 7.

2.1.3 Robust and secure transmission

As already mentioned in section 2.1, coded transmission offers higher security over uncoded transmission, since a knowledge of the used code sequence is unavoidable in order to properly detect the transmitted signal. If an illicit intruder tries to receive the transmitted signals and is not in possession of the correct code, he will only receive „noise“. Fibre optic CDMA thus offers the advantage of an increased security in an unsecure environment. Furthermore, it is much more difficult to use the irradiation emerging from a fibre in order to detect communication signals as it is in the case of copper cables.

Adding a CDMA component to an existing system, i.e. coding of each transmitted signal, can offer further advantages. High bit rate transmission systems are strongly susceptible to environmental changes such as fibre bends or temperature differences, since the system margin is only in the range of a few dB. WDM systems and especially DWDM systems with channel spacings of only 0.8 nm or less are very much dependent on the long term stability of their components, especially their laser sources [11][29]. Recent experiments [55] showed, that in the case of uncontrolled temperature influence, wavelength deviations can reach up to 2 GHz within 24 hours. Whereas short-term fluctuations and fast temperature changes can be compensated, long-term drifts, e.g. aging-induced, can not be economically controlled by state-of-the-art techniques. These long-term drifts can reach up to ± 0.4 nm [13]. If only temperature dependence is considered and aging-induced shifts neglected, the wavelength dependence in the 3rd optical window can e.g. be expressed as [23]

$$\Delta\lambda = 6.67 \cdot 10^{-6} \cdot 1550\ \text{nm} \cdot \Delta T\ . \tag{2.10}$$

Uncompensated systems would drift due to temperature changes during infield operation of up to 1 nm, approx. Keeping in mind, that channel spacings can go down to 0.4 nm for high bit rate systems, a drift of more than 0.2 nm would certainly mean a breakdown in the bit error rate, see also Chapter 6.

However, even the techniques for compensating short-term drifts require costly system components. So far, optical feedback, electronic feedback locking to a frequency reference and absolute frequency stability by locking to molecular absorption lines have been implemented [74]. Optical feedback systems suffer from instability, while locking to a molecular absorption reference prevents flexibility in the choice of operating wavelength. Electrical feedback loops in high bit rate environments need to operate at high bit rates (equalling the data bit rate) which make them an extremely costly component. Finally, these control mechanisms lead to very bulky transmitters, rendering them unsuitable for LAN applications.

Furthermore, the range of tunability of the widely used distributed feedback (DFB) lasers is narrow (in the order of several hundred GHz) and its center frequency cannot be precisely controlled during manufacturing. Even lasers from the same wafer will typically have different center frequencies and tuning ranges that may even not overlap, making DFB lasers a very costly component, since only lasers with designated center frequencies can be used in WDM transmission systems.

Thus, coding adjacent channels with orthogonal codes can be an interesting alternative to complex channel wavelength monitoring [17]. If adjacent channels are orthogonally coded, they can be detected without additional errors even in the case of a complete spectral overlap, see Chapter 3 and Chapter 6.

Codewords of an additional CDMA component in a DWDM transmission link must meet similar requirements as the ones used in TDM point-to-point links as described in section 2.1.2. Therefore, their necessary characteristics are not described here but can be found in section 2.1.2. The codes that can be used for these applications are developed in Chapter 3, their influence on the performance of existing transmission systems is examined in Chapter 7.

2.2 Code generation and detection

As in the whole of this chapter, only direct sequence (DS) CDMA is of concern. The manifold possibilities of code generation for spectral or spatial coding will not be mentioned here, since this work only deals with temporal coding mechanisms which are easy to implement for upgrading existing systems.

Depending on the application, the data signal can be coded either in the electrical or in the optical domain. Advantages and disadvantages will be compared in section 2.2.1 and section 2.2.2.

2.2.1 Code generation by electrical signal processing

In an uncoded fibre optic system, the injection current of the laser source carries the relevant bit sequence. Alternatively, the laser diode is not directly modulated but the output bitbeam is sent through a modulator, mostly an electroabsorption modulator (EAM) that transfers the on-off bit sequence onto the constant laser output. In a coded fibre optic system, in order to modulate the bit stream with the chip stream (the code sequence), it is necessary to logically „AND“ the bit stream with the much faster chip stream (see Figure 2.5). Another possibility is the triggering of the code generator with the bit sequence. Since in fibre optic DS CDMA, a „1“ is encoded into a code sequence and „0“ is not encoded (i.e. a code sequence consisting only of „0“s), the data generator can supply the code generator with the necessary triggering signal. The transmitter complexity can be simplified by the structure in Figure 2.6.

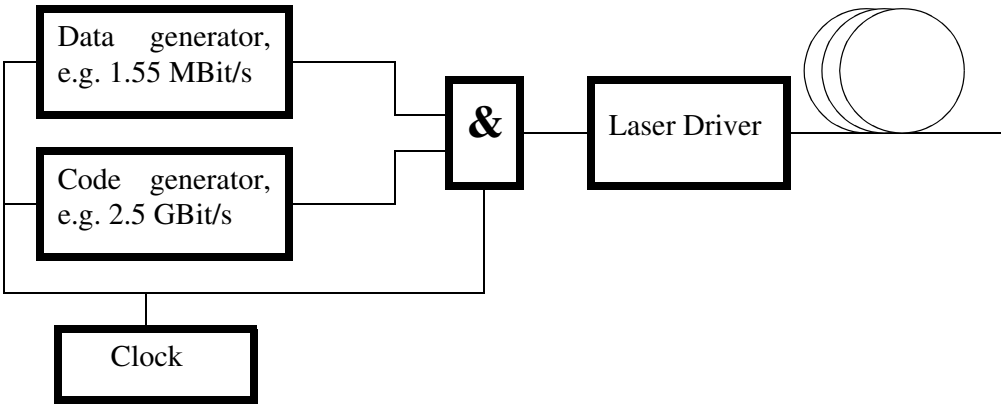

Figure 2.5: Block diagram of transmitter with electrical coding and common clock of data and code generator

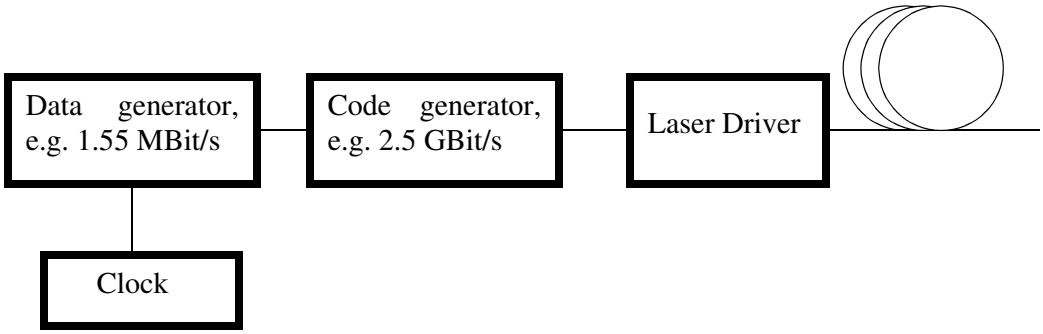

Figure 2.6: Block diagram of transmitter with electrical coding, triggering of code generator by data generator

Especially in high bit rate systems, electronic components that are capable of handling the high data rates severely increase system costs. Since with conventional codes, see section 2.3, code words reach lengths of 1000 and more, even originally low bit rate signals need very fast code generators. What makes the electrical coding attractive is its simple capability to switch to different codewords. By this, all users participating in the network can be addressed. This method of coding is thus to be preferred in a local area network scenario as described in section 2.1.1.

2.2.2 Code generation by optical signal processing

Instead of coding in the electrical domain, coding in the optical domain offers the advantage of the speed of optical processing. The data generator is directly connected to the laser driver,

which only needs to be capable of producing a low duty cycle, narrow pulse width bit stream, see Figure 2.7.

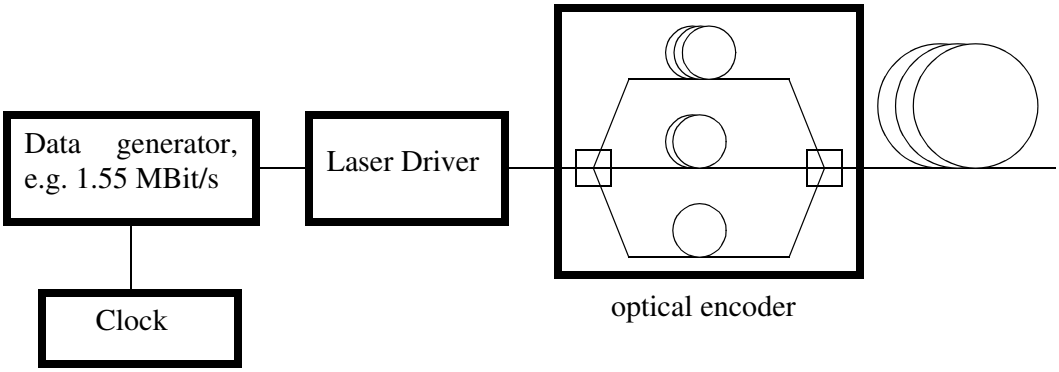

Figure 2.7: Block diagram of transmitter with optical coding

The laser source is followed by a fibre optic tapped delay line which is configured so that each arm of the encoder introduces the appropriate delay. By this, the encoder emits the desired code sequence. In high bit rate systems, the delay lines have lengths of only a few mm. Figure 2.8 shows a basic example.

The optical encoder thus emulates the multiplication function of the uncoded input signal with the code sequence. The input signal sequence $b(\mu)$ is split up into w equal parts[2] in the w arms of the encoder. No arm is necessary for the „0“s in the code sequence. After travelling through the different arms having different lengths, each of the w pulses has its own runtime delay. The pulses are then added up, forming the specific codesequence. The encoded signal $s(\mu)$ thus consists of

$$s(\mu) = \frac{1}{w} b(\mu - x_0 M_c) + \frac{1}{w} b(\mu - x_1 M_c) + \dots , \tag{2.11}$$

where x_i are the introduced delays in each arm and M_C is the duration of the data sequence $b(\mu)$. The sum on the righthandside of (2.11) has w terms.

Thus

$$\begin{aligned} s(\mu) &= \frac{1}{w} b(\mu) * (\delta(\mu - x_0 M_c) + \delta(\mu - x_1 M_c) + \dots) \\ &= \frac{1}{w} b(\mu) * \sum_{j=-\infty}^{\infty} a_j \delta(\mu - j M_c) \end{aligned} \tag{2.12}$$

[2] w corresponds to the weight of the code.

which is analogous to (2.3), if $M_c < M$ is assumed. $\delta(\mu)$ denotes Kronecker's delta and $h(\mu) = \frac{1}{w}\sum_{j=-\infty}^{\infty} a_j \delta(\mu - jM_c)$ the fibre tapped delay line's pulse response.

No fast switching „AND" gate or code generator is necessary for this transmitter structure. However, in order to change the code implied on a bit sequence, one would have to operate with add-drop multiplexers and a number of delay lines, each with different delays. This expenditure of components can not be bypassed. Therefore, the most interesting field of application of this kind of coding would be the high-bit rate point-to-point links and the robust transmission as they were described earlier. In these scenarios, each transmitter has a designated receiver to send the signal to and thus, the associated codes to each signal stay the same during the whole time of operation.

Recently, all-serial encoders, also called lattice-like encoders have been proposed [35] [82]. Their advantage is that they consist of serial 1/2 splitters, so that there is a high efficiency in the power budget of the encoding process. The number of splitters can be reduced to a coding process by tapped delay lines [35].

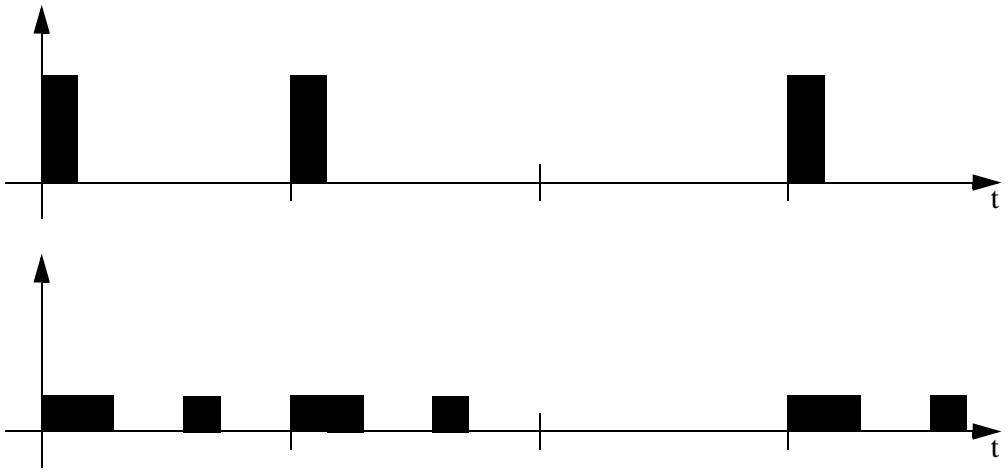

Figure 2.8: Low duty cycle bit stream (above) is coded into high chip rate code sequence (below) by splitting and introducing individual delays

However, this lattice structure of the encoder poses a strong limitation to the freedom of choice of the applied code words and has proven to offer disadvantages with respect to new codes that are proposed in Chapter 3.

2.2.3 Code detection

No matter what kind of coding structure is employed, the structure of the decoder is a fibre optic tapped delay line with its taps arranged in such a way, that it serves as a matched filter

to the appropriate transmitter code with $h(-\mu)$ (see section 2.2.2) as its pulse response. The optical decoder thus forms the convolution of the received signal $r(\mu)$ with $h(-\mu)$

$$\begin{aligned} \varphi(i) &= r(\mu) * h(-\mu + i) \\ &= r(\mu) \lozenge h(\mu - i) \end{aligned} \tag{2.13}$$

where $\lozenge$ denotes the correlation. If the coded signal arrives at the correct destination, the decoder thus forms the ACF of the codeword, otherwise a CCF.

Behind the matched filter, the optical signal falls onto a receiving diode, followed by a threshold detector, see Figure 2.9. Although avalanche photodiodes would offer a high power sensitivity, thus relaxing the link output power level, they cannot come to use in high bit rate links due to their relatively low rise time; this being the reason for the use of pin diodes in most high bit rate point-to-point links.

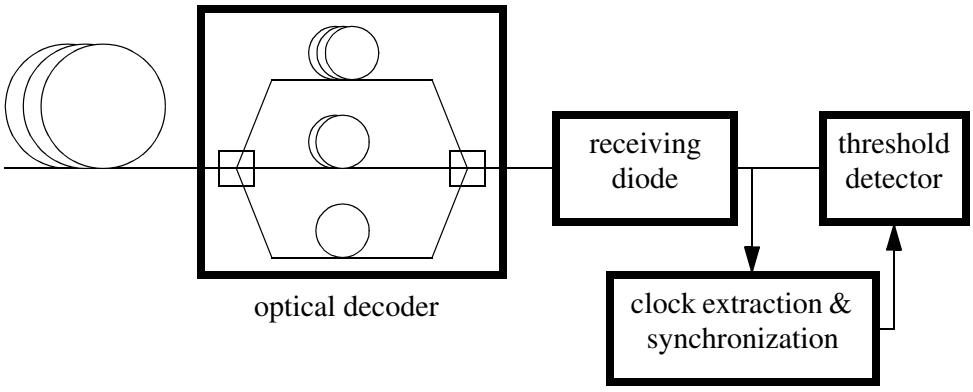

Figure 2.9: Block diagram of decoder and receiver with optical decoding

Synchronization is usually not necessary in CDM systems. If the codes presented in Chapter 3 are used, the synchronization block ensures proper sampling.

With a simple receiver structure like this, it is not possible to use a scheme similar to duobinary coding [3] [55], which modulates the phase of the optical carrier. Using an externally modulated DFB laser shifting the carrier's phase between π and $-\pi$, a decoding would only be possible, if all receivers include an MZ interferometer, emulating a synchronized replica of the specific code sequence. Alternatively, fibre tapped delay lines with an MZ interferometer adjusted to a π phase shift in about every 2nd arm of the delay lines (bipolar codes employ about an equivalent number of both amplitude values) many could be used for the signal reception. Since the aim of this work was a system structure that could be realized as simple as possible, duobinary coding has thus not been pursued further.

2.3 Current codes

The optical codes that were developed throughout the last years ([12] [35] [46] [61] [62] [63] [69]) have been entitled as conventional codes to distinguish between them and the newly developed ones as proposed in chapter 3. The following sections deal with the most important codes for (DS) fibre optic CDMA. Codes for a bipolar transmission have not been considered due to the necessary complex transmitter and receiver structure as explained earlier. Common to all codes is the ability to extract a user's code, also called signature sequence, in the presence of other users' signature sequences. A set of signature sequences for which any two signature sequences are easily distinguishable from a possibly time-shifted version of each other is needed. Strict orthogonality between different codewords would require $\rho_a = \rho_c = 0$, see (2.8) and (2.9). Due to the positive nature of an intensity-modulated, direct-detection system, this cannot be met. This is one of the starting points for the different code families in 2.3.1 to 2.3.4. All code families should fulfill the following points:

- Minimization of code word length F. The shorter the codeword, the lower the chip rate B_c, thus higher bitrates B_b can be coded before running into problems with electronic component speeds.
- Maximization of code weight w. w equals the peak value of the ACF. The higher this peak, the better the SNR.
- Minimization of ρ_a. The lower the value of ρ_a, the more resembles the ACF a clear and distinct peak. Important for easy tracking and synchronization.
- Minimization of ρ_c. The lower the value of ρ_c, the more users can simultaneously transmit, since the overall interference is limited by $K \cdot \rho_c$, K being the number of simultaneous users. Error-free detection is possible if $n \cdot \rho_c < w$.
- Maximization of code size $|C|$ being identical to the number of possible codewords N
- Maximization of possible simultaneous code words, which must not necessarily be equal to $|C|$.

Generally, these conditions cannnot be met at the same time and compromises have to be found. The conventional codes in sections 2.3.1 to 2.3.4 emphasize different requirements of those mentioned above.

2.3.1 Optical orthogonal codes

An optical orthogonal code (OOC) is characterized by the quadruple (F, w, ρ_a, ρ_c) with $\rho_a = \rho_c = 1$. All codewords of an (F, w, ρ_a, ρ_c) OOC have length F and weight (number of marks) w. An OOC can be constructed by using a variety of methods [12] such as iterative construction methods, the Greedy algorithm, algebraic coding theory, techniques with the help of projective geometry or set theory. By stipulating code word length F and code weight w, the appropriate OOC's are found by optimizing the relative delays between the chips within a codeword with respect to the other codewords [61]. It follows that for given F and w, a maximum of N possible OOC can be constructed with

$$N \leq \left\lfloor \frac{F-1}{w(w-1)} \right\rfloor, \tag{2.14}$$

where the brackets denote the integer portion of the real value. An upper bound on the BER can be found by assuming a chip synchronous overlap of the codewords (worst case). To derive the BER of OOC's, it is first necessary to determine the probability density function (pdf) of one mark in a codeword to overlap with a mark in another codeword.

Since there are $w \cdot w$ possibilities for the marks in the codewords to overlap and the probability of each individual overlap is $1/F$, the probability of an overlap is

$$p = \frac{w^2}{F}. \tag{2.15}$$

The pdf of the event of overlap k can then be derived as

$$p_k(k) = \left(1 - \frac{w^2}{F}\right)\delta(k) + \frac{w^2}{F}\delta(k-1), \tag{2.16}$$

δ being Dirac's delta distribution. Considering the on-off modulation of the bit sequence that has to be encoded, a random variable $u = \frac{1}{2}k$ can be defined, since the bit sequence contains marks and spaces with equal probability. It follows that

$$p_u(u) = \left(1 - \frac{w^2}{2F}\right)\delta(u) + \frac{w^2}{2F}\delta(u-1). \tag{2.17}$$

To derive the BER, it is now necessary to determine the pdf for the interference term in (2.6) and (2.7). One obtains

$$p_I(I) = \sum_{i=0}^{N-1} \binom{N-1}{i} \left(\frac{w^2}{2F}\right)^i \left(1 - \frac{w^2}{2F}\right)^{N-1-i} \delta(I-1) \quad . \qquad (2.18)$$

The exact BER follows from

$$BER = p(\varphi_{r,p_1} \geq Th \,|\, b_0=0) \cdot p(b_0=0) + p(\varphi_{r,p_1} < Th \,|\, b_0=1) \cdot p(b_0=1), \qquad (2.19)$$

Th being the signal threshold at the detector, $\varphi_{r,p_1}(i)$ has been defined in (2.6). Since $w \leq \varphi_{r,p_1}$ in the case of $b_0 = 1$ and $Th \leq w$, the second term of (2.19) is zero, see also Figure 2.4. The BER can thus be obtained by

$$BER = \frac{1}{2} \cdot \sum_{i=Th}^{N-1} \binom{N-1}{i} \left(\frac{w^2}{2F}\right)^i \left(1 - \frac{w^2}{2F}\right)^{N-1-i} \quad . \qquad (2.20)$$

(2.20) is the upper bound for the BER, since it assumes a chip synchronized transmission. Figure 2.10 shows the upper bounded BER for varying threshold Th and codeweight w.

As Figure 2.10 indicates, in order to achieve low a BER, long codeword lengths have to be employed. This is confirmed by Figure 2.11 and Figure 2.12. Figure 2.11 shows the upper bound BER for a code word length of $F = 1000$ and a code weight of $w = 7$.

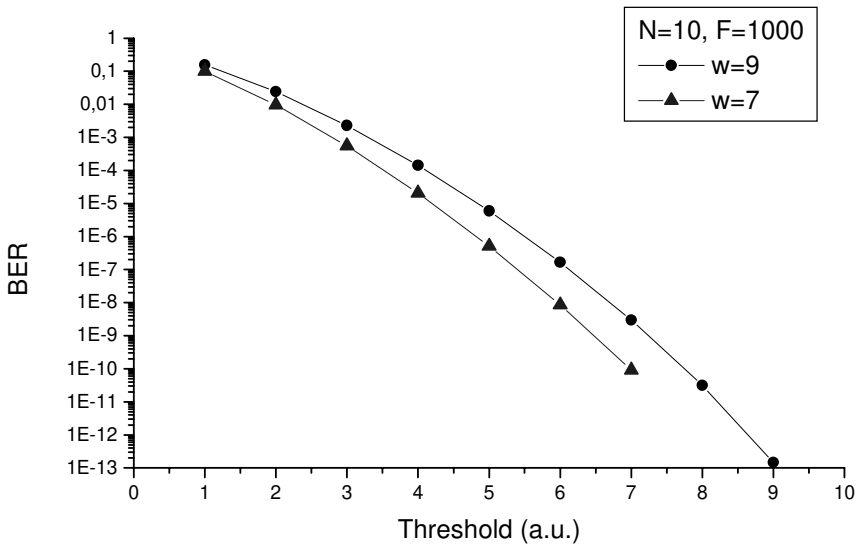

Figure 2.10: BER of OOC versus detector threshold with various codeweight

As a rough rule of thumb, a usual requirement for the BER has become the inverse of the bitrate, i.e. a BER of 10^{-6} can be tolerated at bitrates of 1 MBit/s and a BER of at least 10^{-9} or better in high bit rate systems with 10 GBit/s transmission rate. Employing a code word length of $F = 1000$, about 25 simultaneous users can be accommodated in a CDMA system with conventional OOC codes, having a bit rate of 1 MBit/s and thus a chip rate of 1 GBit/s. For a system with a bit rate of 10 GBit/s, only 10 simultaneous users could be accommodated. It must be noted, that the chip rate in this case is already as high as 10 TBit/s, and even higher, if more than 10 users need to transmit at the same time, see Figure 2.12. In spite of the fact, that most of the signal processing is performed in the optical domain, these high chip rates indicate that conventional OOC are only feasible for low bit rate applications, applications with a low number of simultaneous users or applications with a high number of simultaneous users at the expense of a high bit rate.

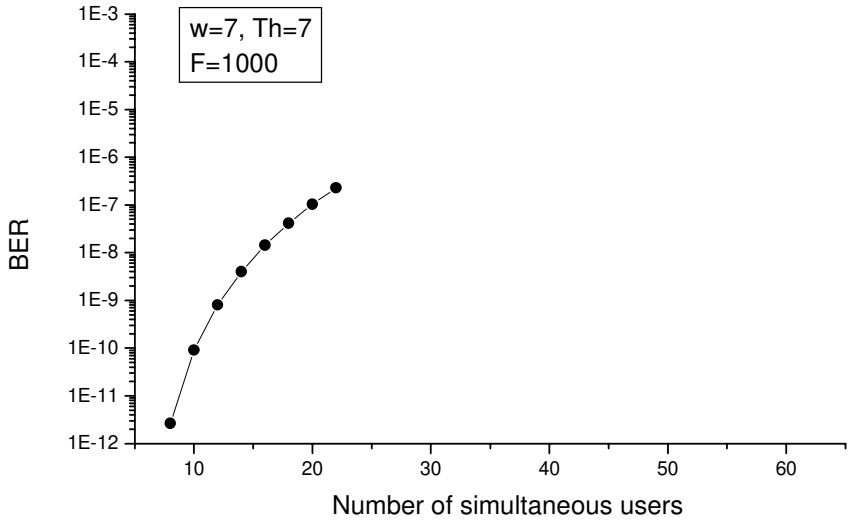

Figure 2.11: BER of OOC versus number of simultaneous users, code word length 1000

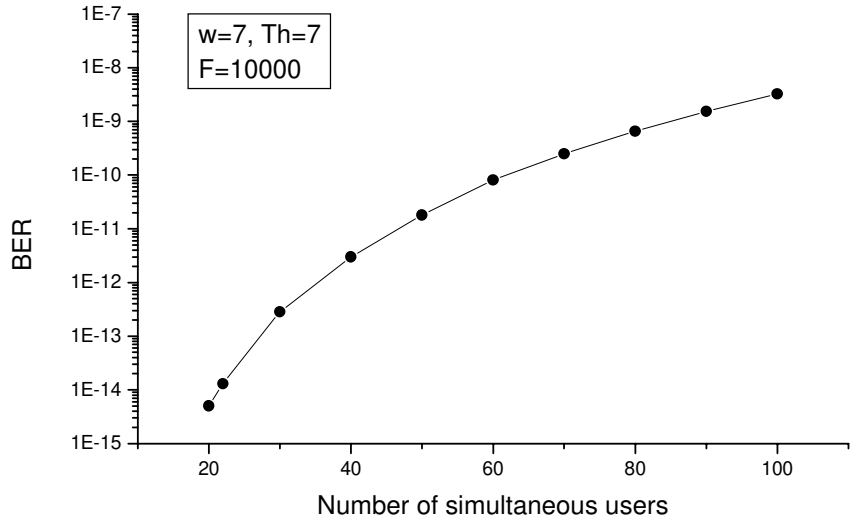

Figure 2.12: BER of OOC versus number of simultaneous users, code word length 10000

2.3.2 Prime sequence codes

Prime sequence (PS) codes can also be characterized by a quadruple (F, w, ρ_a, ρ_c) with $\rho_a = w - 1$ and $\rho_c = 2$. All codewords have the same weight w, where $w = P$, P being a prime number. The code word length equals F with $F = P^2$. PS code words are constructed by using the multiplication table of the elements of the Galois Field $GF(P)$ [63]. Codewords are divided into P time frames. By this, the distances between marks within a codeword are different for different sequences and every time frame contains only one mark. Each family of PS code words thus contains exactly

$$N = P \tag{2.21}$$

different codewords. The BER can be Gaussian approximated by using the central limit theorem and follows as [42]

$$BER = \Phi\left(\frac{-P}{\sqrt{1.16 \cdot (N-1)}}\right) \tag{2.22}$$

with N being the number of simultaneous users and $\Phi(x)$ is the unit normal cumulative distribution function

$$\Phi(x) = \frac{1}{\sqrt{2\pi}} \int_{-\infty}^{x} e^{-\frac{y^2}{2}} dy \ . \qquad (2.23)$$

The BER of PS codes is shown in Figure 2.13. It can be concluded, that PS codes offer less possible code words within a code family, but the BER for a given code word length and number of simultaneous users is some orders of magnitude lower compared to an equivalent OOC code. With a code word length of $N = 961$, a BER of 10^{-10} can be achieved with 22 simultaneous users, approx. Employing an OOC code with code length $N = 1000$ leads to a BER of 10^{-7} if 22 users transmit simultaneously. However, if a higher BER at the expense of increased user number can be tolerated, prime sequence codes are not advisable. If 50 simultaneous users are to be accommodated, PS codes must have a code word length of at least $51^2 = 2601$. An OOC code can offer this user number with a code length of only 1000. The BER then is in the order of 10^{-4} which can only be tolerated for certain applications. Furthermore, a disadvantage not to be underestimated is the poor ACF constraint $\rho_a \leq w - 1$ of PS codes, which renders those codes unfeasible for fully asynchronous systems.

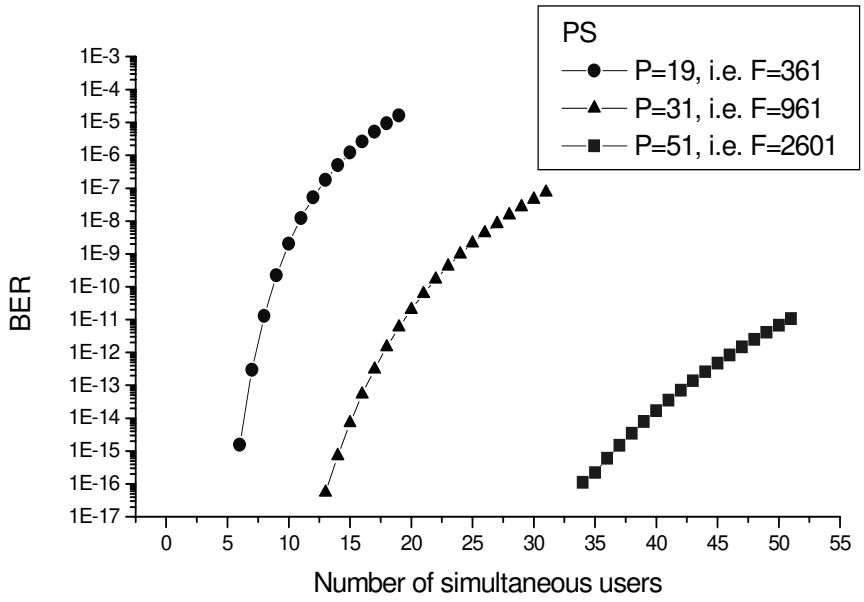

Figure 2.13: BER of PS codes versus number of simultaneous users with varying code length

2.3.3 Quadratic congruence codes

Quadratic congruence (QC) codes are developed with the help of the number theoretic con-

cept [46]. They can also be characterized by a quadruple (F, w, ρ_a, ρ_c), where $F = P^2$ denotes the code word length, $w = P$ the code weight, P being a prime number, the ACF constraint $\rho_a = 2$ and the CCF constraint $\rho_c = 2$. Similar to PS codes, there are exactly $N = P$ different code words within a code family for a specified prime number P. Superior to PS codes, their ACF constraint enables their use in fully asynchronous environments. Their ACF's are almost ideal in a sense of optical codes at the expense of having slightly increased number of coincidences, its impact on the BER can be seen in Figure 2.14.

The BER can, similar to the BER of PS codes, be computed by [46]

$$BER = \Phi\left(\frac{-P}{\sqrt{1.78 \cdot (N-1)}}\right), \tag{2.24}$$

with N being the number of simultaneous users and $\Phi(x)$ the unit normal cumulative distribution function. The most important advantage of QC codes lies in the much lower sidelobes of the ACF, so that tracking and synchronization to the transmitter is much easier due to the sharp peak in the ACF. The higher number of coincidences in the CCF ($\rho_c = 4$) leads to higher interference and a worse BER compared to PS codes ($\rho_c = 2$).

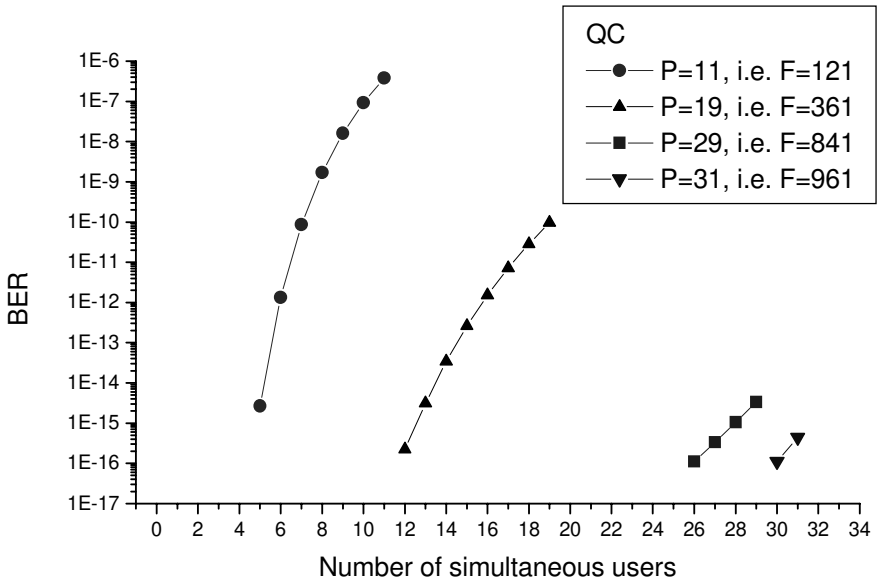

Figure 2.14: BER of quadratic congruence codes versus number of simultaneous users with varying code length

2.3.4 Two-dimensional codes

Separated from the other code classes are the so-called two-dimensional codes. In order to prevent lengthy codes and still keep the BER in a sensible range, these codes use both the temporal as well as the spatial or spectral domain, resp., to encode the information. Common to all two-dimensional codes is that the temporal length of underlying one-dimensional codes[3] is reduced by a factor R which at the same time equals the number of spatial or spectral channels. A two-dimensional code can then be characterized by the quintuple $(F_T, R, w, \rho_a, \rho_c)$, where the index T denotes the temporal length of the code. The advantage of possibly higher bit rates due to lower chip rates is taken at the expense of a more complex network structure. Figure 2.15 shows a typical structure for the use of two-dimensional fibre-optic code division multiple access. The disadvantage of a temporal/spatial network structure is the absolute stringent requirement of all optical paths between encoder and decoder to be equally long. Otherwise, code integrity can not be guaranteed, i.e. a proper decoding is impossible, since propagation time differences between different propagation paths lead to an unintended shift of single time slots into neighboring slots. However, unlike in the temporal case, codes can be constructed which show no sidelobes in the ACF, i.e. $\rho_a = 0$ and a CCF peak $\rho_c = 1$ [65].

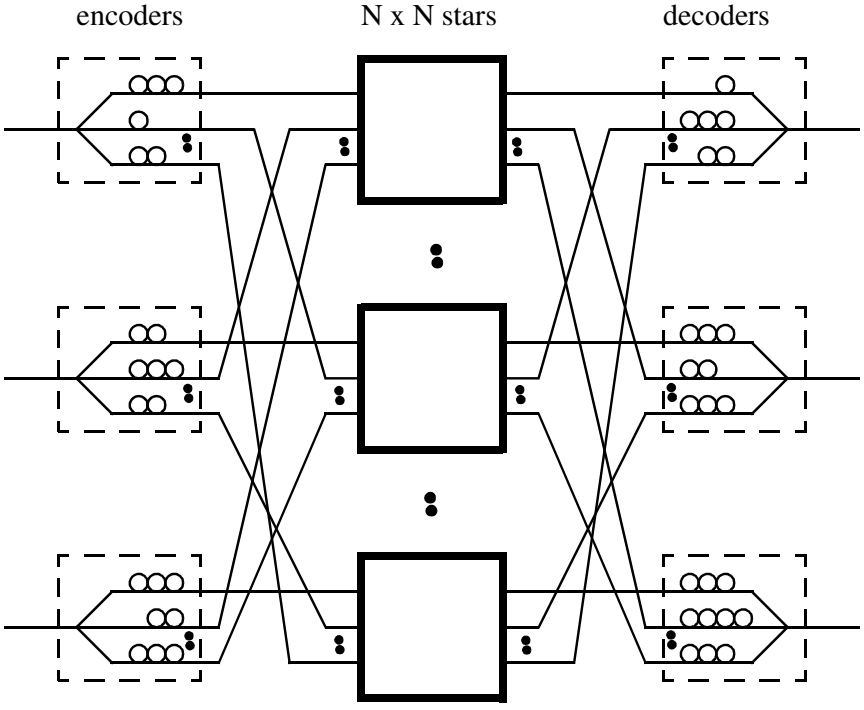

Figure 2.15: Schematic structure of two-dimensional fibre-optic CDMA network

[3] In fibre optic CDMA, two-dimensional codes are built starting from OOC [56].

The BER of these codes follows as [65]

$$\mathrm{BER} = \frac{1}{2} \cdot \sum_{i=\mathrm{Th}}^{N-1} \binom{N-1}{i} \left(\frac{R}{2F}\right)^{i} \left(1 - \frac{R}{2F}\right)^{N-1-i} \quad , \tag{2.25}$$

R being the number of spatial channels. The BER has been visualized in Figure 2.16. A comparison of (2.25) with (2.20) shows the close relationship between two-dimensional codes and optical orthogonal codes.

Though these codes seem very advantageous for use in fibre-optic CDMA systems, their main drawback remains the complex system architecture. If employing temporal/spatial codes, all propagation paths need to have the same length, not to speak of the numerous star couplers. Since this is never the case in existing networks, new fibres would have to be deployed, a measure which is unacceptable from an economic point of view. If temporal/spectral coding is used, as much as R different wavelength channels need to be employed in each encoder/transmitter pair, either by adjustable laser sources and optical filters or by broadband laser sources and fibre gratings, where the time frequency hopping pattern is determined by the order of the grating frequencies in the fibre [22]. Similar to the temporal/spatial coding, applying the temporal/spectral scheme to existing networks means a tremendous investment in system components which no network carrier would want to spend.

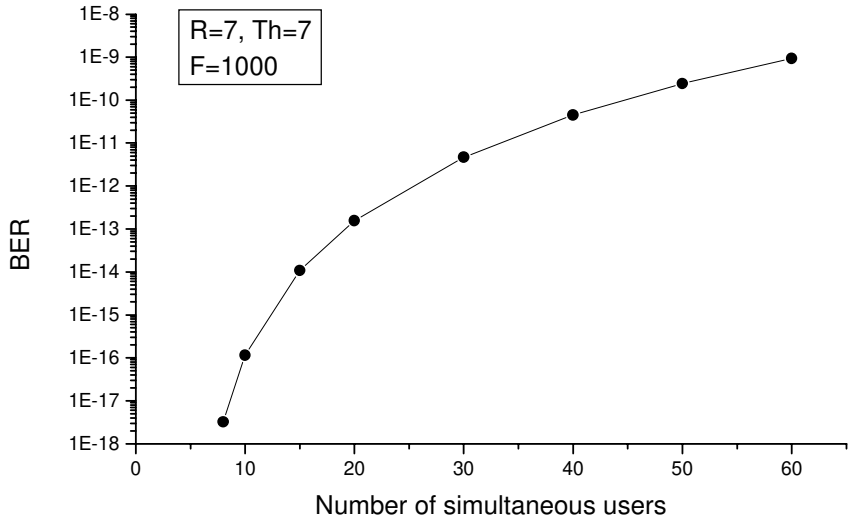

Figure 2.16: BER versus number of simultaneous users, temporal code word length: 1000, number of spatial channels: 7

Chapter 3

New codes for OCDMA and hybrid OCDMA/WDMA-techniques

This chapter deals with the development of new codes and their potential applications.

In order to bring OCDMA to an interesting multiplex alternative with adequate overall transmission capacity, it is necessary to develop powerful codes that exhibit low multiple access interference (MAI) and have short codeword lengths at the same time. Since, in a unipolar environment, low MAI can originally only be achieved by long codewords with few marks and many spaces, the codes known so far ([12] [35] [46] [61] [62] [63] [69]) are not feasible for the coded transmission of high bitrate signals.

Whereas the chiprate is mainly limited by the speed of electronic components, the net bit rate per channel is determined by the chip rate (the coded bit rate) divided by the code word length. In order to maximize the net bit rate, it is thus necessary to develop codes with short word lengths. The idea behind short code words is the use of various time-shifted versions of one distinct code word which corresponds to a necessary synchronization of the different (uncoded) input signals. Whereas CDMA originally is a purely asynchronous technique, a clear temporal fixing of the uncoded signals is inevitable to reduce code word lengths by this means. Since in existing WDM and DWDM transmission systems, the different wavelength channels are synchronized in any way due to monitoring reasons, this restriction is of no further concern.

Section 3.1 describes the generation of the newly developed codes. 3.2 covers the characteristics of this code family in terms of code size, i.e. the number of different code words within a family, number of simultaneous users, bit-error rate, etc. In 3.3, simulation results of these codes are presented, 3.4 finally deals with possible applications of these codes.

3.1 Code generation

Since it is the aim of this work to find appropriate codes for an OCDMA or a hybrid OCDM/DWDM transmission system with a system structure as simple and thus as cheap as possible, it is necessary to comply with certain conditions. The numbers of necessary transmitter and receiver components is to be kept as low as possible and they should be of-the-shelf products. The same holds for the transmission fibers. Since a hybrid OCDM/ DWDM system should be installed as an upgrade of existing DWDM systems, it is necessary to use the same, already deployed fiber links but still show improved system performance. Altogether, by choosing the system to be proposed, the overall system costs, including components and maintenance, related to the system capacity and reliability can significantly be lowered.

The claim for a system structure as easy as possible is inherently combined with an incoherent reception of the transmitted signals, as taking advantage of a cohererent transmission would demand the use of highly cohererent laser sources [40]. For similar reasons, a spectral or phase coding of the input signals has not come into account. Both methods would require costly laser sources, modulators and detectors [14] [22] [28].

The transmission format widely spread is the intensity modulation, direct detection format (IM-DD). It makes use of on-off-keying (OOK) which means that a „1“ (mark) is transmitted with full power (set to an appropriate value depending on the fiber link), a „0“ (space) is transmitted by emitting no power. In the DS (direct sequence)-CDMA environment, this kind of transmission is maintained and developed further, i.e. if a mark is to be transmitted, a whole code sequence emits from the laser diode, in case of a space, nothing is transmitted, see Figure 3.1. All relevant DS coding schemes in fibre optics make use of this coding principle.

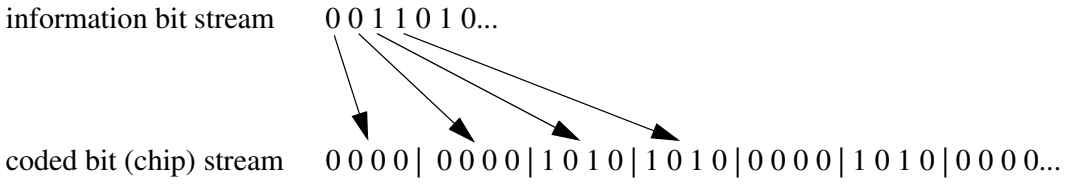

Figure 3.1: Principle of encoding a bit stream in DS-CDMA

Figure 3.1 also shows one of the major tasks in finding suitable codes for a coded transmission: by coding the incoming information bit stream, the necessary bandwidth is multiplied by a factor that equals the length of the code sequence (4 in Figure 3.1). So, the necessary demands for codes that could be used in incoherent OOK OCDMA can be defined as follows.

(1) The length F of the code sequences within a code family has to be equal and must be minimized.

(2) For reasons of easy implementation in existing systems, the length F of a code sequence needs to be a power of 2.

(3) All code sequences within a code family must contain the same number of marks, so that the ACFs show the same peak value.

$$\varphi_{a_j,\,a_j}(0) = \sum_{\mu=0}^{F-1} a_j(\mu)a_j(\mu) = \text{const} \qquad \text{for all } j \tag{3.1}$$

This is necessary due to the threshold device at the receiver, since the threshold value is - for ease of receiver structure - to remain constant, regardless of which code sequence has been transmitted.

(4) All code sequences within a code family have to be orthogonal to each other under the assumption of synchronization, i.e. certain thresholds (see also (7)) have to be met at the sampling instant. Since orthogonality in a strict sense

$$\varphi_{a_i,\,a_j}(0) = \sum_{\mu=0}^{F-1} a_i(\mu)a_j(\mu) = 0,\ i \neq j \tag{3.2}$$

cannot be complied in a unipolar environment, only wide-sense orthogonality is required:

$$\varphi_{a_j,\,a_j}(\nu) = \sum_{\mu=0}^{F-1} a_j(\mu)a_j(\mu+\nu) \leq \rho_a = 1,\ \nu \neq 0 \tag{3.3}$$

$$\varphi_{a_i,\,a_j}(\nu) = \sum_{\mu=0}^{F-1} a_i(\mu)a_j(\mu+\nu) \leq \rho_c = 1,\ \nu \neq 0 \tag{3.4}$$

ρ_a and ρ_c have been chosen to the value of 1, in order to ensure the lowest possible MAI (see also (7)).

(5) The number of orthogonal code sequences $|C|$ within one family is to be maximized.

(6) The number of orthogonal code sequences $|\Omega|$ that can be used simultaneously without producing bit errors is to be maximized. Together with (1), this leads to the demand for the minimization of the „weighted“ processing gain

$$\gamma = F/|\Omega| . \tag{3.5}$$

(7) Due to the positive nature of the transmission system, the MAI is to be minimized through the prevention or the minimization of superposition of marks in the CCF.

(8) If the codes are to be used in a hybrid OCDM/WDM system, additional bit errors must not be introduced through the coding, since using an additional coded multiple access scheme represents an upgrade of the original WDM scheme. This leads to the demand, that the summation of the MAI of all users at the sampling instant must remain below the peak of the ACF of the code sequences.

$$\sum_{\mu=0}^{F-1} \sum_{n=2}^{N} p_1(\mu) \cdot p_n(\mu) < \sum_{\mu=0}^{F-1} p_1(\mu) \cdot p_1(\mu), \tag{3.6}$$

see also equation (2.6).

(9) With respect to the high (information) data rates of 10 GBit/s, the overall bit error rate has to remain below 10^{-9}.

The codes that are developed below are based on the optical orthogonal codes (OOC) as proposed by Chung, Salehi and Wei in [12]. Similar to them, the new codes will be characterized by the tuple (F, w). Since $\rho_a \equiv 1$ and $\rho_c \equiv 1$ for all new codes, ρ_a and ρ_c have been omitted in the tuple.

As starting point for the search for the codes that come into question serves the accelerated „greedy“ algorithm which is described in [12]. The greedy algorithm is altered and adapted to the specific needs, so that the requirements mentioned in (1)-(9) can be fulfilled. Input parameters to the algorithm are the code length F and the code weight w. The modified greedy algorithm originally starts with an empty code. In an outer loop, a new codeword is attempted to include in the code in each iteration; in the inner loop, a new mark is tried to be included in the codeword that is actually formed until all w marks are included. The inner

loop stops if the codeword at hand cannot be included due to the autocorrelation or the cross-correlation boundaries (3.3) and (3.4). Due to (8), the outer loop stops if $w-1$ codewords are included in the code. These $w-1$ codewords could be used in an asynchronous environment without causing bit errors. In order to increase the number of allowable simultaneous users, new codewords are subjoined to the code by adding temporally shifted codewords from the $w-1$ codewords found above. By choosing an appropriate set of code sequences from all possible time-shifted versions which minimize the cross-correlation peak at the expected position of the autocorrelation peak, i.e. the sampling instant, the number of different code sequences as well as the number of simultaneous users can greatly be enhanced. It turns out, that beyond the $w-1$ possible simultaneous users, a system using these so-called „modified optical orthogonal codes“ (with respect to the optical orthogonal codes from [12]) can accommodate up to $\frac{F}{2(w-1)}$ simultaneous users without leading to bit errors. With these new code sequences, the cross-correlation peak between two time-shifted versions of a code sequence can be as high as the autocorrelation peak, but always occurs delayed from the autocorrelation peak. By synchronizing the receiver to the expected position of the autocorrelation peak for the code sequence under consideration, the autocorrelation peak can easily be distinguished from adjacent cross-correlation peaks.

The algorithm for the generation of the code sequences that are designated as „modified optical orthogonal codes“ (MOOC) is generally described with the help of a flowchart, see Figure 3.2 and Figure 3.3. As an example, the development of a $(F = 16, w = 3)$ MOOC is performed. Please refer to Figure 3.2 and Figure 3.3 for connotations.

- As input parameters serve the code length $F = 16$ and the code weight $w = 3$, in the case of $F = 16$, $\Gamma = \{0, 1, 2, 3, 4, 5, 6, 7, 8, 9, 10, 11, 12, 13, 14, 15\}$.
- Randomly allotted $w-1$ positions of marks are 0 and 1, i.e. $\Lambda_1 = \{0, 1\}$. In order to demonstrate the algorithm in a quick and clear way, the random choices of positions of marks have been chosen such that the algorithm leads to the MOOC codewords straightly.
- Calculate x: $x = 0$, $x = 1$, $x = 2$, $x = 15 \rightarrow \Delta = \{0, 1, 2, 15\}$, i.e. $\bar{\Delta} \cap \Gamma = \{3, 4, 5, 6, 7, 8, 9, 10, 11, 12, 13, 14\}$
- Choose $7 \in \{\bar{\Delta} \cap \Gamma\}$ and add this element to Λ_1: $\Lambda_1 = \{0, 1, 7\}$. First codeword completed: $a_1(\mu) = \delta(\mu) + \delta(\mu - 1) + \delta(\mu - 7)$

- Clear Δ: $\Delta = \varnothing$. Allocate w-1 marks on w-1 positions of next codeword. This loop finally creates $\Lambda_2 = \{2, 4\}$.
- Calculate x with a, b and c from Λ_2: $x = 0$, $x = 2$, $x = 4$, $x = 6$
  $\rightarrow \Delta = \{0, 2, 4, 6\}$
- Calculate x with a from Λ_2, b and c from Λ_1: $x = 1$, $x = 3$, $x = 5$, $x = 8$, $x = 9$, $x = 10$, $x = 11$, $x = 12$, $x = 13$, $x = 14$.
  $\rightarrow \Delta = \{0, 1, 2, 3, 4, 5, 6, 8, 9, 10, 11, 12, 13, 14\}$, i.e.
  $\bar{\Delta} \cap \Gamma = \{7, 15\}$
- Choose $7 \in \bar{\Delta} \cap \Gamma$ and add this element to Λ_2: $\Lambda_2 = \{2, 4, 7\}$. Second codeword completed: $a_2(\mu) = \delta(\mu - 2) + \delta(\mu - 4) + \delta(\mu - 7)$.
- $w - 1 = 2$ OOC codewords found, start search for MOOC codewords (Figure 3.3)
- Start with first OOC codeword: $j = 1$
- Starting with $a_{1,0}(\mu) = a_1(\mu)$, $a_{1,4}(\mu) = a_{1,0}(\mu - 4)$, $a_{1,8}(\mu) = a_{1,0}(\mu - 8)$ and $a_{1,12}(\mu) = a_{1,0}(\mu - 12)$ fulfill the shift constraint
- Search for time-shifted versions of 2nd OOC codeword: $j = 2$
- $a_{2,0}(\mu)$, $a_{2,4}(\mu)$, $a_{2,8}(\mu)$, $a_{2,12}(\mu)$ fulfill the shift constraint.
- No more than $\frac{F}{2(w-1)} = 4$ time-shifted versions per OOC codeword can be found.
- Overall, the algorithm delivers in this special case 8 codewords ($a_{1,i}(\mu)$, $a_{2,i}(\mu)$, $i = 0, 4, 8, 12$) that can be used in a sychronized CDMA application without leading to bit errors. It must be noted that the equidistance between the shifted versions of codewords is purely coincidental.

The found codewords in this example are shown in Table 3.1.

In the case of short code lengths F as in the example, the greedy algorithm yields only few orthogonal codewords (two in the above example). Surely, if this number is less than the code weight w, no bit errors can occur due to the crosscorrelation constraint. However, with increasing code length F, it is possible to form more than w-1 codewords. In this case, bit errors solely due to the coding are inevitable. Analog to the example above, the modified greedy algorithm then also yields MOOC words for the use in a sychronized environment. The bit error performance and more properties of the MOOC codes are discussed in section

3.2.

OOC codeword j	Sequence	MOOC sequences
1	$a_{1,0}$	1100 0001 0000 0000
	$a_{1,4}$	0000 1100 0001 0000
	$a_{1,8}$	0000 0000 1100 0001
	$a_{1,12}$	0001 0000 0000 1100
2	$a_{2,0}$	0010 1001 0000 0000
	$a_{2,4}$	0000 0010 1001 0000
	$a_{2,8}$	0000 0000 0010 1001
	$a_{2,12}$	1001 0000 0000 0010

Table 3.1: Overview of MOOC sequences for (F=16,w=3)

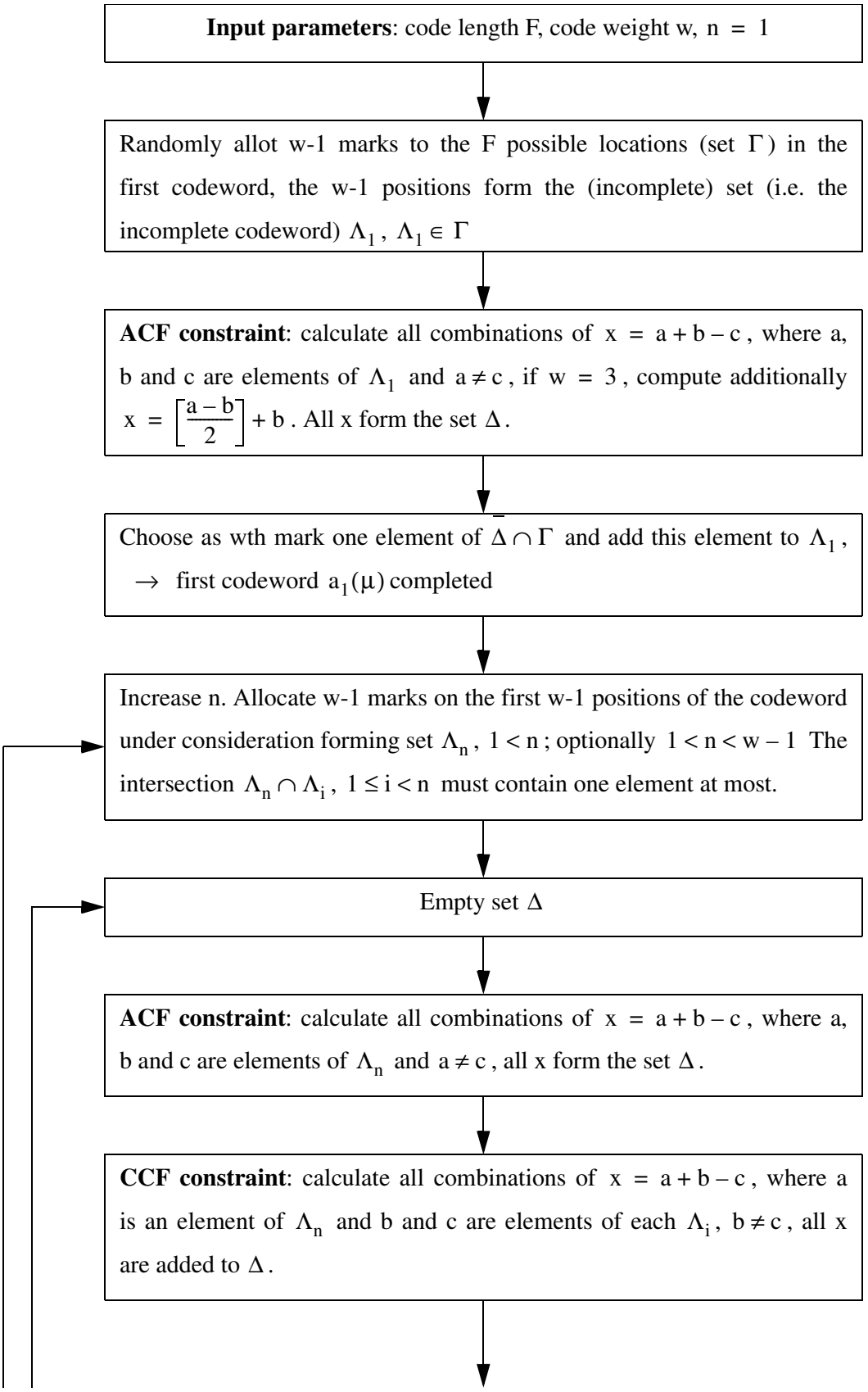
Input parameters: code length F, code weight w, $n = 1$
Randomly allot w-1 marks to the F possible locations (set Γ) in the first codeword, the w-1 positions form the (incomplete) set (i.e. the incomplete codeword) Λ_1, $\Lambda_1 \in \Gamma$
ACF constraint: calculate all combinations of $x = a + b - c$, where a, b and c are elements of Λ_1 and $a \neq c$, if $w = 3$, compute additionally $x = \left[\frac{a-b}{2}\right] + b$. All x form the set Δ.
Choose as wth mark one element of $\Delta \cap \Gamma$ and add this element to Λ_1,
$\rightarrow$ first codeword $a_1(\mu)$ completed
Increase n. Allocate w-1 marks on the first w-1 positions of the codeword under consideration forming set Λ_n, $1 < n$; optionally $1 < n < w - 1$ The intersection $\Lambda_n \cap \Lambda_i$, $1 \leq i < n$ must contain one element at most.
Empty set Δ
ACF constraint: calculate all combinations of $x = a + b - c$, where a, b and c are elements of Λ_n and $a \neq c$, all x form the set Δ.
CCF constraint: calculate all combinations of $x = a + b - c$, where a is an element of Λ_n and b and c are elements of each Λ_i, $b \neq c$, all x are added to Δ.

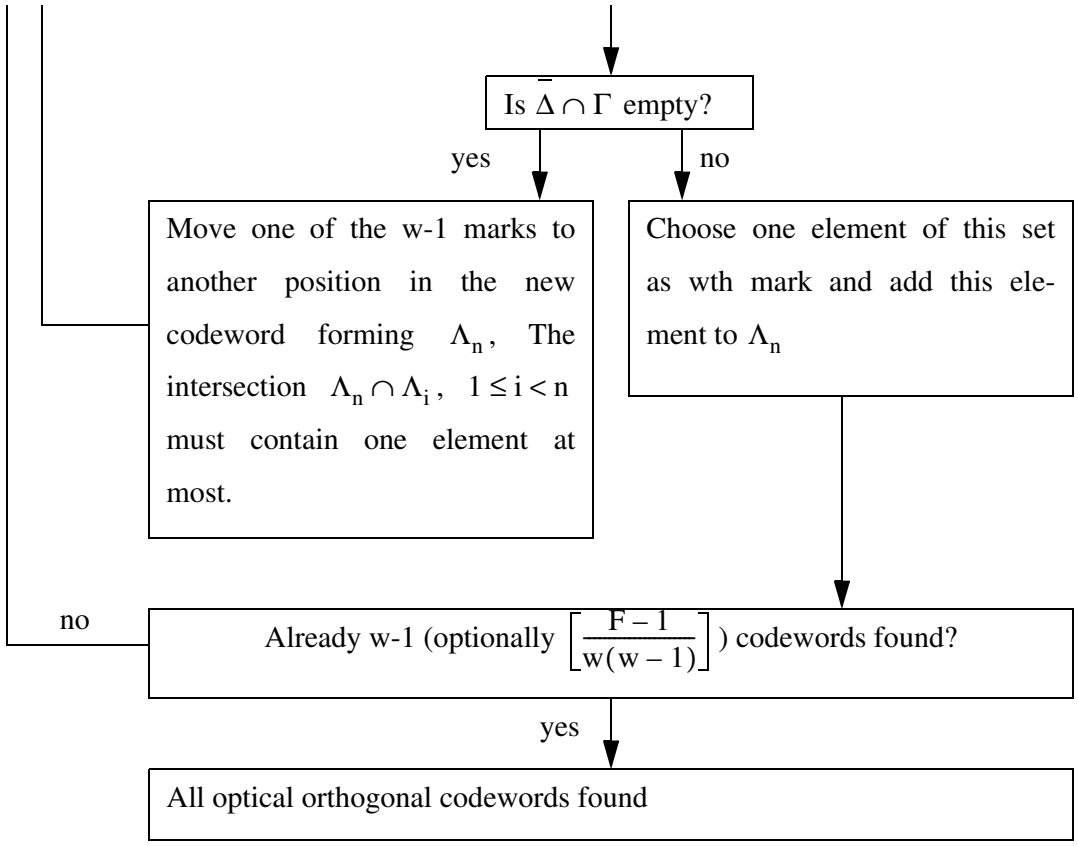

Figure 3.2: Flowchart I, describing the algorithmic search for an OOC word family

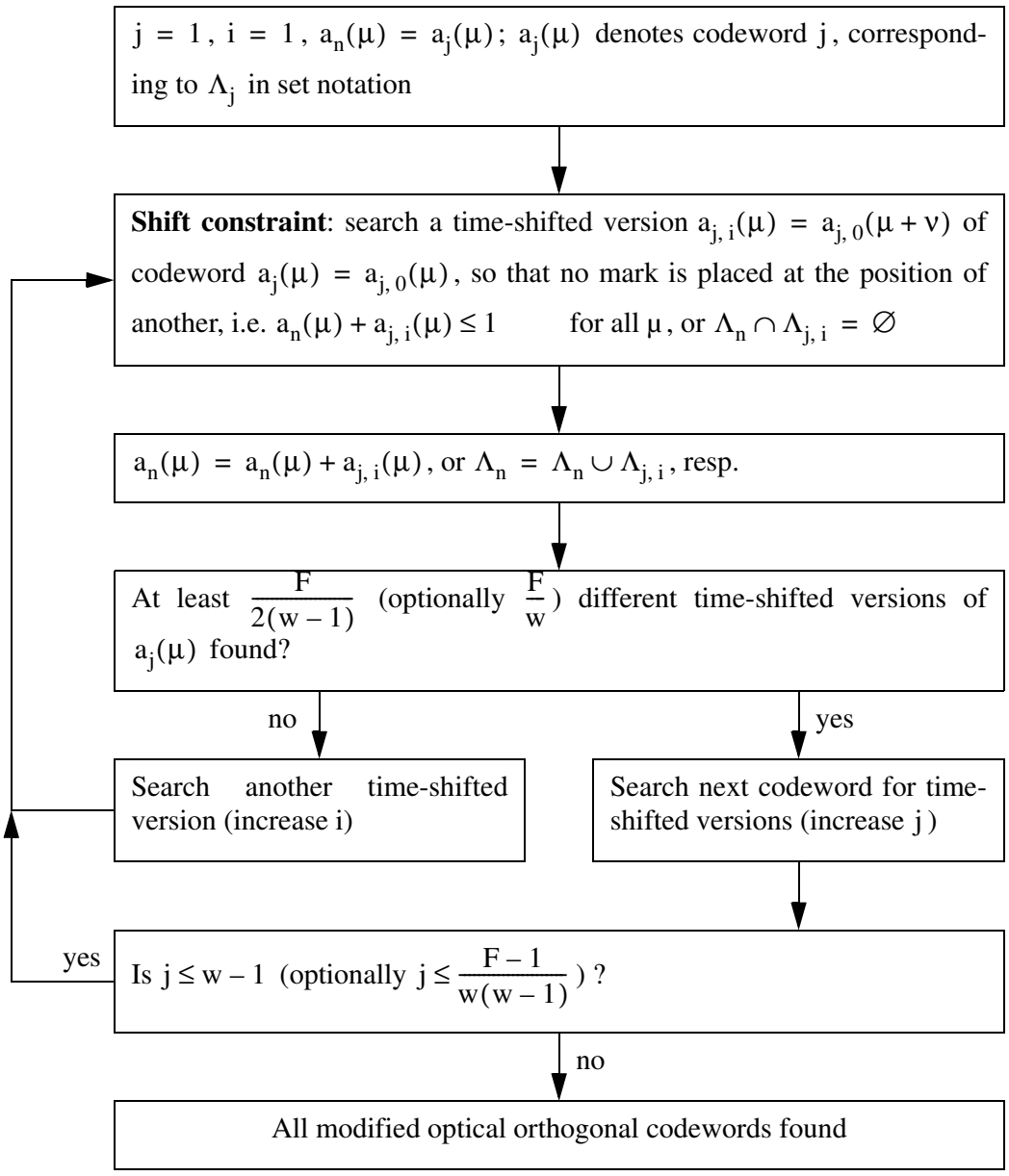

Figure 3.3: Flowchart II, describing the algorithmic search for MOOC words based on an OOC family

3.2 Code properties

3.2.1 Correlation constraints

As has been stated before, a typical characteristic of optical orthogonal codes is their strong autocorrelation and crosscorrelation constraint:

$$\varphi_{p_j,\,p_j}(\nu) = \sum_{\mu=0}^{F-1} a_j(\mu)a_j(\mu+\nu) \le \rho_a = 1 \qquad \text{for } 1 \le \nu \le F-1 \tag{3.7}$$

$$\varphi_{p_j,\,p_k}(\nu) = \sum_{\mu=0}^{F-1} a_j(\mu)a_k(\mu+\nu) \le \rho_c = 1 \qquad \text{for } 0 \le \nu \le F-1,\ j \ne k \tag{3.8}$$

Whereas (3.7) ensures easy synchronization and temporal locking to a certain signal by shaping a sharp peak in the ACF, (3.8) is necessary for low interference terms of simultaneous users. Since OOC form the basis for the MOOC words, (3.7) and (3.8) can slightly be altered and hold for MOOC. The autocorrelation constraint then yields

$$\varphi_{p_{j,i},\,p_{j,i}}(\nu) = \sum_{\mu=0}^{F-1} a_{j,i}(\mu)a_{j,i}(\mu+\nu) \le \rho_a = 1 \qquad \text{for } 1 \le \nu \le F-1\,. \tag{3.9}$$

The crosscorrelation constraint can now be separated into

$$\varphi_{p_{j,i},\,p_{k,h}}(\nu) = \sum_{\mu=0}^{F-1} a_{j,i}(\mu)a_{k,h}(\mu+\nu) \le \rho_c = 1 \qquad \text{for } 0 \le \nu \le F-1,\ j \ne k \tag{3.10}$$

and

$$\varphi_{p_{j,i},\,p_{j,h}}(\nu) = \sum_{\mu=0}^{F-1} a_{j,i}(\mu)a_{j,h}(\mu+\nu) \le \rho_c^* \qquad \text{for } 0 \le \nu \le F-1,\ i \ne h\,, \tag{3.11}$$

where $\rho_c^* = w$.

First index in (3.10) and (3.11) denotes the underlying optical orthogonal codeword, second index denotes the time shift of the modified codeword with respect to its underlying OOC, see Figure 3.3 and Table 3.1.

Since MOOC are only suitable and specifically designed for the use in a synchronized scheme, arbitrary temporal shifts between codewords based on one optical orthogonal codeword do not occur during transmission. (3.11) thus yields

$$\varphi_{p_{j,i},\,p_{j,h}}(0) = \sum_{\mu=0}^{F-1} a_{j,i}(\mu)\,a_{j,h}(\mu) = 0 \qquad \text{for } i \neq h\,. \tag{3.12}$$

To give an example of how these correlation constraints manifest, autocorrelation and crosscorrelation functions of typical MOOC words are shown in the following figures. The codewords of the (16,3) code are the same as presented in Table 3.1.

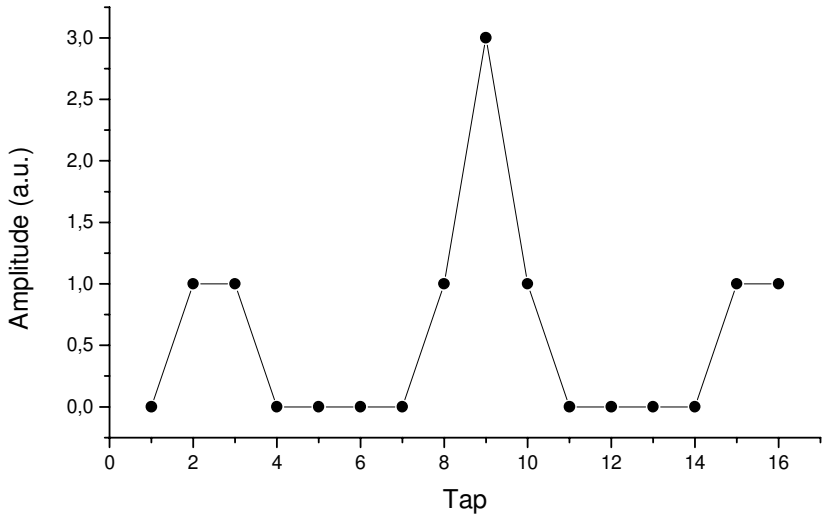

Figure 3.4: Autocorrelation function $\varphi_{p_{1,0}p_{1,0}}$ of code sequence $a_{1,0}$

Figure 3.4 and Figure 3.5 show typical autocorrelation functions of modified optical orthogonal codewords or their underlying optical orthogonal codewords, resp.

Due to the codeweight of $w = 3$, the maximum peak of the ACF equals this value. The secondary maxima of all ACFs are bounded by 1 due to (3.9). Because of the positive nature of the transmission scheme, i.e. all codewords consist of logical *and* physical „1“s and „0“s (i.e. they are unipolar), it is not possible to lower the correlation sidelobes below the value of 1. By prolonging the code length F or reducing the codeweight w, it is possible to decrease the ratio of correlation sidelobes to code length, a state that one would try to reach, since this ratio impacts on the interference term that finally leads to bit errors. However, reducing the codeweight is inherently connected with a reduction of the maximum peak of the ACF, so that it is easier for the interference to reach that very same level. Furthermore, prolonging the code length is not always advisable, since the information data rate is fixed and an increased

code length means higher chip rates and thus higher demands for all implicated components.

As a matter of course, the autocorrelation functions of $a_{j,i}$ code sequences are identical to those of the $a_{j,0}$ words.

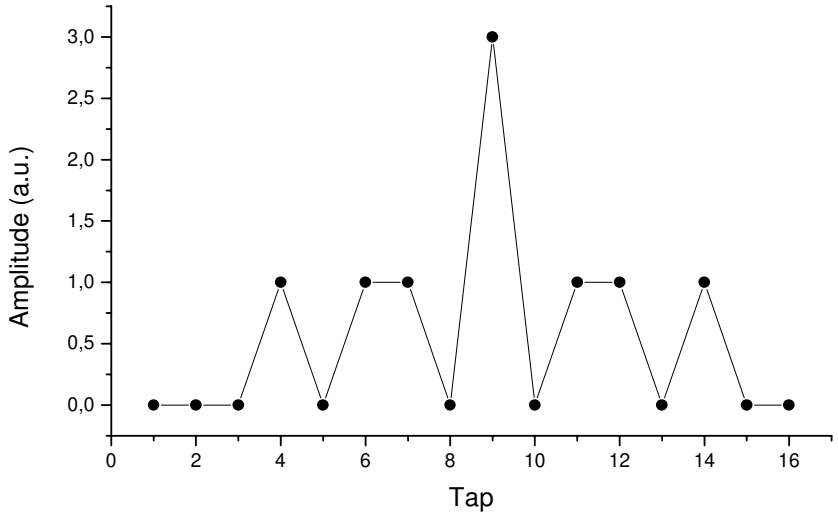

Figure 3.5: Autocorrelation function $\varphi_{p_{2,0}p_{2,0}}$ of code sequence $a_{2,0}$

Following (3.10), the crosscorrelation $\varphi_{p_{j,0}p_{k,0}}$ (i.e. the CCF of two optical orthogonal codewords) is bounded by 1 (see Figure 3.6). By this, a clear distinction between desired (reception of ACF) and undesired user (reception of CCF) can be made simply through the usage of a threshold detector. The value of the threshold detector would best be set equal to 2.5 (compare to Figure 3.9).

Different to that, the crosscorrelation $\varphi_{p_{j,i}p_{j,h}}$ of two code sequences that have the same underlying optical orthogonal codeword resembles the ACF of an OOC with an additional time shift (see Figure 3.7). Figure 3.7 corresponds to a received signal, where the user with the code $a_{1,4}$ transmitted a data „1“ and the receiver of the user with code $a_{1,0}$ correlates this signal.

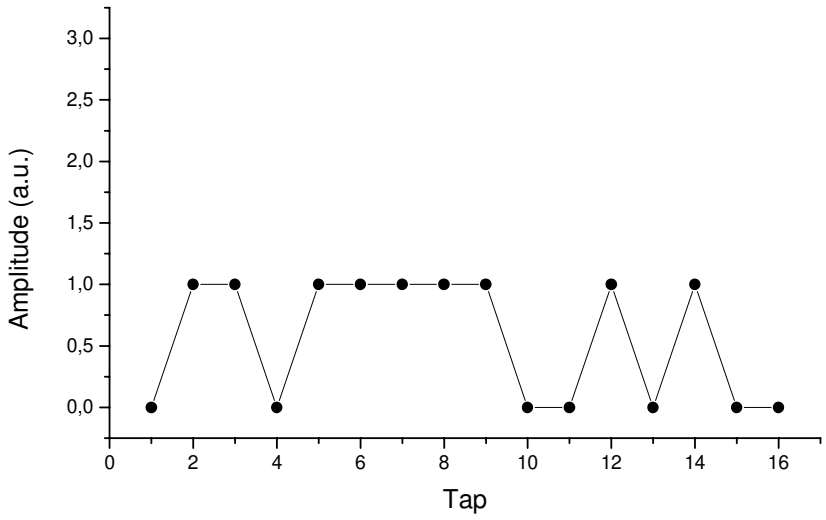

Figure 3.6: Crosscorrelation function $\varphi_{p_{1,0}p_{2,0}}$ of code sequences $a_{1,0}$ and $a_{2,0}$

A distinction between $\varphi_{p_{j,i}p_{j,h}}$ and $\varphi_{p_{j,i}p_{j,i}}$ can no longer be made simply by using a threshold device, but it is necessary to sample the incoming temporal regime of the correlation function at the right moment, here, as in all figures of this chapter, at tap no. 9, the exact centre of the time frame. The condition for this scheme is the synchronization of the transmitters to each other. In the case of missynchronization or a complete lack of synchronization, the peak of the CCF in Figure 3.7 might slip into the time slot of tap no. 9, indicating a transmitted data „1“ of the user who uses code sequence $a_{1,0}$, thus leading to a bit error.

In order to further illustrate the characteristics of the ACF and CCF, Figure 3.8 shows the crosscorrelation $\varphi_{(p_{1,0}+p_{2,0})p_{1,0}}$ of the code sequences $(a_{1,0}+a_{2,0})$ and $a_{2,0}$, the signal one would receive if both transmitters (the one coded with $a_{1,0}$, the other with $a_{2,0}$) send a data bit „1“ and the receiver listens to code $a_{1,0}$ (i.e. its detector correlates the incoming signal with $a_{1,0}$). Since the threshold is set to a value of 2.5, the incoming signal is detected as a transmitted „1“ despite the isochronous transmission of a data „1“ of another transmitter. Figure 3.9 depicts the same situation, if the two applied code sequences originate from the same underlying optical orthogonal code sequence. It can clearly be seen that in this case, a time-adjusted sampling is necessary in order to avoid bit errors. By this, the peak of the ACF and the peak of the CCF of two MOOC using the same underlying codeword arrive at different times at the receiver and can clearly be distinguished.

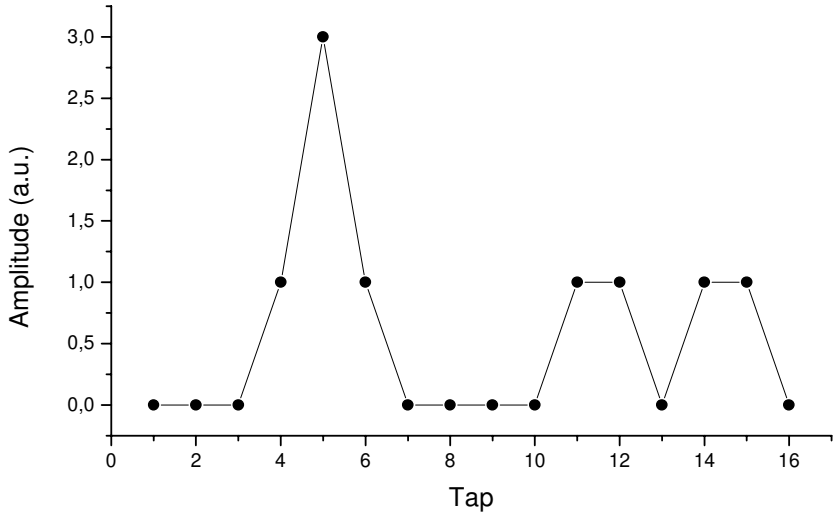

Figure 3.7: Crosscorrelation function $\varphi_{p_{1,0}p_{1,4}}$ of code sequences $a_{1,0}$ and $a_{1,4}$

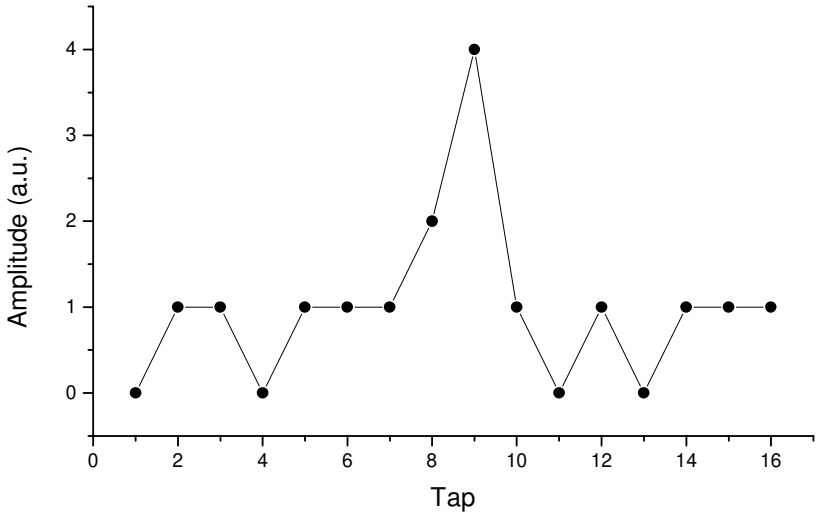

Figure 3.8: Crosscorrelation function $\varphi_{(p_{1,0}+p_{2,0})p_{1,0}}$ of code sequences ($a_{1,0}$+$a_{2,0}$) and $a_{1,0}$

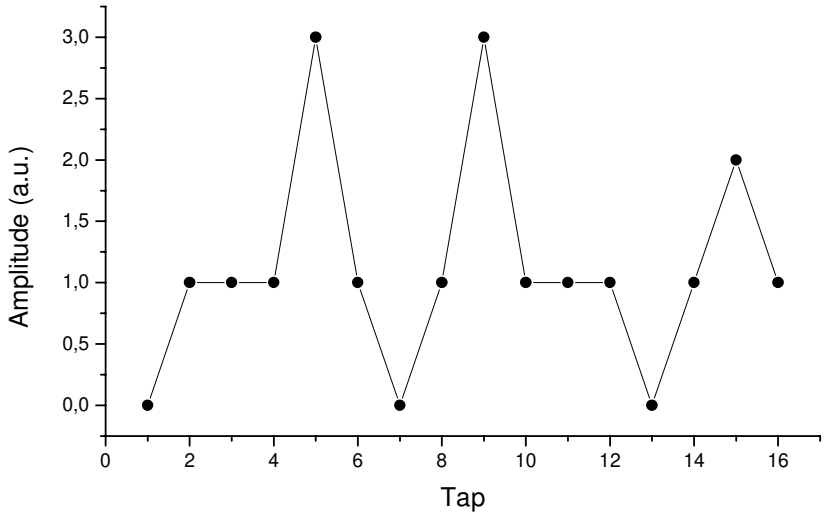

Figure 3.9: Crosscorrelation function $\varphi_{(p_{1,0}+p_{1,4})p_{1,0}}$ of code sequences ($a_{1,0}$+$a_{1,4}$) and $a_{1,0}$

3.2.2 Size

Since MOOCs are based on OOCs, the size of an OOC is developed first. From that on, the size of an MOOC is obtained. Both lower and upper bounds will be presented.

The interpretation of the elements of set Λ_i (see Figure 3.2) as marks in a codeword can - without loss of generality - be changed to an interpretation as differences $x - x'$ between any two marks (x, x'), $x, x' \in \Lambda_i$, $x \neq x'$ in the codeword, see [12], [61]. In a code with $\rho_a = \rho_c = 1$, there are no repeated differences (otherwise, two or more marks of different code words would be placed at the same distance leading to a cross correlation peak of 2 or more). Thus, in a code with w marks, each of the w marks has $w - 1$ different distances to other marks in the same codeword, see an example in Figure 3.10.

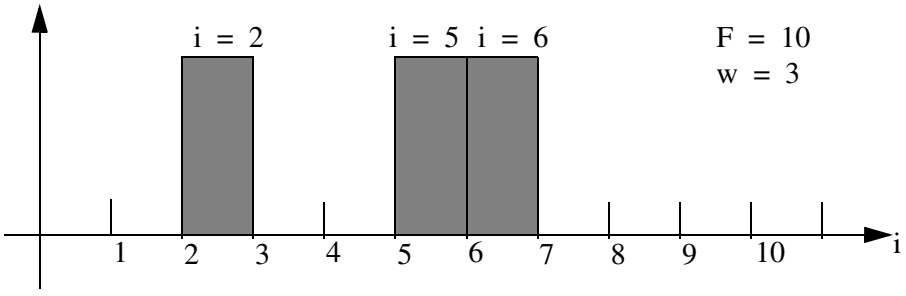

Figure 3.10: Illustration of w-1 different differences for each mark in an OOC

Since the number of possible distances in a code of length F is $F-1$, the maximum size of an OOC is

$$N_{OOC} \leq \left\lfloor \frac{F-1}{w(w-1)} \right\rfloor , \tag{3.13}$$

where $[z]$ denotes the integer (pre-decimal) part of the real value of z. If F is even, (3.13) can be enforced to

$$N_{OOC} \leq \left\lfloor \frac{F-2}{w(w-1)} \right\rfloor , \tag{3.14}$$

since a distance of $\frac{F}{2}$ between x and x' cannot be realized obeying the correlation constraints of $\rho_a = \rho_c = 1$.

It is also possible to derive a lower bound. For this reason, it is necessary to take a closer look at the code generation process from Figure 3.2. The autocorrelation constraint implies that there are $(w-1)^2(w-2)$ different possibilities to form $x = a + b - c$ in the codeword under consideration (a, b and c from the same codeword). This comes from the fact, that already $w-1$ marks have been positioned, i.e. there are $w-1$ different possibilities for a as well as for b, but only $w-2$ possibilities for c, since $a \neq c$. Assuming that $m-1$ codewords have already been included in the code, the crosscorrelation demands, that there are $(m-1)w(w-1)^2$ different possibilities to form $x = a + b - c$, (a from the codeword under consideration, $b \neq c$ from the same, already existing codewords). $m-1$ codewords have already been found, b and c can take values of the w or $w-1$ (since $b \neq c$) positions of marks in these codewords; a can take $w-1$ different values. That means, that considering the $w-1$ marks, that have been positioned in the codeword under consideration, a new mark can *always* be placed to complete a codeword, if

$$(w-1)^2(w-2) + (m-1)w(w-1)^2 + (w-1) < F \tag{3.15}$$

From (3.15), it follows that

$$m < \frac{(F-w+1) - (w-1)^2(w-2)}{w(w-1)^2} + 1 \quad . \tag{3.16}$$

A codeword can in any case and for sure be completed if (3.16) holds. The borderline case

can thus be designated as

$$m \approx \frac{(F - w + 1) - (w - 1)^2 (w - 2)}{w(w - 1)^2} + 1 \quad . \tag{3.17}$$

Since there might be cases, in which a codeword can be included in the code even if the bound in (3.15) is exceeded, one can write

$$N \geq \frac{(F - w + 1) - (w - 1)^2 (w - 2)}{w(w - 1)^2} + 1 \quad . \tag{3.18}$$

Since each OOC word serves as basis for the MOOC words, one must now obtain the number of MOOC words that can be generated from one OOC word. This can be fulfilled by looking at the inner structure of MOOC words. MOOC words are time-shifted variants of their underlying OOC word. In order to be able to get as many as possible MOOC words, the available F positions must all be occupied by marks of the different MOOC words, see Figure 3.11.

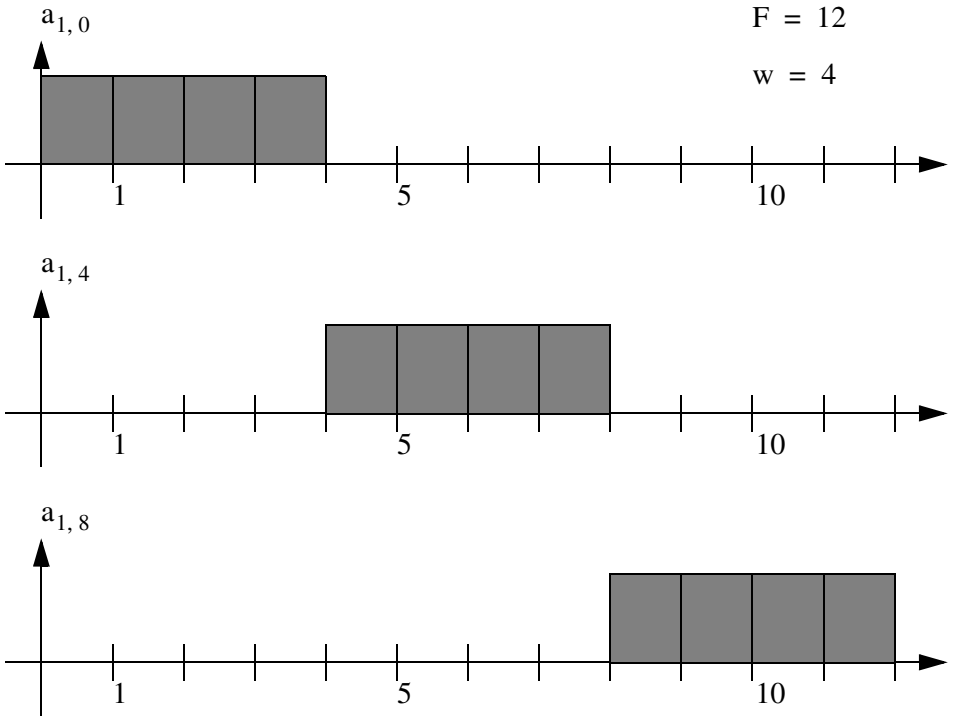

Figure 3.11: Best case of inner structure referring to temporal shift between MOOC $a_{1,i}$ -words

This „best case“ scenario can deliver up to

$$N_{MOOC} < \left\lceil \frac{F}{w} \right\rceil \tag{3.19}$$

different MOOC words per OOC word. However, it must be noted that this best case does not comply with the proposed correlation constraints. Four consecutive marks would inherently lead to $\rho_a = 3$. Yet, (3.19) serves as an upper bound.

Similar to that, a worst case scenario is depicted in Figure 3.12. This case occurs, if the $a_{1,0}$-word consists of a block of $w-1$ marks, followed by $w-2$ spaces. By this, it is not possible to create new $a_{1,i}$ words without leaving these $w-2$ positions empty. This worst case thus leads to the lower bound

$$N_{MOOC} \geq \left\lceil \frac{F}{w + (w-2)} \right\rceil = \left\lceil \frac{F}{2(w-1)} \right\rceil . \tag{3.20}$$

Again, it must be noted that the explicit example from Figure 3.12 does not comply with the proposed correlation constraints due to the three consecutive marks. Still, even for codewords with w marks (no consecutive ones), the worst case is that $w-2$ positions remain free while shifting. Thus, (3.20) holds as lower bound for the number of MOOC words N_{MOOC} per underlying OOC word.

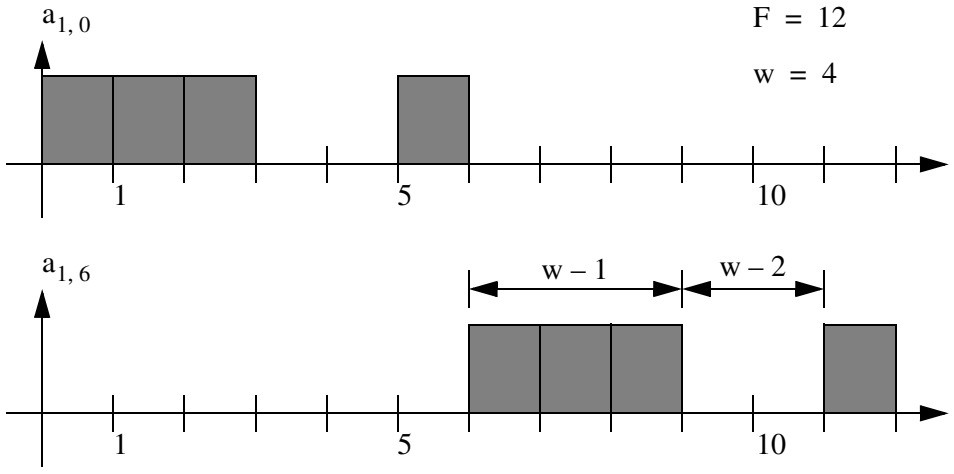

Figure 3.12: Worst case of the inner structure referring to temporal shift between MOOC $a_{1,i}$-words

Following from (3.13) and (3.20), an upper bound for the overall size of a modified optical orthogonal code $N_{total} = N_{OOC} \cdot N_{MOOC}$ can be derived as

$$N_{total} \leq \left\lceil \frac{F}{2(w-1)} \right\rceil \cdot \left\lceil \frac{F-1}{w(w-1)} \right\rceil , \tag{3.21}$$

whereas an upper bound results in

$$N_{total} \geq \left\lceil \frac{F}{2(w-1)} \right\rceil \cdot \frac{((F-w+1)-(w-1)^2(w-2))}{w(w-1)^2} \quad . \tag{3.22}$$

As mentioned in 3.1, OOC and MOOC can be used for error free multiple access transmission by limiting the number of simultaneous users, thus not exploiting the size of the code. Still, a lower bound can be given for that case.

Given an OOC with length F, weight w and $\rho_a = \rho_c = 1$, w users can be allowed to transmit simultaneously without leading to any bit errors. Since each CCF peaks with a maximum of 1, the overall sum of all CCF peaks may be as high as $w-1$. Since the ACF peak is as high as w, the receiver can discriminate the different signals. The lower bound for OOC in the case of „errorfree“ transmission thus follows as

$$N_{OOC,\,ef} = w , \tag{3.23}$$

where index „ef“ stands for errorfree. As long as an OOC can be found for a given code length F and a given code weight w, the lower bound for the possible overall size of MOOC for „errorfree“ transmission yields

$$N_{total,\,ef} \leq \left\lceil \frac{2F}{w+1} \right\rceil . \tag{3.24}$$

$N_{total,\,ef}$ thus is the size of the so-called errorfree subset of MOOC. To explain (3.24), it is necessary to take a look at the composition of the MAI, when using only codes of this errorfree subset. The codewords from Table 3.1 serve as an example.

Let us suppose that all 8 users are transmitting a data „1“, so that each of the 8 codewords is emitted by the lasers at the same time. User #1 with sequence $a_{1,0}$ is the desired user. The received signal before correlation thus is the sum of all 8 codewords as shown in Table 3.2.

OOC codeword j	Sequence	MOOC sequences
1	$a_{1,0}$	1100 0001 0000 0000
	$a_{1,4}$	0000 1100 0001 0000
	$a_{1,8}$	0000 0000 1100 0001
	$a_{1,12}$	0001 0000 0000 1100
2	$a_{2,0}$	0010 1001 0000 0000
	$a_{2,4}$	0000 0010 1001 0000
	$a_{2,8}$	0000 0000 0010 1001
	$a_{2,12}$	1001 0000 0000 0010
	$r(\mu)$	2112 2112 2112 2112

Table 3.2: Summation of all codewords to explain the MAI

The correlation $\varphi_{r,\,p_{1,0}}(i)$ of the received signal $r(\mu)$ leads to a value of 5, resulting in a detection of a transmitted data „1“ from user #1, since the threshold device has been set to the codeweight $w = 3$. As long as $r(\mu)$ ensures that $\underline{\varphi}_{r,\,p_{j,i}}(i) < 2w$ while all users transmit their sequence, an errorfree transmission is possible. Therefore, $r(\mu)$ needs to have the structure from Table 3.2 or a rotation of that structure. The maximum size $N_{total,\,ef}$ can be reached with $\underline{\varphi}_{r,\,p_{j,i}}(i) = 2w - 1$. To illustrate (3.24), $r(\mu)$ is rotated by two taps and is - for demonstrational reasons - composed by fictive sequences that would not meet the correlation constraint, but serve only as example.

	MOOC sequences
	1110 0000 0000 0000
	0111 0000 0000 0000
	0000 1110 0000 0000
	0000 0111 0000 0000
	0000 0000 1110 0000
	0000 0000 0111 0000
	0000 0000 0000 1110
	0000 0000 0000 0111
$r(\mu)$	1221 1221 1221 1221

Table 3.3: r(μ) composed by fictive (demonstrational) MOOC sequences

As can be seen from Table 3.3 the structure of $r(\mu)$ can be reached, when $w+1$ consecutive taps are covered by two code sequences, each with w marks within these $w+1$ taps. Since there are $\left\lfloor \frac{F}{w+1} \right\rfloor$ segments in the codewords with length F, a total of max. $2\left\lfloor \frac{F}{w+1} \right\rfloor$ users can simultaneously transmit their codesequences.

3.2.3 Bit error ratio

3.2.3.1 Bit error ratio of modified optical orthogonal codes

The amplitude of the crosscorrelation peak between two MOOC sequences is at most 1. Since the autocorrelation peak has an amplitude equal to the codeweight w, at least $w-1$ users can simultaneously be accommodated without errors. However, when the number of simultaneous users K equals or exceeds the codeweight w, the cumulative amplitude of the interference in the sampled chip position can be as high as the autocorrelation peak or even higher, resulting in a detection error. The bit error ratio is calculated by considering all possible cases, for which a receiver makes a wrong decision. It is further assumed, that each user transmits data bits „1“ or „0“ with equal probability. The probability of error with K simultaneous users is given by

$$\begin{aligned} P_e &= P(\text{error, K users}) \\ &= \sum_{i=0}^{K} P(\text{error, K users} \mid \text{i sent 1}) \cdot P(\text{i sent} \mid \text{K users}) \end{aligned} \tag{3.25}$$

for $0 \le K \le \left\lfloor \frac{F}{2(w-1)} \right\rfloor \left\lfloor \frac{F-1}{w(w-1)} \right\rfloor$. Since each of the K simultaneous users can transmit data bits „1" and „0“ with equal probability, there is a total of 2^K different cases to consider. There are $\binom{K}{i}$ ways to pick i users out of K that transmit data bits „1“. I.e.,

$$P(\text{i sent 1} \mid \text{K users}) = \frac{\binom{K}{i}}{2^K}. \tag{3.26}$$

Now, the first term on the right side in (3.25) has to be examined.

If the number of simultaneous users, that transmit „1“ exceeds the number $N_{\text{total, ef}}$ of users that can possibly be accommodated errorfree (see (3.24)) i.e. $i > 2\frac{F}{w+1}$, at least one receiver will in any case detect an error. If $i < w$, then there will be no error. The case $w \le i \le 2\frac{F}{w+1}$ needs a closer examination.

Bit errors for simultaneous users of number $w \le i \le 2\frac{F}{w+1}$ can occur, if more than w users have marks (or „1"s, resp.) on one of the chip positions of the desired user. Thus the mean value m_b has to be determined of sequences of a total of $N_{total} = \left\lfloor \frac{F}{2(w-1)} \right\rfloor \left\lfloor \frac{F-1}{w(w-1)} \right\rfloor$ that have marks on the chip positions of the desired user.

The sequence of the desired user (e.g. $a_1(\mu)$) shows w marks on F positions, i.e. that the probability that a certain position holds a mark equals $\frac{w}{F}$. Each other user's sequence ($a_i(\mu)$, $i \neq 1$) also has w marks, so that the probability P_m for exactly one overlap is given by

$$P_m = \binom{w}{1}\frac{w}{F}\left(1-\frac{w}{F}\right)^{w-1} = \frac{w^2}{F}\cdot\left(1-\frac{w}{F}\right)^{w-1} . \tag{3.27}$$

More than one overlap between two different sequences cannot occur due to the defined correlation constraints. The mean m_b thus follows as

$$m_b = \left\lfloor \frac{F}{2(w-1)} \right\rfloor \left\lfloor \frac{F-1}{w(w-1)} \right\rfloor \cdot P_m . \tag{3.28}$$

Thus, one would expect m_b sequences out of $N_{total} = \left\lfloor \frac{F}{2(w-1)} \right\rfloor \left\lfloor \frac{F-1}{w(w-1)} \right\rfloor$, that have one mark at the same chip position as the desired one.

The probability of error for $w \le i \le 2\frac{F}{w+1}$ simultaneous users follows as

$$P(\text{error, K users} \mid \text{i sent 1}) = \frac{\sum_{j=w}^{\min(i,\,m_b)} \binom{m_b}{j}\binom{N_{total}-m_b}{i-j}}{\binom{N_{total}}{i}} . \tag{3.29}$$

To recapitulate, the probability of error for K users, if all send data bits „1" can be expressed as

$$P(\text{error, K users} \mid \text{i sent 1}) = \begin{cases} 0 & \text{if} \quad i < w \\ \dfrac{\sum_{j=w}^{\min(i,\,m_b)} \binom{m_b}{j}\binom{N_{total}-m_b}{i-j}}{\binom{N_{total}}{i}} & \text{if} \quad w \le i \le \dfrac{2F}{w+1} \\ 1 & \text{if} \quad i > \dfrac{2F}{w+1} \end{cases} \tag{3.30}$$

In the case of $w \le i \le \frac{2F}{w+1}$, at least w of the transmitters with one of the m_b sequences must furthermore transmit a data „1“ for an error to occur. Thus, for $w \le i \le \frac{2F}{w+1}$, it follows, that

$$\begin{aligned} P(\text{i sent 1} \mid \text{K users}) &= \sum_{k=w}^{j} \binom{j}{k} \cdot 0.5^{k} \cdot 0.5^{j-k} \\ &= \sum_{k=w}^{j} \binom{j}{k} \cdot 0.5^{j} \\ &= \sum_{k=w}^{j} \frac{\binom{j}{k}}{2^{j}} \end{aligned} \tag{3.31}$$

Combining (3.26), (3.30) and (3.31) in (3.25), the probability of error (or the bit error ratio, resp.) for K simultaneous users ($N_{total} \ge K \ge w$) is given by

$$P_e = \frac{\sum_{j=w}^{\min\left(K,\, m_b,\, \frac{2F}{w+1}\right)} \binom{m_b}{j} \binom{N_{total}-m_b}{K-j} \sum_{k=w}^{j} \binom{j}{k} \cdot 0.5^{j}}{\binom{N_{total}}{K}} + \sum_{i=\frac{2F}{w+1}+1}^{K} \frac{\binom{K}{i}}{2^{K}}. \tag{3.32}$$

For $K < w$, the bit error ratio is equal to zero.

3.2.3.2 Bit error ratio of the errorfree subset of modified optical orthogonal codes

It must be noted, that there exist combinations of up to $N_{total,\,ef} = \left\lfloor \frac{2F}{w+1} \right\rfloor$ code sequences that can be used by $\left\lfloor \frac{2F}{w+1} \right\rfloor$ transmitters, all transmitting data „1“, without an occurrence of bit errors (see 3.2.2). If this errorfree subset is chosen for the first $[2F/(w+1)]$ users, and further users are assigned to remaining code sequences from the total set, the BER for a number of users lower than its maximum (which equals the size of the code) is expected to be significantly lower.

To obtain the BER, it is necessary to analyze, where the bit errors are generated. Starting again with (3.25) and (3.26), one can write

$$\begin{aligned} P_e &= \sum_{i=0}^{K} P(\text{i sent} \mid \text{K users}) \cdot P(\text{error, K users} \mid \text{i sent 1}) \\ &= \sum_{i=0}^{w} \frac{\binom{K}{i}}{2^{K}} \cdot 0 + \sum_{i=w+1}^{N_{total,\,ef}} \frac{\binom{K}{i}}{2^{K}} \cdot P(\text{error, K users} \mid \text{i sent 1}) + \sum_{i=N_{total,\,ef}+1}^{K} \frac{\binom{K}{i}}{2^{K}} \cdot 1 \\ &= \sum_{i=w+1}^{N_{total,\,ef}} \frac{\binom{K}{i}}{2^{K}} \cdot P(\text{error, K users} \mid \text{i sent 1}) + \sum_{i=N_{total,\,ef}+1}^{K} \frac{\binom{K}{i}}{2^{K}} \end{aligned} \tag{3.33}$$

where

$$
\begin{aligned}
P(\text{error, K users} \mid \text{i sent 1}) &= P((n_{nef} \geq 1) \wedge (m_{nef} > m_{ef})) \\
&= \sum_{k=1}^{N_{nef}} \frac{\binom{i}{i-k}\binom{K-i}{k}}{\binom{K}{i}} \cdot \\
&\quad \cdots \sum_{j=0}^{k-1} \sum_{m=j+1}^{k} \binom{k}{j} P_m^j (1-P_m)^{(k-j)} \binom{k}{m} P_m^m (1-P_m)^{(k-m)}
\end{aligned}
\tag{3.34}
$$

N_{nef} is the actual size of the not-errorfree subset of MOOC ($N_{nef} = K - N_{ef}$) and $1 \leq n_{nef} \leq N_{nef}$, m_{nef} ($1 \leq m_{nef} < n_{nef}$) the number of not-errorfree codes out of n_{nef} that have a mark on a same position as the desired user, m_{ef} ($0 \leq m_{ef} < n_{nef}$) the number of codes out of the errorfree subset that have a mark on a same position as the code sequence of the desired user.

(3.33) will now be evaluated with the help of an example. With code length $F = 32$, code weight $w = 3$, code size $N_{total} = 32$, size of the errorfree subset $N_{ef} = 16$, number of simultaneous users $K = 20$, it follows that $N_{nef} = 4$. Bit errors occur in the following cases:

- •• 17, 18, 19 or 20 users transmit simultaneously a data „1“ (last term on right-hand side of (3.33)).
- •• 16 users transmit simultaneously a data „1“ *and*
  - from these 16 have 15 users code sequences from the errorfree subset (1 user has a code sequence that is not from the errorfree subset) *and*
    - this 1 code sequence has a mark at the same position as the desired user *and* the code sequence from the errorfree subset that is not used does not have a mark on a position of the code sequence of the desired user; *or*
  - from these 16 have 14 users code sequences from the errorfree subset (2 users have a code sequence that is not from the errorfree subset) *and*
    - 1 of these 2 sequences has a mark at the same position as the desired user *and* 0 of the code sequences from the errorfree subset that are not used do not have a mark on a position of the code sequence of the desired user, *or*

- 2 of these 2 sequences have a mark on a same position as the desired user and none *or* one of the code sequences from the errorfree subset that are not used do not have a mark on a position of the code sequence of the desired user; *or*

- from these 16 have 13 users code sequences from the errorfree subset (3 users have a code sequence that is not from the errorfree subset) *and*

  - 1 of these 3 sequences has a mark on a same position as the desired user *and* 0 of the code sequences from the errorfree subset that are not used do not have a mark on a position of the code sequence of the desired user, *or*

  - 2 of these 3 sequences have a mark on a same position as the desired user and 0 *or* 1 of the code sequences from the errorfree subset that are not used do not have a mark on a position of the code sequence of the desired user, *or*

  - 3 of these 3 sequences have a mark on a same position as the desired user and 0, 1 *or* 2 of the code sequences from the errorfree subset that are not used do not have a mark on a position of the code sequence of the desired user; *or*

- from these 16 have 12 users code sequences from the errorfree subset ($4 = N_{nef}$ users have a code sequence that is not from the errorfree subset) *and*

  - 1 of these 4 sequences has a mark on a same position as the desired user *and* 0 of the code sequences from the errorfree subset that are not used do not have a mark on a position of the code sequence of the desired user, *or*

  - 2 of these 4 sequences have a mark on a same position as the desired user and 0 *or* 1 of the code sequences from the errorfree subset that are not used do not have a mark on a position of the code sequence of the desired user, *or*

  - 3 of these 4 sequences have a mark on a same position as the desired user and 0, 1 *or* 2 of the code sequences from the errorfree subset that are not used do not have a mark on a position of the code sequence of the desired user; *or*

  - 4 of these 4 sequences have a mark on a same position as the desired user and 0, 1, 2 *or* 3 of the code sequences from the errorfree subset that are not used do not have a mark on a position of the code sequence of the desired user; *or*

•• 15 users transmit simultaneously a data „1“ *and*

- from these 15 have 14 users code sequences from the errorfree subset (1 user has a code sequence that is not from the errorfree subset *and*
  - this 1 code sequence has a mark at the same position as the desired user *and* the code sequence from the errorfree subset that is not used does not have a mark on a position of the code sequence of the desired user; *or*
- ... (analogous to above)

down to

•• 4 users transmit simultaneously a data „1“ *and* ... (analogous to above)

The BER curves are plotted in 3.3.2.

3.3 Simulation results

3.3.1 Size

The size of a code specifies the maximum number of users that can be assigned a specific code sequence that is orthogonal to each other sequence in the code. It is thus desirable to design a code that delivers as many sequences as possible. From 3.2.2, the size of an ordinary and known OOC has been found to be $N_{OOC} \leq [(F-1)/(w(w-1))]$. For small code lengths $F = 16$ and $F = 32$, suitable for data signals at high bit rates in the order of GBit/s, the number of available codes is shown in Figure 3.13, for large code lengths ($F = 1000$ and $F = 10000$), suitable for low data rates, in Figure 3.14.

To compare the newly MOOC with the OOC from which the MOOC were developed, Figure 3.15 and Figure 3.16 show the size of the corresponding MOOC codes with lengths $F = 16$ and $F = 32$ as well as $F = 1000$ and $F = 10000$.

Whereas the usual optical orthogonal codes can deliver only few orthogonal code sequences compared to the number of chips within a sequence (or the code length, resp.), this disadvantage is removed by the introduction of modified optical orthogonal codes. Usually, the data bit rate is given for a system under examination. In order to keep the demands for system components in terms of switching times as low as possible, it would be advisable to have code sequences of short length, thus keeping the chip rate (which equals the bit rate times the code sequence length) low. With usual OOC and sequence lengths of $F = 16$, only two dif-

ferent user could be assigned a specific code sequence at a code weight of $w = 3$. Shifting to MOOC and keeping the same sequence length, 8 different users could be accommodated.

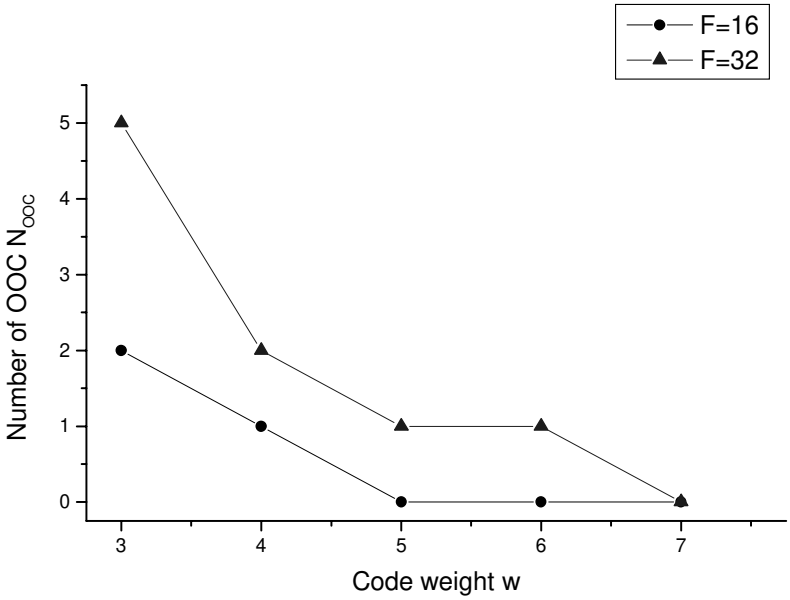

Figure 3.13: Size of OOC with length F=16 and F=32, resp.

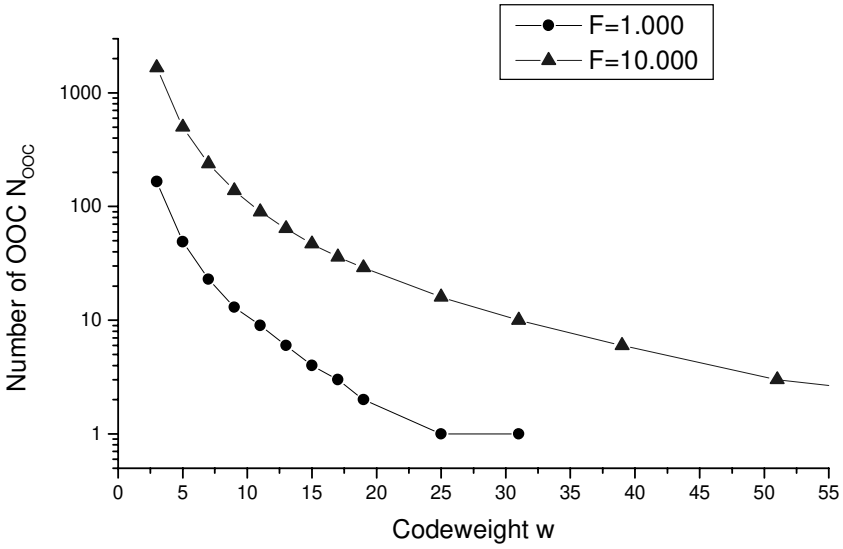

Figure 3.14: Size of OOC with length F=1000 and F=10000, resp.

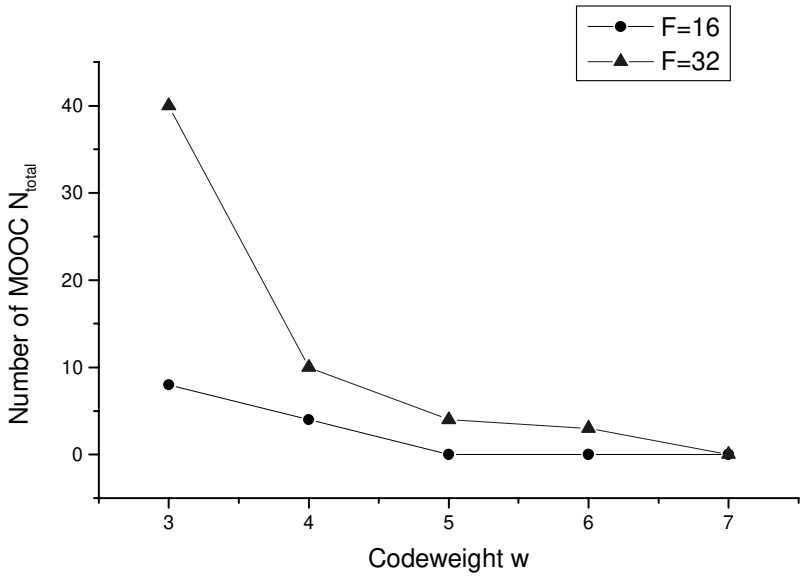

Figure 3.15: Size of MOOC with length F=16 and F=32, resp.

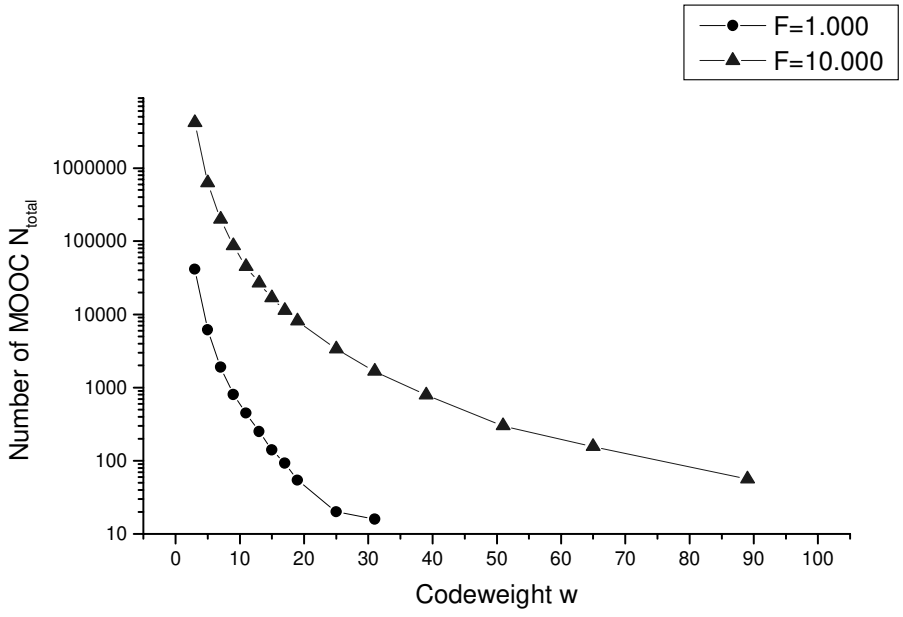

Figure 3.16: Size of MOOC with length F=1000 and F=10000, resp.

The difference between sizes of OOC and MOOC gets even more obvious with increasing sequence lengths. While in a system with OOC of length 32, max. 5 users could get assigned a unique code sequence, this number eightfolds in a system with MOOC to 40. It is important to notice that the bit error ratio for a system with 5 users and OOC is about the same as with MOOC, see section 3.3.2. Furthermore, for sequence lengths of $F = 1000$ or $F = 10000$, more than 250 times as many users can be accommodated with roughly the same bit error ratio.

It might seem odd that there can exist more unique code sequences than chips per sequence (see Figure 3.15 and Figure 3.16), a fact completely unknown to the conventional codes described in 2.3. However, this vast potential cannot completely be exploited since the bit error ratio reaches values close to 1, when all sequences are allotted to users that are simultaneously active.

The greatest advantage of the new codes can be shown, if only sequences of the errorfree subset are chosen and assigned to users. These code sequences are not only orthogonal to each other, but can also be used simultaneously by their users (even if all transmit a data „1“ at the same time) and no bit error will occur. This errorfree subset allows - in the case of $F = 16$ and $w = 3$ up to 8 simultaneous users, all being active without any bit errors. In the case of the conventional OOC, only 2 users could be supplied with code sequences. The interesting feature about the errorfree subset of MOOC, also called errorfree MOOC, is that at low code weights, both the code size can be greatly increased and at the same time, the bit error rate can be reduced to zero (see Figure 3.17 and Figure 3.18).

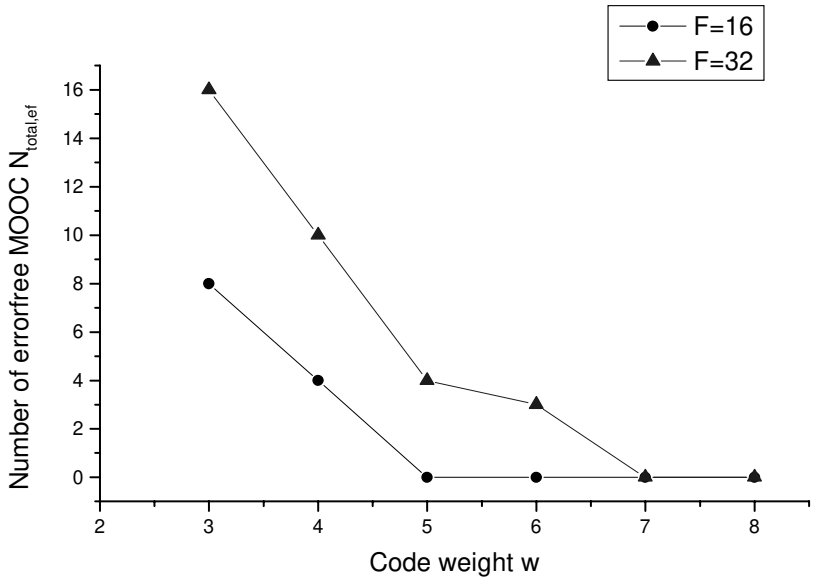

Figure 3.17: Size of the errorfree subset of MOOC with lengths F=16 and F=32

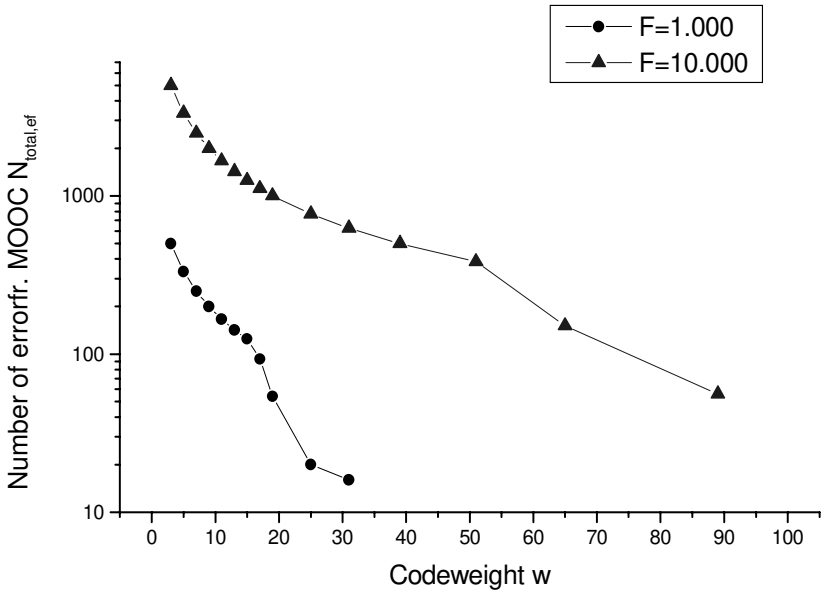

Figure 3.18: Size of the errorfree subset of MOOC with lengths F=1000 and F=10000

From a certain code weight on to higher code weights, (3.24) delivers higher values for the

maximum number of errorfree MOOC $N_{total,\,ef}$ than the maximum number of MOOC N_{total}. Since the errorfree MOOC are a subset of the MOOC, $N_{total,\,ef} \leq N_{total}$ is preconditioned and the slope of the curve in Figure 3.17 and Figure 3.18 increases. I.e. that from a certain code weight on, all found MOOC words belong to the errorfree subset.

3.3.2 Bit error ratio

As important for the suitability of a code in a CDMA system as the size of the code is its probability of error, or the bit error ratio (BER), resp. Besides creating codes with large code sizes, it is necessary that as many as possible simultaneous users can access the transmission medium without causing too many errors at the receivers. Though these two demands are more than somewhat conflictive, a compromise can be found by using the MOOC. For comparative reasons, Figure 3.19, Figure 3.20 and Figure 3.21 show the BER of OOC for $F = 16$ and $F = 32$ as well as $F = 1000$ and $F = 10000$. In order to maximize the number of possible users (i.e. the size of the code), code weight w has been chosen to $w = 3$. An OOC with $F = 16$ and $w = 3$ can deliver only two different code words. Since the code weight is greater than the number of users, the BER in this case is equal to zero. For demonstrational reasons, the black curve in Figure 3.19 appears as 10^{-6}. BER curves for low values of code length F and code weights $w > 3$ are trivial since these code sizes are equal to zero.

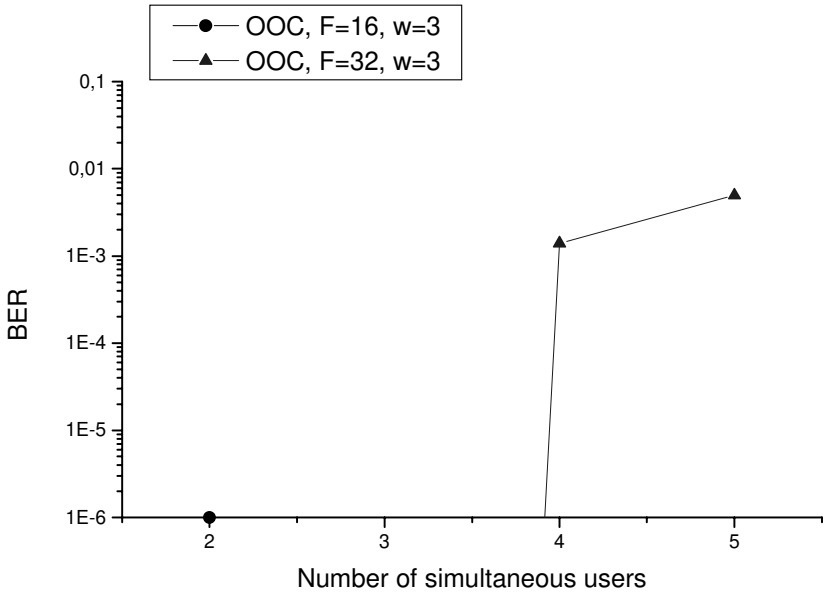

Figure 3.19: BER of OOC with lengths F=16 and F=32, codeweight w=3

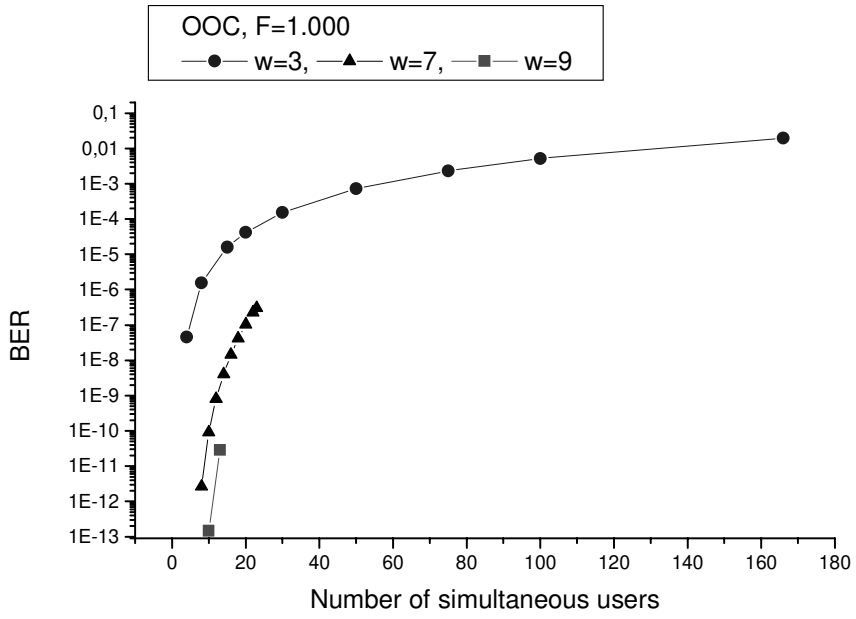

Figure 3.20: BER of OOC with length F=1000, codeweight w=3, 7 and 9, resp.

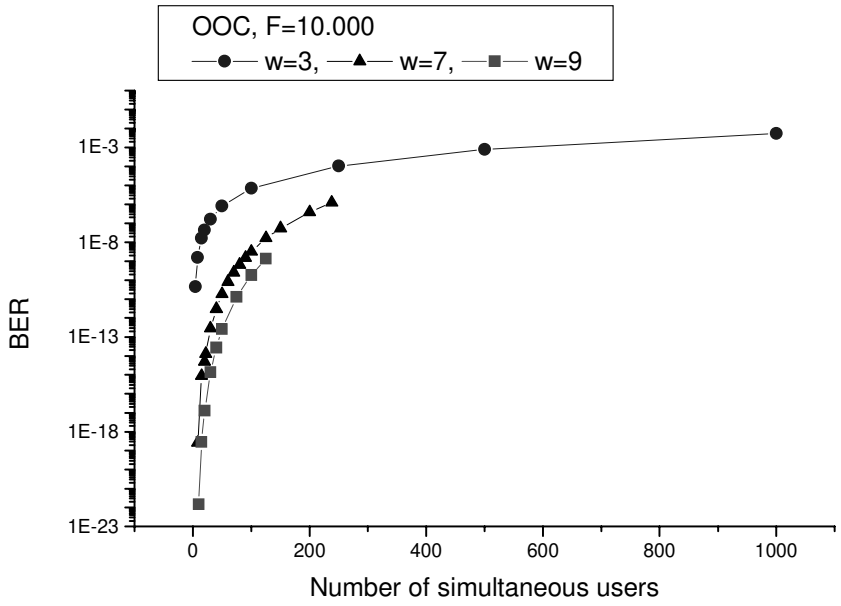

Figure 3.21: BER of OOC with length F=10000, codeweight w=3, 7 and 9, resp.

The triangled line in Figure 3.19, representing an OOC with $F = 32$ and $w = 3$ stops at five simultaneous users, since only 5 code words can be created by this code. In the case of less than four simultaneous users, the BER is equal to zero again.

Figure 3.20 and Figure 3.21 show the BER curves for OOC with $F = 1000$ and $F = 10000$ with varying code weights. Each curve stops at the maximum number of code sequences that each code can generate. The low number of maximum users in spite of long sequence lengths is flashy and a clear disadvantage for OOC.

On the other hand, MOOC have BERs that are in the same range as the corresponding OOC, but can generate much more orthogonal code sequences, see Figure 3.22 compared to Figure 3.19. The MOOC with $F = 16$ and $w = 3$ has a size of 8, a bit error ratio of zero for up to all 8 users. Only for demonstrational reasons, it is shown as a BER of 0.002 in Figure 3.22.

The fact that MOOC allow many more users than OOC gets even more obvious when turning to longer code sequences as shown in Figure 3.23 and Figure 3.24. With a code length of $F = 1000$, OOC allow only max. 20 users with BERs better than 10^{-4}. With MOOC, this value can be more than doubled to over 50 users. As expected, the BER decreases with higher codeweights. The disadvantage, that higher codeweights are inevitably connected with very low code sizes is eliminated.

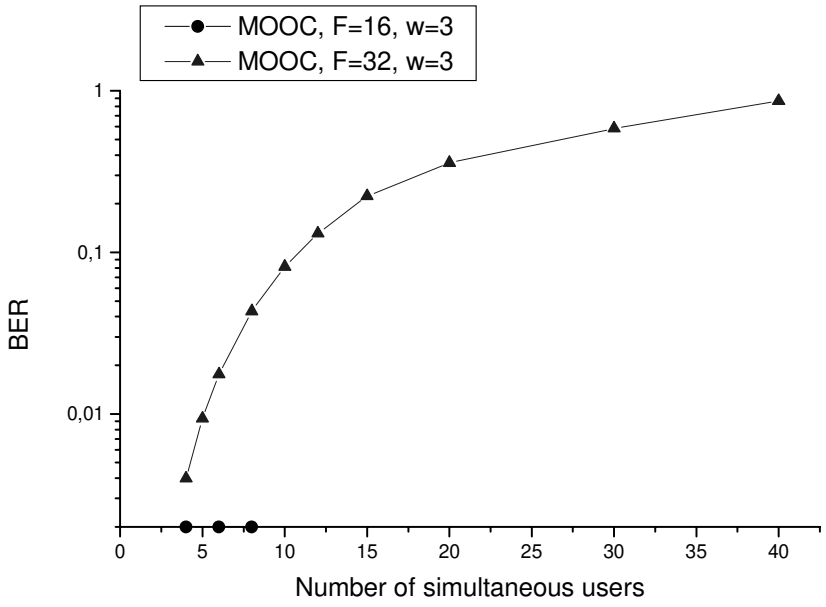

Figure 3.22: Bit error rate of MOOC with length F=16 and F=32, codeweight w=3.

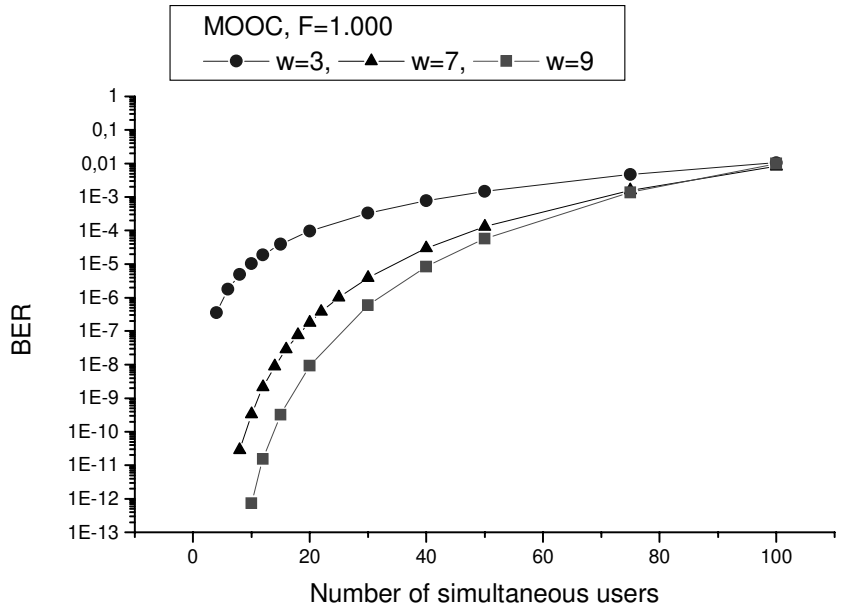

Figure 3.23: BER of MOOC with length F=1000, codeweight w=3, 7 and 9, resp.

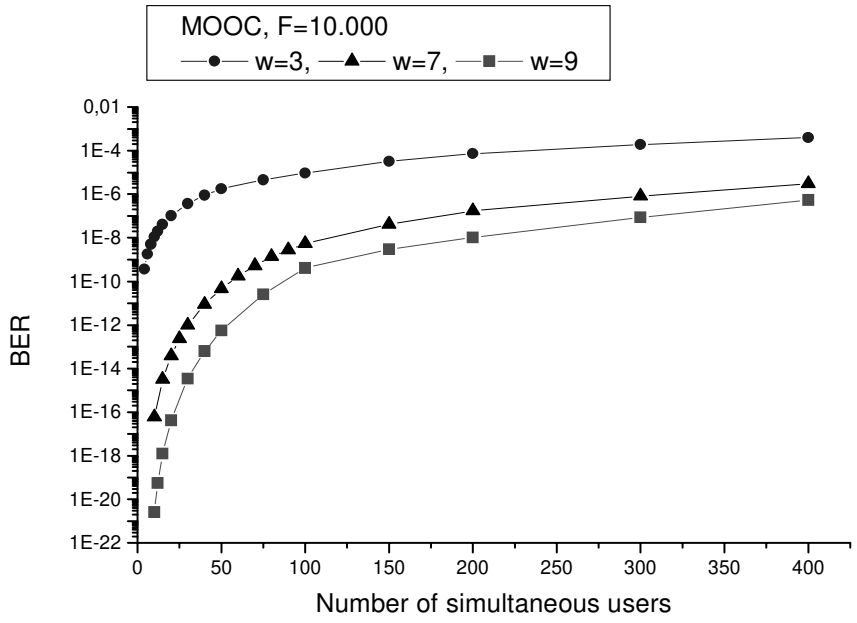

Figure 3.24: BER of MOOC with length F=10000, codeweight w=3, 7 and 9, resp.

Most interesting though is the BER performance of the errorfree subset of the MOO codes, given as an example with $F = 16$, $F = 32$ and $F = 1000$ in Figure 3.25, Figure 3.26 and Figure 3.27. An MOOC with $F = 32$ and $w = 3$ has a subset of 16 errorfree code sequences. If 16 of all users are allotted these errorfree sequences, and the other users are allotted to the remaining sequences of the MOO code, the BER curve equals zero up to 16 simultaneous users and then rises to its maximum at 40 simultaneous users. I.e. that with a code length of only $F = 32$, 16 simultaneous users without leading to bit errors can be accommodated. With a code length of $F = 16$, the size of the errorfree subset is 8 as is the total number of MOOC. Thus, with $F = 16$, up to 8 users can access the system simultaneously without causing bit errors due to the multiple access scheme. Figure 3.26 shows the comparison of the MOOC and its errorfree subset for $F = 32$ and $w = 3$. As expected, the BER of the errorfree subset is lower than the BER of the usual MOOC, but reaches the same BER at the maximum number of simultaneous users.

With longer code lengths, e.g. $F = 1000$ and a code weight of $w = 3$, more than 800 users can use the transmission medium simultaneously and still cause a system wide BER of less than 10^{-9}.

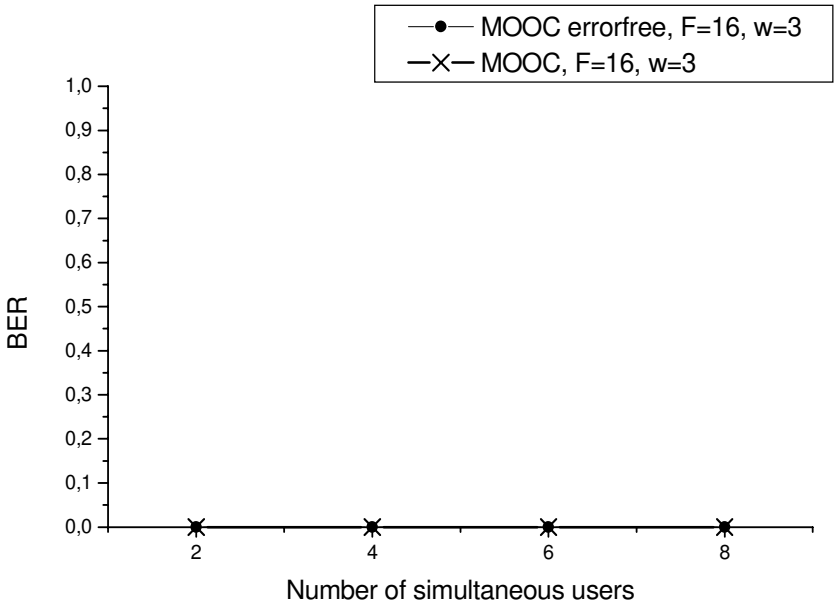

Figure 3.25: Comparison of BER of MOOC and its errorfree subset, length F=16, w=3. Size of MOOC and its errorfree subset is identical in this special case. No additional errors are introduced by this MOOC, i.e. the BER equals zero.

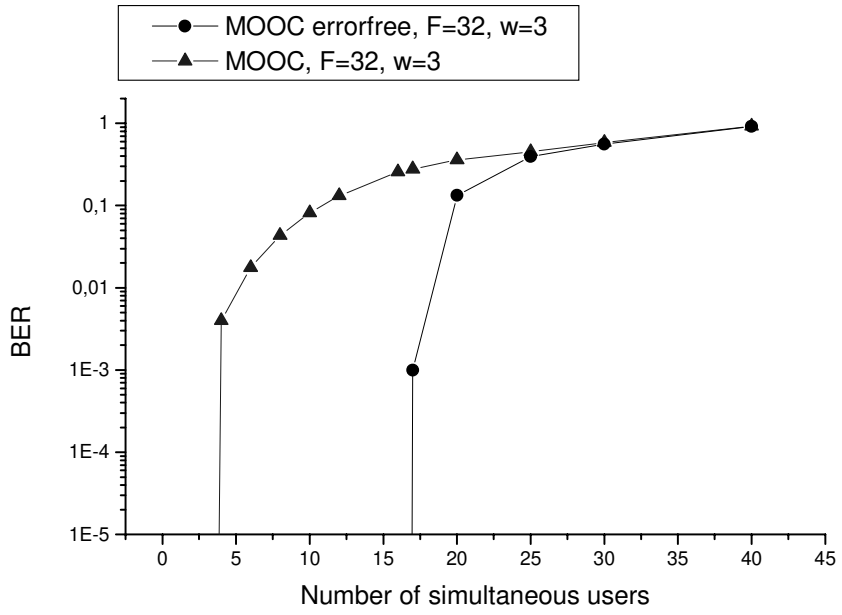

Figure 3.26: Comparison of BER of MOOC and its errorfree subset, length F=32, weight w=3.

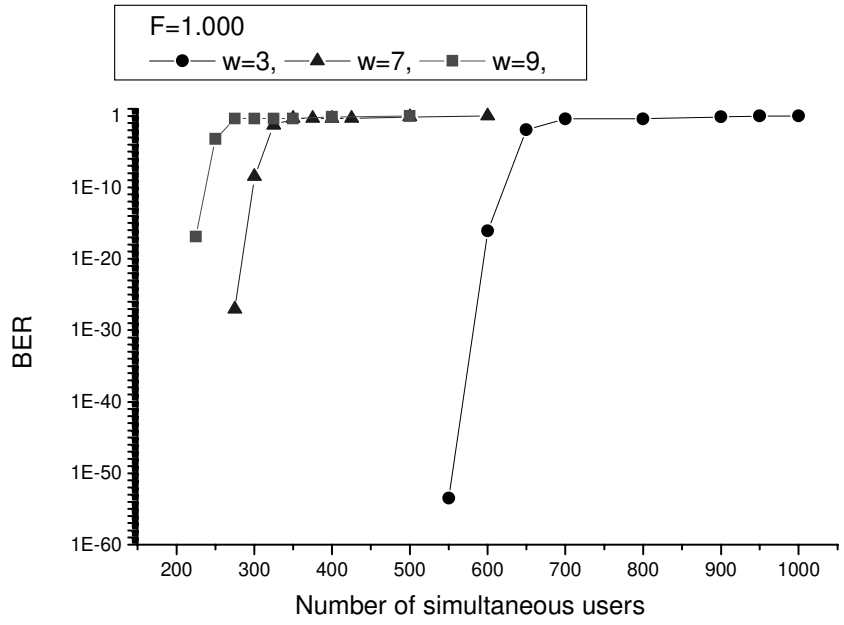

Figure 3.27: BER of the errorfree subset of MOOC, length F=1000, code weight w=3, 7 and 9, resp.

3.4 Potential fields of application

The codes as proposed in 3.2 can serve as spreading sequences of transmitter/receiver pairs in several multiple access scenarios.

3.4.1 Synchronized CDMA system

The modified optical orthogonal codes with their superior size over the conventional OOC at comparable bit error rate can serve as orthogonal spreading sequences in a synchronized CDMA (S/CDMA) transmission system where there is network synchronization among all users. In contrast to an asynchronous CDMA system with no waiting time for the users to access the system, the synchronized version allows more users to access the system by not only providing more orthogonal code sequences, but also - at the same time - increasing the number of simultaneous users without exceeding a specified bit error rate. Since synchronous accessing schemes generally produce higher throughput than asynchronous ones [42], they are most efficient in applications where real time requirements or high bit rates are of utmost important concern. For applications where the transmission channel is continuously used at high bit rates, the time division multiple access scheme shows best performance in terms of network throughput. However, if the channel is sparsely used or bursty traffic like IP traffic occurs, S/CDMA with the proposed codes allows access to the channel with less synchronization effort than in a TDMA system, especially at the receivers. Low traffic density, combined with low data rates in the order of tens or hundreds of kbit/s allow the usage of code sequences with lengths of several thousands chips.

The synchronization effort is significantly reduced compared to TDMA due to the usage of code sequences that are detected at the receiver not only by sampling and thresholding at a specified time slot, but also by the correlation of the orthogonal code words with the sequence of the desired user. Whereas in a TDMA system, each time slot can only contain the signal of one user, this number is increased by the factor $N_{OOC} = \left\lfloor \frac{F-1}{w(w-1)} \right\rfloor$, see 3.2.2 and Figure 3.28. Meanwhile, the sampling frequency at the demultiplexer and the receiver is reduced by the same amount, allowing to design cheaper receivers with less requirements for components for which switching speeds is of high concern.

This ease of receiver structure is bought with a chiprate that is increased by a factor of F compared to the bitrate of the original data signal which equals the datarate in the TDMA system. Whereas the receiver components are simplified in S/CDMA system, the trans-

mitter components need to fulfill higher speed requirements. S/CDMA is therefore superior in any kind of point-to-point or even more in point-to-multipoint applications, where a high number of receivers must be connected to the transmission system. Figure 3.29 shows the regime of N_{OOC} for $w = 3$ in dependence of code length F. I.e. that with code lengths of $F = 10000$, switching speeds at the receivers can be reduced by up to a factor of 1666 compared to a bit rate equivalent TDMA system.

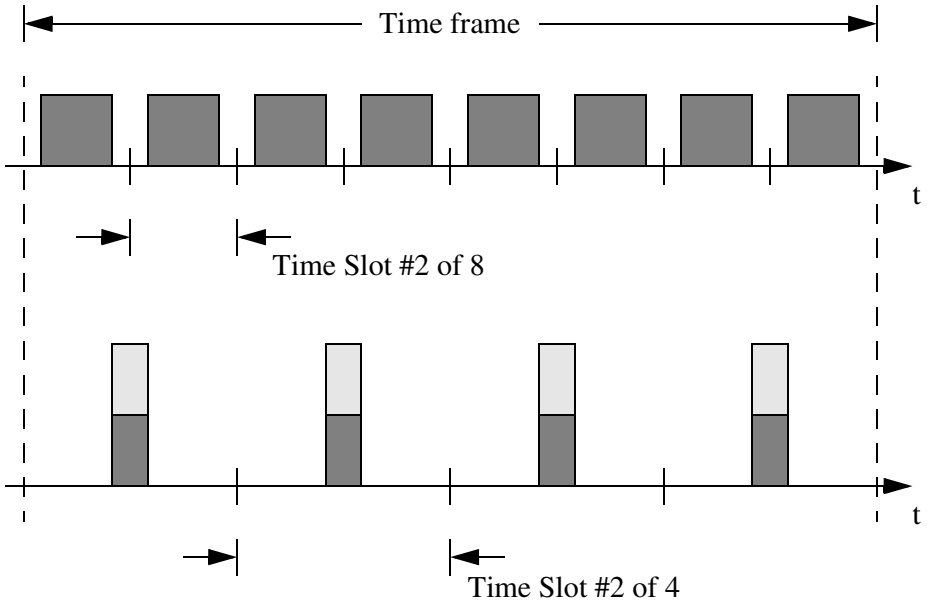

Figure 3.28: Schematic pulse streams at receivers in TDMA (above) and S/CDMA system (below)

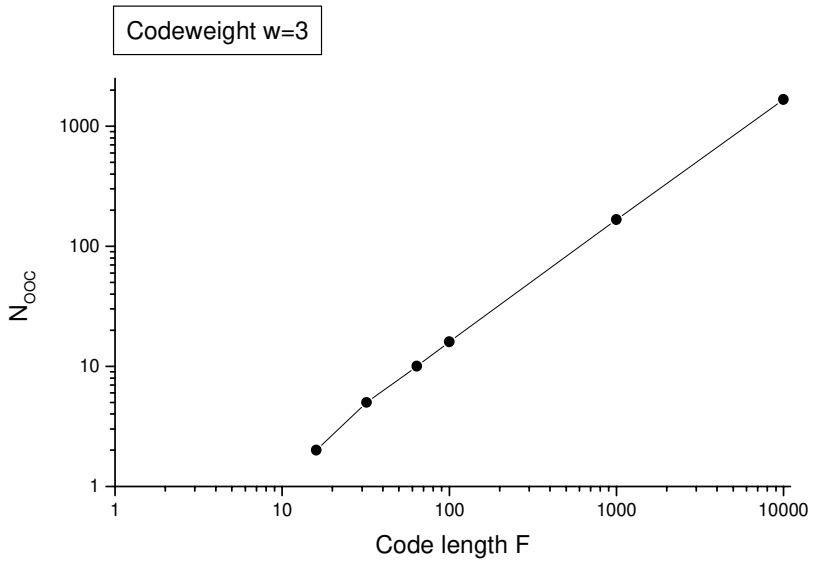

Figure 3.29: Size N_{OOC} in dependence of code length F

3.4.2 Hybrid WDMA/CDMA system

To increase the overall bit rate in a fiber optic transmission system, network carriers have swept from pushing the bit rate ahead on to transmit via multiple carrier wavelengths, since bit rates have already achieved values that can no more easily be handled by the involved electronic components. However, a transmission with multiple carrier wavelengths poses new problems to the transmission link design, e.g.

- generation of new frequencies by four-wave mixing effect, see 4.2.2,
- interference between different channels due to crossphase modulation, see 4.2.1,
- clear and sharp separation of the different channels by the use of costly bandpass filters see 6.3 and 6.4,
- intensive channel monitoring and carrier frequency control to reduce wavelength drifts of transmitter laser diodes to a minimum, see 2.1.3.

To battle the last three effects which are the most dominant ones (see Chapter 4), it is possible to assign one of the code sequences of the errorfree subset of a modified optical orthogonal code (named code sequences #1 to #8) to each of the signals on separate carrier wavelengths.

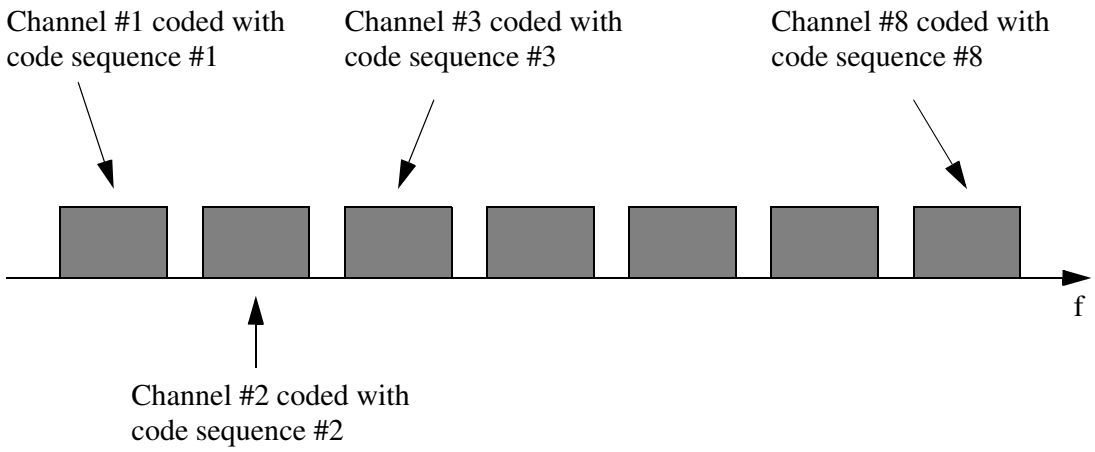

Figure 3.30: Coding of the spectrally adjacent wavelength channels

Through the orthogonality of the used sequences, the received signals can be separated at the receiver by an easy correlation, performed by fiber optical tapped delay lines, as proposed in Chapter 2. By this, the adjacent channel wavelengths need not longer be subject

of exact carrier tracking, since even a complete overlap of all involved channels can be tolerated and does not lead to an increased bit error rate, see Chapter 7. The otherwise necessary and very costly frequency control of the carrier wavelengths can be omitted. Furthermore, even the numerous bandpass filters that are necessary in the demultiplexing unit can be left out, thus reducing the number of complex and expensive filters and exchanging them to inexpensive and easy-to-handle optical delay lines. Even the effect of crossphase modulation is effectively reduced, see Chapter 7. Since WDM systems operate with high signal bit rates, only short code lengths in the order of 10 come into question as they were proposed in section 3.2.

Chapter 4

The propagation characteristics of single-mode fibres

The propagation of electromagnetic waves is thoroughly described by Maxwell's equations which relate the electrical field distribution to the magnetic one. Solving Maxwell's equations numerically requires computational methods (e.g. the **F**inite-**D**ifference **T**ime-**D**omain FD-TD, [43]) which consumes enormous CPU time and calls for extensive memory usage. The reason for this lies in the fact that Maxwell's equations describe the phenomenon of electromagnetic wave propagation in the most general way. They can be used for solving propagation problems in free space, in linear nondispersive media, for interfering signals in scattering media, etc. Since we are only interested in propagation of light in dispersive nonlinear media, namely an optical fibre, we can, starting from Maxwell's equation, obtain a basic equation which fulfills this need and, at the same time, requires only a fraction of computing time of that which would be necessary using the FD-TD method in connection with Maxwell's equation. In section 4.1, a brief overview of optical fibres and its distinctive characteristics will be given. Furthermore, a nonlinear differential equation, the so-called **n**on**l**inear **S**chrödinger **E**quation (NLSE), will be deduced by making some general assumptions which are characteristic for the propagation in an optical fibre. Section 4.2 describes the effects that occur during transmission of multiple wavelengths on the same fibre and develops the NLSE for the WDM case. 4.3 finally describes the consideration of the effects described in 4.2 in the simulations.

4.1 Propagation of single wavelength light in optical transmission fibres

In order to transmit guided light, a media which is „transparent“ for the wavelength or frequency range, resp., of interest is absolutely necessary. Transparent in the scientific sense means, that the injected lightwave discovers as little attenuation as possible. As a suitable substance which provides not only little attenuation, but also feasibility in terms of production processes as well as high transmission bandwidth, fused silica (SiO_2) has been found [33]. An alternative to the silica based fibres is often seen in plastic optical fibres (POF). Unfortunately, their advantage of being rather cheap compared to their silica counterpart is clouded by their high attenuation. Whereas silica fibres have attenuation levels as low as down to 0.2 dB/km, POF attenuate the signal with more than 20 dB/km. Furthermore, their dispersion, another fibre characteristics which will be explained in 4.1.3 reaches manifold levels of the silica based ones, making it impossible nowadays to use POF for long transmission links. Their application is to be found in inhouse networks, where transmission lengths and speeds are relatively low compared to those in trunk traffic networks which are treated in this work. Therefore, POF will not be of further consideration here.

One can distinguish between three important (glass) fibre types, [33], [45]:

- step-index fibre
- graded-index fibre
- single-mode fibre

Common to all of them is their principal structure which consists of an inner core, the surrounding cladding and a sheath to protect the fibre.

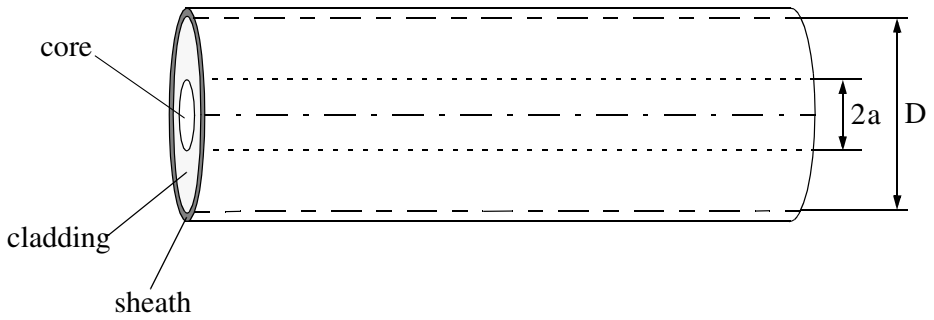

Figure 4.1: Longitudinal section through a fibre with diameter D and core radius a

Whereas the diameter D has been internationally standardized and is fixed to 125 µm, the core radius a differs between the different fibre types. Step-index and graded-index fibres usually have a diameter of 50 µm [33], single mode fibres of not more than 7 µm. The local refractive index of the material can be changed by doping, where GeO_2 is a widely used dopant to increase the refractive index. The core always has a higher optical refractive index than the cladding (approx. 1% higher), thus leading to the guiding of the light which is based on total reflection (step-index type) or continuous refraction (graded index and single mode fibre) at the core-cladding interface. In step-index and graded-index fibres, the core diameter is much greater than the free-space wavelength of the transmitted light (around 1.3 µm and 1.5 µm), resulting in very many different electromagnetic waveforms (the so-called *modes*) which can propagate within the fibre. These types of fibres are called *multimode fibres*. The propagation of many modes leads to impulse distortion, because every single mode has its own run-time for a certain link length. These run-times are slightly different for each mode which results in a temporal and spectral widening of the impulse at the receiver. In single mode fibres, the small core prevents all modes from propagating except the ground mode with two orthogonal directions of (linear) polarizations. In ideally rotation-symmetric and isotropic fibres, both modes have the same propagation constant and thus show identical propagation behaviour. Thus, impulse distortion is very much weaker in single mode fibres which, in reality, have a slight rotational asymmetry due to little imponderabilities during the production process. Only single-mode fibres can therefore be used for high bit-rate links [27].

4.1.1 The Nonlinear Schrödinger Equation

The propagation of impulses through a fibre can be described by the *nonlinear Schrödinger equation* (NLSE) [1]. In order to understand the NSLE, it is useful to derive it from Maxwell's basic electromagnetic wave equations:

$$\nabla \times \vec{e} = -\frac{\partial \vec{b}}{\partial t} \tag{4.1}$$

$$\nabla \times \vec{h} = \sigma \vec{e} + \frac{\partial \vec{d}}{\partial t} \tag{4.2}$$

$$\nabla \cdot \vec{d} = \rho \tag{4.3}$$

$$\nabla \cdot \vec{b} = 0 \tag{4.4}$$

where $\vec{e} = \vec{e}(\vec{r}, t)$ and $\vec{h} = \vec{h}(\vec{r}, t)$ are electric and magnetic field vectors, resp., $\vec{d} = \vec{d}(\vec{r}, t)$ and $\vec{b} = \vec{b}(\vec{r}, t)$ are corresponding electric and magnetic flux densities, ρ being the space charge density and σ the electrical conductivity. $\vec{b}$ and $\vec{d}$ are connected by the parameters ε and μ which describe dielectric and magnetic properties of the medium:

$$\vec{d} = \varepsilon\vec{e} = \varepsilon_0\vec{e} + \varepsilon_r\vec{e} = \varepsilon_0\vec{e} + \vec{p} \tag{4.5}$$

$$\vec{b} = \mu\vec{h} = \mu_0\vec{h} + \mu_r\vec{h} = \mu_0\vec{h} + \vec{m} \tag{4.6}$$

where $\vec{p}$ and $\vec{m}$ is the electric or the magnetic polarization of the wave, resp.

An SiO_2 transmission medium which is of infinite extension has the following properties:

- $\sigma = 0$, the medium is free of losses, its conductivity equals zero.
- $\rho \equiv 0$, there are no space charges within the medium.
- $\mu \equiv \mu_0$ or $\mu_r \equiv 0$, resp., the dielectric medium is not magnetic.
- $\varepsilon = \varepsilon_0\varepsilon_r(\vec{r})$, the medium is inhomogenous (because of the dependence of place), but isotropic (because of the independence of direction).

With these values, (4.1) to (4.4) take the following form:

$$\nabla\times\vec{e} = -\frac{\partial\vec{b}}{\partial t} \tag{4.7}$$

$$\nabla\times\vec{h} = \frac{\partial\vec{d}}{\partial t} \tag{4.8}$$

$$\nabla\cdot\vec{d} = 0 \tag{4.9}$$

$$\nabla\cdot\vec{b} = 0 \tag{4.10}$$

By taking the curl of (4.7) and making use of (4.5) as well as of

$$\frac{1}{c^2} = \mu_0\varepsilon_0, \tag{4.11}$$

c being the velocity of light, one obtains

$$\nabla\times\nabla\times\vec{e} = -\frac{1}{c^2}\frac{\partial^2\vec{e}}{\partial t^2} - \mu_0\frac{\partial^2\vec{p}}{\partial t^2} . \tag{4.12}$$

The behaviour of a dielectric medium to intense electromagnetic fields is nonlinear. This effect is due to the anharmonic motion of bound electrons under the influence of an outer field [7]. Therefore, the induced polarization $\vec{p}$ from the electric dipoles is not linear in the electric field $\vec{e}$ and obeys the relation

$$\vec{p} = \varepsilon_0(\chi^{(1)}*\vec{e} + \chi^{(2)}*\vec{e}\vec{e} + \chi^{(3)}*\vec{e}\vec{e}\vec{e} + \ldots) \tag{4.13}$$

where $\chi^{(j)}$ is the jth order susceptibility of the dielectric medium. $\chi^{(j)}$ is a tensor of rank $j+1$, $*$ denotes the convolution. $\chi^{(1)}$, the linear susceptibility, is responsible for the two linear effects of refraction and attenuation, represented by the refractive index n and the attenuation coefficient α. The second-order susceptibility is responsible for nonlinear effects as second-harmonic generation and sum-frequency generation. Because of the inversion symmetric molecular structure of fused silica, $\chi^{(2)}$ is zero [8]. Nonlinear effects like third order harmonic generation, four-wave mixing and nonlinear refraction are caused by the third-order susceptibility $\chi^{(3)}$. By neglecting higher-order nonlinearities because of their weak effects, (4.13) can therefore be written as

$$\begin{aligned}\vec{p} &= \varepsilon_0(\chi^{(1)}*\vec{e} + \chi^{(3)}*\vec{e}\vec{e}\vec{e}) \\ &= \varepsilon_0\left(\int_0^\infty \chi^{(1)}(\vec{r},\tau)\vec{e}(\vec{r},t-\tau)d\tau + \right. \\ &\qquad \left. \int_0^\infty\int_0^\infty\int_0^\infty \chi^{(3)}(\vec{r},\tau_1,\tau_2,\tau_3)\vec{e}(\vec{r},t-\tau_1)\vec{e}(\vec{r},t-\tau_2)\vec{e}(\vec{r},t-\tau_3)d\tau_1 d\tau_2 d\tau_3\right)\end{aligned} \tag{4.14}$$

In isotropic media, the susceptibility tensors $\chi^{(1)}$ and $\chi^{(3)}$ consist of only one element so that $\chi^{(1)}(\vec{r},t) = \chi^{(1)}_{x;x}(\vec{r},t)$ and $\chi^{(3)}(\vec{r},t_1,t_2,t_3) = \chi^{(3)}_{x;xxx}(\vec{r},t_1,t_2,t_3)$ and (4.12) and (4.14) can further be simplified. Still, their complexity prevents a straightforward solution, and it is necessary to make some simplifying approximations. The nonlinear response can be assumed to be instantaneous which originates in neglecting the contribution of molecular

vibrations to $\chi^{(3)}$. For silica fibres, this response time is in the range of 60 fs [1], thus this approximation holds for pulse widths > 1 ps.

Another simplification is to treat the second term on the right hand side of (4.14), which can be viewed as the nonlinear induced polarization, as a small perturbation to the total induced polarization. Because of the relatively weak nonlinear effects in silica fibres, this is justified [32]. So by setting the nonlinear part of the polarization to zero, the simplified (4.14), together with (4.12) and taking it into the Fourier domain, we obtain:

$$\nabla\times\nabla\times\vec{E}(\vec{r},\omega)-\frac{\omega^2}{c^2}\varepsilon(\vec{r},\omega)\vec{E}(\vec{r},\omega) = 0 \tag{4.15}$$

where we made use of the definition of the frequency-dependent dielectric constant

$$\varepsilon(\vec{r},\omega) = 1+\tilde{\chi}^{(1)}(\vec{r},\omega)+\varepsilon_{NL}(\vec{r},\omega). \tag{4.16}$$

$\varepsilon_{NL}(\vec{r},\omega)$ is the nonlinear contribution to the dielectric constant and is defined by

$$\varepsilon_{NL}(\vec{r},\omega) = \frac{3}{4}\chi^{(3)}_{x;xxx}(\vec{r})\left|\vec{E}(\vec{r},\omega)\right|^2 \tag{4.17}$$

With the help of the development theorem of Graßmann[1] and an estimation for $\nabla(\nabla\vec{e})$ [33] as well as the relation $\nabla\nabla = \Delta$, (4.15) leads to

$$\Delta\vec{E}(\vec{r},\omega)+\frac{\omega^2}{c^2}\varepsilon(\omega)\vec{E}(\vec{r},\omega) = 0 \tag{4.18}$$

where we dropped the notification of $\vec{r}$ as a parameter of ε, since the permittivity ε is not dependent on $\vec{r}$ within the fibre core. (4.18) is the time-free wave equation or the Helmholtz equation. It is obvious, that by using the definition

$$\varepsilon(\omega) = \left(\tilde{n}-j\frac{c}{\omega}\frac{\tilde{\alpha}}{2}\right)^2 = \underline{\tilde{n}}(\omega)^2 \tag{4.19}$$

where $\underline{\tilde{n}}(\omega)$ the complex refractive index, $\tilde{n} = \tilde{n}(\omega)$ the refractive index of the fibre core and $\alpha(\omega)$ the attenuation coefficient, $\tilde{n}$ and α become intensity dependent because of ε_{NL}. It has become common to introduce $\tilde{n} = n+n_2\left|\vec{E}(\vec{r},\omega)\right|^2$ and $\tilde{\alpha} = \alpha+\alpha_2\left|\vec{E}(\vec{r},\omega)\right|^2$. The

[1]The development theorem of Graßmann reads: $\nabla\times\nabla\times\vec{x} = \nabla(\nabla\vec{x})-(\nabla\nabla)\vec{x}$

nonlinear parts of $\tilde{n}$ and α are then given by

$$n_2 = \frac{3}{8n}\mathrm{Re}(\chi^{(3)}_{x;xxx}) \tag{4.20}$$

$$\alpha_2 = \frac{3\omega_0}{4nc}\mathrm{Im}(\chi^{(3)}_{x;xxx}) \; . \tag{4.21}$$

In order to solve (4.18), it is necessary to choose a suitable system of coordinates. We identify the vector $\vec{E}$ with its component E_x, assuming that $E_y \equiv E_z \equiv 0$ without loss of generality. For reasons of simplicity E denominates the x-component of $\vec{E}$ in the following. By separating the electric field into

$$E(\vec{r}, \omega) = F(x, y)A(z, \omega - \omega_0)e^{j\beta z} \tag{4.22}$$

where $F(x, y)$ describes the modal distribution of the fundamental fibre mode, $A(z, \omega - \omega_0)$ is the *slowly varying envelope approximation* (SVE) and $\beta = \beta(\omega)$ the propagation constant[2], the Helmholtz equation leads to two differential equations in F and A. The differential equation for A can be transformed and by expanding $\beta(\omega)$ in its Taylor series about ω_0

$$\begin{aligned} \beta(\omega) &= \omega\sqrt{\varepsilon\mu_0} \\ &= \frac{\omega}{c}\tilde{n} \\ &= \beta_0 + (\omega - \omega_0)\beta_1 + (\omega - \omega_0)^2\beta_2 + \ldots \end{aligned} \quad , \tag{4.23}$$

with $\beta_j = \left(\frac{d^j}{d\omega^j}\beta(\omega)\right)_{\omega = \omega_0}$, $j = 0, 1, 2, \ldots$

the nonlinear Schrödinger equation is derived

$$\frac{\partial A}{\partial z} + \beta_1\frac{\partial A}{\partial t} + j\frac{1}{2}\beta_2\frac{\partial^2 A}{\partial t^2} + \frac{\alpha}{2}A - j\frac{\omega_0}{c}n_2|A|^2A = 0 \; . \tag{4.24}$$

β_1 is related to the group velocity v_g by $\beta_1 = \frac{1}{v_g}$, β_2 is the second order dispersion coefficient.

By introducing the retarded and normalized time [44]

[2] If $\chi^{(3)}$ is neglected, the fibre's transfer function reads $H(j\omega) = e^{-j\beta L}$, L being the fibre length.

$$\tau = t - \beta_1 z \ , \tag{4.25}$$

which leads to a fixed „observation window“ that travels with the envelope of the information signal, and the definition of the normalized complex envelope

$$U(z, \tau) := \sqrt{\frac{1}{2}\varepsilon_0 n_0 c A_{eff}}\, A(z, t) = \sqrt{\frac{1}{2}\varepsilon_0 n_0 c A_{eff}}\, A(z, \tau + \beta_1 z) \tag{4.26}$$

where A_{eff} is the effective core area and given by

$$A_{eff} = \frac{\left(\int_{-\infty}^{\infty} \int_{-\infty}^{\infty} |F(x, y)|^2 dx dy \right)^2}{\int_{-\infty}^{\infty} \int_{-\infty}^{\infty} |F(x, y)|^4 dx dy} \ , \tag{4.27}$$

(4.24) can be transformed into

$$\frac{\partial U}{\partial z} + j\frac{1}{2}\beta_2 \frac{\partial^2 U}{\partial \tau^2} + \frac{\alpha}{2} U - j\gamma_{nl} |U|^2 U = 0 \ . \tag{4.28}$$

The medium power referred to the effective core area is hereby related with the square of the absolute value of the complex envelope by

$$P(z, t) = |U(z, \tau)|^2 = A_{eff} \cdot I(z, t) \, , \tag{4.29}$$

$I(z, t)$ being the slowly varying intensity of the electrical field. The effective area A_{eff} is a measure for that part of the cross section of the fibre, in which most of the modal energy is distributed. In equation (4.28), γ_{nl} is the nonlinearity coefficient which is defined by

$$\gamma_{nl} = \frac{n_2^I \omega_0}{c A_{eff}} \tag{4.30}$$

and is known as the coefficient of nonlinear phase shift, n_2^I is the Kerr coefficient referred to the intensity $I(z, t)$.

(4.28) can be solved numerically by using the split-step-Fourier algorithm which is described in [1]. This numerical algorithm is not subject of this work, for a detailed descrip-

tion of this method, please refer to [1]. (4.28) describes the propagation of a single wavelength signal including the linear effects of *attenuation*, *dispersion* and the nonlinear effect of *self-phase modulation* due to the Kerr effect. Further nonlinear effects like the *stimulated Brillouin scattering* (SBS) and the *stimulated Raman scattering* are not included. Both linear and nonlinear effects will be described in the next sections.

4.1.2 Attenuation

The attenuation characteristics of typical standard telecommunication fibres originates from a combination of several effects. At wavelengths less than 1.3 µm, the attenuation is mainly caused by scattering of the electromagnetic wave at microscopic inhomogenities [5], [66]. Since the spatial extension of these inhomogenities is smaller than the wavelength of the incident light wave, these scattering losses can be viewed as Rayleigh scattering which is proportional to the wavelength of the light by $1/\lambda^4$. The Rayleigh scattering represents a lower boundary for the attenuation which can by no means be fallen below (see Figure 4.2).

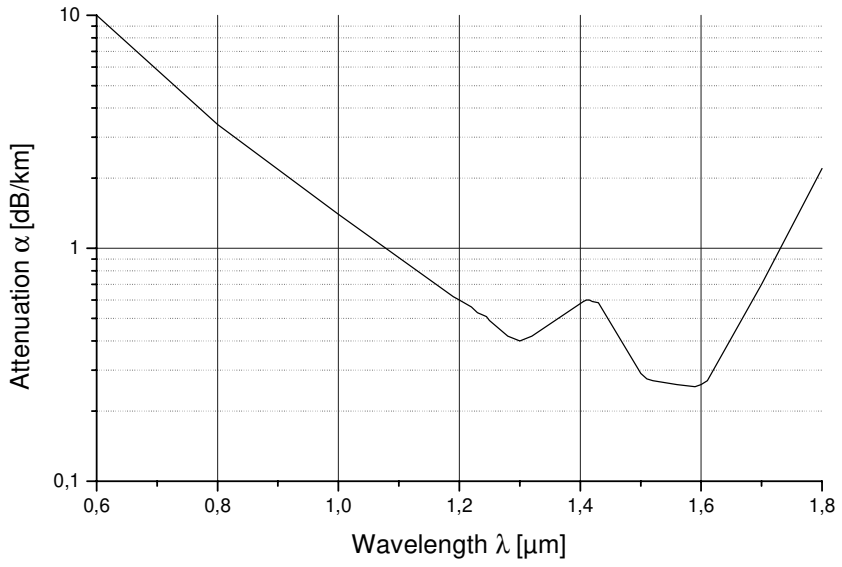

Figure 4.2: Attenuation of a standard single mode fibre (according to [33])

Doping of the core in order to adjust the refractive index profile leads to further scattering and thus increases the attenuation. Above 1.6 µm, the losses result from strong absorption (IR absorption) due to resonance vibrations of the silica molecules. The absolute minimum of the fibre attenuation determined by the effects just mentioned is situated at around 1.6 µm. A lot of fibres show a peak of the attenuation curve close to 1.4 µm.

This peak originates from absorption losses due to resonances of OH ions which get into the fibre core during the production process. The fundamental oscillation of the OH resonance is at $\lambda = 2.73\ \mu m$, so that the first harmonic oscillation is excited with a wavelength of 1.37 µm. Newly fabricated fibres show a very much smaller attenuation peak at 1.4 µm. According to Figure 4.2, there are two attenuation minima, at 1.3 µm with an attenuation of approximately 0.2 dB/km and at 1.55 µm with 0.4 dB/km. Both wavelengths are to be preferred for fibre optic signal transmission.

Going back to (4.28), setting $\beta_2 \equiv 0$ and $\gamma \equiv 0$, we obtain for the electric field or the square root of the normalized power, resp.

$$\frac{\partial U(z,\tau)}{\partial z} = -\frac{\alpha}{2} U(z,\tau) . \tag{4.31}$$

Solving this equation leads to the simple relation

$$U(z,\tau) = U(z=0,\tau) \cdot e^{-\frac{\alpha}{2}z} \tag{4.32}$$

where α is the wavelength dependent attenuation factor.

Neglecting the absorption due to OH impurities (which is, as mentioned above, thoroughly realistic for newer fibres), the wavelength dependence of α can be described by the emprical formula [27]

$$\alpha(\nu) = \left(\frac{\nu}{3057\text{THz}}\right)^4 \text{m}^{-1} + \left(\frac{156,6\text{THz}}{\nu}\right)^{58} \text{m}^{-1} , \tag{4.33}$$

ν being the optical carrier frequency ranging from 175 THz to 350 THz or λ ranging from 857 nm to 1700 nm, resp. The first term on the right hand side of (4.33) describes the attenuation due to the Rayleigh scattering, whereas the second term stems from the IR absorption. α can be converted to the more practically oriented unit dB/km by $\alpha[\text{dB/km}] = \alpha \cdot 10\log e$ [1]. The wavelength dependence can be neglected if the bandwidth of the information signal, be it single- or multiwavelength, is very much less than the carrier frequency. Since this is the usual case, α is not regarded as wavelength dependent for the information signal in this work.

4.1.3 Dispersion

While the wavelength dependence of the attenuation α can be neglected when focussing on the information signal, the chromatic dispersion shows a wavelength dependence which has a strong influence on the system performance. The chromatic dispersion is, like the attenuation, another linear effect of light propagation in optical fibres. It is made up of two different parts:

- the material dispersion and
- the waveguide dispersion [33].

The *material dispersion* is based on the wavelength dependence of the refractive index $n(\lambda)$. The response of the medium generally depends on the optical frequency, when an incident light wave propagates through the fibre and interacts with the bound electrons of the dielectric.

The *waveguide dispersion* originates from the wavelength dependence of the transverse field distribution of the modal energy in core and cladding. With increasing wavelength, the part of the modal energy which propagates in the cladding of the fibre increases. Due to the smaller refractive index in the cladding of the fibre, the part of the light wave in the cladding propagates faster than the one in the core, leading to run-time differences and to pulse broadening.

Since the waveguide dispersion depends on fibre-design parameters such as core radius and core-cladding index difference, it can be adjusted according to desired values. Eventually, both kinds of dispersion can compensate each other. By taking advantage of this fact, fibres with dispersion minima at different nulls can be fabricated. Whereas older standard fibres had their dispersion minima of $1\,\mathrm{ps}/(\mathrm{nm}\cdot\mathrm{km})$ at 1.3 µm, the newer dispersion-shifted fibres (DSF) have a dispersion minimum which falls together with the attenuation minimum at 1.55 µm. Still, most telecommunication fibres deployed in the last years are SSMF with a high dispersion. The broader the spectrum of the pulse (the narrower in the time domain), the stronger the distortion of the pulse is, since different spectral components associated with the pulse travel at different speeds.

The frequency dependence of the refractive index can empirically be described by the Sellmeier equation [47], [1]

$$n^2(\nu) = 1 + \sum_{j=1}^{3} \frac{B_j}{1 - \left(\frac{\nu}{\nu_j}\right)^2}, \tag{4.34}$$

where ν is the optical carrier frequency, ν_j the characteristic resonance frequency at which the medium absorbs the electromagnetic radiation through oscillations of bound electrons and B_j the strength of the jth resonance.

In order to describe the phenomenon of dispersion mathematically, it is useful to expand the mode-propagation constant β in a Taylor series as has already been mentioned in (4.23). β_1 can then be identified with the specific group delay τ_g, the inverse of the specific group velocity v_g, which is the velocity, at which the envelope of the pulse moves along the fibre.

$$\beta_1 = \left.\frac{d\beta(\omega)}{d\omega}\right|_{\omega=\omega_0} = \tau_g = \frac{1}{v_g}. \tag{4.35}$$

β_2 characterizes the dispersion of the fibre and is often called group-velocity dispersion (GVD) parameter or dispersion coefficient. It is related to the dispersion parameter D_ν which is used more commonly by

$$\beta_2 = \left.\frac{d\beta_1(\omega)}{d\omega}\right|_{\omega=\omega_0} = \frac{d}{d\omega}\left(\frac{1}{v_g}\right) = \frac{1}{2\pi} D_\nu. \tag{4.36}$$

Another common quantity is the dispersion parameter D_λ which can be obtained by

$$D_\lambda = \left.\frac{d\beta_1(\lambda)}{d\lambda}\right|_{\lambda=\lambda_0} = \frac{-2\pi c}{\lambda^2}\beta_2 \tag{4.37}$$

A measured variation of D_λ can be seen in Figure 4.3. A remarkable point of that curve is the crossover at approx. 1.3 µm. This wavelength is often referred to as the zero-dispersion wavelength λ_D. If pulse propagation close to or in the 1.29 µm regime or pulses of duration shorter than 0.1 ps are to be examined, the third order term of the Taylor series of $\beta(\omega)$ has to be considered in the calculations. The crossover divides the transmission band in two distinct parts. Carrier wavelengths $\lambda < \lambda_D$ which is equivalent to $\beta_2 > 0$, $D_\nu > 0$ or $D_\lambda < 0$ are said to be in the *normal dispersion* regime, whereas the fibre exhibits *anomalous dispersion* at wavelengths $\lambda > \lambda_D$ or $\beta_2 < 0$, $D_\nu < 0$, $D_\lambda > 0$ resp. A pulse which travels in the normal dispersion regime is subject to a pulse broadening which originates from the fact, that the higher frequency components (shorter wavelengths) of the pulse travel slower than the lower frequency components (longer wavelengths).

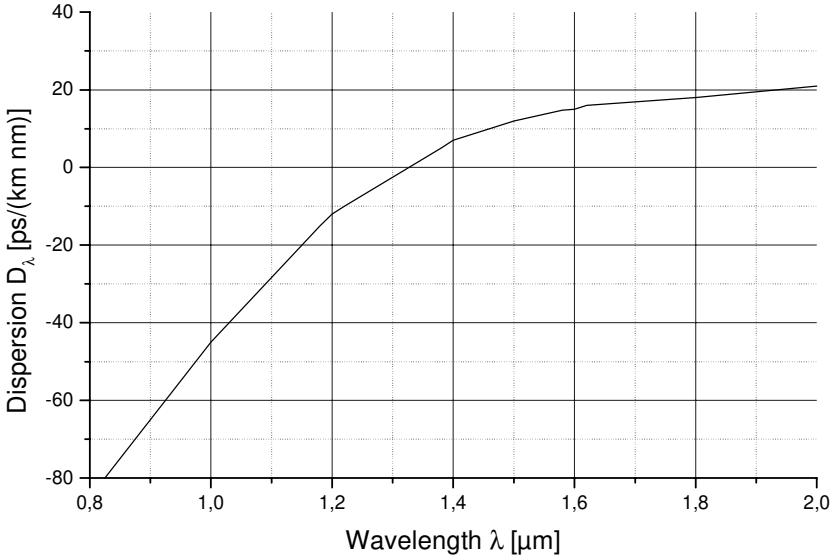

Figure 4.3: Measured wavelength dependence of chromatic dispersion (according to [33])

As already mentioned, fibre optic communication usually takes place in the so-called 2nd and 3rd optical window at 1.3 µm and 1.55 µm. Both wavelengths lie in the anomalous dispersion regime. Keeping in mind that $\beta_2 < 0$ in the anomalous dispersion regime, it becomes clear that higher frequency components (shorter wavelengths) travel faster than the lower frequency components (longer wavelengths). It is in this regime that the effects of GVD and self-phase modulation (SPM), which is to be explained in 4.1.4, can compensate each other. This phenomenon is taken advantage of in the transmission of optical solitons where dispersion and SPM are brought into balance by a careful choice of pulse shape and pulse power [1]. Optical solitons will not be of further consideration in this work.

A useful measure for the impact of the group-velocity dispersion is the dispersion length L_D which is defined by

$$L_D = \frac{T_0^2}{|\beta_2|}, \tag{4.38}$$

T_0 being the initial half-width of the pulse at intensity of $1/e$. The dispersion length represents the propagation distance after which the effect of GVD becomes clearly visible, i.e. the pulse distortion caused by the GVD can no longer be neglected.

In order to study the physical effects of GVD, it is useful to examine (4.28) in a linear, loss-free medium by setting $\gamma \equiv 0$ and $\alpha \equiv 0$. (4.28) then becomes

$$\frac{\partial U}{\partial z} = -j\frac{1}{2}\beta_2\frac{\partial^2 U}{\partial \tau^2} \tag{4.39}$$

which is readily solved using the Fourier transform. Given an initial Gaussian pulse shape with its electrical field distribution

$$U(z = 0, \tau) = U_0 e^{-\frac{\tau^2}{2T_0}}, \tag{4.40}$$

U_0 being the amplitude, the pulse thus develops into

$$U(z, \tau) = \frac{U_0 T_0}{\sqrt{T_0^2 - j\beta_2 z}} e^{-\frac{\tau^2}{2(T_0^2 - j\beta_2 z)}}. \tag{4.41}$$

It must be noted that it has become common practice to use the full width half maximum (FWHM) instead of the half-width at intensity $1/e$. For a Gaussian pulse, these two are related by $T_{FWHM} = 2\sqrt{\ln 2}T_0 \approx 1.665T_0$.

Looking at (4.41), it can be seen that a Gaussian pulse maintains its shape during propagation, but its amplitude decreases (even in the absence of attenuation) by a factor of $T_0^2/(T_0^2 + \beta_2 z)^2$, whereas the width of the pulse increases by a factor of $\sqrt{1 + (z/L_D)^2}$, as follows from extending the fraction of the exponent of (4.41) with its complex conjugate and comparing the result with (4.40). After a Gaussian pulse has propagated over a length of the dispersion length L_D, its width has broadened by a factor of $\sqrt{2} \approx 1.414$.

(4.41) may furthermore serve as explanation of the *chirp*, a modulation of the phase $\phi(\tau)$. Whereas (4.40) has no time-dependent phase, this does not hold for (4.41). By separating the right-hand side of (4.41) into amplitude and phase, one obtains a time-dependent phase term, where its deviation with respect to time is proportional to the sign of β_2 (corresponding to normal or anomal dispersion), to the normalized time τ and to the propagation distance z by $z/(1 + z^2)$:

$$\Delta\omega = -\frac{d\phi}{d\tau} \sim \mathrm{sgn}(\beta_2) \cdot \tau \cdot \frac{z}{(1 + z^2)} \tag{4.42}$$

Thus, the chromatic dispersion inevitably introduces a frequency shift which leads not

only to pulse spreading in the time domain as discussed above, but also to pulse spreading in the frequency domain. Since the right-hand side of (4.42) is linear in τ, (4.42) is often referred to as the linear frequency chirp.

In the anomalous dispersion regime ($\beta_2 < 0$), e.g., this leads to a shift to higher frequencies (shorter wavelengths) $\Delta\omega > 0$ at the front flank ($T < 0$) of the pulse and to a shift to lower frequencies (longer wavelengths) at the back flank of the pulse.

4.1.4 Nonlinear refraction - Self-phase modulation

As mentioned in section 4.1.1 in (4.30), the refractive index of silica is not independent of the power of the propagating lightwave. The lightwave itself changes its propagation constant by its own intensity, leading to a nonlinear phase shift. This effect, which occurs at power levels easily reached in common transmission systems operating at 1.3µm and 1.55µm, is called the *Kerr-effect*. Starting with (4.23) and replacing $\tilde{n}$ by

$$\tilde{n} = n + n_2 \frac{P(z, \omega)}{A_{eff}}, \tag{4.43}$$

where $P(z, \omega) = |U(z, \omega)|^2$ and A_{eff} the effective core area of the fibre as defined in (4.27), n the refractive index which is responsible for the chromatic dispersion as described in 4.1.3 and n_2 the Kerr coefficient[3], (4.23) holds for

$$\underline{\beta}(\omega) = \frac{\omega}{c}\left(n + n_2 \frac{P(z, \omega)}{A_{eff}}\right) - j\frac{\alpha}{2} = \frac{\omega}{c}(n + n_2 I(z, \omega)) - j\frac{\alpha}{2}, \tag{4.44}$$

$I(z, \omega)$ being the intensity of the lightwave. Typical values are $n = 1.445$ and $n_2 = 3.0 \cdot 10^{-20}\ m^2/W$ for single mode silica fibres at 1.55µm.

In order to derive the nonlinear phase shift caused by the Kerr-Effect, it is usual to solve the nonlinear Schrödinger equation while neglecting the chromatic dispersion and the attenuation. The same result can be obtained much more easily by setting (4.44) in the idealized fibre's transfer function $H(j\omega) = e^{-j\underline{\beta}(\omega)z}$. This leads to

$$H(j\omega) = e^{-\frac{\alpha}{2}z} e^{-j\phi(z, \omega)} = e^{-\frac{\alpha}{2}z} e^{-j\frac{2\pi}{\lambda}nz} e^{-j\frac{2\pi}{\lambda}n_2 I(z, \omega)z}. \tag{4.45}$$

The first term on the right-hand side of (4.45) describes the attenuation, the second term the

[3] n_2 is related to n_2^I by $n_2^I = \frac{2n_2}{\varepsilon_0 c n}$

linear phase shift and the third term the nonlinear (due to the dependence on the intensity) phase shift caused by the Kerr-Effect. Thus, the instant frequency $\Delta\omega = -\frac{\partial\phi}{\partial t}$ is

$$\Delta\omega = -2\pi n_2 \frac{z}{\lambda}\frac{\partial I}{\partial t}. \tag{4.46}$$

The intensity of the lightwave thus changes its own frequency and phase. Therefore, the Kerr-Effect or its consequences, resp., is also called *self-phase modulation* (SPM).

The change in frequency relative to the carrier frequency is called frequency chirp. Analyzing (4.46), it can be seen that the front part of an impulse (the incline, $\partial I/\partial t > 0$) is shifted towards lower frequencies ($\Delta\omega < 0$) or longer wavelengths, resp. The opposite holds for the back part of the impulse (decline, $\partial I/\partial t < 0$), which is shifted to higher frequencies or shorter wavelengths, resp. [31].

The SPM can be used to compensate the chromatic dispersion. Since in the anomalous dispersion regime, the higher frequency parts of an impulse travel faster than the lower ones, the higher frequency parts are shifted towards the front end of the impulse, the lower ones towards the back end. This effect is perfectly oppositional to the one caused by SPM. By carefully choosing of impulse form and power, both effects can completely compensate each other. The so-called solitons make use of this phenomenon.

In the normal dispersion regime, both effects coincide together and lead to even further pulse broadening.

A practical measure to assess the impact of the SPM on a transmission system is the nonlinear length which is defined by

$$L_{NL} = \frac{1}{\gamma_{nl} P_0} = \left(\frac{n_2^I \omega_0}{c A_{eff}} P_0\right)^{-1}, \tag{4.47}$$

where P_0 is the peak power of the impulse at $z = 0$. The nonlinear length is the effective propagation distance at which the nonlinear phase induced by the Kerr-Effect is 1 (rad), a value at which the effect on the propagating impulse is clearly visible. For SSMF, $L_{NL} \approx 150$ km at peak powers of 5 mW.

4.1.5 Stimulated Raman Scattering

The process of stimulated Raman scattering (SRS) leads to a significant loss of signal energy in the fibre, especially at high input powers. SRS results from stimulated inelastic scattering of incident laser light at molecules of the nonlinear transmission medium, where energy of the optical field is transferred partially to the silica molecules (see Figure 4.4). It describes the parametric interaction of light with molecular vibrations.

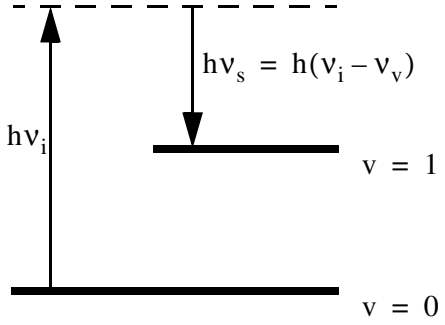

Figure 4.4: Energy levels of silica molecule involved in Raman scattering (schematic)

An incident photon of the irradiating laser light of frequency ν_i is absorbed by the silica molecule while, simultaneously, a so-called Stokes photon with frequency $\nu_s < \nu_i$, the *Stokes frequency*, is emitted [79]. To conserve the total energy of the process, the silica molecule is excited to the vibrational level $v = 1$, i.e. a phonon with suitable energy and momentum is produced. The Stokes frequency is determined by the vibrational modes of the medium. This property is oppositional to elastic scattering processes such as the Rayleigh scattering, where the scattering process is accompanied without any frequency conversion.

In another point of view, the incident lightwave acts as a pump for the frequency-shifted wave. With increasing fibre length, more and more energy from the incident lightwave with frequency ν_i is transferred to the generated lightwave at ν_s, leading to an attenuation of the incident wave and an amplification of the generated wave. Keeping this in mind, the Raman-gain coefficient g_R can be defined in order to estimate the impact of SRS on a propagating light wave. The threshold power P_{th}, which is defined as the incident power at which half of the power is lost to the generated Stokes wave at the output end of a fibre of length L, can be estimated by [2]

$$g_R P_{th} \frac{L_{eff}}{A_{eff}} \approx 16 . \tag{4.48}$$

A_{eff} is the previously mentioned effective core area, sometimes referred to as the effective mode cross section, and L_{eff} the effective length of the fibre which can be computed from the actual fibre length L and its attenuation coefficient α by

$$L_{eff} = \frac{1 - e^{-\alpha L}}{\alpha} . \tag{4.49}$$

Since silica is an amorphous material and not crystalline, there exists not only one energy level with a Stokes frequency of ν_s but a whole continuum. The spectral behavior of the Raman-gain coefficient can be seen in Figure 4.5, it scales inversely with the pump wavelength [68].

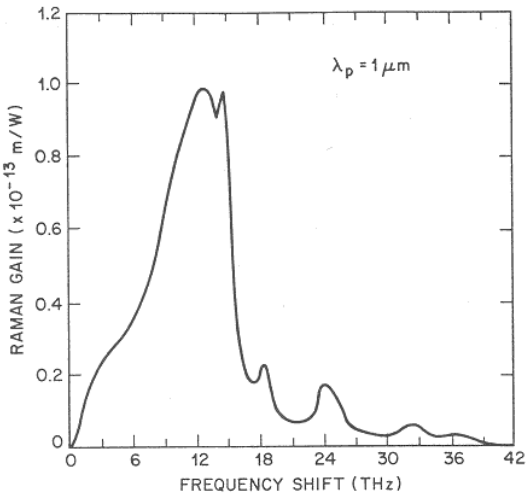

Figure 4.5: Measured Raman-gain spectrum for fused silica at a pump wavelength of 1µm [10]

In the usual case of a standard single mode fibre at 1.55 µm, P_{th} equals 410 mW approx. This threshold is well over the used power levels in communication systems of 10 mW approx. Stimulated Raman scattering is therefore not to be taken into consideration in single channel applications.

4.1.6 Stimulated Brillouin Scattering

Stimulated Brillouin scattering (SBS) is a nonlinear process that can occur in optical fibres at input power levels much lower than those needed for SRS. SBS manifests through a depletion of the incident wave and, in addition, generates a potentially strong

scattered beam propagating back towards the launch origin.

The underlying process is - classically seen - the generation of acoustic waves, travelling at the speed of sound, which is less than 5 km/s in glass, through the incident light wave by electrostriction. While travelling through the solid, transparent silica material, these sound waves induce spatially periodic local compressions and expansions that in turn cause local increases and decreases in the refractive index. This is called the photoelastic effect. The magnitude of the photoelastic effect increases with increasing input optical power. The pump-induced index grating scatters the incident (pump) light through Bragg diffraction.

Quantum-mechanically spoken, the pump photon is annihilated and a (Stokes) photon of lower frequency and an acoustic phonon are created simultaneously. In this inelastic hit incident, both energy and momentum of the involved particles must be conserved:

$$E_a = E_p - E_s \tag{4.50}$$

$$\vec{k}_a = \vec{k}_p - \vec{k}_s \tag{4.51}$$

where $E_a = h\nu_a$ is the photon energy of the acoustic phonon, E_p and E_s the energy of the (incident) pump wave and the (scattered) Stokes wave, resp., and $\vec{k}_a$, $\vec{k}_p$ and $\vec{k}_s$ the wave vectors. The newly generated wave is therefore downshifted in frequency by a value determined by [68]

$$\nu_a = 2n\nu_p \frac{v_a}{c} \sin\left(\frac{\theta}{2}\right) \tag{4.52}$$

where n is the refractive index of the SSMF, $\nu_p = 193\ \text{Thz}$ the frequency of the pump wave, $v_a \approx 5\text{km/s}$ the velocity of the acoustic wave in glass, c the speed of light and θ being the angle between scattered and acoustic wave. The relevant directions in a SSMF are certainly the forward and backward directions. From (4.52), it can be seen that SBS does not occur in the forward direction ($\theta = 0$), but has a maximum in the backward direction ($\theta = \pi$). Using $n = 1.45$, $\nu_a \approx 10\text{GHz}$. According to (4.50), a part of the energy of the incident wave is transferred into the acoustic wave and the scattered wave is generated at a frequency 10 Ghz lower than the carrier frequency of the incident wave. This energy transfer manifests as an additional loss of the input signal. Using a similar approach as for SRS, the

threshold power P_{th} can be estimated by [68]

$$g_B P_{th} \frac{L_{eff}}{A_{eff}} \approx 21 \tag{4.53}$$

where g_B is the Brillouin gain coefficient, L_{eff} and A_{eff} the effective length and the effective core area, resp., as defined in 4.1.5. For silica fibres, $g_B \approx 5 \cdot 10^{-11} \frac{m}{W}$ [68] which is more than two orders of magnitude larger than g_R, the gain coefficient of SRS. Using typical values of $A_{eff} = 50\mu m^2$, $L_{eff} = 50km$, (4.53) leads to a threshold power of only $P_{th} \approx 3$ mW.

Because of its low threshold, SBS can limit the launch power in SSMF. However, (4.53) neglects both the effect of spectral width associated with the incident light and its modulation. The optical bandwidth of SBS is only approx. 30 MHz. Maximum SBS gain will therefore only occur for pump lasers with linewidths less than 30 MHz. For laser diodes with linewidths usually much larger than 30 MHz, SBS gain decreases. Furthermore, unlike SRS, the SBS gain depends on the signal modulation, because the origin of SBS involves a process which is not instantaneous on the time scale of the information rate. High modulation rates lead to broad optical spectra and, thus, a further reduction of SBS gain. In ASK systems, the SBS gain g approaches $g_B/4$ for bit rates much higher than the Brillouin spectral width.

In typical fibre communication systems with bit rates of 625 Mbit/s and higher, the SBS power threshold is approx. 12 mW. Though it is much less than SRS power thresholds, it can still be neglected, since typical modulated signals have average channel powers below this threshold. Another possibility to increase the critical power threshold is to low-frequency dither the bias current of the laser diode which increases the effective bandwidth of the signal.

4.2 Propagation of multiple-carrier wavelength light signals in optical transmission fibres

There are several possibilities in order to increase the capacity of an optical transmission link. Going beyond data rates of 40 Gbit/s in a single channel is getting more and more difficult because of the limitation of switching speeds of electronic circuits. Currently, fast electronic devices can handle signals up to 40 GHz.

Another possibility is to transmit signals at different wavelengths on the same optical

fibre. These signals have to be spectrally separated, so that they can be distinguished at the receiver by bandpass filters. In a strongly linear transmission medium, these different channels would not interact with each other. Because of the nonlinearities occurring in optical fibres, these signals interfere with each other leading to signal distortions and creation of new wavelengths. These additional effects are to be studied in the following paragraphs.

4.2.1 Cross-phase modulation

Similar to the self-phase modulation, cross-phase modulation (XPM) occurs, because the effective refractive index of the transmission medium depends on the signal intensity being transferred through the medium. In the case of a single wavelength transmission, it is only the intensity of the particular wave which can change the effective refractive index and which leads to the effect of SPM. In the case of multiple wavelengths, the effective refractive index which a wave sees is not only changed by its own intensity, but is additionally influenced by the intensity of other copropagating waves.

In order to derive the nonlinear Schrödinger equation in the case of two or more copropagating waves, we define the electric field of the propagating wave as being proportional to

$$\vec{e}(\vec{r}, t) \sim E_1 e^{j\omega_1 t} + E_2 e^{j\omega_2 t}\,, \tag{4.54}$$

where ω_1 and ω_2 are the angular carrier frequencies of the two signals and E_1 and E_2 are the slowly varying amplitudes. The evolution of E_1 and E_2 is governed by the wave equation and their derivation is analogous to the single wavelength case in 4.1.1 [1]. Both waves are influenced by an intensity-dependent nonlinear phase which can be depicted as

$$\phi_1^{nl} = \frac{\omega_1 z n_2}{c}\left(|E_1|^2 + 2|E_2|^2\right) \text{ and} \tag{4.55}$$

$$\phi_2^{nl} = \frac{\omega_2 z n_2}{c}\left(|E_2|^2 + 2|E_1|^2\right) \tag{4.56}$$

for signal 1 and signal 2, resp. Whereas the first term on the right-hand side of (4.55) and (4.56) describes the SPM, the second term is responsible for the XPM. It is noteworthy to say that XPM is twice as effective as SPM for a given intensity as indicated by the factor of 2 in

(4.55) and (4.56).

Analogous to 4.1.1, the coupled nonlinear Schrödinger equations in the case of two propagating waves at different wavelengths can be derived as [1]

$$\frac{\partial A_1}{\partial z} + \beta_{11}\frac{\partial A_1}{\partial t} + j\frac{1}{2}\beta_{21}\frac{\partial^2 A_1}{\partial t^2} + \frac{\alpha_1}{2}A_1 - j\frac{\omega_1}{c}n_2(|A_1|^2 + 2|A_2|^2)A_1 = 0, \tag{4.57}$$

$$\frac{\partial A_2}{\partial z} + \beta_{12}\frac{\partial A_2}{\partial t} + j\frac{1}{2}\beta_{22}\frac{\partial^2 A_2}{\partial t^2} + \frac{\alpha_2}{2}A_2 - j\frac{\omega_2}{c}n_2(|A_2|^2 + 2|A_1|^2)A_2 = 0, \tag{4.58}$$

where β_{2j} is the group-velocity dispersion coefficient of wave j, α_j its attenuation coefficient and

$$\gamma_{nl,j} = \frac{n_2^I \omega_j}{c A_{eff}} \qquad (j=1, 2) \tag{4.59}$$

its nonlinearity coefficient as defined in 4.1.1. Since

$$\beta_{21} = \frac{d\beta_{11}}{d\omega} \approx \frac{d\beta_{12}}{d\omega} = \beta_{22}, \tag{4.60}$$

we denote the GVD coefficient by β_2. By introducing the retarded time $\tau = t - \beta_{11}z$ and the normalized complex envelope U (see 4.1.1), (4.57) and (4.58) can be transformed into

$$\frac{\partial U_1}{\partial z} + j\frac{1}{2}\beta_2\frac{\partial^2 U_1}{\partial \tau^2} + \frac{\alpha_1}{2}U_1 - j\gamma_{nl,1}(|U_1|^2 + 2|U_2|^2)U_1 = 0, \tag{4.61}$$

$$\frac{\partial U_2}{\partial z} + \Delta\beta_{112}\frac{\partial U_2}{\partial \tau} + j\frac{1}{2}\beta_2\frac{\partial^2 U_2}{\partial \tau^2} + \frac{\alpha_2}{2}U_2 - j\gamma_{nl,2}(|U_2|^2 + 2|U_1|^2)U_2 = 0, \tag{4.62}$$

where $\Delta\beta_{112} = \beta_2(\omega_1 - \omega_0)$ from (4.60).

While the two waves have equal group-velocity dispersion coefficients, their group velocity β_{1j} is different, i.e. they propagate at different speeds. This group-velocity mismatch leads to a continual alteration of the temporal overlap between the transmitted data patterns. This effect is called the walk-off effect of the pulses, which finally results in a limitation of the XPM.

On the other hand, if pulses are transmitted over dispersion-shifted fibres, where β_{11} equals β_{12}, i.e. a propagation without walk-off effects, a strong impact of XPM on the

signals can be expected.

If more than two waves are simultaneously propagating through the fibre, their evolution is best evaluated by the nonlinear Schrödinger equation in the following form

$$\frac{\partial U_j}{\partial z} + \beta_2(\omega_j - \omega_{ref})\frac{\partial U_j}{\partial \tau} + j\frac{1}{2}\beta_2\frac{\partial^2 U_j}{\partial \tau^2} + \frac{\alpha_j}{2}U_j - j\gamma_{nl,j}\left(2\sum_{i=1}^{N} |U_i|^2 - |U_j|^2 \right)U_j = 0, \quad (4.63)$$

where ω_{ref} is the angular frequency of the reference carrier wave.

Similar as SPM, XPM creates with every rising and falling transition in one channel a time dependent phase to the impulses of other channels whenever two or more spectrally separated impulses temporally overlap. This time dependent phase leads to a frequency shift analog to 4.1.4. Since each frequency component has its own group velocity in a dispersive medium, the frequency shift is converted into run-time differences between various frequency components within the impulse, finally leading to intensity distortions [72].

Furthermore, because of the different group velocities of the carrier frequencies of the various channels, the frequency shifted components propagate at slightly different speeds, resulting in timing jitter. Principally, timing jitter in a certain channel accumulates until the frequency shift from one edge in an interfering channel is cancelled by the following edge, since rising and falling transitions cause opposite frequency shifts [20]. However, scattering losses in actual fibres reduce the signal power such that the frequency shift induced by the first interfering edge is much larger than the opposite frequency shift created by the following edge. Therefore, the frequency shift is not fully compensated, and timing jitter due to the frequency shift accumulates along the whole length of the fibre.

The influence of XPM strongly depends on such factors as the bitrate, channel powers of the involved channels, dispersion parameters and channel spacings. Further details and simulation results will be presented in Chapter 6.

As a rough rule of thumb for SSMF, (4.64) may serve [10].

$$P_{cr,\,XPM} = \frac{10}{N}\ \text{mW}, \quad (4.64)$$

where $P_{cr,\,XPM}$ is the critical power threshold per channel and N the number of channels, so that the maximum allowable power penalty is 0.5 dB. (4.64) assumes a directly phase modulated laser diode which shows a much broader output spectrum than an externally modulated

laser diode, leading to a stronger XPM impact. (4.64) can thus only be seen as a lower limit for the threshold, in most cases, XPM effects will not occur when obeying (4.64). Figure 4.6 illustrates this aspect in a graphical way. As Figure 4.6 indicates, XPM must be taken into account in system simulations since its critical threshold power is quite low and is exceeded in a usual application scenario.

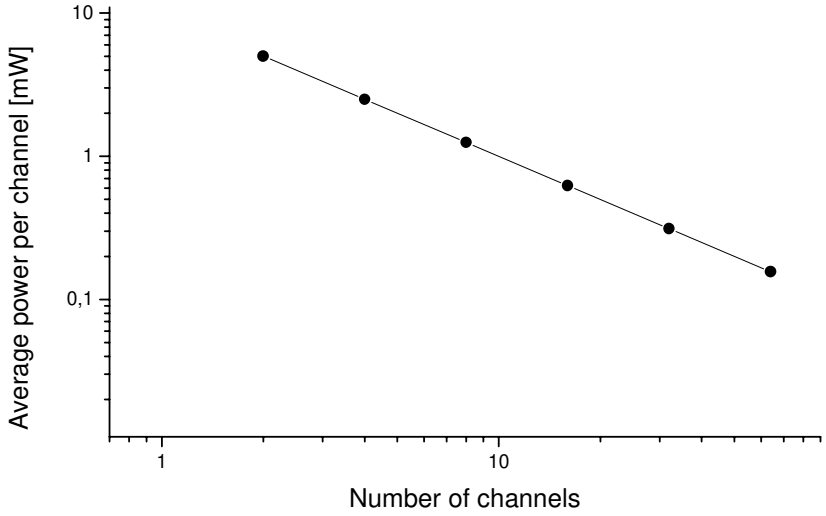

Figure 4.6: Critical average power per channel due to XPM for a typical SSMF fibre at 1.55 µm, bitrate 10 Gbit/s and channel spacing 100 GHZ or 0.4 nm, resp. Maximum allowable power penalty has been 0.5 dB.

Nevertheless, as already been mentioned, dispersion is a limiting factor of XPM because of the walk-off effect. In conjunction with a dispersion compensation scheme, the intensity distortions and the timing jitter caused by XPM can be minimized.

4.2.2 Four-wave mixing

Four-wave mixing (FWM) belongs to the parametric processes which have their name from the fact that they originate from light-induced modulation of a medium parameter such as the refractive index. Alas, an applied optical field leads to a nonlinear response of bound electrons of the propagation medium.

The derivation of the physical facts of FWM runs from (4.14), where $\vec{e}$ has to be inserted as

$$\vec{e} \sim \sum_j E_j e^{j(k_j z - \omega_j t)} \tag{4.65}$$

where $k_j = \frac{n_j \omega_j}{c}$, n_j being the refractive index of wave j and the same direction of propagation z has been assumed. (4.14) can then be converted to a result which includes intermodulation products such as [1]

$$E_1 E_2 e^{j(k_1 \pm k_2 \pm k_3)z} e^{j(\omega_1 \pm \omega_2 \pm \omega_3)t} \tag{4.66}$$

where $j = 3$ has been used as example. How many of these $j^2 = 9$ terms are effectively producing parametric coupling depends on the relative phase term in (4.66). Significant four-wave mixing occurs only if the phase terms in (4.66) are almost zero. The requirement of the first phase term in (4.66) to be almost zero is often referred to as *phase-matching condition*.

Qualitatively speaking, if three waves with angular carrier frequencies ω_1, ω_2 and ω_3 propagate at the same time in a single mode fibre, nine new waves at frequencies $\omega_1 \pm \omega_2 \pm \omega_3$ are generated (see Figure 4.7). These sidebands copropagate with the initial waves and grow at their expense. The efficiency of FWM depends on channel spacing and fibre dispersion.

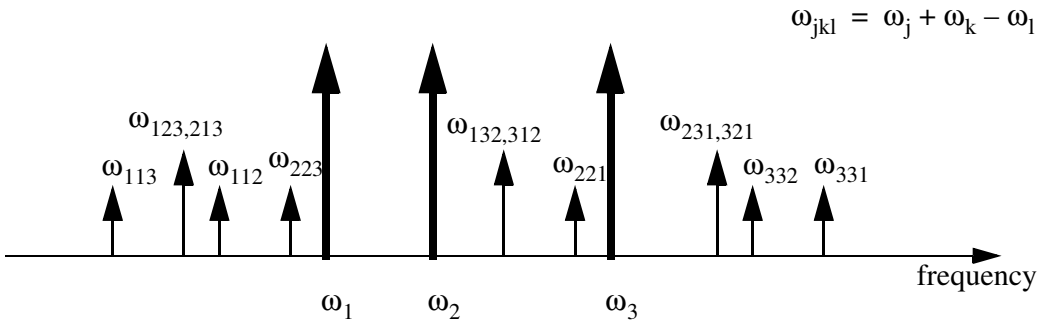

Figure 4.7: Newly generated frequencies by the effect of four-wave mixing

In general, it is difficult to satisfy the phase-matching condition except for the case of

$$\omega_{new} = \omega_1 + \omega_2 - \omega_3 \, . \tag{4.67}$$

Because of the fibre dispersion, the involved waves have different group velocities which destroys the phase-matching condition and lowers the efficiency of the energy transferal process. Thus, all other newly created waves than the one of (4.67) lack of sufficient power.

Nevertheless, the new wave at $\omega_1 + \omega_2 - \omega_3$ leads to a loss of power in all incident

waves, acting like additional losses for the transmission system. Furthermore, if the signal at ω_{new} falls together or close to one of the signals at ω_1, ω_2 or ω_3, interchannel crosstalk occurs, resulting in a further degradation of signal quality. It is interesting to note, that the effects of FWM are bit-rate independent [10].

The power of the generated wave can be estimated from [64]

$$P_{jkl}(z) = \eta \frac{1024\pi^4\omega^2}{4n_0^4c^4}(D\chi_{1111})^2\left(\frac{L_{eff}}{A_{eff}}\right)^2 P_j P_k P_l e^{-\alpha z}, \tag{4.68}$$

where η is the efficiency of FWM, D the degeneracy factor ($D = 3$ in the case of two incident waves and $D = 6$ in the case of three incident waves) and $\chi_{1111} = 6 \cdot 10^{-14} \frac{m^3}{Ws}$ the third-order nonlinear susceptibility, L_{eff} and A_{eff} the effective fibre length and its effective core area, resp. η can be expressed by a relation from [64] and is depicted in Figure 4.8 which serves most interests.

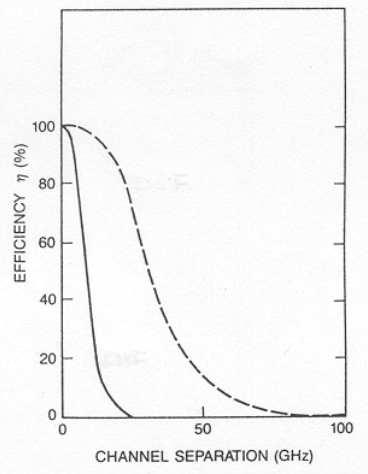

Figure 4.8: Normalized FWM efficiency versus channel separation at 1.55 µm. The solid curve represents FWM efficiency in SSMF with dispersion β_2 = -21.69 ps^2/km, the dashed curve shows FWM efficiency in DSF with dispersion β_2 = -1.5 ps^2/km [64].

In order to estimate the impact of the FWM effect, it is useful to define a threshold power of the involved signals beyond which the FWM effect cannot be neglected. It has become common to set the critical threshold power to a certain value, so that the average power of the generated wave is not more than 10% of the average power of the incident waves. This corresponds to a power penalty of 0.5 dB [2]. Using (4.68), the critical threshold power for FWM effects is

$$P_{th} = \frac{n_0^2c^2A_{eff}}{16\pi^4 D\omega\chi_{1111}L_{eff}} e^{\frac{1}{2}\alpha z}\sqrt{\frac{0.1}{\eta}}, \tag{4.69}$$

where equal input powers for all incident signals has been assumed.

As indicated in Figure 4.8, FWM is 100% efficient only in case of a channel spacing of 0 GHz. The ITU recommendation determines a channel separation of 50 GHz (or 0.4 nm at 1.55 µm, resp.) for DWDM systems. Assuming an abiding of this recommendation, FWM does not occur in SSMF according to Figure 4.8, due to the influence of dispersion. The signals walk off each other because of their group velocity difference, leading to a phase mismatch as mentioned previously. Threshold powers for three or more channels with a spacing according to ITU recommendations are well over 10 W.

On the other hand, DSF fibres exhibit a higher FWM efficiency. Group velocity mismatch is substantially lower due to the low dispersion these fibres exhibit, threshold powers are below 1 W. While transmitting via DSF, FWM has to be taken into account and can be fought with dispersion management techniques. Another possibility is to allocate unequal channel spacing, so that the newly generated waves do not fall together with the spectra of the incident waves. However, many WDM components (e.g. Fabry Perot filters or waveguide grating routers) make use of equal channel spacings, so that this technique is sometimes not a practical solution. Opposite to that, FWM can be neglected in SSMF at 1.55 µm with a channel spacing of 50 GHz or more (see Figure 4.8).

4.2.3 Stimulated Raman scattering

As pointed out in 4.1.5, stimulated Raman scattering (SRS) is of no concern in single channel applications due to its high threshold power. This does not hold for multi channel applications. If two optical waves separated by the Stokes frequency are coinjected into the fibre, the lower frequency wave will be amplified at the expense of the higher frequency wave. Figure 4.5 shows, that the Raman gain spectrum has a spectral width of up to 15 THz (or 100 nm, resp.). This means that any number of channels separated by less than this spectral width are coupled via SRS.

In WDM systems, not only two but numerous channels are injected into the fibre. The signals at higher frequencies amplify the ones at lower frequencies, i.e especially the highest frequency channel is most depleted since it acts as a pump for all other channels. It is important to note that the amplification process is bit pattern dependent, i.e. amplification occurs only when „marks“ are present in the involved channels. Figure 4.9 may give an impression of the crosstalk induced by SRS.

Assuming equal input powers in channel 1 and channel 2 and a carrier frequency of channel 1 which is higher than that of channel 2, SRS induced crosstalk always occurs whenever there is a mark in both channels (first time slot in Figure 4.9). The signal in the higher frequency channel is depleted, whereas the signal in the lower frequency channel is amplified by the same amount. No intensity changes occur, if a space in either channel is present.

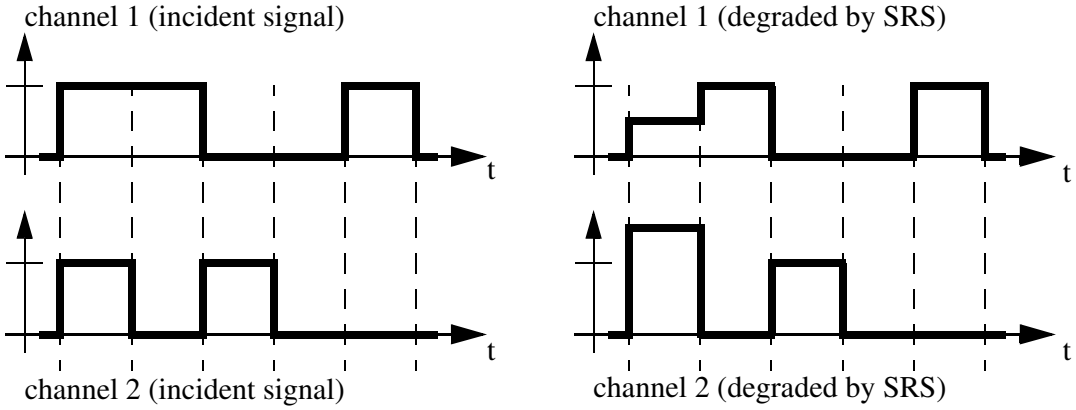

Figure 4.9: Demonstration of bit-pattern dependent crosstalk created by SRS in two-channel WDM system (carrier frequency of channel 1 is higher than that of channel 2, i.e. $\omega_1 > \omega_2$)

The depletion of the signal in channel 1 leads to a closing of the eye pattern opening, leading to a loss in signal quality or an increase of the bit-error ratio. Although the opening in channel 2 is increased in some bit positions, receivers with automatic gain controls can precipitate degradations [10].

In order to avoid crosstalk originating from SRS, it is necessary to limit the input power of each channel to a certain value. This threshold power can be estimated from the total fractional loss which is given by [2]

$$l_{fr} = \sum_{i=2}^{N} g_R(\omega) P_{ch} \frac{L_{eff}}{A_{eff}} \quad , \tag{4.70}$$

where L_{eff} and A_{eff} are effective fibre length and effective fibre core area as defined before, $g_R(\omega)$ the Raman gain coefficient from Figure 4.5, P_{ch} the average power per channel and N the number of channels.

Approximating the Raman gain spectrum from Figure 4.5 by a triangular profile and assuming equidistant channel spacing, the appropriate critical average threshold power per channel

can be calculated from [66]

$$P_{th} = \frac{3.77 \cdot 10^{13}\,\mathrm{Hz} \cdot A_{eff}}{\Delta\omega g_R^{max} L_{eff} N(N-1)}, \tag{4.71}$$

where $g_R^{max} = 7.0 \cdot 10^{-14}\ \frac{m}{W}$, the peak value of the Raman gain at 1.55 µm. l_{fr} has been arbitrarily determined to 0.05, which is necessary to keep the power penalty below 0.5 dB.

Using (4.71), the following table can be calculated which shows that SRS has to be taken into account for WDM systems with 64 channels and more. For WDM systems with less than 32 channels, SRS is of no concern since the critical threshold power is well over 100 mW per channel. Usual channel powers in WDM systems range from 1 to 10 mW. Table 4.1 has been used to draw Figure 4.10. Taking into account the signal modulation, i.e. that each channel carries a random sequence of marks and spaces, SRS effects are lowered by a factor of 2 [25].

no. of channels	2	4	8	16	32	64
Δf [GHz]						
25	58,4	9,73	2,08	0,487	$118 \cdot 10^{-3}$	$29 \cdot 10^{-3}$
50	29,2	4,87	1,04	0,244	$58 \cdot 10^{-3}$	$15 \cdot 10^{-3}$
100	14,6	2,43	0,52	0,122	$29 \cdot 10^{-3}$	$7.2 \cdot 10^{-3}$

Table 4.1: Critical threshold power P_{th} in W in dependance of the (equidistant) channel spacing Δf and the number of channels

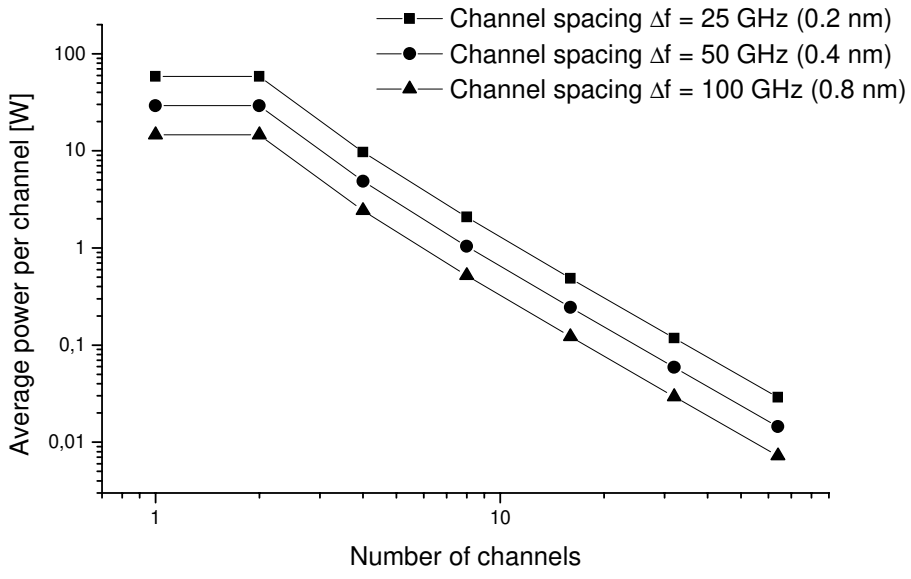

Figure 4.10: Critical average power per channel due to SRS for a typical SSMF fibre at 1.55 µm. Maximum allowable power penalty has been 0.5 dB.

From Figure 4.10, it is clearly visible that the SRS effect is directly related not only to the numbers of channels but also to the channel spacing. It is interesting to note that the critical threshold power decreases with increasing channel spacing. Greater channel separations relate to a greater total bandwidth which leads to a stronger SRS impact due to the nearly triangular form of the Raman gain (see Figure 4.5).

4.2.4 Stimulated Brillouin scattering

Stimulated Brillouin scattering (SBS) creates a backward-propagating wave at a slightly lower frequency[4] than its originating wave as described in 4.1.6. Furthermore, the Brillouin gain spectrum has a spectral width of only about 50 MHz at 1.55 µm. I.e. that for Brillouin amplification to occur in a WDM system, two signals must counter-propagate and must be separated by almost exactly 10 GHz, allowing a range of 50 MHz. Both conditions are easily avoidable.

Since fibres are most often used in unidirectional service in WDM systems, crosstalk originating from SBS cannot occur. But also in bidirectional systems, two channels would have to be spaced 10 GHz apart, which corresponds to 0.08 nm at 1.55 µm. Clearly, this condition will never be met in a WDM or even a DWDM system with high bit rates, since the signal spectrum itself of a 10 GBit/s signal is about 20 GHz wide.

Assuming unidirectional propagation and a channel separation of more than 10 GHz, SBS thus produces only additional losses for all channels. These losses are independent of the number of channels since they are not coupled via the Brillouin gain [1] and occur, if the average channel power is well over the SBS threshold power calculated in 4.1.6. Figure 4.11 shows these facts in graphical description.

It is interesting to note that the threshold power can further be increased up to 100 mW approx. by modulating the phase of the optical carrier wave with frequencies of 200 to 500 MHz. This modulation broadens the laser linewidth which effectively suppresses SBS effects. Another possibility to overcome SBS effects is to low-frequency dither the bias current of the laser diode which also leads to an increases effective bandwidth of the signal.

[4]The Brillouin shift equals 10 GHz approx.

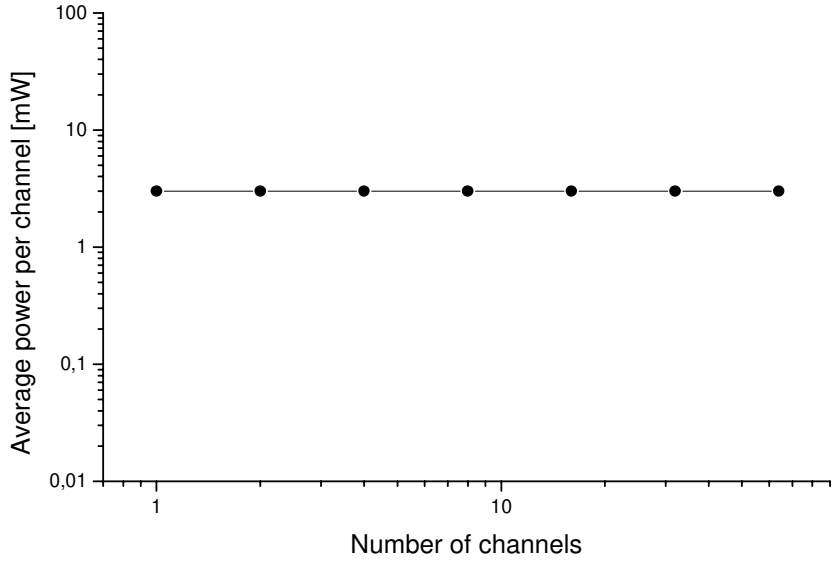

Figure 4.11: Average threshold power per channel due to SBS for a typical SSMF fibre at 1.55 µm. Maximum allowable power penalty 0.5 dB. Threshold power is widely independent of channel spacings and numbers.

4.3 Consideration of nonlinear effects in WDM system simulations

In this section, an overview of all nonlinear effects occurring during transmission of multi-wavelength light in single mode fibres and its appropriate considerations in system simulations will be comprisingly given.

Throughout the last years, millions of kilometers of fibres have been installed all over the world. Whereas this development had started in the early eighties in Europe, Japan and other Asian countries followed some years later, giving them the chance to install the then newly developed **d**ispersion-**s**hifted **f**ibres (DSF). But the ongoing need for higher bitrates has brought up unexpected, but inevitable problems of that fibre type. Due to its low or even almost zero dispersion at the transmission wavelength of 1.55 µm, there is no walk-off effect of the different channels in a WDM transmission environment, leading to an immense impact of FWM. Furthermore, crosstalk due to XPM is increased, likewise due to the almost negligible walk-off effect. If all signals, especially signals on adjacent channels propagate with the same velocity, marks on those channels overlap in the time domain for a sufficing time so that the energy transferal is quite effective. Recent experi-

ments have thus shown, that transmission over a combination of SSMF and DCF is less affected by these nonlinear phenomena [19][6][60].

Since European network companies started to deploy communication fibres some years earlier than their Asian counterparts, SSMF and DCF are the cornerstone of European WDM fibre networks. DSF had not yet been developed in a manner which suited market requirements. What looked as an immense disadvantage at first has turned to a positive property of that network architecture. Networks containing SSMF and DCF structures exhibit a much stronger walk-off effect between different channels, leading to a limitation of FWM and XPM implications. Since this network type is the preferred one in European applications, this work will mostly deal with SSMF and DCF fibres.

XPM converts power fluctuations in a particular channel to phase fluctuations in all other channels, which in turn are converted to power fluctuations in these channels by dispersion, see 4.2.1. Its efficiency strongly depends on factors such as bitrate, channel powers of the involved channels, dispersion parameters and channel spacings, effective core area etc. The threshold power for XPM, i.e. the average power per channel above which the XPM effect distorts the signals by more than 0.5 dB, is in the range of only a few mW, see 4.2.1. XPM therefore has to be taken into consideration in system views and, of course, also in system simulations.

FWM is responsible for the generation of new frequencies. Those waves can lead to strong crosstalk if their spectra fall together with the spectra of the incident waves. However, the threshold power for FWM is well over 10 W, thus its impact on actual fibre transmission systems will be quite low or even negligible, since average channel powers at the transmitter are around 10 mW. The commercial specification for the average launch power at 10 Gbit/s is 9 dBm or 11.3 mW, resp. [19]. FWM has therefore not been taken into account in the system simulations of Chapter 6.

The effect of **SRS** leads to crosstalk, if all involved channels within the Raman gain bandwidth carry a mark. Power is then transferred from the higher frequency channel to the lower frequency channel(s). SRS effects occur in WDM systems with a great number of channels, see Table 4.1. In applications with less than 32 channels and average channel powers less than 20 mW, SRS can be neglected. Since system simulations in this work will be carried out with eight channels, SRS will not be included in the further parts of this work.

SBS leads to crosstalk, if the transmission fibre is used in bidirectional service and the

involved channels are spectrally separated by less than 10 GHz. This is not the case in WDM transmission systems, which are mostly unidirectional. SBS then produces only additional losses which can easily be fought against with a low-frequency dithering of the carrier. For these reasons, SBS will not be included in the system simulations.

It is noteworthy to say, that in a DSF transmission environment, the effects of FWM and SRS cannot be neglected. But as already said, DSF transmission systems are not within the focus of this work.

Figure 4.12 shows all necessary critical threshold powers for a SSMF at 1.55 µm, a bitrate of 10 Gbit/s, a spectral channel separation of $\Delta\lambda = 0.4$ nm, an attenuation of $\alpha = 0.2$ dB/km, an effective core area of $A_{eff} = 95 \cdot 10^{-6} m^2$ and a dispersion of $\beta_2 = -21.69 ps^2/km$.

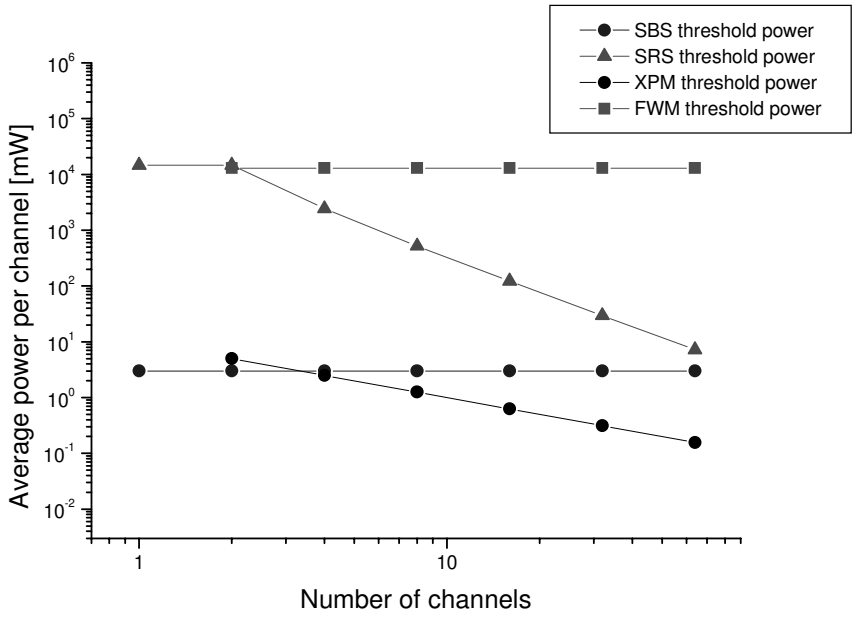

Figure 4.12: Average threshold power for nonlinear effects in SSMF at 1.55 µm. Criterion: Maximum allowable BER penalty 0.5 dB.

Chapter 5

The simulation of the optical transmission system

In previous chapters the optical fibre was treated as a transmission medium and the encoder and decoder, which are necessary to supply the different signals with orthogonal characteristics. This chapter deals with the remaining components of the optical fibre transmission system, which are substantial for its operation.

The optical transmitter as creating the incident lightwave is specially looked upon in section 5.1, since the temperature dependence of its output signal with regard to power as well as carrier frequency, plays an important role for the usually necessary channel monitoring. The physics of the optical fibre link has already been discussed in Chapter 4. In section 5.3, a brief overview of the corresponding simulation model will be given. The receiver finally consists of the demultiplexer, bandpass filters and receiver diodes. They will be presented in section 5.4. Since a bit error ratio can not be calculated by comparing transmitted and received bits due to enormous computing time, other measures, namely the Q factor and the eye penalty factor, serves as bit error indicator. Section 5.5 is dedicated to its explanation and implementation. A complete overview of the system structure can be found in Figure 6.1 and Figure 7.1.

5.1 The optical transmitter

At a carrier wavelength of 1.55 µm, operating with high bit rates, Fabry Perot semiconductor lasers are out of the question, since they oscillate in several longitudinal modes simultaneously due to the relatively small gain difference between neighboring modes of the cavity [2] [5]. Mode changes can appear through modulation or through temperature

changes. Since mode changes always coincide with increased noise and stronger dispersion effects, semiconductor lasers with single-longitudinal-mode operation such as distributed feedback semiconductor lasers (DFB), coupled-cavity semiconductor lasers (CCL) or vertical-cavity surface-emitting lasers (VCSEL) are preferred and are widely in use.

The optical carrier can principally be modulated with the information carrying signal in two different ways. Whereas the external modulation by means of electro-absorption modulators or Mach-Zehnder modulators is often used, if a chirp[1] of the input signal would crucially lower the performance of the whole system, directly modulated semiconductor lasers are preferred for their ease of use and the lower numbers of components in such a system. The chirp is then overcome by the use of dispersion-shifted fibres or, like in this work, by the use of dispersion-compensation schemes.

The transmitter of each channel is thus modeled as ideal DFB semiconductor laser, emitting 100 times the pseudo-random bitsequence 010100010111100 which adds up to 1600 bits. In order to gain results with some practical validity, all other channels, also modeled as ideal DFB semiconductor lasers, emit uniformly distributed random bit sequences which are created before each of the 100 simulational runs. By this, best and worst cases with regard to the nonlinear effects on the fibre are averaged out, and unrealistic bit pattern effects, which could possibly occur in case of fixed bit streams on all channels, are avoided.

The signal format can be changed between RZ and NRZ format. RZ pulses are Fourier-limited sech^2-pulses with a time-bandwidth product of 0.31. Their bitrate, time-width and power are independently adjustable over a wide range and their carrier frequency ν_i can arbitrarily be chosen within the 1.55 µm window or, if necessary, in the 1.3 µm window. NRZ pulses are modeled with a $\cos^2$-like rise and fall with adjustable rise and fall times as well as adjustable time-widths. Again, bitrate and pulse powers can be chosen arbitrarily.

For simulational purposes, signals are oversampled by a factor of 64.

5.2 The optical encoder and decoder

In general, coding a temporal bit sequence can be done in the electrical or in the optical domain. As obeyed in section 2.2, optical coding by the use of optical tapped delay lines

[1] A pulse is said to be chirped if its carrier frequency changes with time.

offers the advantage of a simpler encoder design which makes this solution interesting for low-cost applications. The fibre tapped delay lines are implemented by short pieces of standard single mode fibres, in which signals propagate as described in Chapter 4. The length of these pieces is matched to the delay the pulse needs to experience. The pulse evolution is governed by the nonlinear Schrödinger equation and is solved by the split-step Fourier algorithm, see also section 5.3.

The passive splitters and combiners in front or behind the encoder or decoder, resp., are assumed to be lossfree and nonfrequency selective. The principal structure of the encoder and decoder can be seen in Figure 5.1.

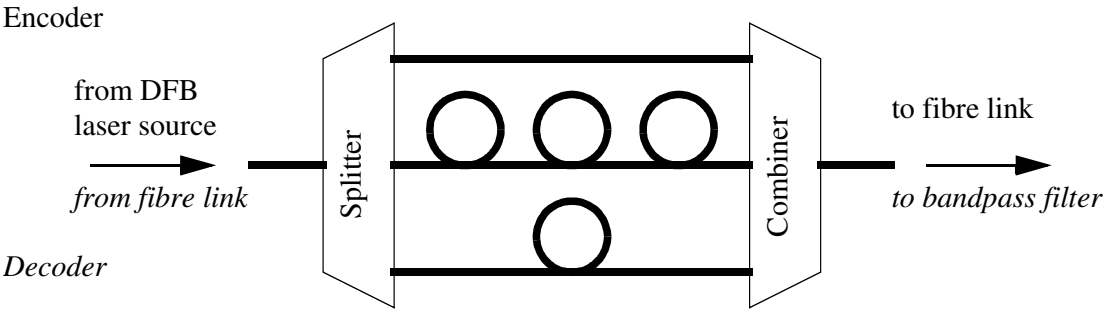

Figure 5.1: Principal structure of the encoder/*decoder*. Splitters and combiners are assumed to be loss free and frequency independent.

5.3 The optical link

High bit rate transmissions in the 1.55 µm regime need to be dispersion compensated [66]. This can be done by the use of dispersion-shifted fibres, which exhibit zero dispersion in the 3rd optical window, or by the use of **d**ispersion **c**ompensating **f**ibers (DCF), which seems attractive if usual SSMF with low dispersion in the 2nd optical window have to be used to bridge the distances. Since European telecommunication companies have started early in the eighties to install SSMF at large scale when transmitting at 1.3 µm, they nowadays make use of these fibres at 1.55 µm by the help of DCF.

Thus, the optical link consists of any desired number of N serial fibre pieces of standard single mode fibre, each of $L = 50$ km length. Each link is pre- and postcompensated (see also Chapter 6), so that the 2nd order group velocity dispersion is completely removed for a carrier wavelength of 1552.5 nm. The most important parameters of each fibre type can be viewed in Table 5.1.

	length L [km]	attenuation α [dB/km]	GVD β_2 [ps^2/km]	eff. core area A_{eff} [μm^2]	Kerr coefficient n_2 [m^2/W]
SSMF	50	0.2	-21.69	95	$2.6 \cdot 10^{-20}$
pre-DCF	2.82	1.0	200	100	$2.6 \cdot 10^{-20}$
post-DCF	2.60	1.0	200	100	$2.6 \cdot 10^{-20}$

Table 5.1: Important fibre parameters

The propagation equations of the optical wave (4.63) are solved by the split-step Fourier algorithm [1]. It obtains an approximate solution of the wave by assuming, that dispersive and nonlinear effects on the fibre act independently, when the optical field propagates over a small distance. The split-step Fourier method is well introduced in literature and is not subject of further discussion in this work.

Each fibre span, consisting of pre-DCF, SSMF and post-DCF, see Figure 5.2, is followed by a nonfrequency selective EDFA with 6dB noise figure. Its amplification is tuned to compensate the attenuation that the signal went through during propagation on the previous span, also including the coupling losses. After the last fibre span, i.e. right in front of the receiver, an optical bandpass filter, which is described in 5.4, is inserted..

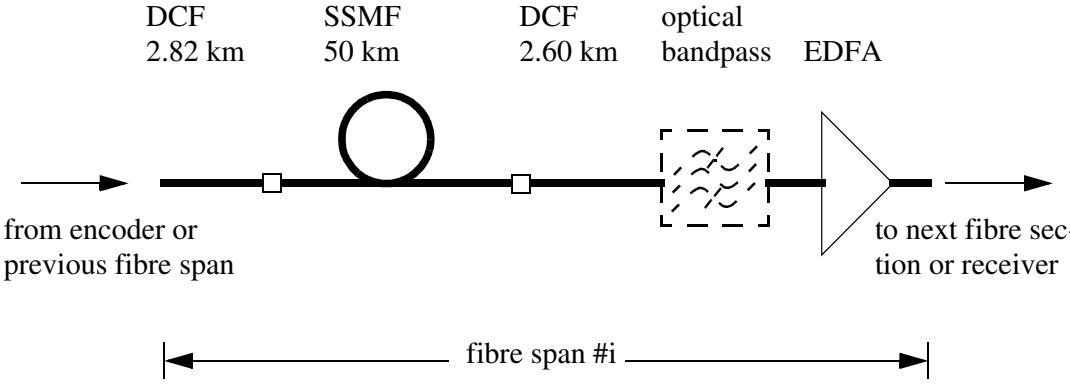

Figure 5.2: Principle structure of fibre span, consisting of SSMF and DCF, optical bandpass and optical amplifier.

5.4 The optical receiver

The optical receiver consists of an optical and an electrical part. The optical part, also called the *front end*, turns the optical signal in an electrical and hands the electrical signal over to the electrical part, where the bit error ratio is determined, see section 5.5.

In an intensity modulated, direct-detection system, the front end consists of an optical preamplifier, which is an EDFA just like the in-line amplifier between two fibre spans, an optical bandpass filter and the p-i-n diode. In order to reduce noise from the amplifying process, a lowpass filter with a 3dB bandwidth below the bitrate is introduced in the electrical section. Its bandwidth must be carefully chosen, so that the intersymbol interference which may be introduced, is as little as possible. Before the decision circuit, the signal has to be synchronized to the middle of the timing. Only by this, the optimal sample point can be realized and the maximum amplitude can be sent to the threshold device. All components except the preamplifier will be described in the next paragraphs.

5.4.1 The optical filters

The optical filter is one of the basic building blocks of a WDM system, which provides the necessary wavelength selection, so that independent channels can be isolated. Especially in WDM applications, the filter passband characteristic and its roll-off slope in relation to the channel spacing must be optimized to ensure minimum crosstalk. Figure 5.3 shows a comparison of common filter types. The normalized spacing $\Delta\Lambda$ has been defined as the ratio of channel spacing to the 3 dB bandwidth of the filter. Since for DWDM systems, $\Delta\Lambda \approx 1\ldots2$, grating based filters have been chosen for the wavelength selection process.

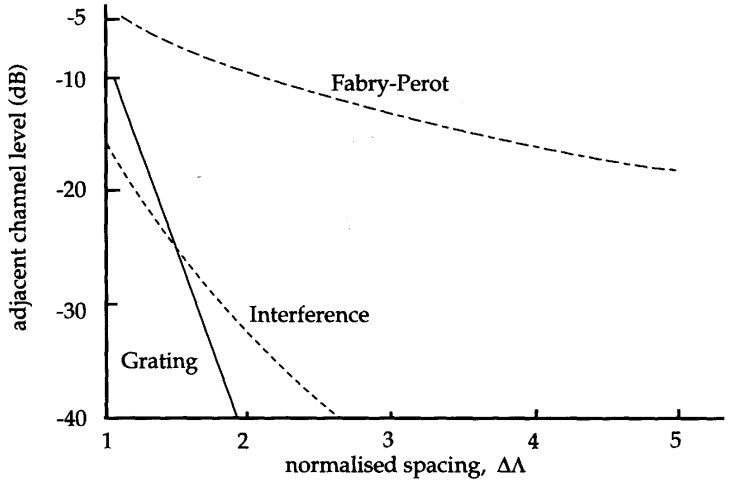

Figure 5.3: Comparison of filter characteristics [66], adjacent channel level versus normalized spacing.

Fibre Bragg gratings can act as optical filter because of the existence of an optical stopband due to reflection of incident light. The stopband is located at the Bragg wavelength

λ_B . The transfer function of a fibre Bragg grating is

$$\underline{H}(j\omega) = \frac{j\kappa \sin(qL_g)}{q\cos(qL_g) - j\delta \sin(qL_g)}, \tag{5.1}$$

where $\delta = 2\pi/\lambda - 2\pi/\lambda_B$ is the detuning from the Bragg wavelength λ_B, κ the coupling coefficient, $q = \sqrt{\delta^2 - \lambda^2}$ and L_g the grating length. For most applications, the power transfer function of (5.1) can be approximated by [2] [38]

$$|H(j\omega)|^2 = e^{-(4\ln 2)\Lambda^2}, \tag{5.2}$$

$\Lambda = (\lambda - \lambda_B)/\lambda_{3dB}$ being the normalized wavelength, where λ_{3dB} is the 3dB bandwidth of the filter. Figure 5.4 shows the power transfer function of the bandpass according to (5.2).

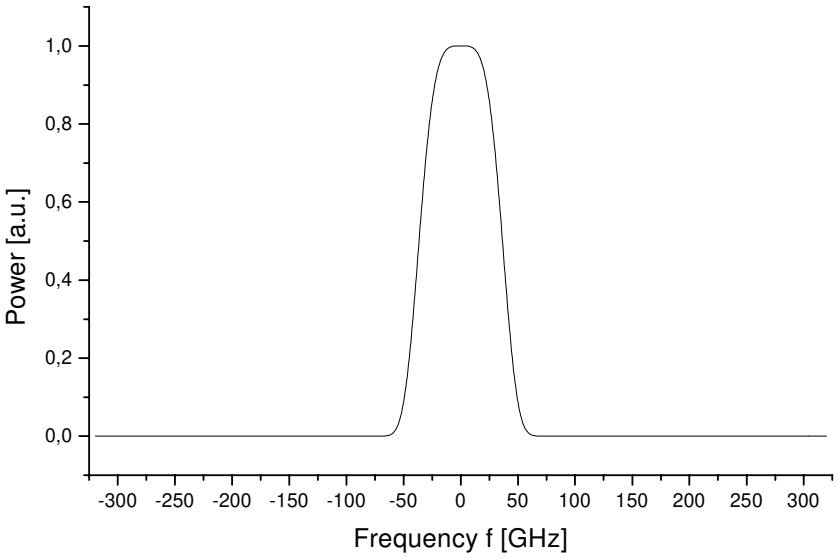

Figure 5.4: Power transfer function of optical bandpass with 3 dB bandwidth of 60 GHz

Filtering is then performed by multiplication of the Fourier transform of the propagating wave with the filter's transfer function.

5.4.2 The receiving diodes

The optical signal is converted to an electrical by the use of pin diodes. A realistic pin-diode model can be described by

$$i(t) = q\frac{n_e}{T_s} + i_T(t), \tag{5.3}$$

$i(t)$ being the instantaneous photodetector output current, q the elementary charge, n_e the number of electrons emitted in time T_s. n_e is a Poisson distributed random variable with expectancy value l.

$$l = \frac{\eta}{h\nu}P(t)T_s + n_d T_s . \tag{5.4}$$

η is called the quantum efficiency, i.e. the relation of emitted carriers to photons, usually 0.8...1, ν the optical carrier frequency, $P(t)$ the optical power arriving at the diode and T_s the sampling time. n_d denotes the emitted carriers per second, if no light falls onto the diode and thus indicates the dark current. High bit rate systems usually employ InGaAs diodes, showing dark currents of 2...10 nA. Since the output current $i(t)$ is several orders of magnitude higher, the dark current contribution can be neglected.

The model first computes the expectancy value of l, then generates the poisson distributed number of emitted electrons n_e. Finally, the thermal noise $i_T(t)$ is included. It is modeled as a stationary Gaussian process with spectral power density $S_T(f)$, which is frequency independent up to 1 THz.

$$S_T(f) = 2k_B T\frac{1}{R_L} \tag{5.5}$$

k_B denotes Boltzmann's constant, T the absolute temperature and R_L the input resistance. The variance of this stochastic process follows as

$$\sigma_T^2 = 4k_B T\frac{1}{R_L}\Delta F , \tag{5.6}$$

ΔF being the total sampling bandwidth in the simulation.

5.4.3 The equalizer and synchronizer

The receiver diode is followed by an electrical lowpass filter with transfer function

$$H(j\omega) = \frac{1 - 2\left(\frac{\omega}{\omega_{3dB}}\right)^2 + j\left(\frac{\omega}{\omega_{3dB}}\right)\left[\left(\frac{\omega}{\omega_{3dB}}\right)^2 - 2\right]}{1 + \left(\frac{\omega}{\omega_{3dB}}\right)^6}. \tag{5.7}$$

The transfer function corresponds to a 3rd order Butterworth filter [71]. Its main objective is the reduction of intersymbol interference, which may have been introduced to the signal by imperfect dispersion compensation and a resulting temporal pulse broadening. In order to equalize a signal of bitrate B, a lowpass filter with Nyquist bandwidth B/2 is sufficient [67].

In order to examine the received signal, it is important to synchronize it to the input signal of the fibre link. The synchronizer correlates the received signal with the link input signal with variable delay. Best synchronization is achieved, if the correlation product finds its maximum.

5.5 Performance evaluation measures

To determine the bit error ratio (BER) of a high bit rate transmission system, it is not advisable to transmit several thousand bits, compare the received bits with the transmitted bits and compute the ratio of „wrong“ to the total number of bits. Specifications for high bit rate systems of today and the future with bit rates of more than 10 GBit/s require a BER of 10^{-9} or even 10^{-12}. In order to achieve reliable statements concerning the BER, at least $100 \cdot 10^{9}$ or $100 \cdot 10^{12}$, resp. bits would have to be transmitted[2]. Simulation times of several months on usual PCs would be the consequence. Therefore, more qualitative than quantitative measures for the performance evaluation come into account. Both the Q factor and the eye penalty factor are widely in use and are discussed in 5.5.1 and 5.5.2.

5.5.1 The Q factor

The estimation of the probability densities of sampling values of the electrical signal at the decision device is the base for calculating the Q factor. Assuming a Gaussian distribution of these values, a „Q factor“ and from that, the BER can be calculated. The assumption of a Gaussian distribution is widely used, though it means an acceptance of negative optical power values. Recent results indicate not a Gaussian, but a Bose-Einstein distribution of the power of transmitted spaces [75][76]. However, due to the wide acceptance of the Q factor as comparative measure of optical transmission system, it is also used in this work.

Since a Gaussian distribution is assumed, the probability densities of the sampling values of the photocurrent for the „zero“- and „one“-bits are

[2]For a detailed description of Monte Carlo Simulation, see [39].

$$p_0(I) = \frac{1}{\sigma_0\sqrt{2\pi}}\exp\left(-\frac{(I-I_0)^2}{2\sigma_0^2}\right) \tag{5.8}$$

and

$$p_1(I) = \frac{1}{\sigma_1\sqrt{2\pi}}\exp\left(-\frac{(I-I_1)^2}{2\sigma_1^2}\right). \tag{5.9}$$

σ_0 and σ_1 are the standard deviations, I_0 and I_1 the corresponding expectancy values, see Figure 5.5.

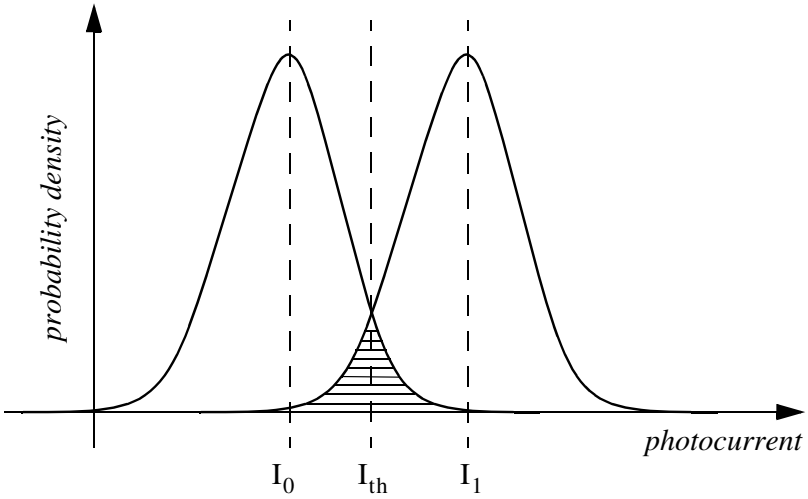

Figure 5.5: Probability density function of sampling values of photocurrent. I_{th} threshold current at threshold device.

With the conditional probability of a transmitted „zero“ detected as „one“

$$P(1|0) = \int_{I_{th}}^{\infty} p_0(I)dI = \frac{1}{2}\mathrm{erfc}\left(\frac{I_{th}-I_0}{\sqrt{2}\sigma_0}\right) \tag{5.10}$$

and the conditional probability of a transmitted „one“ detected as „zero“

$$P(0|1) = \int_{-\infty}^{I_{th}} p_1(I)dI = \frac{1}{2}\mathrm{erfc}\left(\frac{I_1-I_{th}}{\sqrt{2}\sigma_1}\right), \tag{5.11}$$

one obtains the BER as

$$BER = \frac{1}{2}P(0|1) + \frac{1}{2}P(1|0), \tag{5.12}$$

where $P(0) = P(1) = \frac{1}{2}$ has been assumed, i.e. „zero“ and „one“ are transmitted with equal probability.

The BER is minimized by finding the optimum threshold current I_{opt} which is obtained from solving the partial differentiation equation $\partial BER / \partial I_{th}$. The optimum threshold value then results in

$$I_{opt} = \frac{\sigma_0 I_1 + \sigma_1 I_0}{\sigma_0 + \sigma_1}, \tag{5.13}$$

and since the Q factor is defined as

$$Q := \frac{I_1 - I_{opt}}{\sigma_1} = \frac{I_{opt} - I_0}{\sigma_0}, \tag{5.14}$$

Q finally is obtained by

$$Q = \frac{I_1 - I_0}{\sigma_0 + \sigma_1}, \tag{5.15}$$

and the minimum BER resolves as

$$BER = \frac{1}{2}\operatorname{erfc}\left(\frac{Q}{\sqrt{2}}\right). \tag{5.16}$$

Since this method of calculating the BER neglects bit pattern effects which might occur through interaction of following or predecessing pulses due to the Kerr nonlinearity of the fibre or its chromatic dispersion, it is advisable to determine a Q factor or bit error ratio, resp., that takes significant contributions of pattern effects into account [4]. Transient processes of the lowpass filter represent another source of bit pattern effects.

Taking both the direct predecessor and successor into account, there exist four different Q factors and thus four different BER, see also Table 5.2.

i	0	1
1	0**0**0	0**1**0
2	0**0**1	0**1**1
3	1**0**0	1**1**0
4	1**0**1	1**1**1

Table 5.2: The four combinations of various predecessing and following bit (standard numbers) with fixed middle bit (bold numbers).

Since the channel under supervision emits a pseudorandom, but fixed bit sequence, the position of each specified middle bit within the bit stream of the synchronized output signal is known. Thus, standard deviations σ_0^i, σ_1^i and mean values I_0^i, I_1^i of all four combinations can be calculated[3]. After calculating the four different Q factors by help of (5.15), the resulting minimum Q_{res} factor is then obtained by

$$BER_{res} = \frac{1}{4}\sum_{i=1}^{4} BER^i \tag{5.17}$$

and solving

$$\frac{1}{2}\mathrm{erfc}\left(\frac{Q_{res}}{\sqrt{2}}\right) = BER_{res}\,. \tag{5.18}$$

Clearly, the resulting Q factor Q_{res} is mainly determined by the maximum BER^i of the four combinations. A Q factor of 6 corresponds to a BER of 10^{-9}, a Q of 7 to a BER of 10^{-12}.

It must be noted, that quoting a BER leads to the association of being able to exactly predict the quantitative behavior of a transmission system. Numerical simulations, though, can only be auxiliary means to give a qualitative prediction of the system performance, since not all influence factors (e.g. exact coupling losses, mechanical stress of fibres or components) can be considered. Instead of a BER, system performance is given as Q factor in this work which is a perfect measure for qualitative evaluation.

In the pure WDM system, the amplitude values of the sampled electrical output signals are Gaussian distributed in a first approximation [30] due to the Gaussian distribution of the ASE. The WDM system is mainly a noise and nonlinearity-limited system. In contrast to that, the hybrid OCDM/WDM system which will be presented in Chapter 7 is mainly affected by the possible interference between the different users, the so-called multiple access interference. The hybrid system thus is an interference-limited system. However, the distribution of the amplitude values of the output signals are no more Gaussian distributed (except for a very high number of simultaneous users; in the case of 8 simultaneous users like in the simulated system, this assumption can not be made). Consequently, the performance of the system can no longer be estimated by the help of the Q factor, which inherently assumes Gaussian distributed values.

[3] All four combinations of zeros and ones depicted in Table 5.2 occur twice. The appropriate mean value I^i is the average of the sampling values at both sampling times. Standard deviations are then calculated with averaged mean squares.

5.5.2 The eye diagram and the eye penalty factor

The eye diagram is more a qualitative than a quantitative measure for the evaluation of a optical transmission system. The decision threshold can also be determined by the help of the eye diagram, and even timing jitter is clearly indicated.

By putting all time slots of the synchronized signal one over another, the traces of the signal amplitude build up to a pattern which resembles the shape of a human eye. Lower traces stem from the transmitted spaces, while the upper traces originate from transmitted marks. It has become common to place two eyes side by side. The larger the untraced area is, the easier is the signal detection and the better the bit error ratio.

The widely used eye penalty factor ε_p [dB] (e.g. [18][53]) can then be measured from the eye diagram. It expresses the closure of the eye diagram compared to the back-to-back case in dB, will be employed (see Figure 5.6). The eye penalty factor is defined as

$$\varepsilon_p[\mathrm{dB}] := 10 \cdot \log \frac{\hat{s}_1}{\min(s_1) - \max(s_0)}, \tag{5.19}$$

where $\min(s_1)$ and $\max(s_0)$ are the minimum and maximum values of the sampled „0“ and „1“-level values s_0 and s_1 in the eye diagram, resp. and $\hat{s}_1$ being the loss-corrected input power level.

Generally, the eye penalty factor ε_p cannot be directly transferred into a bit error ratio. It only serves as a qualitative measure for a relative comparison of the same system under different conditions. However, in the case of Gaussian distributed amplitude values, a connection between the Q and the ε_p factor can be drawn. Both factors will be evaluated in Chapter 6. It follows that - generally speaking - ε_p factors greater than 3.5 dB lead to bit error ratios that are less than 10^{-9}.

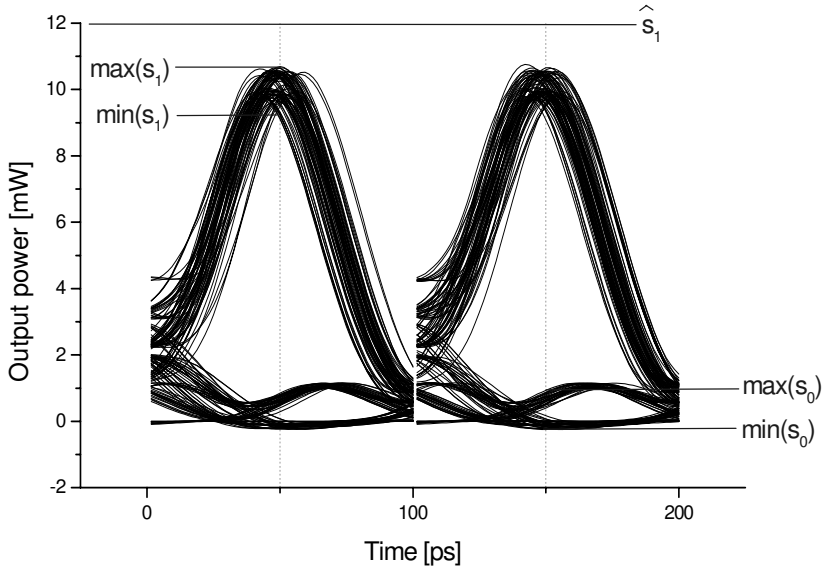

Figure 5.6: Explanatory diagram for the eye penalty factor ε_p

Chapter 6

Crossphase modulation as dominant nonlinear effect in a SSMF/DCF based WDM transmission system

The performance of a WDM transmission system is highly influenced by nonlinear effects which stems from the non-vanishing third-order susceptibility of silica glass. Fortunately, signal input powers in actual transmission systems are low enough, so that only crossphase modulation must be taken into account, whereas the nonlinear effects four-wave mixing, stimulated Raman and Brillouin scattering can be neglected, see section 4.3.

The impact of XPM occurring in a WDM transmission system depends on a variety of parameters, such as the channel bitrate, the average input powers of the channels, the number of channels and their spectral spacing, the applied in-line optical filters and, of course, the link length. The influence of these crossphase modulation related parameters on a WDM transmission system will be evaluated in this chapter. Simulation results will be obtained and then compared to the ones of the hybrid OCDM/WDM system in Chapter 7.

As has been depicted in Chapter 5, a system with up to 8 input channels and a link length of 400 km SSMF, dispersion compensated by DCF, is simulated. The link consists of 8 spans, each span of precompensating DCF of 2.82 km length, a 50 km SSMF and a postcompensating DCF of 2.60 km length. Figure 6.1 shows the simulated system in its principal structure.

Whereas channel #4 emits the fixed 16 bit pseudo-random bitsequence 010100010111100 in NRZ format, bit sequences of all other channels were chosen randomly for each simulational run. By this means, the statistical behavior of the XPM in a realistic transmission scenario with uncorrelated input signals can be taken into account. Multiplexer and demultiplexer are assumed to be ideal. Since the primary target of this chapter is the influence

of XPM on system performance, a more realistic approach to the simulation of the couplers including crosstalk would blur the sheer effects of XPM on the transmission fibre. Similar reasons hold for the simulation of the EDFA's.

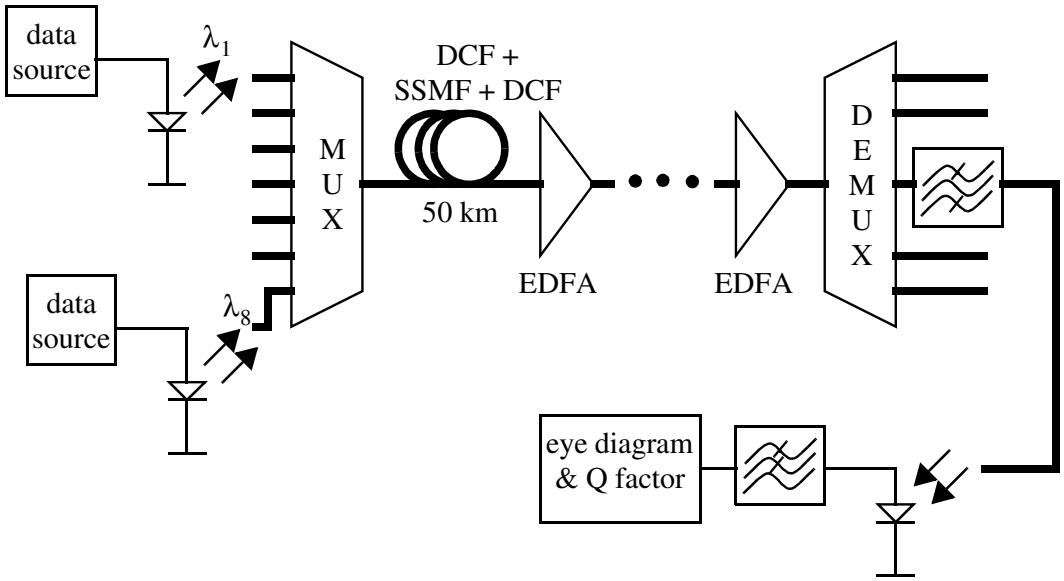

Figure 6.1: The simulated lightwave system. MUX: optical multiplexer, e.g. 8x1 coupler, lossfree; SSMF + DCF: standard single monomode fibre with pre- and postcompensation; EDFA: (ideal[1]) erbium-doped fibre amplifier; DEMUX: optical demultiplexer, e.g. 1x8 coupler, lossfree. For Q factor computation, see section 5.5.

Numerous publications (e.g. [9], [51], [73]) confirm that the compensation of accumulated dispersion shows best results if both each span is compensated (and not the whole link for once) and within each span, pre- and postcompensation is performed. Simulation results in [34] suggest a ratio of 52% to 48% of pre- to postcompensation which has been applied to the simulations in this work.

During the simulations, several parameters were changed in order to study the dependence of XPM of different system characteristics. Of the total parameter set, only one parameter was changed at a time, thus the examination of the dependence of XPM on a certain parameter is made possible. The standard set of parameter which was used is shown in Table 6.1.

Bitrate [GBit/s]	Input power [mW]	Signal format	Number of channels	Channel spacing [GHz]	Wavelength of channel #4 [nm]	3dB Filter bandwidth [GHz]	Link length [km]
10	12	NRZ	8	50	1552.5	30	400

Table 6.1: Standard set of parameters used in the simulation of the WDM system

[1] EDFA's are assumed to be ideal in the sense of wavelength dependence. Their noise contribution is considered by a noise figure of 6 dB.

Channel #4 has been used as center channel, its carrier wavelength was kept fixed. Fibre parameters are chosen as exemplified in section 5.3. In the following paragraphs, one parameter of the set will be changed and its effects on system performance discussed.

6.1 Input powers

Input powers of the signals in an optical transmission system have to be carefully chosen and then kept very fixed. This holds especially for a WDM transmission system, let alone a DWDM system, since a trade-off has to be made between high input powers, which would be desirable with respect to the signal noise ratio, and low input powers, by which means nonlinear effects would be negligible. The International Telecommunication Union (ITU) recommends a maximum launch power of 9 dBm or 7.94 mW, resp. for each channel in DWDM systems [52], which are defined as WDM systems with channel spacings of less than 0.8 nm or 100 GHz, resp. Therefore, maximum input powers have been changed in the simulation between 3 dBm (2 mW) and 13 dBm (20 mW), resulting in average powers of -1.4 dBm (0.7 mW) to 8.6 dBm (7.3 mW).

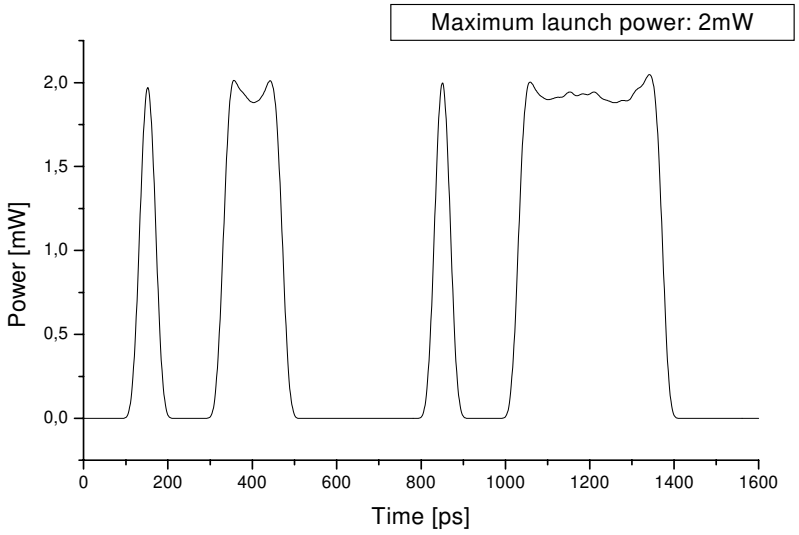

Figure 6.2: The bandpass filtered output signal with 2 mW launch power. Crosstalk stems from crossphase modulation of surrounding channels. Signal degradation 0.5 dB approx. Clock samples at $50 + i \cdot 100$ **ps.**

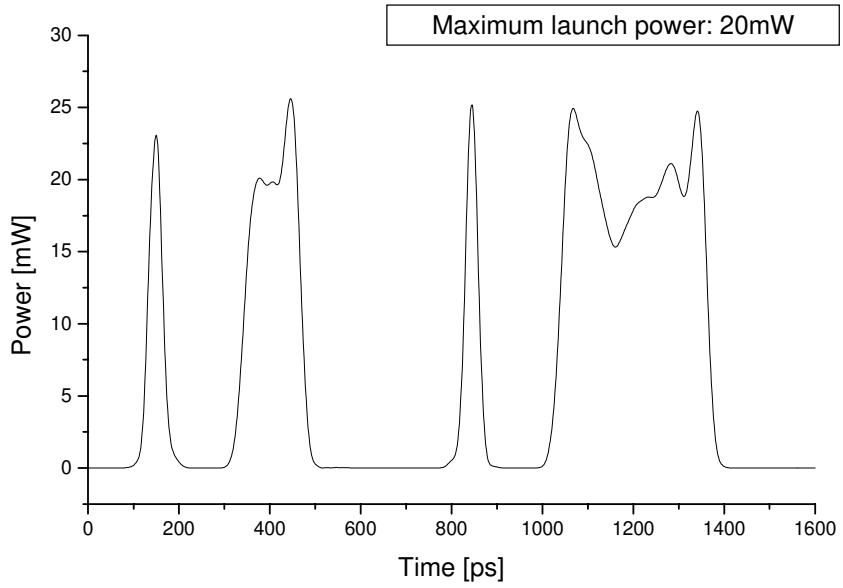

Figure 6.3: The bandpass filtered output signal with 20 mW launch power. Crosstalk stems from crossphase modulation of surrounding channels. Signal degradation 2.25 dB approx. Clock samples at $50 + i \cdot 100$ **ps.**

Figure 6.2 shows the bandpass-filtered time signal before the optical-electrical conversion at the receiver for a maximum launch power of 2 mW. The NRZ signal format helps to indicate the crosstalk since consecutive marks show variances in their power levels which are flat if not disturbed by XPM. This modulation strongly depends on the launch power of the involved channels, as Figure 6.3 confirms. Whereas in the 2 mW case, signal distortion due to XPM is 0.5 dB approx., an input power of 20 mW leads to an additional deterioration of 2.25 dB. The standardized launch power of 9 dBm (7.94 mW) shows an average deterioration of 1.3 dB.

The optical-electrical conversion and the following lowpass filtering slightly averages the XPM induced power fluctuations in the consecutive marks. This can be seen in the eye diagram, which is sketched in Figure 6.4. Furthermore, Figure 6.4 shows the traces of 50 simulative runs and points out the stochastic behavior of the XPM in the realistic case of uncorrelated and random bit sequences in the adjacent channels of the observed channel #4. Another important result is the occurrence of timing jitter which is also due to XPM, see 4.2.1 or [20].

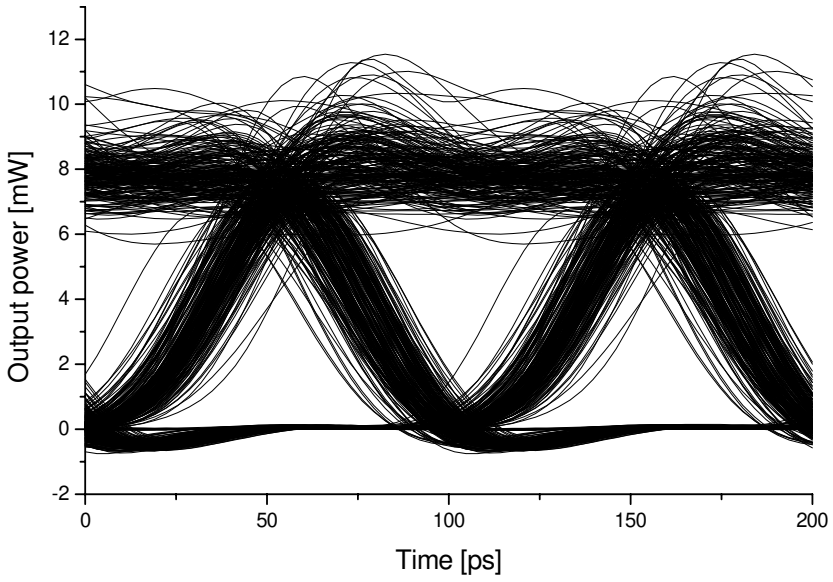

Figure 6.4: Eye diagram of channel 4, showing 50 simulative runs, launch power 8 mW. Power fluctuations and jitter due to XPM. Each run draws two traces.

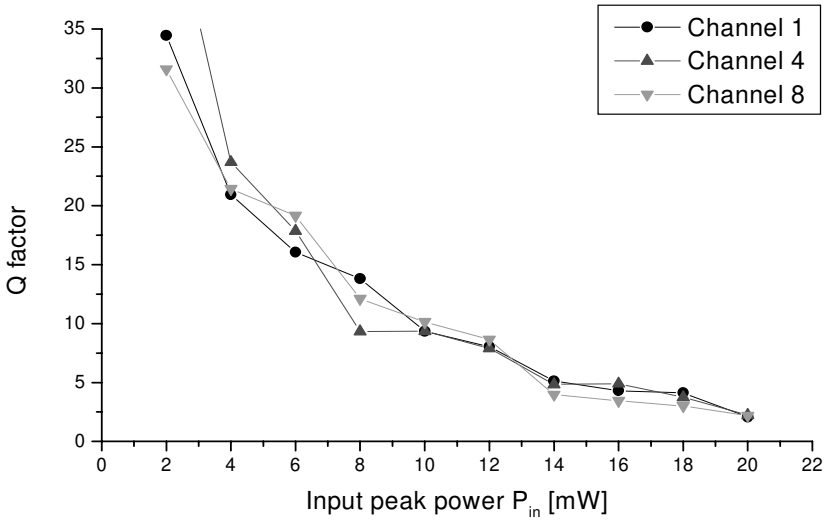

Figure 6.5: Q factors of channel #1, #4 and #8 versus input peak power. Link length and channel spacings were fixed at 400 km and 0.4 nm, resp. All 8 channels were active.

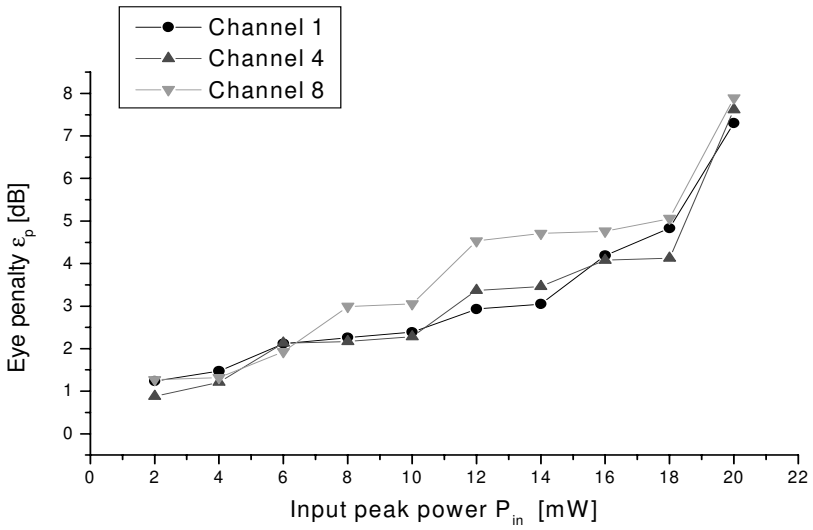

Figure 6.6: Eye penalty ε_p of channels #1, #4 and #8 versus input peak power. Link length and channel spacings were fixed at 400 km and 0.4 nm, resp. All 8 channels were active.

In order to assess the dependence of the system performance due to XPM, Figure 6.5 shows the Q factor of the received signals of channels #1, #4 and #8 with varying maximum launch power.

Since a Q factor of 6 corresponds to a bit error ratio of 10^{-9} in the case of a jitterfree signal, an input power of more than 12 mW can not be recommended. The Q factor curve shows an incursion at input powers of 8 mW at channel #4 and channel #8, which can be traced to a hapless distribution of the random bitsequences on adjacent channels, which were chosen randomly for each simulation run. A further increase of simulative runs (100 were performed if not stated otherwise, having a simulation run time of 40 hours) would have prolonged the simulation time in an inconvenient manner.

In order to get results that are comparable to those obtained with the hybrid system (see Chapter 7), Figure 6.6 additionally shows the eye penalty ε_p in dB (see 5.5), computed for the same results as Figure 6.5. In contrast to the Q factor, the eye penalty factor does not assume a Gaussian distribution of the sampled output amplitude values which is necessary for a comparison with results from Chapter 7, since the assumption of a Gaussian distribution is not justified in case of a coded transmission. Comparing Figure 6.5 and Figure 6.6, one can see that as long as $\varepsilon_p < 3.5$ dB (corresponding to $Q \approx 6$), a transmission with acceptable bit

error rate is possible.

Q factor curves and eye penalty factor curves must not necessarily be analog to each other, there might be small differences, e.g. at an input power at 12 mW, where Q factors for the three channels are similar, but the eye penalties ε_p are different. This can be traced back to the fact, that the lowest sampled amplitude value of a transmitted mark ($\min(s_1)$) is very determining for ε_p, but is less important for the variance σ_1 of the Q factor due to an averaging effect of all sampled marks.

Figure 6.5 and Figure 6.6 suggest, that the XPM impact on all channels is of linear characteristic, a fact that is confirmed by Figure 6.7, where the modulation of the signal of channel #4 is shown versus the signal input power. These results conform with experimental results reported in [21].

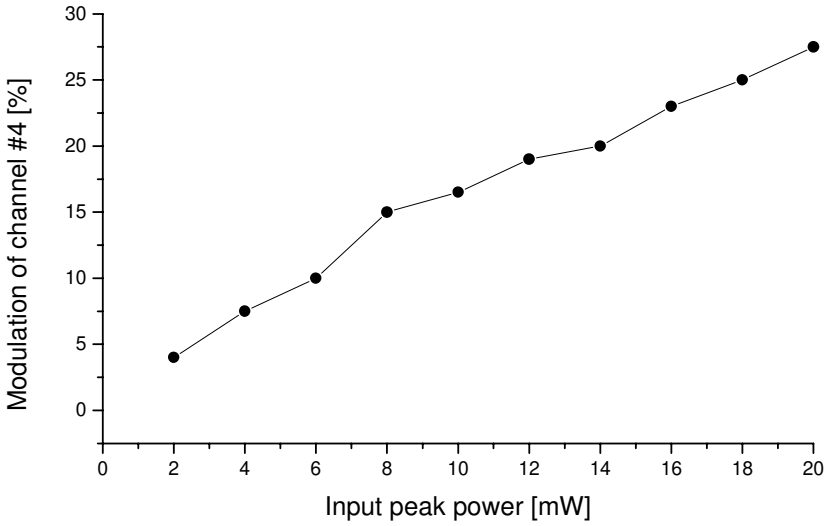

Figure 6.7: Modulation of channel #4 by other channels due to XPM versus input peak power

6.2 Channel numbers

In order to examine the impact of channel numbers on system performance, a simulation series with increasing channel numbers, starting from only one channel, has been run. Having channel #4 as the only transmitting channel, no XPM effects are visible, as Figure 6.8 indicates. Different to other simulations within this chapter, a link length of only 50 km has been chosen. By this, results are only little influenced by self-phase modulation, since the nonlin-

ear length $L_{nl} \approx 75$ km. Thus, Figure 6.8 shows an eye diagram of an undistorted signal with respect to XPM. Besides the electric lowpass filter, only noise of the laser diode and slight SPM effects alter the received signal. Chromatic dispersion is equalized as told in the introduction to Chapter 6.

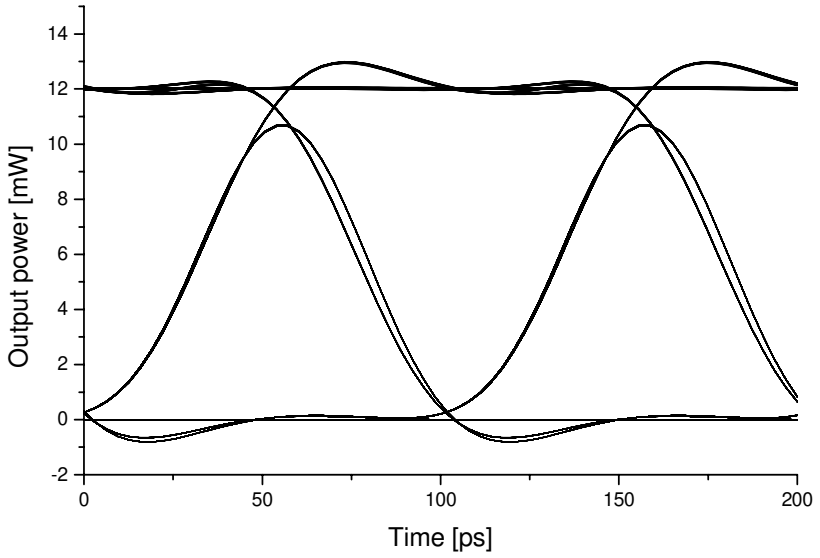

Figure 6.8: Eye diagram of channel #4 with no other transmitting channels present.

If a second transmitter (channel #5) is turned on, spaced 0.4 nm from the first one, XPM immediately leads to timing jitter and power fluctuations, as can be seen in Figure 6.9 and Figure 6.10. Figure 6.9 shows the bandpass-filtered optical time signal before amplification in the pre-amplifier, Figure 6.10 the corresponding eye diagram of the amplified and converted electrical signal. Here, the strong power fluctuations of the time signal in Figure 6.9 are slightly averaged by the lowpass filter applied to the signal.

As expected, with a total of 8 active channels, XPM shows a further increased influence on the signal (see Figure 6.11). However, Figure 6.11 also suggests that the influence of the additional channels (channels #1 to channel #3 and channel #6 to channel #8) is of minor importance than that of channel #5, an assumption which is confirmed by Figure 6.12. This should be due to the fact, that the added channels #1 and #2 and also #6 to #8 are spaced at least 0.8 nm from channel #4. Channel separation is one of the most important parameters for the XPM effect and will be evaluated in 6.3. Bit error rates based on Q factor from Figure

6.12 may well serve as a qualitative assessment.

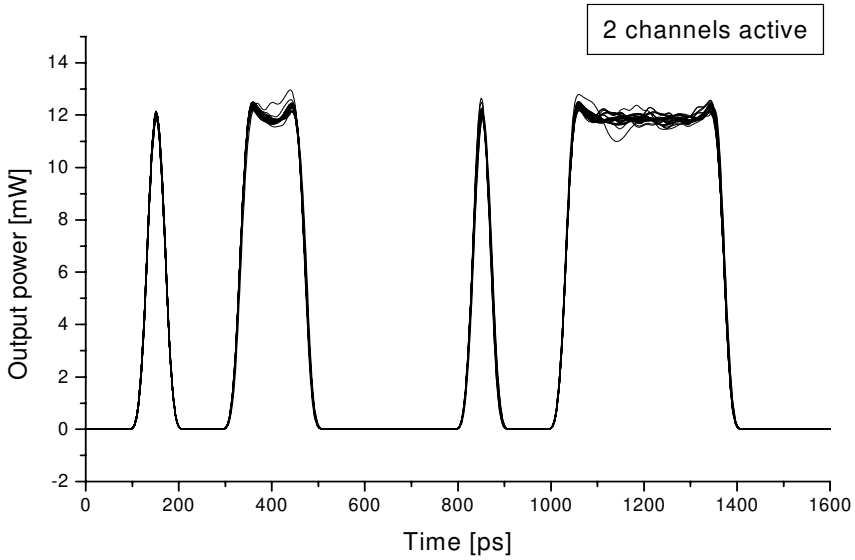

Figure 6.9: Time signal of channel #4 of 50 simulative runs with two transmitting channels. Power fluctuations due to XPM. Clock samples at $50 + i \cdot 100$ ps.

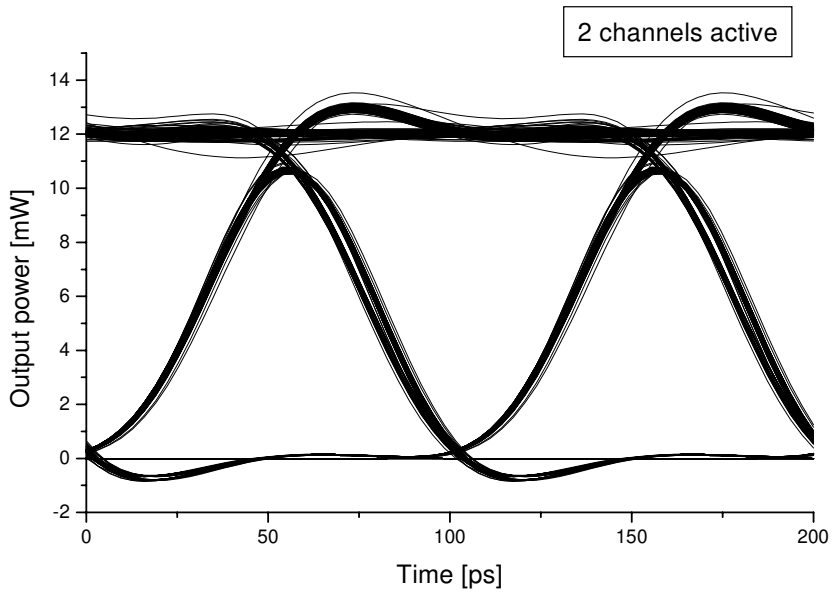

Figure 6.10: Eye diagram of channel #4 with one other transmitting channel present.

The assumption that channel #4 is most influenced by the channels #3 and #5 is further confirmed by Figure 6.13 showing the grade of modulation due to SPM (in case of channel #4 being the only active channel) and SPM and XPM (in case of two or more active channels).

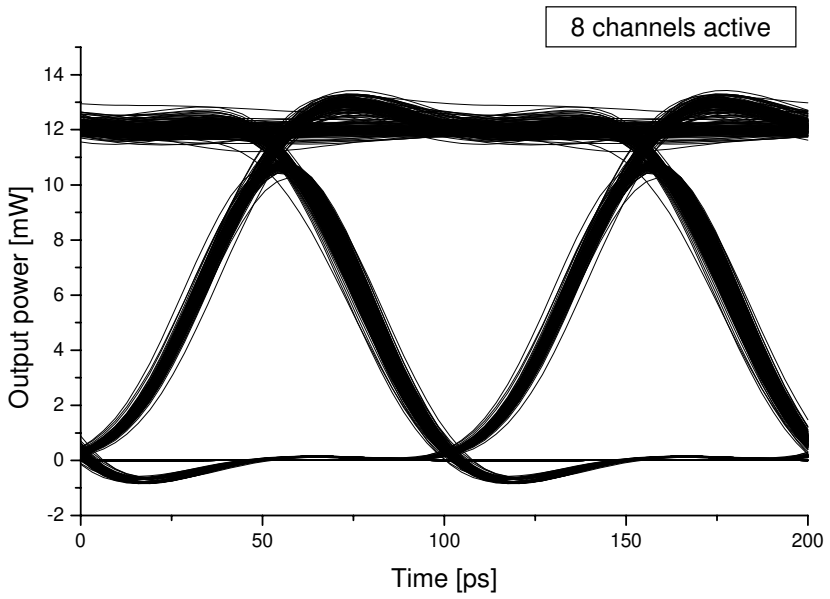

Figure 6.11: Eye diagram of channel #4 with a total of 8 transmitting channels.

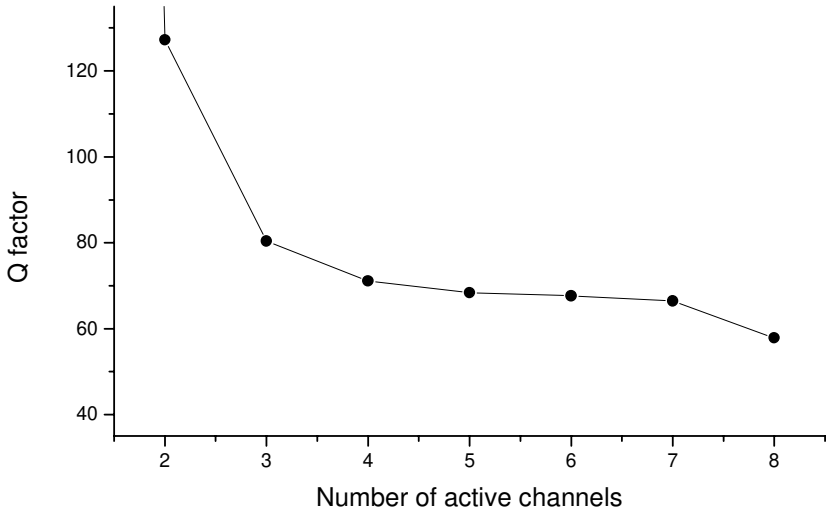

Figure 6.12: Q factor of channel #4 versus total number of transmitting channel. Two channels active connotes channel #4 and channel #5, three channels active connotes channel #4, channel #3 and channel #5, etc.

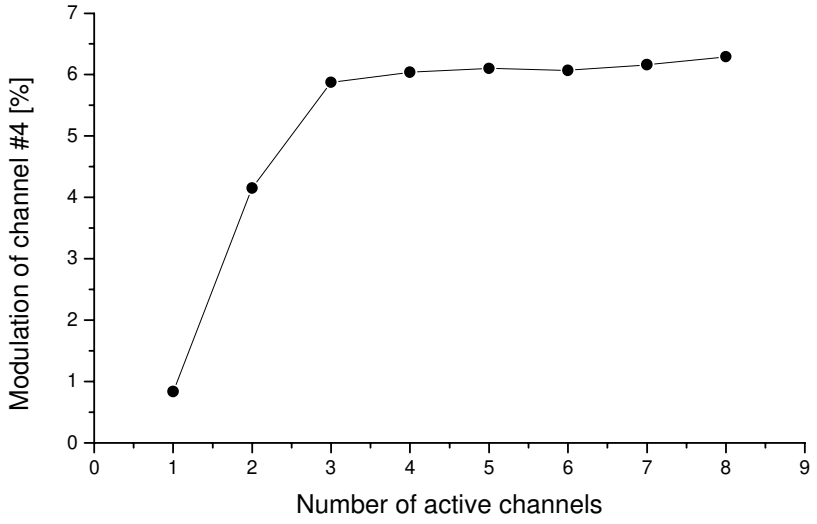

Figure 6.13: Modulation of channel #4 due to SPM and XPM versus number of active channels.

It is interesting to note, that the grade of modulation is not doubled when switching from two to three active channels, although the newly added channel (channel #3) has the same spectral separation as channel #5 from channel #4. This stems from the random bit sequences on all channels except channel #4, which in turn leads to a stochastic distribution of the power fluctuations for each transmitted bit. Assuming a Gaussian characteristic of the power fluctuations, one would expect a grade of modulation in case of three active channels of $\sqrt{4.06^2 + 4.06^2}\% = 5.75\,\%$, where 4.06% is the grade of modulation in case of two active channels, reduced with the SPM share. The measured value equals 5.81% which thus is very close to the predicted value. This sheds an interesting light on the behavior of the bit error rate performance when new channels are added. Since in this system configuration, the bit error rate strongly depends on the XPM effects, it will not be doubled by adding a new channel with the same spectral separation as the compared channel.

6.3 Channel spacing

One important parameter in a WDM transmission system, if not the most important, is the spectral separation of the active channels, also called the channel spacing. In order to increase total system capacity and to efficiently use the possible transmission bandwidth, channels

have to be separated as little as possible, keeping in mind that a 10 Gbit/s signal has a spectral width of up to 60 GHz or 0.48 nm, resp. One speaks of a DWDM transmission system, if channels are separated by less than 100 GHz or 0.8 nm, resp. In this environment, only little deviations in the precise carrier allocation immediately lead to crosstalk due to spectral overlapping of the signals. But not only the transmitters have to be exactly allocated, the bandpass filters also need careful attention. Their 3 dB bandwidth must completely cover the signal bandwidth and at the same time, must show a great sharpness to attenuate adjacent signals, see also section 6.4.

All eight channels were active in the simulation, the channel under examination transmitting the pseudorandom bit sequence 010100010111100, all other channels transmitting random bit sequences which are changed for each simulation run. Since interesting applications for WDM systems have channel spacings between 0.4 nm and 1.0 nm, the channel spacing has been changed from 0.3 nm to 1.3 nm. Figure 6.14 shows the Q factors for the 400 km link. No simulations were performed for channel #1 with channel spacings greater than 0.8 nm and for channel #8 with spacings greater than 0.7 nm, since these channels would then have been outside the spectral simulation window.

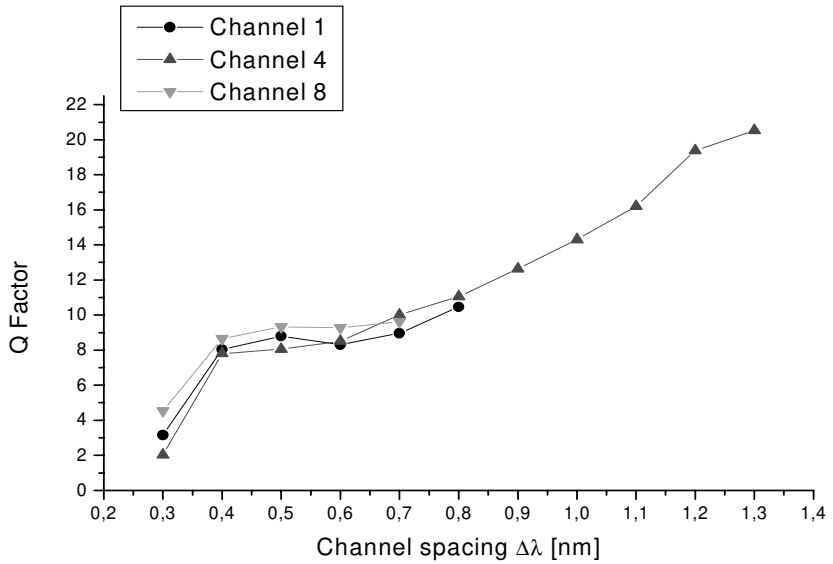

Figure 6.14: Q factors of channels #1, #4 and #8 versus the equidistant channel spacing. All eight channels are active.

As expected, the Q factors suddenly drop as soon as the channel spacing goes below 0.4 nm and the spectra of adjacent channels start to overlap. Simulations with channel spacings of

less than 0.3 nm would lead to bit error ratios of about 0.5 due to this overlap.

The realistically high Q factor of channel #4 at a spacing of 1.2 nm should be due to the stochastic effects in connection with the random input signals. As Figure 6.14 shows, a channel spacing of $\Delta\lambda$=0.4 nm is the absolute minimum value for a realistic system scenario, leading to a Q factor of approximately 8, but leaving almost no margin for further error sources such as splices or connectors. Again, for comparative reasons with simulations of the hybrid system, the eye penalty is shown in Figure 6.15.

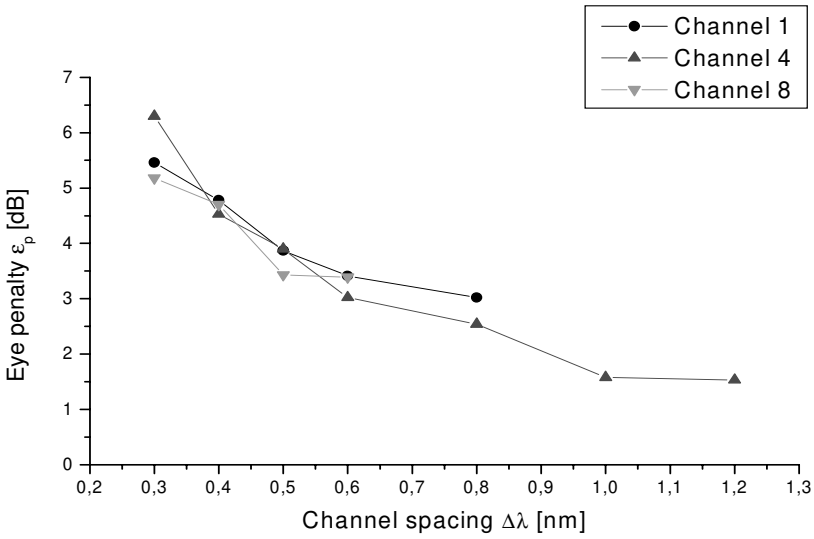

Figure 6.15: Eye penalty ε_p of channel #1, #4 and #8 versus channel spacing. Link length and input peak powers were fixed at 400 km and 12 mW, resp. All eight channels were active.

Taking the modulation of channel #4 versus the equidistant channel spacing as shown in Figure 6.16, the grade of modulation is linear proportional to the inverse of the channel spacing, a result which confirms experiments carried out in [21].

The results of [48] can thus also be confirmed by the performed simulations. The performance of a multichannel transmission system approaches a singlechannel state, as soon as the spectral separation of the involved channels is well over 1.0 nm.

Changing the horizontal axis to a $1/\Delta\lambda$ scale as done in Figure 6.17, the linear nature of the grade of modulation with respect to inverse of the channel spacing becomes obvious.

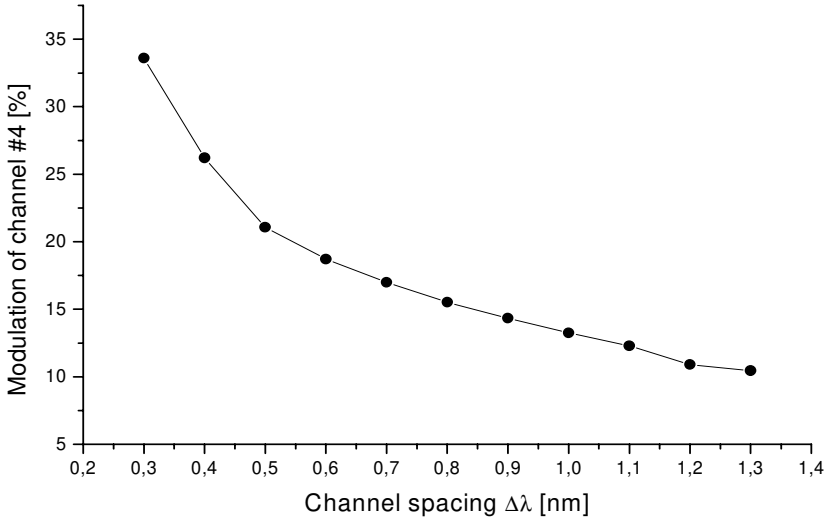

Figure 6.16: Modulation of channel #4 due to SPM and XPM versus channel spacing. All 8 channels are active.

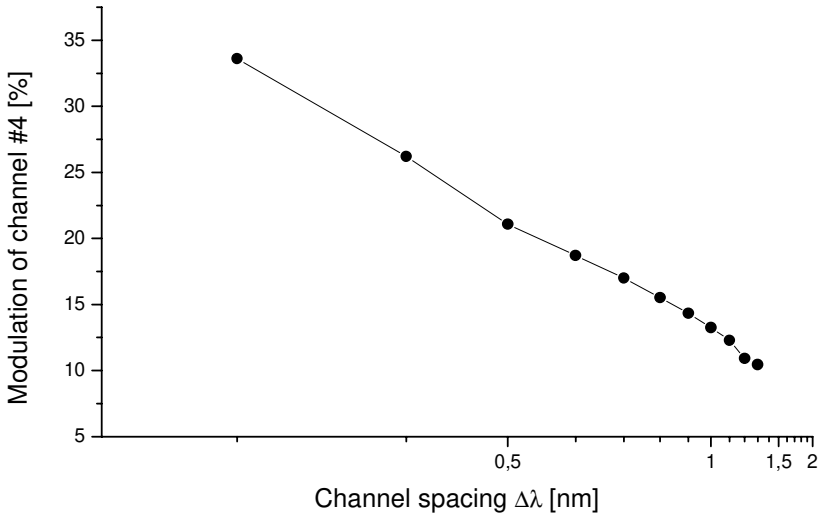

Figure 6.17: Modulation of channel #4 due to SPM and XPM versus channel spacing on a reciprocal scale of the horizontal axis. All eight channels are active.

6.4 Bandpass filter characteristics

Whereas in a single channel transmission, the only task of the bandpass filter in front of the receiver is the reduction of accumulated noise originating from the optical amplifiers, in a WDM and even more in a DWDM system, bandpass filters additionally have to block intrachannel interference. The most important design parameter is thus its 3 dB filter bandwidth $B_{3\,dB}$ and its sharpness, i.e. the attenuation of the adjacent channels. As pointed out in section 5.4, grating filters meet both demands with satisfying results. Figure 6.18 shows the Q factor of the DWDM system with varying 3 dB bandwidths.

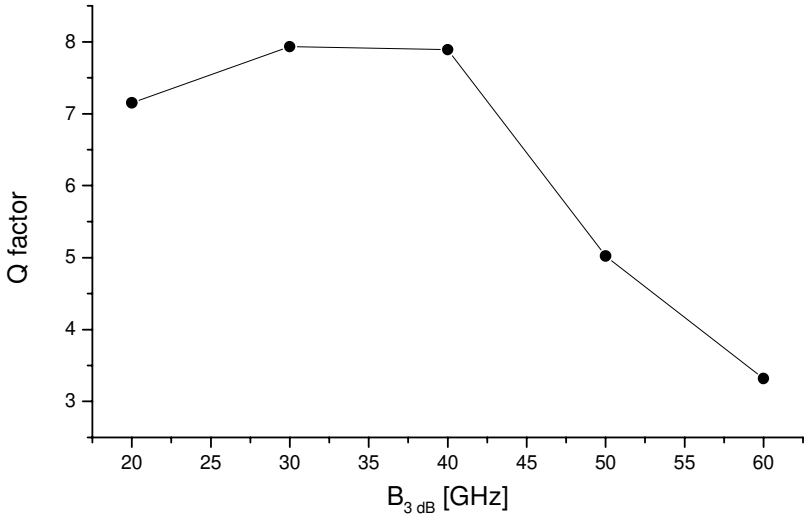

Figure 6.18: Q factor of channel #4 versus the single-sided 3dB bandwidth of the optical bandpass filter in front of the receiver diode. Adjacent channels active.

A single-sided 3 dB bandwidth $B_{3\,dB}$ smaller than 30 GHz (60 GHz double-sided) or 0.67 nm at 1.55 µm leads to an attenuation of the selected signal, since its spectral width is 25 GHz approx. If the 3 dB bandwidth exceeds 40 GHz, adjacent channels are no more suppressed effectively and the Q factor falls down immediately due to intrachannel interference. As Figure 6.18 suggests, the optimum 3 dB bandwidth is 35 GHz (single sided) approx., leaving some margin for filter instabilities like temperature or aging drifting, to which grating based filters are especially susceptible.

6.5 Link length

In a dispersion compensated transmission system, single channel applications experience no distortions from the chromatic dispersion, but only from accumulated noise and self-phase modulation. Since self-phase modulation effects at 1.55 µm occur in noticeable measures only at higher power levels, the system performance is mainly noise-limited. Link lengths of several thousands of kilometers have thus been reached to date [2].

In a WDM system, though, cross-phase modulation hinders the use of long transmission links. The longer the link, the longer the time in which copropagating signals can interact and transfer power. Furthermore, in a DWDM system with very low walk-off effects in adjacent channels, the cross-phase modulation effect strongly reduces the maximum link length. Figure 6.19 shows the Q factor for channels #1, #4 and #8 for various link lengths of the 10 GBit/s-system described at the beginning of this chapter.

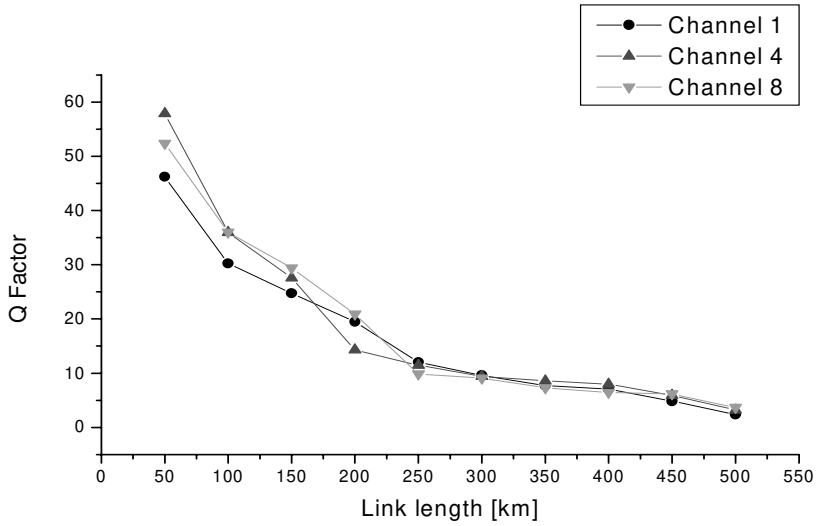

Figure 6.19: Q factor of channel #1, #4 and #8 versus link length. Decline of Q factor mainly due to XPM.

Link lengths of more than 400 km (corresponding to a Q factor of approx. 8) are not advisable for this specified system, since there is almost no power margin left. At 450 km, the Q factors drop down to 4.82, 5.92 and 6.16 for channel #1, #4 and #8, resp., and at 500 km, there is a dramatic drop to Q factors of only 2.37, 3.18 and 3.68, resp., allowing no useful transmission. This fact is also shown in Figure 6.20 by the eye penalties versus the link length.

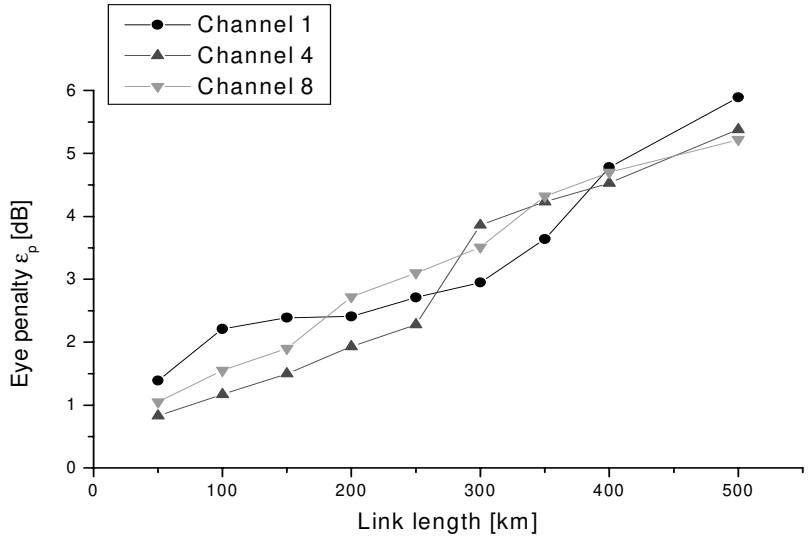

Figure 6.20: Eye penalty ε_p of channels #1, #4 and #8 versus link length. Input peak powers and channel spacings were kept fixed at 12 mW and 0.4 nm, resp. All 8 channels were active.

The same picture is drawn by Figure 6.21, showing the modulation of channel #4 due to XPM of the copropagating channels.

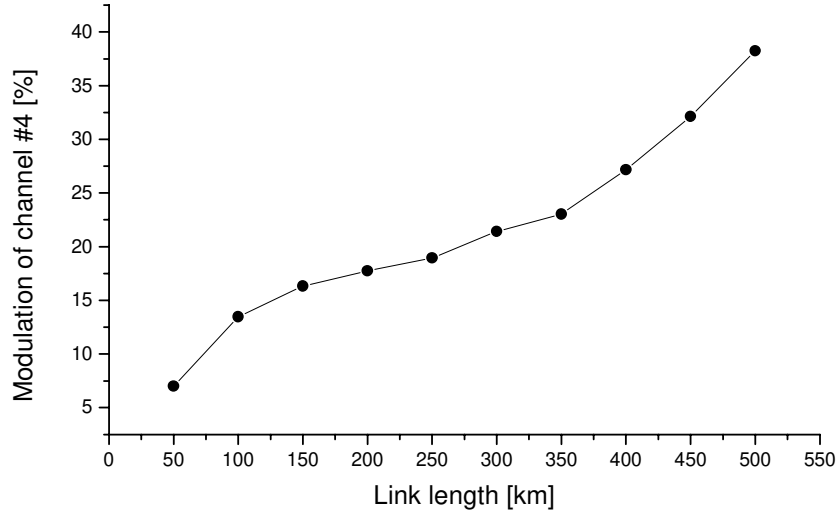

Figure 6.21: Modulation of channel #4 due to XPM versus link length. All eight channels are active.

It is interesting to note, that the curve representing the grade of modulation shows two

inflection points. Alas, the changes in Q factor as well as in the grade of modulation are smallest in the 250 km regime. Systems operating with that length should thus be especially robust against parameter deviations. In order to get a feeling for Q factor values in terms of eye diagrams, Figure 6.22 and Figure 6.23 shows the eye diagrams of 50 km and 400 km link lengths, resp. It must be noted that the Q factor of 57.87 is a qualitative statement. Its corresponding bit error ratio is not realistic.

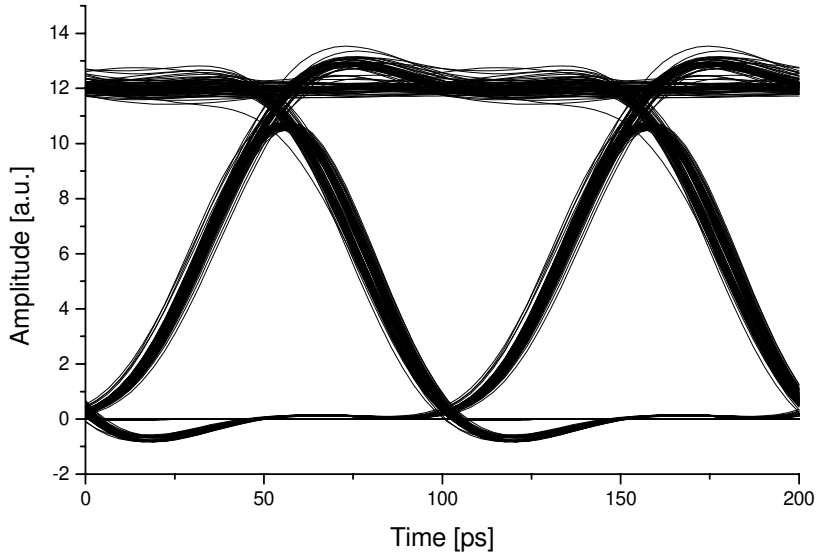

Figure 6.22: Eye diagram of channel #4, link length 50 km, Q factor: 57.87.

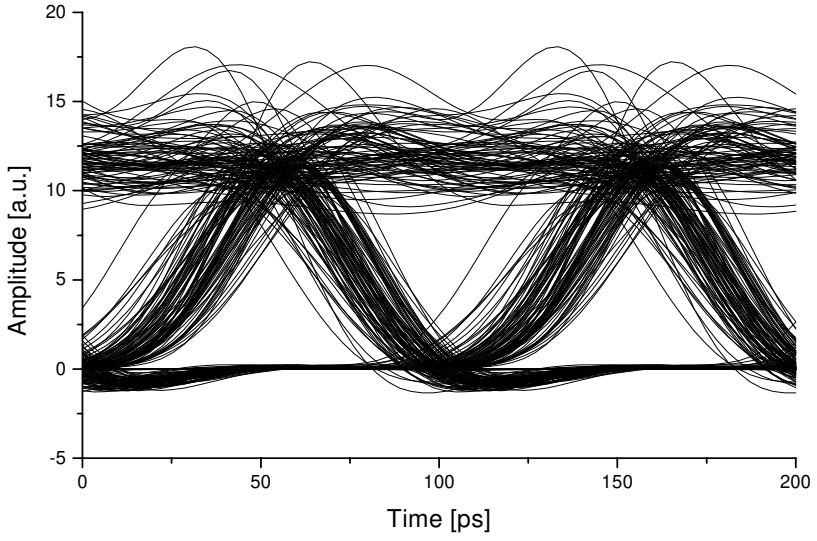

Figure 6.23: Eye diagram of channel #4, link length 400 km, Q factor: 7.98.

Chapter 7

Characteristics of the hybrid OCDMA/ WDMA transmission system

This chapter deals with the examination of a hybrid CDMA/WDMA transmission system. The performance of this system with 8 wavelength channel, each of which is optically direct sequence encoded by its own specific code sequence, is evaluated by varying sensitive system parameters such as input power level, link length and channel spacing, thus making a comparison with the results received in Chapter 6 possible.

In section 7.1, the system structure is described. The components were already described in Chapter 5 and Chapter 6. Section 7.2 proposes the code sequences that will be used in the simulation of the hybrid system. Section 7.3 finally presents the very attractive simulation results.

7.1 The structure of the system model

The modeled optical hybrid transmission system is shown in Figure 7.1. It allows the simulation of the transmission of up to eight data channels, each with arbitrary carrier wavelength, signal format, specific code sequence and random bit sequence over a fibre optic link with selectable link length.

Each **transmitter** consists of a data source, a laser diode and the CDMA encoder:

- The **data source** of the user under examination generates a 16 bit long pseudo-random bit sequence (0101100010111100), all other data sources emit a random distributed bit sequence of 16 bit length. The bitrate can be chosen arbitrarily and is the same for all channels, its default value has been set to 10 GBit/s.

- These data signals serve as input signal for the **laser diodes**. The carrier wavelength of each diode as well as the spectral spacing between the diodes can be chosen arbitrarily. The default value of channel #4, one of the middle channel, has been set to 1552.5 nm, the default value for the channel spacing is 0.4 nm (50 GHz, approx.). The simulated direct modulation emits a chirp- and noisefree NRZ signal with a temporal width of T_{FWHM} = 3.125 ps and a repetition time of 1600 ps, thus optimized for a 10 GBit/s data signal and a 16 chip code sequence. The output power of the emitted light can also be chosen arbitrarily. The default value of the oversampling factor has been set to 64.
- The **encoders** are a configuration of fibre optic tapped delay lines, each adjusted to the specific code of each channel which is shown in Table 7.1, thus each having a length of 1.25 mm (corresponding to a delay of one chip position) to 18.75 mm (15 chip positions). The delay lines consist of the same standard single mode fibres as used for the link, coupling losses are neglected.

The following **multiplexer** (MUX) combines all 8 different signals and transfers them into the fibre. It is assumed to be lossfree, coupling losses as well as crosstalk are neglected.

The **fibre optic link** consists of an arbitrary number of fibre units, each including a L_{pre} = 2.82 km piece of DCF for precompensation of the chromatic dispersion, a L_{SMF} = 50 km piece of SSMF, a L_{post} = 2.60 km piece of DCF for postcompensation and finally an ideal[1] **Erbium Doped Fibre Amplifier** (EDFA) with a noise figure of 6 dB. The lengths of pre- and postcompensating fibres have been chosen to reduce the total chromatic dispersion of each fibre unit closely to zero. The amplification of the amplifiers has been set to 15.4 dB in order to compensate for the loss the signal experiences when travelling over the fibre. The fibre parameters of the SSMF are: attenuation α = 0.2 dB/km at λ = 1552.5 nm, chromatic dispersion β_2 = -21.69 ps^2/km, effective area $A_{eff} = 95 \cdot 10^{-12}$ m^2 at λ = 1552.5 nm. Parameters of the DCF are: attenuation α = 1.0 dB/km at λ = 1552.5 nm, chromatic dispersion β_2 = 200 ps^2/km, effective area $A_{eff} = 95 \cdot 10^{-12}$ m^2 at λ = 1552.5 nm. The underlying propagation equations have been described in Chapter 4.

[1] Ideal in the sense of not introducing signal distortions (as crosstalk, carrier frequency shifts, saturation effects et al.) except noise.

The **demultiplexer**'s only task is to distribute the combined signal of all 8 channels to eight different spatial channels, i.e. fibre pieces. It does not contain any bandpass filters. It is, as the multiplexer, assumed to be loss- and distortionfree.

The **receivers** consist of the subsequent components:

- The **decoder** in each receiver consists - like the encoder - of fibre optic tapped delay lines that emulate the actual code word of Table 7.1, thus correlating the incoming signal with the desired code sequence.
- The **receiving** diodes, modeled as pin-diodes, convert the optical signal into an electrical. Their characteristics are described in 5.4.2.
- To remove unnecessary noise from the data signal, the decoded bit stream then passes a **lowpass filter**, implemented as a 3rd order Butterworth filter with a 3 dB bandwidth of 80 % of the actual bitrate (default value: 8 GHz). The transfer function of the filter is described in 5.4.3.
- In the final **signal analysis block**, the Q factor and the eye penalty ε of each channel is calculated as well as the eye diagram drawn. This block is the same as the one used in the WDM system. Further specifications of this block can therefore be found in 5.4.3.

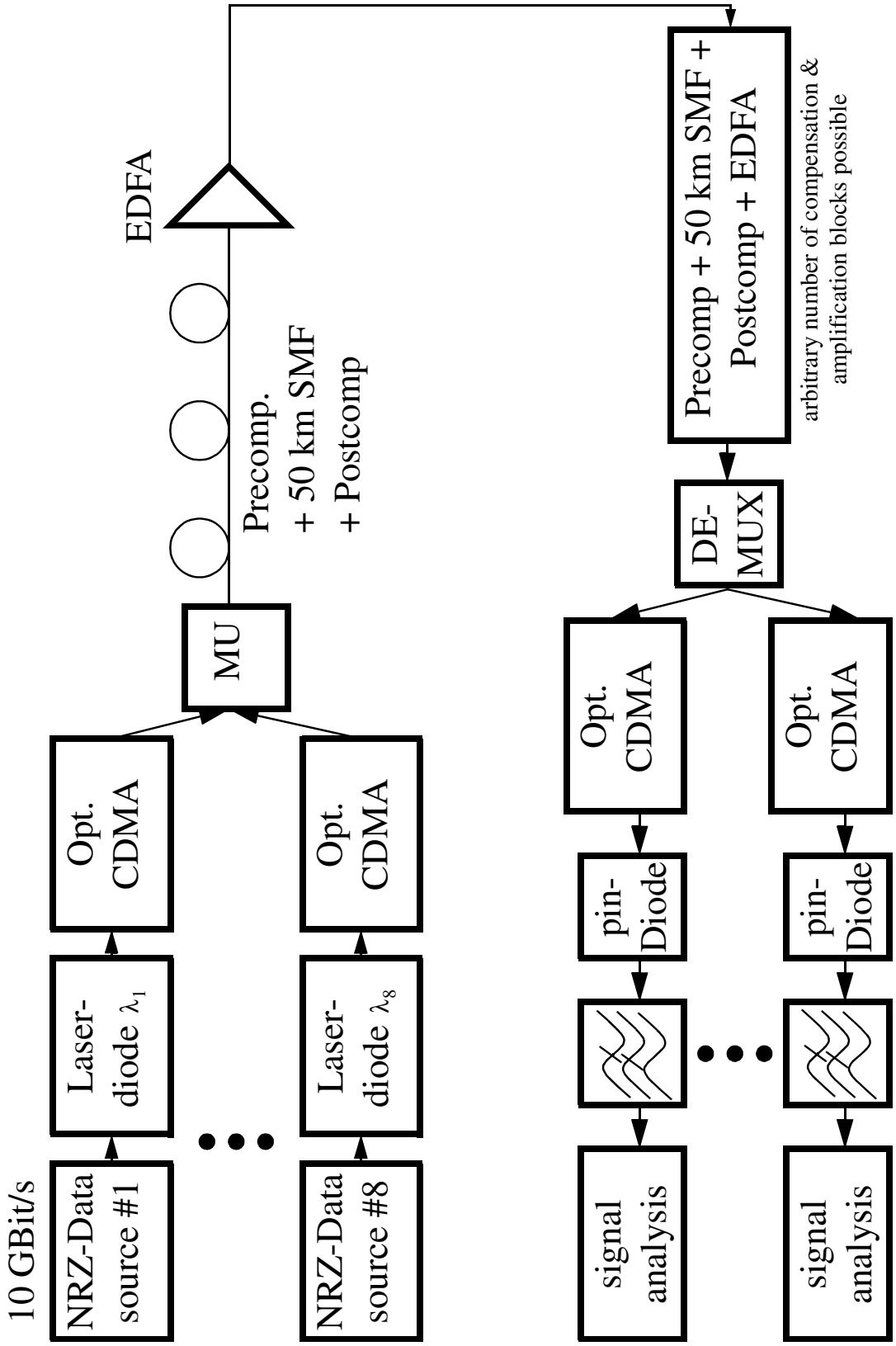

Figure 7.1: The structure of the simulated hybrid OCDMA/WDMA lightwave system

7.2 Appropriate codes for a hybrid system

The discrete, spectrally separated wavelength channels usually operate at bitrates of up to B_{Signal} = 10 GBit/s in commercially available and widely common WDM transmission systems. Since switching speeds of the involved electronic components reach up to approx 100 GBit/s, it is evident that it is a costly task to increase bit rates so that these 100 GBit/s can be exceeded. OTDM (optical time division multiplex) is one of the techniques which enable transmission speeds which lie above the 100 GBit/s barrier. However, if this technique is used both in the transmitter as well as in the receiver (demultiplexer) system complexity and costs increase dramatically.

Since in a hybrid OCDM/WDM system the total transmission rate (or chip rate, resp.) equals the product of the original (signal) bitrate times the code sequence length $B = B_{Signal} \cdot F$ and B_{Signal} = 10 GBit/s, sequence lengths F should lie well below 100 chips per bit, see Figure 7.2. To minimize the MAI stemming from the usage of a pseudo orthogonal coding of the involved channels and maximizing at the same time the number of channels with which this is possible, it is advisable to focus on the errorfree subset of a modified optical orthogonal code as proposed in Chapter 3. Furthermore, as a result of chapter 3.3, the code weight should be minimized in order to maximize the number of simultaneous users (or channels in a hybrid system, resp.).

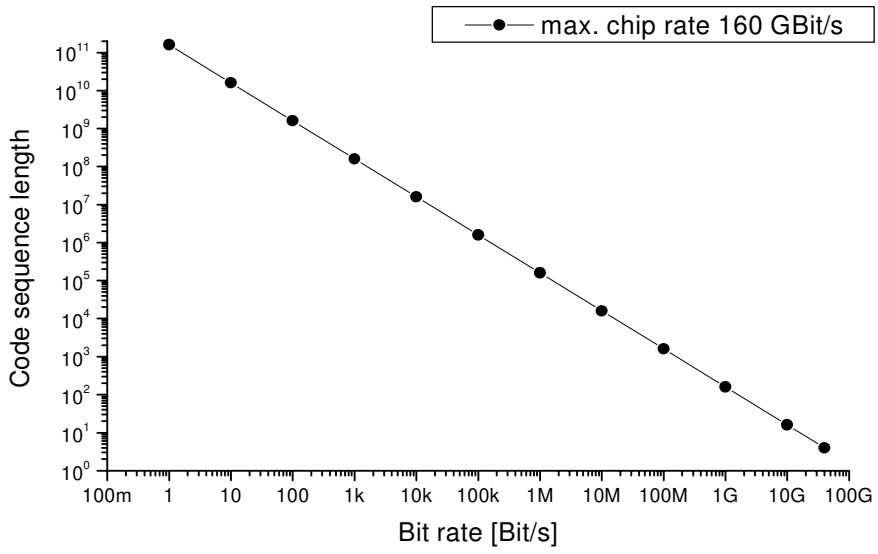

Figure 7.2: Max. allowed code sequence length depending on signal bit rate. Code sequence length times bit rate equals a maximum that was set to 160 GBit/s due to expected signal degradations originating from the fibre characteristics.

For simulational reasons and because of practical feasibility, a (16,3) MOOC has been chosen for the simulation of the hybrid OCDM/WDM system. This code offers the possibility to encode $N_{ef} = 8$ channels with a code length of $F = 16$ which suites the demands for the simulated system presented in 7.1 perfectly. The eight different code words, selected through the greedy algorithm as presented in Chapter 3, are shown in Table 7.1.

Sequence and channel number	Code word
1	1100 0001 0000 0000
2	0000 1100 0001 0000
3	0000 0000 1100 0001
4	0001 0000 0000 1100
5	0010 1001 0000 0000
6	0000 0010 1001 0000
7	0000 0000 0010 1001
8	1001 0000 0000 0010

Table 7.1: Code words of a (16,3) modified optical orthogonal code.

7.3 Simulation results

This section presents the simulation results that were achieved with the hybrid transmission system that was presented in section 7.1. Analogous to Chapter 6, where simulation results were presented for a pure WDM system, parameters like input power, channel spacing and link length are varied and their impact examined.

7.3.1 Input powers

In a fibre optic transmission system, it is very important to choose the right power level that is adjusted to the specific link. The system behavior is usually very sensitive to variations in the input power levels of the various wavelength channels. To evaluate the behavior of the hybrid OCDMA/WDMA system, system simulations with a link length of 400 km and a channel spacing of $\Delta\lambda = 0.2$ nm between adjacent channels were performed, while the carrier wavelength of channel #4 was fixed to 1552.5 nm. All 8 channels were active. As Figure 7.3 shows, the hybrid system offers bit error rates that are well below levels that are demanded for high bit rate transmissions. All channels behave equally. With increasing input powers, the XPM is responsible for interchannel modulation products and the eye gets more closed. However, the eye penalty factor ε always stays below 3 dB due to the correlation

reception of the signals.

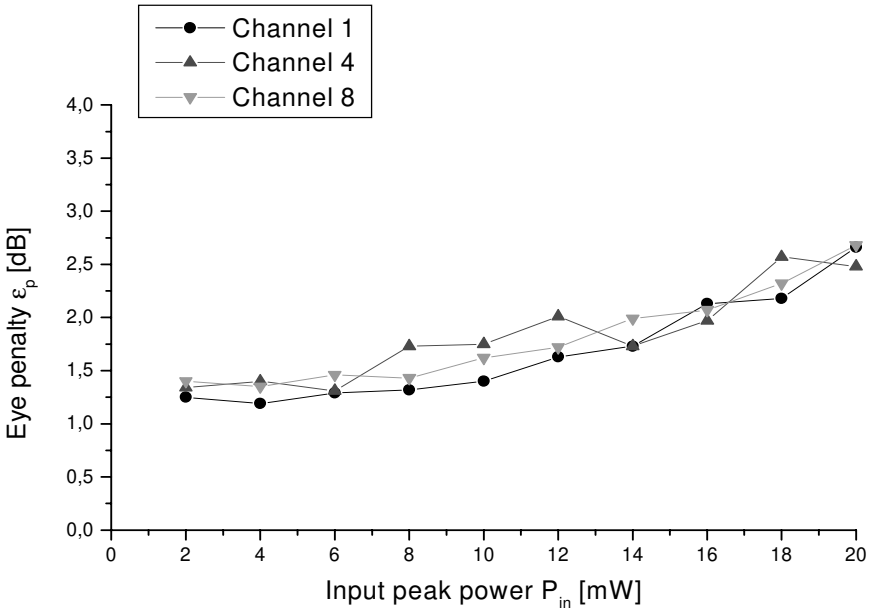

Figure 7.3: Eye penalty factor ε_p versus input peak power for channels #1, #4 and #8. Channel spacings and link lengths were fixed to 0.2 nm and 400 km, resp.

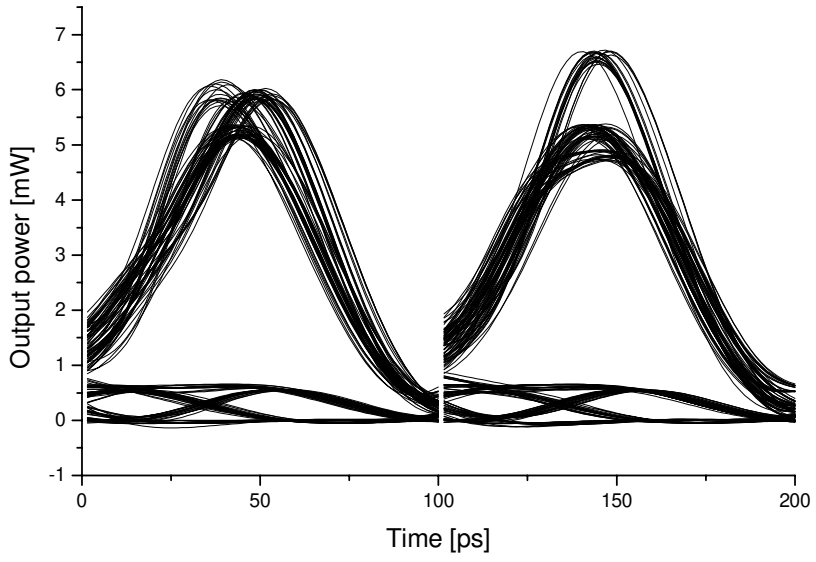

Figure 7.4: Eye diagram of channel #4, input power 6 mW, link length 400 km, channel spacing 0.2 nm, all 8 channels active

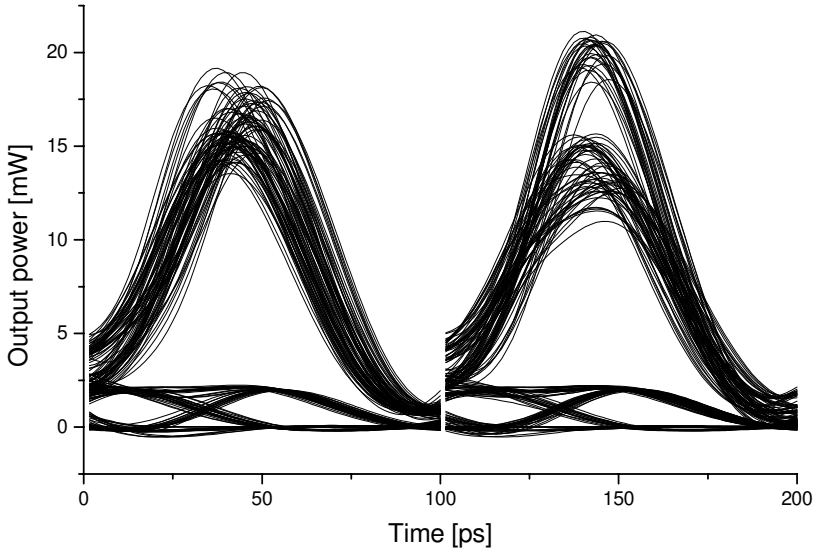

Figure 7.5: Eye diagram of channel #4, input power 20 mW, link length 400 km, channel spacing 0.2 nm, all 8 channels active

The different amplitude levels on the left and on the right of Figure 7.4 and Figure 7.5 are due to disadvantageous XPM effects that result from the fixed input signals on the neighboring channels. For subsequent simulations, these fixed bit streams were replaced by random bit streams.

Figure 7.4 and Figure 7.5 show the eye diagram of channel #4 for a link length of 400 km, a channel spacing of 0.2 nm and input powers of 6 mW and 20 mW per channel, resp. In both cases, the eye is widely open, resulting in a clearly detectable signal.

l

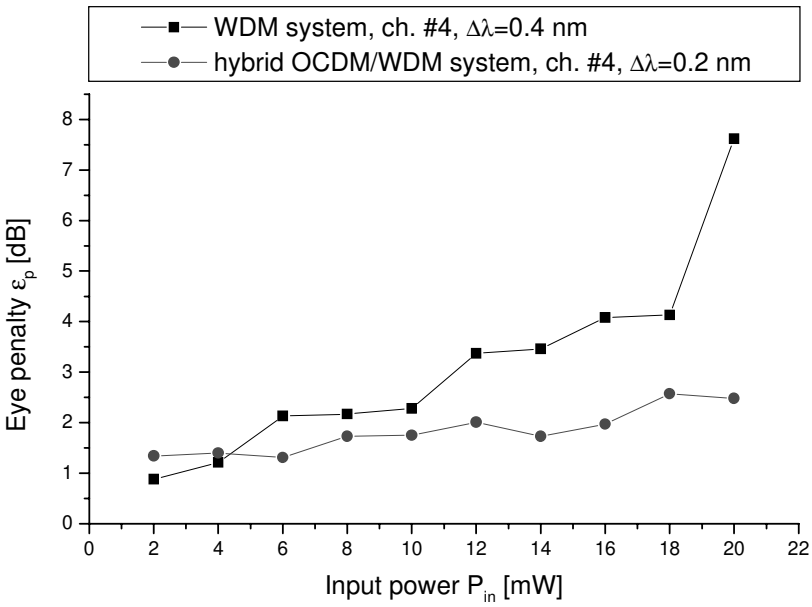

Figure 7.6: Eye penalty ε_p of channel #4 in both the WDM and the hybrid OCDM/WDM system. Channel spacing 0.2 nm in the hybrid system, 0.4 nm in the WDM system, link length 400 km, all 8 channels active.

Figure 7.6 shows a comparison of the pure WDM system with a channel spacing of 0.4 nm and the hybrid system with a spacing of 0.2 nm. Although the channel spacing of the hybrid system is thus only half the spacing of the WDM system, the BER is much lower for almost all input powers. Without the coded transmission, the XPM greatly degrades the transmitted signals, making a decent BER for input powers greater than approx. 14 mW impossible. It must be mentioned, that a transmission with a spacing of only 0.2 nm in the WDM system would lead to unacceptable bit error rates (see Figure 6.14).

7.3.2 Channel spacing

One of the main aims of the simulation was to evaluate the dependence of the (hybrid) transmission performance on the channel spacing. Whereas in a pure WDM system, transmissions at 10 GBit/s can not be performed with a channel spacing of less than 0.3 nm, see section 6.3, the hybrid system shows a valuable robustness against variations in the carrier wavelengths of the different channels. The carrier wavelength of channel #4 was kept at 1552.5 nm. During the simulations, all 8 channels were active with a fixed peak input

power of 12 mW per channel and a transmission link length of 400 km. As can be seen in Figure 7.7, a safe and reliable transmission for all channels can be guaranteed for all possible channel spacing values $\Delta\lambda$. It is interesting to note, that the worst eye penalty factors are obtained in the case of a channel spacing of 0.0 and 0.1 nm. In the case of zero channel spacing, no crossphase modulation occurs and the eye penalty factor is mainly determined by the orthogonality of the used code sequences. With a spectral separation greater than zero, crossphase modulation occurs which is - in conjunction with residual crosscorrelation products - responsible for the eye closure. The greater the channel spacing, the less the spectral overlap of the different channels, the lower the crosscorrelation products and thus, the better the eye penalty factor. The high eye penalty of channel #1 at $\Delta\lambda = 0.4$ nm should be due to stochastic coincidences of channels #2 to #8 which were fed with random input bit sequences.

No results were obtained for channel #1 with channel spacings greater than 0.8 nm and channel #8 for spacings greater than 0.6 nm, since these channels were then outside the spectral window that was simulated.

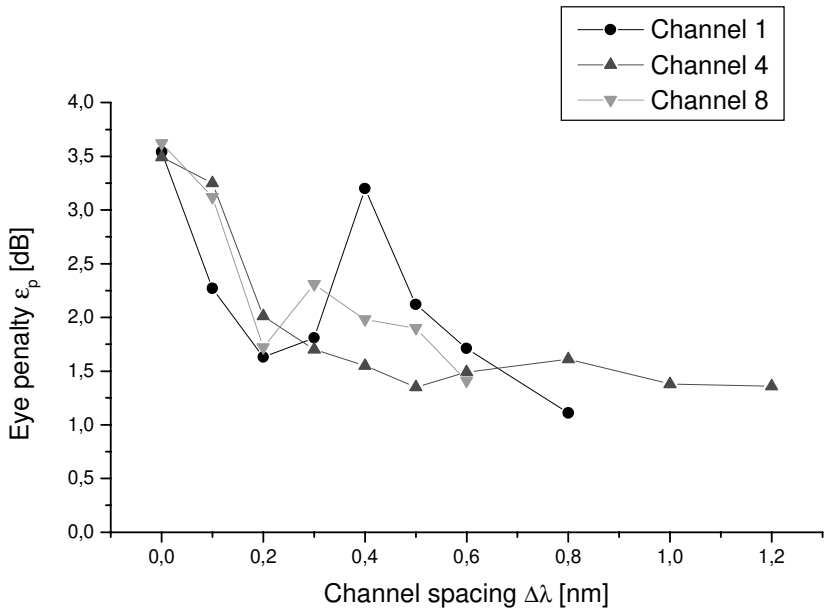

Figure 7.7: Eye penalty factor ε_p versus channel spacing for channels #1, #4 and #8. Input powers and link lengths were fixed to 12 mW and 400 km, resp.

Figure 7.8 and Figure 7.9 show the eye diagram for channel #4 in the case of complete spectral overlap of all channels ($\Delta\lambda = 0$ nm) and a spacing of $\Delta\lambda = 0.6$ nm. It is interesting to note, that the eye diagram in the case of the 0 nm spacing is mainly influenced by the multiple access interference(„0“ level corresponds to amplitude values of 0, 1 and 4; „1“ level corresponds to amplitude values of 10, 12 and 14), whereas in the case of 0.6 nm, crossphase modulation and crosscorrelation products are responsible for the deviations in the „1“ level and mainly crosscorrelation products for the deviations in the „0“ level.

Following from Figure 7.7, Figure 7.8 and Figure 7.9, a safe transmission on all 8 channels even in the case of total spectral overlap can be guaranteed.

A direct comparison between the WDM and the hybrid OCDM/WDM system shows Figure 7.10, where the eye penalty factor of channel #4 in both systems is shown. Whereas in the WDM system, a spectral spacing of 0.4 nm or less is critical or even impossible with regard to an acceptable bit error rate, the hybrid system offers superior signal quality. The pure WDM system can offer similarly good results as the hybrid system only for channel spacings greater than 0.9 nm.

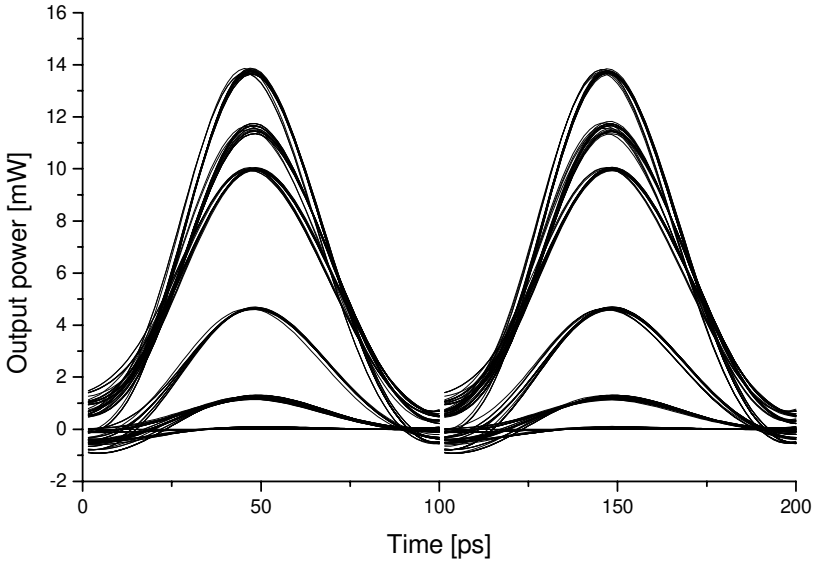

Figure 7.8: Eye diagram of channel #4, input power 12 mW, link length 400 km, channel spacing 0 nm, all 8 channels active

.

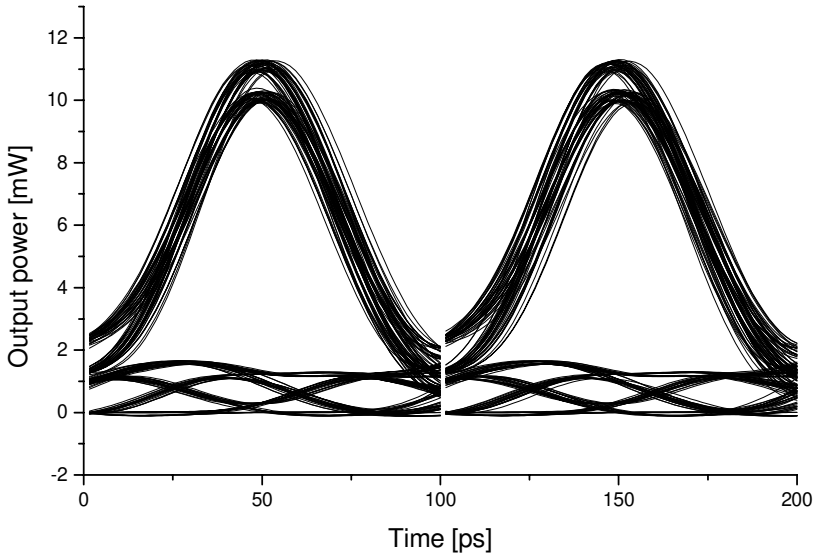

Figure 7.9: Eye diagram of channel #4, input power 12 mW, link length 400 km, channel spacing 0.6 nm, all 8 channels active.

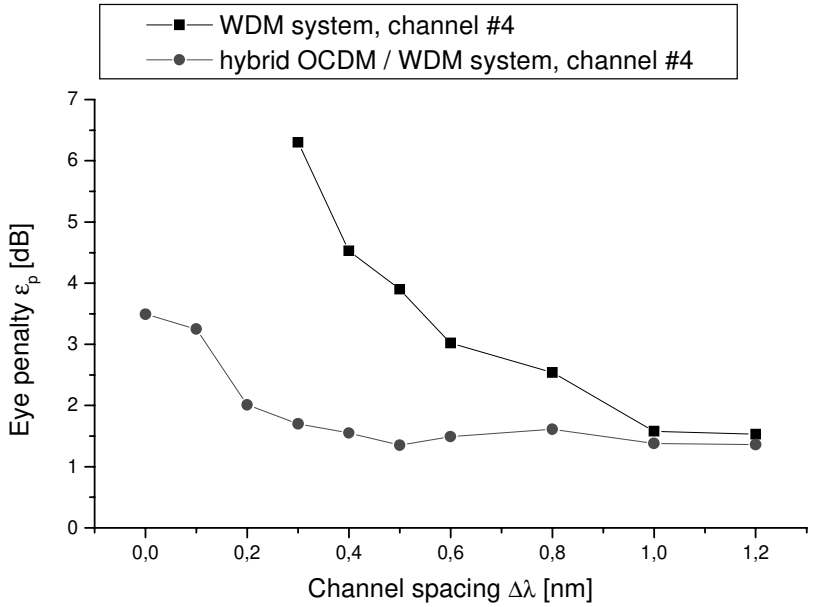

Figure 7.10: Eye penalty ε_p of channel #4 in both the WDM and the hybrid OCDM/WDM system. Input power 12 mW, link length 400 km, all 8 channels active.

7.3.3 Link length

Analogous to 6.5, the link length of the hybrid system was examined. Again, all 8 channels were simultaneously transmitting 10 GBit/s signals, the input peak power of each channel was 12 mW, the channel spacing $\Delta\lambda = 0.4$ nm and the carrier wavelength of channel #4 was fixed at $\lambda_4 = 1552.5$ nm. Figure 7.11 shows the eye penalty factors of channel #1, channel #4 and channel #8. All channels behave similarly. As expected and analogous to a sole WDM transmission, the eye penalty factor increases as the link length increases. The difference in the eye penalty factors between the different channels, especially for longer link lengths greater than 200 km, can be reduced to the passive dispersion compensation which has been adjusted to channel #4, in order to keep overall dispersion as low as possible for this channel. No dispersion slope compensation has taken place, so that a small residual dispersion remains for every channel except channel #4, including namely channel #1 and channel #8.

A comparison between Figure 6.20 and Figure 7.11 shows, that the decrease in output signal performance is much less in the case of a coded transmission, an effect due to the correlation reception of the transmitted signals. Whereas in the uncoded transmission, the eye penalty factor exceeds 4 dB at a link length of 300 km or more, all channels show a much less eye closure if the hybrid transmission scheme is employed. Even at 400 km, $\varepsilon < 3.5$ dB, ensuring bit error levels that are more than sufficient. Furthermore, Figure 7.11 shows that the hybrid system is very stable against different link lengths, making renewed link calculations in the case of a link shortage or extension an easy task.

Figure 7.12 shows the eye diagram of channel #8 for a link length of 50km. XPM has not yet had much influence on the signal and the eye is widely open. Small residual crosscorrelation products can be seen in the „1“ level due to a partial spectral overlap. In Figure 7.13, the eye is only a little bit more distorted. Comparing Figure 7.13 with Figure 6.23 shows a much better resistance against XPM in the case of coded transmission, a fact that is substantiated by Figure 7.14. Whereas at little link lengths, the WDM system is slightly better than the hybrid system (due to the missing of crosscorrelation products in the WDM system), the hybrid system keeps a much lower eye penalty throughout the whole link length.

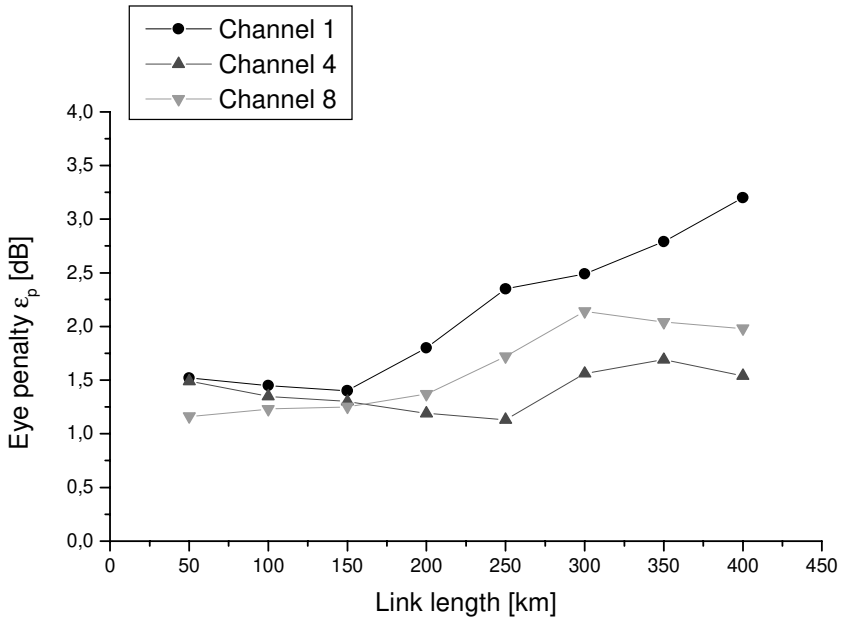

Figure 7.11: Eye penalty factor ε_p versus link length for channels #1, #4 and #8. Input powers and channel spacings were fixed to 12 mW and 0.4 nm, resp.

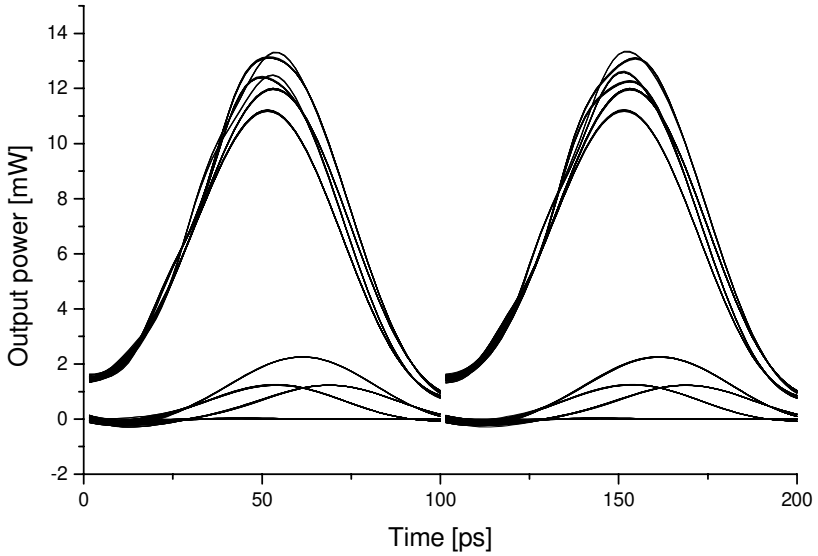

Figure 7.12: Eye diagram of channel #8, input power 12 mW, link length 50 km, channel spacing 0.4 nm, all 8 channels active

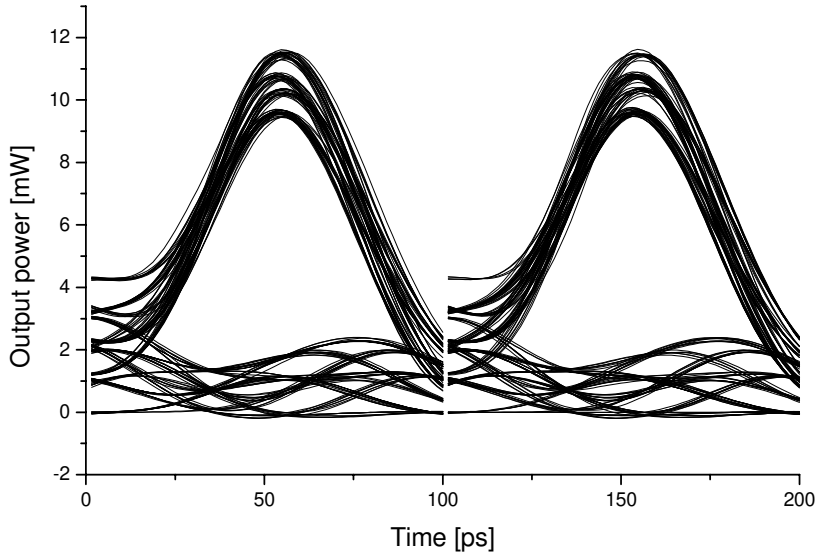

Figure 7.13: Eye diagram of channel #8, input power 12 mW, link length 400 km, channel spacing 0.4 nm, all 8 channels active.

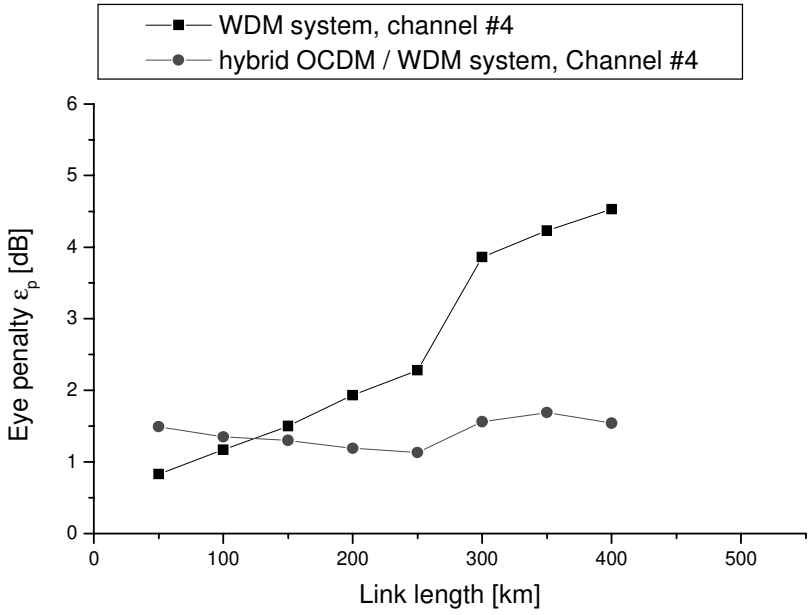

Figure 7.14: Eye penalty ε_p of channel #4 in both the WDM and the hybrid OCDM/WDM system. Input power 12 mW, channel spacing 0.4 nm, all 8 channels active.

Chapter 8

Summary

In this thesis a new family of codes for the use in optical high bit rate transmission systems with a direct sequence code division multiple access scheme component was developed and its performance examined. These codes were then used as orthogonal sequences for the coding of the different wavelength channels in a hybrid OCDMA/WDMA system. The overall performance was finally compared to a pure WDMA system.

The common codes known up to date have the problem of needing very long sequence lengths in order to accommodate an adequate number of users. Thus, code sequence lengths of 1000 or more were necessary to reach bit error ratios of 10^{-12} with only about 10 simultaneous users. However, these sequence lengths are unacceptable if signals with data rates higher than 100 MBit/s are to be transmitted, not to speak about the number of simultaneous users.

Starting from the well known optical orthogonal codes (OOC) and under the assumption of synchronization among the participating transmitters - justified for high bit rate WDM transmission systems -, a new code family called „**m**odified **o**ptical **o**rthogonal **c**odes“ (MOOC) was developed by minimizing the crosscorrelation products of each two sequences. By this, the number of simultaneous users could be increased by several orders of magnitude compared to the known codes so far.

The obtained code sequences were then introduced in numerical simulations of a 80 GBit/s DWDM transmission system with 8 channels, each carrying a 10 GBit/s payload. Usual DWDM systems are featured by enormous efforts to minimize the spectral spacing between the various wavelength channels. These small spacings in combination with the high bit rates lead to very strict demands on the system components like laser diode, filters, multiplexers etc. Continuous channel monitoring and temperature regulations of sensitive components are

inevitable, but often cannot prevent drop downs of the bit error ratio due to aging effects or outer influences like mechanical stress.

The obtained results show that - very different to the pure WDM system - by orthogonally coding adjacent wavelength channels with the proposed MOOC, the overall system performance gets widely independent from system parameters like input powers, channel spacings and link lengths. Nonlinear effects like XPM that insert interchannel crosstalk are effectively fought. Furthermore, one can entirely dispense with the bandpass filters, thus simplifying the receiver structure, which is especially interesting for broadcast networks. A DWDM system upgraded with the OCDMA subsystem shows a very robust behavior against a variety of influences.

Zusammenfassung

Diese Arbeit beschreibt die Entwicklung einer neuen Codefamilie, die sowohl zum Einsatz in optisch hochbitratigen Übertragungssystemen mit reinem Codemultiplexzugriffsverfahren als auch für hybriden Wellenlängen- und Codemultiplexzugriffsverfahren gedacht ist. Sequenzen aus dieser Familie wurden sodann zur orthogonalen Codierung der Signale auf den verschiedenen Wellenlängenkanälen eines kombinierten OCDMA/WDMA-Systems eingesetzt. Das Verhalten dieses hybriden Systems, konzipiert als Upgrade eines bestehenden WDM-Systems, wurde daraufhin mit dem Verhalten eines reinen WDM-Systems verglichen.

1 Optischer Codemultiplex

Die CDMA-Technik geht auf die sogenannte Bandspreiztechnik (engl.: Spread Spectrum) zurück, die Anfang der 40er Jahre des 20. Jahrhunderts entwickelt wurde. Ziel war eine gegen absichtliche Störer resistente und vor unerlaubten Lauschern sichere Übertragung eines Funksignales. Dazu wird das Datensignal mit einem breitbandigeren Signal moduliert, so daß das übertragene Spektrum einen weiteren Bereich belegt als eigentlich notwendig ist. Zum Empfang wird das übertragene Signal erneut mit dem gleichen breitbandigen Signal moduliert, wodurch es spektral gestaucht wird und wieder seine ursprüngliche Form erhält. Gleichzeitig empfangene Störsignale werden durch diese Modulation jedoch weiter gespreizt, so daß der Empfänger diese Störsignale nur als schwaches Rauschen registriert. Zur fehlerlosen Stauchung des Spektrums ist die genaue Kenntnis des Spreizsignales unabdingbar. Greifen nun mehrere Sender/Empfängerpaare gleichzeitig auf das Übertragungsmedium zu, wobei jedes Paar ein nur ihm zugewiesenes, einzigartiges Spreizsignal verwendet, das zudem noch orthogonal zu allen anderen ist, so spricht man von Codemultiplexvielfachzugriffsverfahren.

Während die CDMA-Technik im Funkbereich schon lange bekannt, weithin untersucht und mittlerweile dank der Mobilkommunikation großflächig eingesetzt wird, blieben die Anwendungen im Bereich der faseroptischen Übertragung begrenzt. Dies lag neben dem

im Vergleich zur Funkübertragung recht störungsarmen Charakter des faseroptischen Übertragungskanals an der direkten Energiedetektion, die bei faseroptischen Übertragungssystemen aufgrund der hohen Frequenz der Signalträger (ca. 193 THz) fast ausschließlich vorgenommen wird. Diese bedingt, daß übertragene Signale, ebenso wie die Spreizsignale, nur „unipolar“ sein können (d.h. „0“ und „1“) im Gegensatz zur Funkübertragung, bei der Phasendetektion vorherrscht und bipolare Signale („-1“ und „1“) die Regel sind. Dadurch tritt eine erhebliche Verschlechterung der Korrelationseigenschaften der Spreizsignale (auch Codesequenzen genannt) ein, was letztendlich zu extrem langen Codesequenzen führt, um auf akzeptable „Orthogonalität“ und Anzahl unterschiedlicher Sequenzen zu kommen. Unter akzeptabler „Orthogonalität“ ist hier zu verstehen, dass die summierten Kreuzkorrelationen der Codesequenzen Maximalwerte aufweisen, die unterhalb der Maxima der Autokorrelationen liegen, um so eine Detektion zu ermöglichen.

Da die zu übertragende Datenrate dem Produkt von Eingangssignal und Codesequenzlänge F entspricht ($B_{total} = B_{Signal} \cdot F$), sind Codelängen von 1000 und mehr für hochbitratige Systeme ($B_{Signal} > 100\,\text{MBit/s}$) aufgrund der auch in Zukunft wohl auf etwa 100 GBit/s beschränkten Verarbeitungsgeschwindigkeit elektronischer Komponenten inakzeptabel.

Die Codierung/Decodierung wird aus diesem Grunde optisch durchgeführt, s. Abbildung 1.

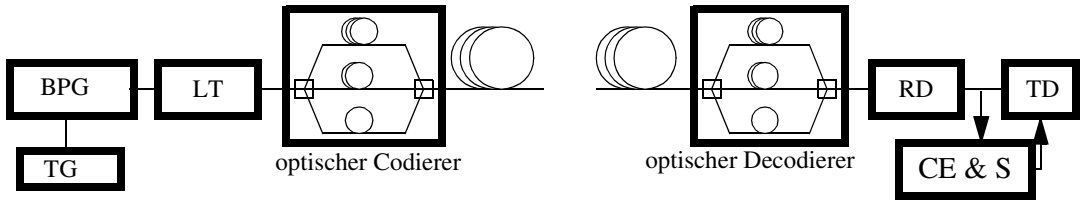

Abbildung 1: Blockdiagramm des optischen Codierers und des optischen Decodierers. BPG: Bitsignalgenerator, TG: Taktgeber, LT: Lasertreiber, ED: Empfangsdiode, SE: Schwellwertentscheider, TR & S: Taktregenerator und Synchronisation.

Die eigentliche Signalverarbeitung erfolgt somit nicht mit der höheren Codedatenrate, sondern nur mit der geringeren Signaldatenrate. Einzig der Bitgenerator bzw. Lasertreiber muß in der Lage sein, kurze Impulse (entsprechend der Periode der Codedatenrate) zu liefern, deren Wiederholrate jedoch der Signaldatenrate entspricht. Zusätzlich werden als Codesequenzen die von mir im folgenden vorgestellten Codesequenzen verwendet. Da von vorneherein das Augenmerk auf der Möglichkeit einer einfachen und wenig komplexen Systemaufrüstung bereits installierter faseroptischen Systeme

lag, wurden nur eindimensionale, temporale Sequenzen in Erwägung gezogen.

1.1 Konventionelle Codes

Die bekannten konventionellen Codes - optisch orthogonale Codes (OOC), Primsequenz (PS) Codes, quadratische Kongruenz (QC) Codes - gehen davon aus, daß die auf das Übertragungsmedium zugreifenden Sender/Empfängerpaare untereinander nicht synchronisiert sind. Alle Codes haben gemeinsam, daß sie sehr große Codelängen benötigen ($F > 1000$), um selbst nur 30 gleichzeitige Sender/Empfängerpaare mit einer Bitfehlerrate von ca. 10^{-12} zu beherbergen. Sie alle werden charakterisiert durch das Quadrupel (F, w, ρ_a, ρ_c), wobei F die Länge einer Codesequenz, w das Codegewicht, ρ_a und ρ_c Beschränkungen der Auto- bzw. Kreuzkorrelationen bedeuten. Im Falle von PS und QC codes entspricht w einer Primzahl p und $F = p^2$. Abbildung 2 zeigt die entsprechenden Bitfehlerratenkurven.

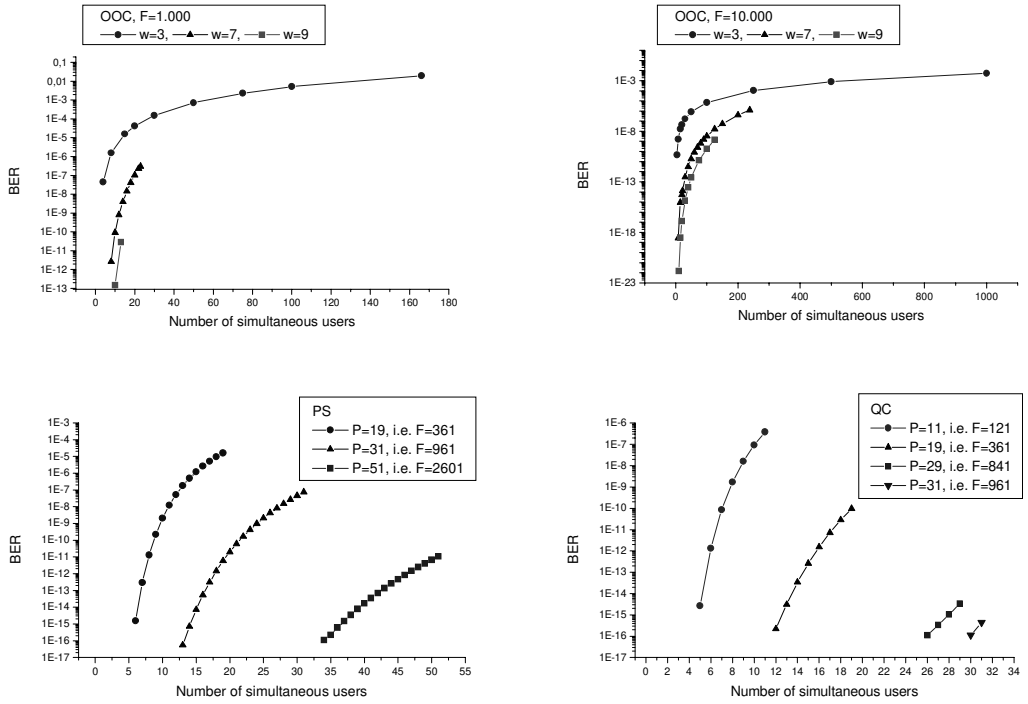

Abbildung 2: Bitfehlerraten von OOC, PS und QC codes.

1.2 Die modifizierten optisch orthogonalen Codes (MOOC)

Ausgehend von der Tatsache, daß in einem WDM- bzw. DWDM-System die verschiedenen Kanäle untereinander synchronisiert sind, wurde mittels dieser Tatsache eine neue Codefami-

lie entwickelt. Zugrunde liegen diesen sogenannten modifizierten optisch orthogonalen Codes (MOOC) die optisch orthogonalen Codes mit den Schranken $\rho_a = 1$ und $\rho_c = 1$. Ein algorithmisches Verfahren (siehe Abb. 3.2 und Abb. 3.3) sucht nach zur jeweiligen OOC-Familie gehörenden Sequenzen, die, bei gleichzeitiger Verwendung mit den bereits bekannten OOC-Sequenzen, nicht zu einer Erhöhung der Bitfehlerrate führen, jedoch eine wesentlich höhere Anzahl von orthogonalen Codesequenzen als die ursprüngliche liefert (siehe Abbildung 3).

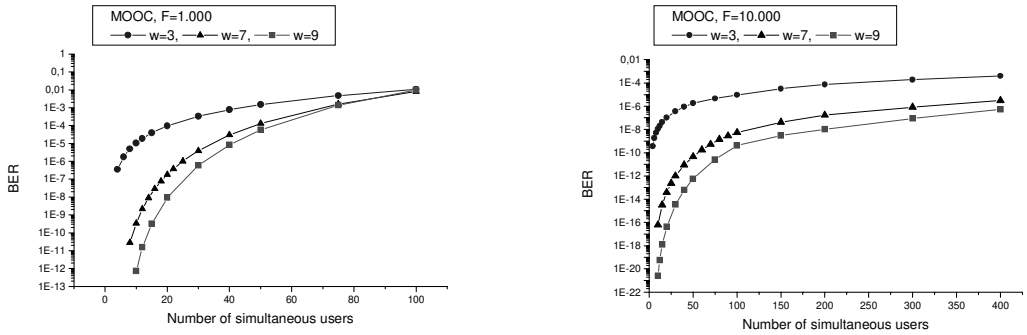

Abbildung 3: Bitfehlerrate der MOOC.

Alternativ kann der Algorithmus auch nur diejenigen Codesequenzen der jeweiligen MOOC-Familie ausgeben, die zu keinerlei Bitfehlern führen (die sogenannte fehlerfreie Teilmenge der MOOC). Somit können bis zu $2F/(w+1)$ unterschiedliche Sender/Empfängerpaare mit orthogonalen Codesequenzen ausgestattet werden, was eine wesentliche Steigerung gegenüber den bisherigen Codes bedeutet. Werden über die $2F/(w+1)$ Codes noch die übrigen Sequenzen verwendet, treten wiederum Bitfehler auf, jedoch erst bei Teilnehmerzahlen, die die der bekannten Codes um ein Vielfaches übersteigt (siehe Abbildung 4).

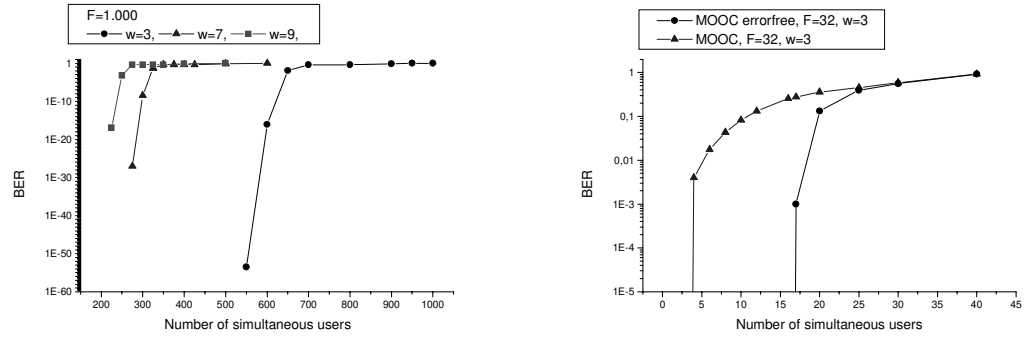

Abbildung 4: Bitfehlerrate der fehlerfreien Teilmenge der MOOC für große (links) und kleine Codelängen (rechts, im Vergleich mit den gesamtem MOOC Sequenzen)

Abbildung 4 zeigt, daß insbesondere die fehlerfreie Teilmenge geeignet ist, um mit kleinen Codelängen hochbitratige Signale zu codieren. Bei einer Länge von $F = 16$ können 8, bei $F = 32$ 16 verschiedene Sender/Empfängerpaare in einem Codemultiplexverfahren eingesetzt werden.

2 Das hybride OCDMA/WDMA-Übertragungssystem

Die so gewonnen Codes wurden nun in einem 80 GBit/s DWDM-System (8 Kanäle mit jeweils 10 GBit/s) verwendet, um dessen Anfälligkeit gegen nichtlineare Verzerrungen, herrührend u.a. von Kreuzphasenmodulation und gegen spektrale Schwankungen der Trägerwellenlängen zu reduzieren. Übliche DWDM-Systeme betreiben einen enormen Aufwand, um das genaue Einhalten des vorgegebenen Kanalrasters einzuhalten. Temperatur- und Alterungseffekte sowie äußere Einwirkungen wie mechanische Belastungen führen zu erhöhten Bitfehlerraten trotz kontinuierlicher Überwachung der Kanäle und steiler Filterflanken der eingesetzten grating-basierten, optischen Bandpassfilter. Werden bei bestehenden DWDM-Systemen die unterschiedlichen Kanäle jeweils mit den entsprechenden MOOC-Sequenzen orthogonal zueinander codiert, so zeigt sich eine große Robustheit gegenüber nichtlinearen Effekten und Schwankungen der Trägerwellenlängen (siehe Abbildung 5).

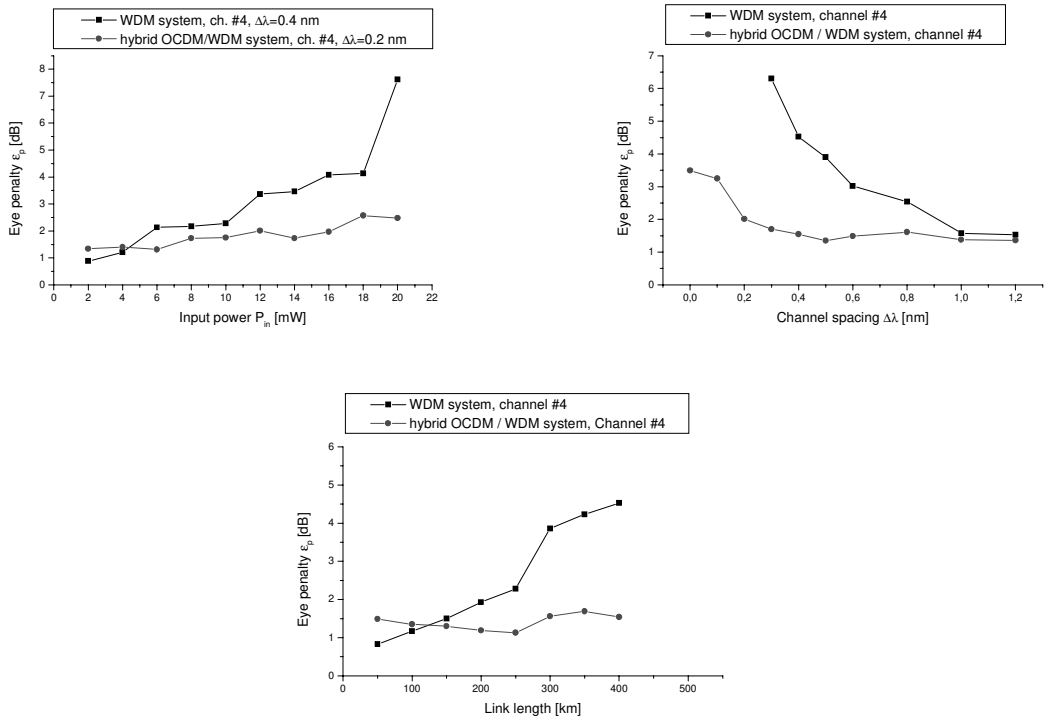

Abbildung 5: Augenfehler des hybriden OCDMA/WDMA(rot) und des reinen WDMA-Systems

Abbildung 5 zeigt, daß mit Hilfe des Codemultiplexaufsatzes auf ein bestehendes WDM- bzw. DWDM-System eine weitreichende Unabhängigkeit des Augenfehlers und damit der Bitfehlerrate von verschiedenen Systemparametern erreicht werden kann[1]. Somit kann selbst bei einer vollständigen Überlappung der Spektren ($\Delta\lambda = 0$ nm) noch mit Bitfehlerraten kleiner als 10^{-12} empfangen werden. Weiterhin können alle Bandpassfilter entfallen, die nicht der Reduzierung des ASE Rauschens dienen sondern der Separierung der verschiedenen Spektren. Die Empfängerkomplexität wird somit reduziert, was diese Systemstrukur insbesondere für Verteilnetze interessant macht.

[1] Ein Augenfehler von ca. 3.5 dB führt unter der Annahme von gaußverteilten Abtastwerten der Amplitude des empfangenen Signales auf eine Bitfehlerrate von etwa 10^{-12}.

List of Symbols

$A(z, \omega - \omega_0)$:	Slowly varying envelope approximation
A_{eff} :	Effective core area
$a_j(\mu)$:	Signature/code sequence
B_c :	Chiprate
B_b :	Bitrate
$\vec{b}$:	Magnetic flux density
$b_t^{(n)}$:	Data sequence of user #n
$b(\mu)$:	Data sequence in temporal dependence
$\|C\|$:	Code size
c :	Velocity of light
$\vec{d}$:	Electric flux density
$\vec{e}$:	Electric field vector
$\vec{E}$:	Fourier transform of electric field vector
F :	Codeword length
$F(x, y)$:	Field distribution of fundamental mode
$\vec{h}$:	Magnetic field vector
$\vec{H}$:	Fourier transform of magnetic field vector
h :	Planck's quantum
$I(z, t)$:	Slowly varying envelope of electric field
$i(t)$:	Electric current
K :	Number of simultaneous users
L_D :	Dispersion length
L_{NL} :	Nonlinearity length
$\vec{m}$:	Magnetic polarization
N :	Number of users

$\tilde{n}$:	Complex refactive index
n_2^I :	Kerr coefficient
P :	Prime number
$P_{el}(z, t)$:	Electric power
p :	Probability density function
$\vec{p}$:	Electric polarization
$p_M(\mu)$:	Unit pulse
q :	Elementary charge
$r(\mu)$:	Received signal at demultiplexer
$\vec{r}$:	Space vector
$s_n(\mu)$:	Encoder output signal
T_0 :	Full width at $1/e^2$ -intensity
T_{FWHM} :	Full width at half maximum
T :	Time period
t, τ :	Time
Th :	Threshold value
$U(z, \tau)$:	Normalized complex envelope
v_g :	Group velocity
w :	Codeweight

$\underline{\alpha}$:	Complex attenuation coefficient
$\beta(\omega)$:	Propagation constant
$\beta_x(\omega)$:	x th order dispersion coefficient
γ_{nl} :	Coefficient of nonlinear phase shift
ε :	Permittivity
ε_p :	Eye penalty factor
η :	Quantum efficiency
$\Delta\Lambda$:	Normalized spacing
λ :	Wavelength of optical carrier
μ :	Permeability
ν :	Optical carrier frequency
$\lvert\Omega\rvert$:	Max. number of simultaneous users
σ :	Electrical conductivity
ρ :	Space charge density
ρ_a :	Threshold for ACF sidelobes
ρ_c :	Threshold for CCF peak values
$\varphi_{r,\,p}(i)$:	Correlated receiver signal
χ :	Susceptibility

List of Acronyms

ACF	Autocorrelation function
BER	Bit error ratio
CCF	Crosscorrelation function
CCL	Coupled-cavity semiconductor laserdiode
CDM	Code division multiplex
CDMA	Code division multiple access
DCF	Dispersion compensating fibre
DD	Direct detection
DFB	Distributed feedback
DS CDMA	Direct sequence code division multiple access
DSF	Dispersion shifted fibre
DWDM	Dense wavelength division multiplex
DWDMA	Dense wavelength division multiple access
EAM	Electroabsorption modulator
EDFA	Erbium doped fibre amplifier
FH CDMA	Frequency hop code division multiple access
FTTH	fibre to the home
GVD	Group velocity dispersion
IM	Intensity modulation
ITU	International Telecommunication Union
LAN	Local area network
MAI	Multiple access interference
MAN	Metropolitan area network
MOOC	Modified optical orthogonal codes
MUX	Multiplexer

MZ	Mach-Zehnder
OADM	Optical add-drop multiplexer
OCDM	Optical code division multiplexing
OCDMA	Optical code division multiple access
OTDMA	Optical time division multiple access
OOC	Optical orthogonal codes
OOK	On-off keying
OXC	Optical cross-connect
PDF	Probability density function
PMD	Polarization mode dispersion
POF	Polymer optical fibre
SBS	Stimulated Brillouin scattering
SC	Star coupler
SPM	Selfphase modulation
SRS	Stimulated Raman scattering
SS	Spread spectrum
SSMF	Standard Single Mode Fibre
UMTS	Universal mobile telecommunication system
VCSEL	Vertival cavity surface emitting laser
WAN	Wide area network
WC	Wavelength converter
WDM	Wavelength division multiplex
WDMA	Wavelength division multiple access
WR	Wavelength routers
XPM	Crossphase modulation

References

[1] *Agrawal, G. P.*: Nonlinear fiber optics. Academic Press, San Diego, 1995

[2] *Agrawal, G. P.*: Fiber optic communication systems. John Wiley & Sons, New York, 1997

[3] *Aisawa S. et. al.*: A 1580-nm band WDM transmission technology employing optical duobinary coding. IEEE Journal of Lightwave Technology, vol. 17, no. 2, pp. 191-199, 1999

[4] *Anderson, C., Lyle, J.*: Technique for evaluating system performance using Q in numerical simulations exhibiting intersymbol interference. IEE Electronics Letters, vol. 20, no. 1, pp. 71-72, 1994

[5] *Barabas, U.*: Optische Signalübertragung. R. Oldenbourg Verlag, München, 1993

[6] *Bigo, S., Bellotti, G., Chbat, M. W.*: Investigation of cross-phase modulation limitation over various types of fiber infrastructures. IEEE Photonics Technology Letters, vol. 11, no. 5, pp. 605-607, 1999

[7] *Boyd, R. W.*: Nonlinear optics. Academic Press, San Diego, 1992

[8] *Butcher, D. N., Cotter, D.N.*: The elements of nonlinear optics. Cambridge University Press, Cambridge, 1990

[9] *Cartaxo, A. V.*: Cross-phase modulation in intensity modulation-direct detection WDM systems with multiple optical amplifiers and dispersion compensators. IEEE Journal of Lightwave Technology, vol. 17, no. 2, pp. 178-190, 1999

[10] *Chraplyvy, A. R.*: Limitations on lightwave communications imposed by optical-fiber nonlinearities. IEEE Journal of Lightwave Technology, vol. 8, no. 10, pp. 1548-1557, 1990

[11] *Chraplyvy, A. R., Tkach, R. W.*: Terabit/second transmission experiments. IEEE Journal of Quantum Electronics, vol. 34, no. 11, pp. 2103-2108, 1998

[12] *Chung, R. K., Salehi, J. A., Wei, V. K.*: Optical orthogonal codes: design, analysis, applications. IEEE Transaction on Information Theory, vol. 35, no. 3, pp. 595-604, 1989

[13] *Chung, Y. C., Jeong, J., Cheng, L. S.*: Aging-induced wavelength shifts in 1.5 µm DFB lasers. IEEE Photonics Technology Letters, vol. 6, no. 7, pp. 792-795, 1994

[14] *Dennis, T., Young, J. F.*: Optical implementation of bipolar codes. IEEE Journal of Quantum Electronics, vol. 35, no. 3, pp. 287-291, 1999

[15] *Eckert, J., Reichel, S., Leppla, R., Zengerle, R., Mattheus, A., Garcia, L.C.*: Experimental verification of bit pattern effects obtained in numerical simulations of a 10 GBit/s 1.3µm optical communication system. Proceedings PIERS '98, Nantes, 1998

[16] *Reichel, S., Eckert, J., Leppla, R., Zengerle, R., Mattheus, A., Garcia, L.C.*: Simulation and experimental verification of a 10-Gb/s NRZ field trial at 1.3µm using semiconductor optical amplifier. IEEE Photonics Technology Letters, vol. 10, no. 10 ,1998, pp. 1498 -1500

[17] *Eckert, J.:* Performance improvement of DWDM communication systems by optical orthogonal coding of adjacent channels. Proceedings PIERS '99, Volume 1, p. 104, Taipeh, 1999

[18] *Eiselt, M.*: Limits on WDM systems due to four-wave mixing: a statistical approach. IEEE Journal of Lightwave Technology, vol. 12, no. 2, pp. 2261-2267, 1999

[19] *Eiselt, M., Garrett, L.D., Tkach, R.W.*: Experimental comparison of WDM system capacity in conventional and nonzero dispersion shifted fiber. IEEE Photonics Technology Letters, vol. 11, no. 2, pp. 281-283, 1999

[20] *Eiselt, M., Shtaif, M., Garrett, L.D.*: Contribution of timing jitter and amplitude distortion to XPM system penalty in WDM systems. IEEE Photonics Technology Letters, vol. 11, no. 6, 1999

[21] *Eiselt, M., Shtaif, M., Garrett, L.D.*: Cross-phase modulation distortions in multi-span WDM systems. Proceedings OFC '99, 46/ThC5-, 1999

[22] *Fathallah, H., Rusch, L. A., LaRochelle, S.*: Passive optical fast frequency-hop CDMA communications system. IEEE Journal of Lightwave Technology, vol. 17, no. 3, pp. 397-405, 1999

[23] *Fathallah, H., Rusch, L. A.*: Robust optical FFH-CDMA communications: coding in place of frequency and temperature controls. IEEE Journal of Lighwave Technology, vol. 17, no. 8, pp. 1284-1293, 1999

[24] *Fathallah, H. et. al.*: Experimental demonstration of optical fast frequency hopping-CDMA communications. Proceedings ECOC '99, I-190, Nice, France, 1999

[25] *Forghieri, F., Tkach, R.W., Chraplyvy, A.R.*: Effect of modulation statistics on Raman crosstalk in WDM systems. IEEE Photonics Technology Letters, vol. 7, no. 1, 1995

[26] *Glisic, S. A., Leppänen, P. A.*: Code division multiple access communications. Kluwer Academic Publishers, Boston, 1995

[27] *Grau, G., Freude, W.*: Optische Nachrichtentechnik - Eine Einführung. 3.Auflage, Springer Verlag, Berlin, 1991

[28] *Griffin, R. A., Sampson, D. D., Jackson, D. A.*: Optical phase coding for code-division multiple access networks. IEEE Photonics Technology Letters, vol. 4, no. 12, pp. 1401-1404, 1992

[29] *Guy, M., et. al.*: Simultaneous absolute frequency control of laser transmitters in both 1.3 and 1.55 µm bands for multiwavelength communication systems. IEEE Journal of Lightwave Technology, vol. 14, no. 6, pp. 1136-1143, 1996

[30] *Hägele, V.*: Optimieren bestehender Übertragungsstrecken mit Standard-Einwellenfasern für Bitraten von 10 GBit/s. Fortschrittsberichte VDI, Düsseldorf, 1997

[31] *Hasegawa, A.*: Optical solitons in fibers. Springer Verlag, Berlin, 1989

[32] *Haus, H. A.*: Waves and fields in optoelectronics. Prentice-Hall, Englewood Cliffs, 1984

[33] *Heinlein, W.*: Grundlagen der faseroptischen Übertragungstechnik. Teubner Verlag, Stuttgart, 1985

[34] *Hirsch, O.*: Impulsausbreitung auf einer Standaradeinmodenfaser unter Berücksichtigung von Dämpfung, Kerr-Nichtlinearität und Dispersionskompensation. Diplomarbeit, Universität Kaiserslautern, 1998

[35] *Holmes, A. S., Syms, R. R. A.*: All-optical CDMA using "quasi-prime" codes. IEEE Journal of Lightwave Technology, vol. 10, no. 2, pp. 279-286, 1992

[36] *Huang, W. et. al.*: Coherent optical CDMA (OCDMA) systems used for high-capacity optical fiber networks-system description, OTDMA comparison and OCDMA/ WDMA networking. IEEE Journal of Lightwave Technology, vol. 18, no. 6, pp. 765-778, 2000

[37] *Huang, W., Andonovic, I.*: OCDMA/WDMA networks based on OCDMA systems with interference cancellation. Proceedings ECOC ’99, I-194, Nice, France, 1999

[38] *Ip, J.*: Component technologies for DWDM multiplexers. Proceedings OFC ’99, 82/ TuH3-1,1999

[39] *Jeruchim, M. C., Balaban, P., Shanmugan, K. S.*: Simulation of communcation systems. Plenum Press, New York, 1992

[40] *Karafolas, N., Uttamchandani, D.*: Local area network communications using optical spread spectrum and serial correlation of bipolar codes. Optical Fiber Technology, vol. 3, pp. 253-266, 1997

[41] *Kitayama, K.*: OCDM/WDM networks for gigabit access: 1.24 GBit/s, 2xOCDM by 2xWDM experiment. Proceedings ECOC ’99, I-194, Nice, France, 1999

[42] *Kwong, W. C., Perrier, P. A., Prucnal, P. R.*: Performance comparison of asynchronous and synchronous code-division multiple-access techniques for fiber-optic local area networks. IEEE Transactions on Communications, vol. 39, no. 11, pp. 1625-1634, 1991

[43] *Leonhard, S.*: Effiziente Simulationsverfahren für die Charakterisierung und das Design von Bauelementen der optische Nachrichtentechnik. Dissertation, Universität Kaiserslautern, 1999

[44] *Linn, J.*: Modellierung der Ausbreitung optischer Solitonen in einem verteilten Faser-

verstärker. Gawl Verlag, Bochum, 1998

[45] *Lochmann, D.*: Digitale Nachrichtentechnik. Verlag Technik, Berlin, 1995

[46] *Maric, S. V., Kostic, Z. I., Titlebaum, E. L.*: A new family of optical code sequences for use in spread-spectrum fiber-optic local area networks. IEEE Transactions on Communications, vol. 41, no. 8, pp. 1217-1221, 1993

[47] *Marcuse, D.*: Light transmission optics. Van Nostrand Reinhold, New York, 1982

[48] *Marcuse, D., Chraplyvy, A. R., Tkach, R. W.*: Dependence of cross-phase modulation on channel number in fiber WDM systems. IEEE Journal of Lightwave Technology, vol. 12, no. 5, pp. 885-890, 1994

[49] *Marhic, M. E.*: Coherent optical CDMA networks. IEEE Journal of Lightwave Technology, vol. 11, no. 5/6, pp. 854-864, 1993

[50] *Midwinter, J.E., Guo, Y.L.*: Optoelectronics and lightwave technology. John Wiley & Sons, Chichester, England, 1992

[51] *Mikhailov, V., Killey, R. I., Prat, J., Bayvel, P.*: Limitation to WDM transmission distance due to cross-phase modulation induced spectral broadening in dispersion compensated standard fiber systems. IEEE Photonics Technology Letters, vol. 11, no. 8, pp. 994-996, 1999

[52] Newsletter of the International Telecommunication Union. Genf, 1992

[53] Nuyts, R. J., Park, Y. K., Gallion, P.: Dispersion equalization of a 10 GBit/s repeatered transmission system using dispersion compensating fibers. IEEE Journal of Lightwave Technology, vol. 15, no. 1, pp. 31-42, 1997

[54] *Onaka, H., et. al.*: 1.1 TBit/s WDM transmission over 150 km 1.3 µm zero-dispersion single mode fiber. OFC 1996, post-deadline paper 19, San Jose, 1996

[55] *Ono, T., Yutaka, Y.*: Key technologies for terabit/second WDM systems with high spectral efficiency over 1 bit/s/Hz. IEEE Journal of Quantum Electronics, vol. 34, no. 11, pp. 2080-2088, 1998

[56] *Park, E., Mendez, A. J., Garmire, E. M.*: Temporal/spatial optical CDMA networks-de-

sign, demonstration and comparison with temporal networks. IEEE Photonics TEchnology Letters, vol. 4, no. 10, pp. 1160-1162, 1992

[57] *Peterson, R. L., Ziemer, R. E., Borth, D. E.*: Introduction to spread-spectrum communications. Prentice Hall, Englewood Cliffs, New Jersey, 1995

[58] *Proakis, J. G.*: Digital Communications. 2nd edition, McGraw-Hill, New York, 1989

[59] *Prucnal, P. R., Santoro, M. A., Fan, T. R.*: Spread spectrum fiber-optic local area network using optical processing. IEEE Journal of Lightwave Technology, vol. 4, no. 5, pp. 547-553. 1986

[60] *Rongqing, H., Demarest, K.R., Allen, C.T.*: Cross-phase modulation in multispan WDM optical fiber systems. IEEE Journal of Lightwave Technology, vol. 17, no. 6, pp. 1018-1026, 1999

[61] *Salehi, J. A.*: Code division multiple-access techniques in optical fiber networks - part I: fundamental principles. IEEE Transactions on Communications, vol. 37, no. 8, pp. 824-833, 1989

[62] *Salehi, J. A., Brackett, C. A.*: Code division multiple-access techniques in optical fiber networks - part II: systems performance analysis. IEEE Transactions on Communications, vol. 37, no. 8, pp. 834-842, 1989

[63] *Shaar, A. A., Davies, P. A.*: Prime sequences: Quasi-optimal sequences for or channel code division multiplexing. IEE Electronics Letters, vol. 19, no. 21, pp. 888-889, 1983

[64] *Shibata, N., Braun, R. P., Waarts, R. G.*: Phase-mismatch dependence of efficiency of wave generation through Four-Wave Mixing in a single-mode optical fiber. IEEE Journal of Quantum Electronics, vol. QE-23, p. 1025, 1987

[65] *Shivaleela, E. S., Sivarajan, K. N., Selvarajan, A.*: Design of a new family of two-dimensional codes for fiber-optic CDMA networks. IEEE Journal of Lightwave Technology, vol. 16, no. 4, pp. 501-508, 1998

[66] *Spirit, D.M., O'Mahony, M.J.*: High capacity optical transmission explained. John Wiley & Sons, Chichester, England, 1995

[67] *Steinbuch, K., Rupprecht, W.*: Nachrichtentechnik, Band II, Nachrichtenübertragung.

3. Auflage, Springer Verlag, Berlin, 1990

[68] *Stolen, R. H., Ippen, E. P., Tynes, A. R:.* Applied Physics Letters, vol. 20, pp. 62 ff., 1972

[69] *Tamura, S.*: Optical code-multiplex transmission by Gold sequences. IEEE Journal of Lightwave Technology, vol. 3, no. 1, pp. 121-127, 1985

[70] *Tancevski, L., Andonovic, I.*: Wavelength hopping/time spreading code division mutliple access systems. IEE Electronics Letters, vol. 30, no. 17, pp. 1388-1390, 1994

[71] *Tietze, U., Schenk, Ch.*: Halbleiter-Schaltungstechnik. 9. Auflage, Springer Verlag, Berlin, 1991

[72] *Wang, J., Petermann, K.*: Small signal analysis for dispersive optical fiber communication systems. IEEE Journal of Lighwave Technology, vol. 10, no. 1, pp. 96-100, 1992

[73] *Wen, S.*: Bi-end dispersion compensation for ultralong optical communication systems. IEEE Journal of Lightwave Technology, vol. 17, no.5, pp. 792-798, 1999

[74] *Winall, S. T., Lindsay, A. C.*: DFB semiconductor diode laser frequency stabilization employing electronic feedback and Bragg grating fabry-perot interferometer. IEEE Photonics Technology Letters, vol. 11, no. 9, pp. 1357-1359, 1999

[75] *Wong, W. S., Haus, H. A., Jiang, L. A., Hansen, P. B., Margalit, M.*: Photon statistics of amplified spontaneous emission noise in a 10 GBit/s optically preamplified direct-detection receiver. OSA Optics Letters, vol. 23, p. 1832, 1998

[76] *Wong, W. S., Haus, H. A., Jiang, L. A., Korn, J.*: Photon statistics of non-return-to-zero (NRZ) signals in a high-bit-rate optically preamplified direct detection receiver. RLE Progress Report 141, 1998

[77] *Yamamoto, Y., Kimura, T.*: Coherent optical fiber transmission systems. IEEE Journal of Quantum Electronics, vol. QE17, pp. 918 ff., 1981

[78] *Yano, Y., et. al.*: 2.6 Terabit/s WDM transmission experiment using optical duobinary coding. ECOC 1996, vol. 5 (post deadline papers), Oslo, 1996

[79] *Yariv, A.*: Quantum electronics. 3rd Edition, John Wiley & Sons, New York, 1989

[80] *Yegnanarayana, S., Bhushan, A., Jalali, B.*: An inchoherent wavelength hopping/time spreading code-division mutliple access system. Proceedings ECOC '99, I-188, Nice, France, 1999

[81] *Yegnanarayana, S., Bhushan, A., Jalali, B.*: Fast wavelength-hopping time-spreading encoding/decoding for optical CDMA. IEEE Photonics Technology Letters, vol. 12, no. 5, pp. 573-575, 2000

[82] *Zhang, J.-G., Chen, L.-K., Kwong, W. C.*: Experimental demonstration of efficient all-optical code-division multiplexing. IEE Electronics Letters, vol. 34, no. 19, pp. 1866-1868, 1998

Lebenslauf

Persönliche Daten

Geb. 16.10.1969 in Saarlouis, ledig, deutsche Staatsangehörigkeit

Schulbildung und universitäre Ausbildung

1975 - 1988	Besuch der Grundschule St. Donatus und des Max-Planck-Gymnasiums in Saarlouis
1988-1989	Wehrdienst in Daun/Eifel und Hermeskeil
1989-1996	Studium der Luft- und Raumfahrttechnik an der Universität Stuttgart und der Elektrotechnik an der Universität Kaiserslautern, Vertiefungsrichtung Nachrichtentechnik Siebenmonatiger Auslandsaufenthalt und Anfertigung der Studienarbeit im Bereich Optische Nachrichtentechnik an der Michigan State University in East Lansing, Michigan, USA Anfertigung der Diplomarbeit auf dem Gebiet der Mobilkommunikation

Berufliche Tätigkeit

Dezember 1996 - September 2000	Wissenschaftlicher Mitarbeiter am Lehrstuhl für Theoretische Elektrotechnik und Optische Kommunikationstechnik an der Universität Kaiserslautern Vorlesungsbetreuung „Theoretische Elektrotechnik I,II“ mit zugehörigen Übungen und Klausuren Forschungsarbeit über das Systemverhalten optischer Halbleiterverstärker im 1300 nm Wellenlängenbereich Teilnahme am EU-Projekt „ACTS Upgrade“, Koordinierung und Lieferung von Simulationsergebnissen zur Abschätzung der Systemperformance von optischen Halbleiterverstärkern Forschungsarbeit über optische Codemultiplex-Schemata zum kostengünstigen Aufrüsten bestehender DWDM Systeme und zur Vereinfachung der Kanalüberwachung Teilnahme und Präsentation von Forschungsergebnissen bei PIERS’98 und PIERS ’99
Seit September 2000	Projektleiter bei der BMW AG, München, Serienentwicklung Sprachverarbeitungssysteme

München, den 04. Juli 2001